INFORMATION TO USERS

This manuscript has been reproduced from the microfilm master. UMI films the text directly from the original or copy submitted. Thus, some thesis and dissertation copies are in typewriter face, while others may be from any type of computer printer.

The quality of this reproduction is dependent upon the quality of the copy submitted. Broken or indistinct print, colored or poor quality illustrations and photographs, print bleedthrough, substandard margins, and improper alignment can adversely affect reproduction.

In the unlikely event that the author did not send UMI a complete manuscript and there are missing pages, these will be noted. Also, if unauthorized copyright material had to be removed, a note will indicate the deletion.

Oversize materials (e.g., maps, drawings, charts) are reproduced by sectioning the original, beginning at the upper left-hand corner and continuing from left to right in equal sections with small overlaps. Each original is also photographed in one exposure and is included in reduced form at the back of the book.

Photographs included in the original manuscript have been reproduced xerographically in this copy. Higher quality 6" x 9" black and white photographic prints are available for any photographs or illustrations appearing in this copy for an additional charge. Contact UMI directly to order.

UMI

A Bell & Howell Information Company
300 North Zeeb Road, Ann Arbor MI 48106-1346 USA
313/761-4700 800/521-0600

MEASURED AND MODELED PARTICLE EXPORT IN EQUATORIAL AND COASTAL UPWELLING REGIONS

by

John P. Dunne

A dissertation submitted in partial fulfillment of the
requirements for the degree of

Doctor of Philosophy

University of Washington

1999

Approved by _____
Chairperson of Supervisory Committee

Program Authorized
to Offer Degree Oceanography

Date 12 march 1999

Doctoral Dissertation

In presenting this dissertation in partial fulfillment of the requirements for the Doctoral degree at the University of Washington, I agree that the Library shall make its copies freely available for inspection. I further agree that extensive copying of this dissertation is allowable only for scholarly purposes, consistent with "fair use" as prescribed in the U.S. Copyright Law. Requests for copying or reproduction of this dissertation may be referred to University Microfilms, 1490 Eisenhower Place, P.O. Box 975, Ann Arbor, MI 48106, to whom the author has granted "the right to reproduce and sell (a) copies of the manuscript in microform and/or (b) printed copies of the manuscript made from microform."

Signature 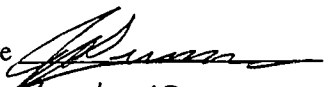

Date March 13 1999

University of Washington

Abstract

Measured and Modeled Particle Export in
Equatorial and Coastal Upwelling Regions

by John P. Dunne

Chairperson of the Supervisory Committee: Professor James W. Murray
Department of Oceanography

The focus of this work was to improve understanding of particle cycling and export from the surface ocean in three areas: 1) methods validation, 2) description of regional and temporal variability and 3) evaluation of particle export mechanisms and implications. To explore the ^{234}Th method of estimating particle export, I first studied the sensitivity of ^{234}Th export to circulation by imposing a hypothetical advection and mixing field on a simple dissolved and particulate ^{234}Th cycle for the central equatorial Pacific. This work confirmed previous studies which estimated particle sinking fluxes using ^{234}Th and implicated vertical advection as a dominant component of the ^{234}Th budget. However, it also suggested that these studies over-estimated sinking particle fluxes in not incorporating horizontal mixing of ^{234}Th. In a second study, I evaluated the role of diatoms in new and export production in the equatorial Pacific by synthesizing data from a suite of cruises. Differential nutrient utilization was shown to be a dominant feature of equatorial biogeochemistry such that large, rapidly sinking and slowly-dissolving diatoms were only dominant in new and export production under high nutrient (iron) conditions. In a third study, I characterized particle export in the western and central equatorial Pacific on two zonal transects and compared these results with data from the JGOFS EqPac program, concluding that the presence of nutrients and the propagation of Kelvin Waves and Tropical Instability Waves were the major determining factors for production variability. In the Santa Barbara Channel, I collected data across the continuum of particle size classes to verify the mechanism by which ^{234}Th traces the particle cycle. Finally, I synthesized data from divergent oceanic regimes to describe the biogeochemical implications of the Two-State ecosystem hypothesis.

TABLE OF CONTENTS

LIST OF FIGURES

LIST OF TABLES

Number *Page*

ACKNOWLEDGMENTS

I wish to thank my advisor, Jim Murray, for all of his efforts to make me a productive and well-rounded scientist. I also wish to thank my committee members: Laurie Balistrieri for her continual support and willingness to help me solve problems, Steve Emerson for his efforts to convert my natural intuition into robust scientific hypothesis testing and Bruce Frost for originally inspiring biological interpretation of much of the data. I have also benefited greatly over the years from conversations with Burke Hales, Russ McDuff, Paul Quay, other UW faculty, many of the JGOFS investigators that I have interacted with and a suite of other students. Barbara Paul helped immensely in the analyses. Jim Bishop and Alice Alldredge taught me sampling methods for the Santa Barbara study. Deanna Akre assisted in the sampling of oxygen during the Santa Barbara study. This work uses published and unpublished data provided by Martine Rodier, Anthony Aufdenkampe, Claudie Navarette, Alice Alldredge, Rebecca Shipe, Alison Murray and Clinton Winant. A majority of this work was supported by a NASA Earth System Science Fellowship (1995-GlobalCh00307) to myself and NSF grants 9504202 and 9633571 to Jim Murray. Finally, I acknowledge Lisa Gilbert's love and support which made the most grueling part of this work, the last year, the most fun.

DEDICATION

I dedicate this dissertation to my parents and to the Sisters of St. Philip's convent who gave me the tools to necessary to complete this work: to my mother for her love and for instilling in me the tenacity to succeed, to my father for his unconditional support, to Sister Romana for making school fun, to Sister Dolores for showing faith in me when I had none in myself, to Sister Catherine for showing me that science is all about asking questions, to Sister Camellias for inspiring my creativity, to Sister Eileen for showing me the importance of self criticism and to all of them for showing me that righteousness comes not from being justified by others but from being true to oneself.

Ode to the Two-State Ecosystem

The plants of the sea,
they produce quite a lot,
but most of them feed
on the ones which have rot.

These leave little trace
on the elements then
but make lots of noise
and are silenced again

The animals keep
a great balance most times
but oft are upset
by those diatom kinds.

These few that are tricky,
they reproduce quick
when the ocean is changing
and their nutrients thick,

but not before long
they will meet a grand fate
and be eaten by copepods
which first had to mate,

and then they'll sink down
in a package of sorts
of the uneaten pieces
and silica forts,

or if they get going,
they may at times stick
and be lost to the depths
aggregating and sick,

but in either case,
they sink through the sea,
and cycle the elements
biogeochemically.

-- John Dunne (1999)

CHAPTER 1: INTRODUCTION TO PARTICLE CYCLING AND EXPORT

BACKGROUND

THE BIOLOGICAL PUMP

The phytoplankton-zooplankton ecosystem of the surface ocean has a profound effect on the global cycling of carbon and other elements. In the presence of sunlit surface waters, phytoplankton convert inorganic nutrients and carbon dioxide into organic material in 'primary production'. Zooplankton and bacteria assimilate some of this organic material while converting a portion of it back into inorganic forms. Some organic material escapes this loop and sinks to the deep ocean. This mechanism of production, processing and sinking of organic material from the surface ocean - the 'biological pump' - is a major component of global elemental cycles as a means transferring carbon and other elements from the surface ocean to the deep sea. One of the most important global effects of the biological pump is to draw down atmospheric carbon dioxide and modulate the extent of the carbon dioxide greenhouse effect (Broecker and Peng, 1982). In addition, the biological pump limits the productivity of ocean ecosystems as it removes the nutrients necessary for further phytoplankton (and subsequently zooplankton) growth.

Primary production is limited by light, major nutrients (e.g. nitrate and silicate) and micronutrients (e.g. iron) and the concentration of phytoplankton which perform it. Oceanographers have extensively studied controls on the rates and mechanisms of the biological pump (e.g. Michaels and Silver, 1988) often using the elements carbon and nitrogen as currency. Available, inorganic nitrogen brought to the sunlit surface ocean is generally in the form of nitrate. Conversion of this nitrate into organic material is termed 'new production'. Ammonia, the inorganic recycling product of zooplankton grazing, is taken up by phytoplankton in 'regenerated production'. Ammonia is taken up preferentially over nitrate (e.g. Price et al., 1994). Zooplankton grazing and phytoplankton regenerated production accounts for a very efficient microbial loop between organic nitrogen and ammonia in many parts of the ocean (McCarthy et al., 1996; Murray et al., 1996). The

sinking flux of organic material which has escaped remineralization is termed 'particle export'. Sinking occurs both directly as phytoplankton single cells and aggregates (Alldredge and Silver, 1988) and indirectly as fecal pellets or other detritus after transfer through the food web (Fowler and Knauer, 1986). Sinking velocity depends both on the excess density (often a function of mineral content) and size of particles (Smayda, 1970). Vertical particle export combines with horizontal exported dissolved and particulate organic matter to account for total export production.

THE EQPAC PROCESS STUDY

Because the presence of nutrients is a critical limiting factor for phytoplankton production, ocean regions which are supplied nutrients from below - via upwelling or mixing - have long been implicated as important for the global cycling of elements (e.g. Eppley and Peterson, 1979). One such area is the equatorial Pacific upwelling zone, where surface waters diverge due to the action of the trade winds at the equator. This divergence brings a near continuous supply of nutrients to the surface. In coastal regions nitrate brought to the surface is utilized by phytoplankton and exported by particles in a matter of weeks (Dugdale and Goering, 1967). In contrast, nitrate upwelled into the equatorial Pacific euphotic zone has a residence time of about a year (McCarthy et al., 1996) and supports relatively low standing stocks of phytoplankton (Barber and Chavez, 1991). This feature of High Nitrate-Low Chlorophyll (HNLC) in the equatorial Pacific has greatly puzzled oceanographers and, in 1992, was the subject of a major oceanographic research process study (EqPac) as part of the US Joint Global Ocean Flux Study (JGOFS).

The EqPac study set out to determine carbon fluxes and understand their controls in the HNLC region of central equatorial Pacific Ocean using a combination of surveys and time-series cruises (e.g. Murray et al., 1994). The EqPac study found that small phytoplankton (Bidigare and Ondrusek, 1996) were recycled by microzooplankton (Landry et al., 1995) in an efficient microbial loop. Primary production was based on recycled nutrients (McCarthy et al., 1996) and the sinking particulate flux was low (Murray et al, 1996). A great deal of temporal variability was observed, however, between boreal spring, El Niño conditions of Survey I and Time-series I, and boreal fall, non-El Niño conditions of Survey II and Time-series II. Synthesis of the EqPac data showed that the

HNLC condition persisted due to intense grazing control of small phytoplankton and iron limitation of large phytoplankton (Landry et al., 1997; Loukos et al., 1997).

ESTIMATION OF PARTICLE EXPORT

The classic means of estimating particle export is through the use of sediment traps. These traps are cylinders which are open at the top but closed at the bottom to collect sinking material. Though this technique has proved invaluable towards the description of sinking material, sediment traps are not quantitative estimators of particle export (Buesseler, 1991). The naturally-occurring, heavily scavenged radioisotope ^{234}Th is currently the most feasible means of calibrating sediment traps for hydrodynamic biases and quantitatively estimating particle export. In this technique the measured sinking flux of ^{234}Th in sediment traps is compared to the predicted ^{234}Th flux from the radioactive disequilibrium with its parent, ^{238}U. Because uranium is unreactive in seawater, long-lived ^{238}U ($t_{1/2}$ = 4.5x10^9 years) is present at high, uniform activities in seawater (~2.4 dpm/l). Thorium, however, is extremely particle reactive such that ^{234}Th ($t_{1/2}$ = 24.1 days) adsorbs onto particles and sinks with them in a process called scavenging, leaving a characteristic radioactive deficiency of ^{234}Th relative to its parent ^{238}U in surface waters. Because the decay of ^{234}Th is of similar timescale as particle production, alteration and export (the biological pump), ^{234}Th can be a sensitive indicator of particle export.

MY CONTRIBUTION TO EQPAC

Our group's main objective during EqPac was to estimate particle export using a combined drifting sediment trap-^{234}Th approach. My first task as a graduate student was to organize, analyze and interpret our group's data set with respect to ^{234}Th-based particle export. In the end, these estimates proved extremely useful in characterizing the equatorial Pacific ecosystem. However, initial interpretation was complicated by two issues. Firstly, the role of advection in the ^{234}Th budget was extremely difficult to accurately account for. When vertical advection (Chai, 1995) and observed gradients in ^{234}Th (Murray et al., 1996) were taken into account, ^{234}Th fluxes at the equator were doubled. Secondly, an equally large amount of variability was observed in the ^{234}Th content of particles, resulting in large differences in estimates of particle export between groups using different methods to collect "sinking" particles (traps, large volume filtration -

Murray et al., 1996; large volume filtration only - Buesseler et al., 1995; Bacon et al., 1996). These issues were extensively debated between investigators. Chapter 2 addresses the first of these issues while Chapters 3 and 5 address the second.

My Master's work focused on interpretation of dissolved and particulate ^{234}Th data taken during EqPac in the context of ^{234}Th scavenging mechanisms - the object being to better understand the mechanism of particle alteration and sinking using ^{234}Th as a tracer. This analysis centered on the comparison between inferred particle remineralization rates which were quite high (0.4 d^{-1}) and observed ^{234}Th particulate distributions and deficiencies from ^{238}U which were also reasonably high. I compared inferred adsorption rates of ^{234}Th from a series of different particle cycling models. Simple models of particle production, remineralization and sinking were inconsistent with previously-described ^{234}Th chemistry. Dunne et al. (1997) concluded that particle sinking was not uniform but depended on a mechanism of differential recycling in the euphotic zone; only a fraction of particles are remineralized while refractory particles sink. In addition, variability in ^{234}Th content of small, large and sinking particles was inconsistent with the mechanism of direct aggregation and sinking of particles. The ^{234}Th content of particles was shown to be a useful constraint on the mechanism of particle export. Use of ^{234}Th scavenging as a constraint on particle dynamics is further explored in Chapters 3 and 5.

My third contribution to EqPac was in the synthesis of observations concerning the "Great Front" (Archer et al., 1997). During EqPac Survey II the equatorial Pacific appeared to bloom as the phytoplankton (the diatom, Rhizosolenia) accumulated at the surface. This dramatic biological response, so extensive that it was observed by space shuttle astronauts (Yoder et al., 1994), was associated with a convergent front at the leading edge of a Tropical Instability Wave. I was able to use EqPac ^{234}Th data to show that these phytoplankton, rather than growing within the front, had been imported to the front on the timescale of a few days. This effort introduced me to the fascinating oceanography associated with Tropical Instability Waves and other mesoscale processes. Observations of additional effects of these waves on the equatorial ecosystem are discussed in Chapters 3, 4 and 6.

OUTLINE OF THIS WORK

This dissertation is a continuation of my efforts to describe the mechanisms and magnitudes of particle export from the surface ocean. It aims to address some of the many questions that arose from my previous work relating to EqPac (Murray et al., 1996; Dunne et al., 1997).

SENSITIVITY OF THE ^{234}TH METHOD TO CIRCULATION - CHAPTER 2

Because the timescale of ^{234}Th scavenging can be long relative to movement of water masses and ecosystem variability, there are inherent uncertainties in the ^{234}Th method. This limitation of the ^{234}Th method was observed during the EqPac because of the sensitivity of ^{234}Th-based particle export estimates to vertical advection. It was necessary to question the general sensitivity of the ^{234}Th method for estimating particle export to advective and diffusive transport in the central equatorial Pacific. In Chapter 2 I develop a two-dimensional model of equatorial circulation and ^{234}Th scavenging to show that, consistent with observations vertical advection is a critical part of the ^{234}Th balance. In addition, I show that horizontal mixing is also important, though less so, while vertical mixing is of negligible effect so long as the depth of interest (the euphotic zone - 120 m) is deeper than the maximum depth of the well-mixed surface layer (50-100 m in the central equatorial Pacific).

PARTICLE EXPORT IN THE EQUATORIAL PACIFIC - CHAPTER 3

One of the issues unresolved after EqPac was the zonal extent of the high nitrate, highly productive water in the central equatorial Pacific with respect to its contact with the western Pacific which is devoid of nitrate in the upper euphotic zone. A second issue unresolved after EqPac was the sensitivity of particle export on seasonal, inter-annual and wave-induced modes of physical variability. Variability in particle export during EqPac may have been associated with inter-annual variability due to the El Niño-Southern Oscillation, seasonal increases in wind-driven upwelling or mesoscale variability induced by Kelvin Waves and Tropical Instability Waves. The two EqPac time periods were not sufficient to distinguish between these effects and ascertain which are the dominant modes of variability.

These two issues are addressed in Chapter 3. New results are presented and discussed from two cruises along the equator from 165°E in the western Pacific to 150°W in the central Pacific collected during the French JGOFS FLUPAC study aboard the R/V l'Atalante in October, 1994 and the Zonal Flux study aboard the R/V Thomas G. Thompson in April, 1996. Both cruises went from New Caledonia to Tahiti. These cruises took place under extremely different ENSO, seasonal and mesoscale conditions: FLUPAC was conducted during a strong El Niño in boreal fall during Kelvin Wave and Tropical Instability Wave activity and Zonal Flux during a mild La Niña in the boreal spring in the absence of mesoscale waves. Particle export in the western equatorial Pacific warm pool is characterized using this new data. The combination of EqPac, FLUPAC and Zonal Flux results is used to examine these potential modes for particle export variability.

SILICON:NITROGEN COUPLING IN THE EQUATORIAL PACIFIC - CHAPTER 4

The EqPac synthesis of Landry et al (1997) provided a convincing argument for limitation of new production and particle export through the combination of zooplankton grazing control of small phytoplankton and iron limitation of larger phytoplankton. More recently, Dugdale and Wilkerson (1998) challenged this hypothesis, suggesting that new production and particle export in the equatorial Pacific are limited by upwelled silicate. Though the Dugdale and Wilkerson (1998) analysis was appealing in its simplicity, it was not fully convincing as it was limited in scope to the EqPac Survey II cruise and only took advantage of nutrient data.

In Chapter 4, I tested the proposal of Dugdale and Wilkerson by compiling nutrient data from 19 equatorial cruises and comparing nutrient data from the EqPac, FLUPAC and Zonal Flux cruises with data from sediment traps and water column particle concentration. This analysis supports the argument that diatom production was tightly coupled to new production in the EUZ during the US JGOFS EqPac Survey II cruise (Dugdale and Wilkerson, 1998). It also shows, however, that the EqPac Survey II cruise took place during a period of atypically high subsurface nutrients. I conclude that, in the equatorial Pacific, diatoms control the biological pump only at times of very high nutrient concentrations and during periods of non-steady state. In this analysis nutrient cycling in the equatorial Pacific is consistent at all times with the proposed mechanism of combined iron and grazing control of phytoplankton size classes (Landry et al., 1997).

^{234}Th scavenging and particle dynamics in the Santa Barbara Channel - Chapter 5

Two years ago, I had the opportunity to step away from the equator and perform an intensive study of particle and ^{234}Th dynamics in another high nutrient region - the coastal upwelling regime of the Santa Barbara Channel. Coastal upwelling regimes are critically different from open ocean upwelling systems like the equatorial Pacific in that phytoplankton are able to more efficiently utilize nutrients and export them in sinking particles. This study had three main goals: 1) to determine particle export in this region, 2) to characterize the ^{234}Th content of particles as a function of particle size using a variety of sampling methods and 3) to determine the mechanism of particle export in this region, focusing on evaluating the role of marine snow. Chapter 5 describes results from this study.

The first of these goals was only partially achieved as particle export could not be adequately calibrated using ^{234}Th; observed sediment trap fluxes were consistent with modeled ^{234}Th fluxes, but these model ^{234}Th fluxes were too uncertain to provide a significant constraint. Though a great deal of variability was also observed with respect to particles, I was able to use address goals 2 and 3 using trends in C:^{234}Th ratios of particles. This analysis showed that: 1) Colloidal particles are not a source of ^{234}Th (they contain almost none) and thus are not a significant source of ^{234}Th to sediment traps. This allows them to be ignored in the particle-^{234}Th model. 2) The dominant removal term in the marine snow budget is disaggregation. This removal is probably a result of zooplankton grazing as was recently suggested by Dilling (1997). As a result, sinking marine snow is created and destroyed repeatedly on its passage from the mixed layer to the depths of sediment traps, steadily being grazed and gaining mineral material until it's excess density and sinking velocity increases enough for it to be exported efficiently.

Biogeochemical Implications of a Two State Ecosystem - Chapter 6

Ecosystem response to nutrient input is extremely variable both spatially and temporally. Coastal upwelling regions and some open ocean regions are prone to intense elevation in phytoplankton biomass (blooms) and mass export of particles while HNLC regions such as the equatorial Pacific, subarctic Pacific and Southern Ocean are typically stable with respect to phytoplankton biomass. A common observation throughout this dissertation is the influence that biological community structure exerts on the

biogeochemical cycling of carbon and other elements. The concept of the two-state ecosystem unifies these observation in a single ecosystem behavior. Chapter 6 serves as a synthesis of the biogeochemical implications of a two-state ecosystem. In Chapter 6, I: 1) define the two-state ecosystem hypothesis as a means of distinguishing between ecosystems under steady-state limitation and those which undergo periodic release from limitation 2) cite examples of the relationship between ecosystem structure and particle export both from the literature and as witnessed in this dissertation and 3) explore the implications of the duality of ecosystem structure for regional and global biogeochemistry.

CHAPTER 2: SENSITIVITY OF ^{234}TH EXPORT TO PHYSICAL PROCESSES IN THE CENTRAL EQUATORIAL PACIFIC

INTRODUCTION

^{234}Th is a tracer of particle transport and cycling in the surface ocean (Coale and Bruland, 1985). The ^{234}Th method consists of using the water column deficiency of ^{234}Th relative to ^{238}U to calculate the sinking flux of ^{234}Th due to particle scavenging. In one application of this method, the calculated sinking flux of ^{234}Th is multiplied by the C:^{234}Th ratio in sinking particles to obtain the sinking flux of carbon (Buesseler et al., 1992, 1994, 1995; Bacon et al., 1996; Murray et al., 1996). If the concentration of ^{234}Th in sinking particles is known, the sinking flux of ^{234}Th can be used to estimate the average sinking velocity of particles (Buesseler et al., 1995; Bacon et al., 1996; Dunne et al., 1998). A second application of the ^{234}Th method is to use the ratio of the calculated sinking flux of ^{234}Th to the measured ^{234}Th flux in sediment traps to correct sediment traps for hydrodynamic biases (Murray et al., 1996). For both approaches, it must be shown (or assumed) that ^{234}Th and carbon are transported by the same particles (Murray et al., 1996).

The accuracy of the ^{234}Th method depends highly on the accuracy of the ^{234}Th deficiency as a diagnostic of the ^{234}Th sinking flux. It is thus important to determine the contribution of advection and diffusion to the calculated ^{234}Th flux, but this is usually difficult to accomplish due to a lack of spatial resolution in the data and weak physical constraints. Fortunately, both of these limitations can be addressed using data from the US JGOFS Process Study in the central equatorial Pacific (EqPac; Murray et al., 1994).

The central equatorial Pacific is well recognized as a regime of intense circulation in which the easterly trade winds drive equatorial divergence (Wyrtki and Kilonsky, 1984). Though zonal currents are stronger than vertical and meridional currents in the upper 300 m, recent model studies have shown that vertical and meridional circulation dominates tracer budgets due to the strength of divergence relative to the long zonal extent of the region. Liu et al. (1994) found that a typical water parcel is upwelled at

the equator in the east and recirculated meridionally 3-6 times while traversing zonally from east to west across the Pacific.

Extensive studies of ^{234}Th were recently conducted in the equatorial Pacific as part of EqPac (Buesseler et al., 1995; Murray et al., 1996; Bacon et al., 1996). The combination of these ^{234}Th data and relatively well-defined physics in the central equatorial Pacific allowed investigation of the advective components of the ^{234}Th balance. In these studies the effect of advection on calculations of ^{234}Th flux was estimated using advection velocities generated from general circulation model results of Chai (1995). Qualitatively, these studies showed that vertical and meridional advection had a major effect on the ^{234}Th flux balance and on calculations of the flux of ^{234}Th from the upper water column. For example, Murray et al. (1996) suggested that at the equator the flux of ^{234}Th into the surface due to upwelling was about half the downward flux of ^{234}Th on particles. Buesseler et al. (1995) reported that vertical advective fluxes at the equator were approximately equal to the radioactive deficiency flux while zonal fluxes were generally less that 5% and always less than 25% of the radioactive deficiency flux. A general lack of zonal ^{234}Th gradients was also observed on the recent FLUPAC and Zonal Flux cruises along the equator from 165°E to 150°W (Dunne et al., in prep.). Results from these studies showed that ^{234}Th scavenging and vertical advection had similar magnitudes of opposing impact on the ^{234}Th flux balance in the equatorial surface ocean while zonal advection was negligible. These fluxes, however, were calculated by multiplying observed gradients in ^{234}Th times the flow field and have large relative errors, generally over 100%, leading to a large uncertainty in the advection-corrected ^{234}Th flux balance. In addition, these studies did not estimate the impact of diffusion.

The geochemical importance of ^{234}Th is its potential as a method for predicting the export flux of particulate carbon and calibrating sediment traps (Buesseler, 1991). The focus of this study is to critically evaluate the sensitivity of the ^{234}Th method to circulation in the central equatorial Pacific and assess the uncertainty in the ^{234}Th method as a calibration tool for sediment traps. We calculated ^{234}Th fluxes due to scavenging, advection and diffusion on a two dimensional flow field adopted from general circulation models to evaluate the sensitivity of the modeled ^{234}Th flux to advection and diffusion. This method has the advantage of being numerically fully consistent and exact, and allowed us to look at the individual effect of each process on the ^{234}Th flux balance. In this chapter

we present model predictions that: 1) Vertical advection at the equator has a dramatic effect on the ^{234}Th flux balance such that vertical advection must be incorporated into ^{234}Th-based estimates of export. 2) Horizontal diffusion also has a significant effect on ^{234}Th flux balance such that ^{234}Th-based export estimates corrected only for advection over-estimate the sinking flux by up to 63%. 3) A scavenging mechanism involving rapid particle sinking predicts that advection and diffusion are only approximately half as important on the ^{234}Th mass balance as does one involving slow particle sinking.

MODEL DESCRIPTION

We simplified the conceptual model of equatorial circulation (e.g. Philander 1990) in order to simulate only the most essential components of the complex four dimensional circulation in the central equatorial Pacific. These components are equatorial upwelling and meridional recirculation. A 2-dimensional advection stream function of upwelling and meridional recirculation between the equator and 5°N and 5°S was patterned after the vertical advection fields of Liu et al., (1994) and Chai (1995).

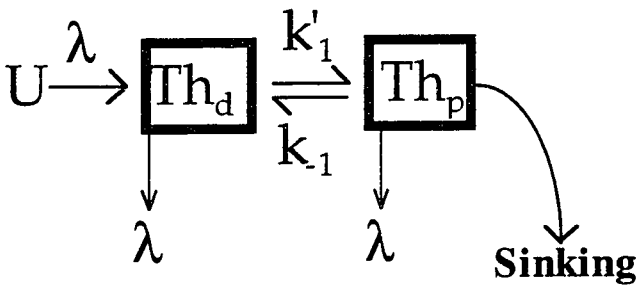

Figure 2.1: Diagram of the thorium scavenging model (Bacon and Anderson, 1982) where boxes indicate reservoirs and arrows indicate fluxes.

We then superimposed the thorium scavenging model of Bacon and Anderson (1982) on the circulation field. The thorium scavenging model was a two-component model shown schematically in Figure 2.1 in which dissolved ^{234}Th, Th_d, undergoes first-order, reversible sorption to become particulate ^{234}Th, Th_p, which sinks through the water column. As discussed above, zonal gradients and subsequently zonal advective and diffusive fluxes have been shown to be small and can be neglected. Ignoring these zonal terms, the continuity equations for dissolved and particulate ^{234}Th are:

$$\partial Th_d/\partial t = U\cdot\lambda - (\lambda+k'_1)\cdot Th_d + k_{-1}\cdot Th_p - v\cdot\partial Th_d/\partial y - w\cdot\partial Th_d/\partial z + (\partial K_h \cdot (\partial Th_d/\partial y))/\partial y + (\partial K_z\cdot(\partial Th_d/\partial z))/\partial z \quad (2.1)$$

$$\partial Th_p/\partial t = k'_1\cdot Th_d - (\lambda + k_{-1})\cdot Th_p - (S + w)\cdot\partial Th_p/\partial z - v\cdot\partial Th_p/\partial y + (\partial K_h\cdot(\partial Th_p/\partial y))/\partial y + (\partial K_z\cdot(\partial Th_p/\partial z))/\partial z \quad (2.2)$$

All parameters used in this study are described in Table 2.1. We assumed single values of the ^{234}Th decay constant (λ), desorption rate constant (k_{-1}) and horizontal diffusion constant (K_h), two values of the vertical diffusion constant (K_z), and fields of meridional (v) and vertical (w) advection as described below. We estimated the apparent adsorption rate constant (k'_1) and sinking velocity (S) from the dissolved ^{234}Th (Th_d), particulate ^{234}Th

Table 2.1: Summary of parameters used in the scavenging/two-dimensional circulation model

Symbol	Definition	Units	Description
U	total ^{238}U activity	dpm m^{-3}	U_{data}=0.0686·Salinity·(1+σ_θ/1000); U_{model}=2440
Th_t	total ^{234}Th activity	dpm m^{-3}	Unfiltered Go-Flo samples
Th_d	dissolved ^{234}Th activity	dpm m^{-3}	Go-Flo samples passing a 0.4 µm filter
Th_p	particulate ^{234}Th activity	dpm m^{-3}	$Th_p = Th_t - Th_d$
P	particle concentration	mmol C m^{-3}	CTD beam attenuation·18.547
λ	decay constant	d^{-1}	λ = 0.02876
k_{-1}	desorption constant	d^{-1}	k_{-1} = 0.0068, Clegg and Whitfield (1993)
k'_1	apparent adsorption constant	d^{-1}	calculated from data using Equation 2.3
v	meridional velocity	°lat d^{-1}	stream function (Chai, 1995; Liu et al., 1994)
w	vertical velocity	m d^{-1}	stream function (Chai, 1995; Liu et al., 1994)
K_h	horizontal diffusion	°lat^2 d^{-1}	K_h = 0.007 (Pacanowski and Philander, 1981)
K_z	vertical diffusion	m^2 d^{-1}	K_z = 2450 above 70 m and K_z = 2.6 below 70 m (Pacanowski and Philander, 1981)
k_1	inherent adsorption constant	mmol C^{-1} m^3 d^{-1}	calculated from regression of k'_1 against P
S	sinking velocity	m d^{-1}	calculated by tuning model to observed deficiency
R_{def}	deficiency flux:sinking flux ratio	----------	calculated by integrating the model deficiency to 120 m and dividing by S·P_{120}
$R_{def+adv}$	deficiency and advection flux:sinking flux ratio	----------	calculated by integrating the model deficiency to 120 m, adding advection terms and dividing by S·P_{120}

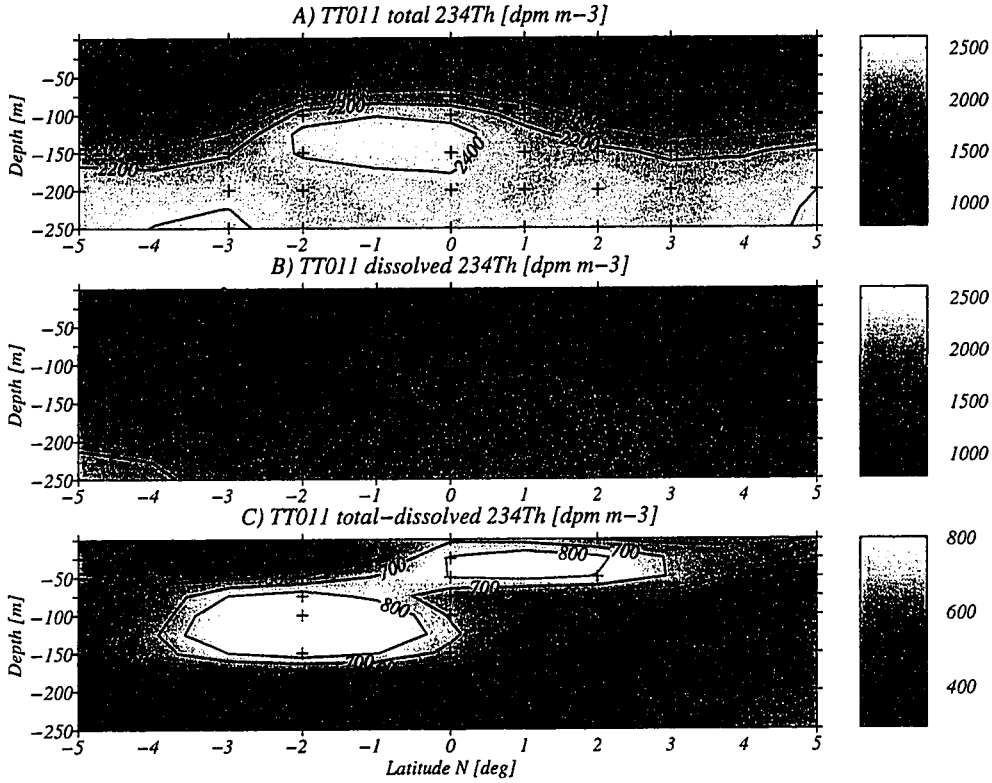

Figure 2.2: Data contours of total ^{234}Th (2.2A) dissolved ^{234}Th (2.2B) and particulate ^{234}Th (= total - dissolved; 2.2C) (dpm m^{-3}) between 5°N and 5°S in the upper 250 m from JGOFS-EQPAC Survey II.

(Th_p) and total ^{238}U (U) data also described below.

Data for Th_t (Murray et al., 1996) and Th_d (Dunne et al., 1998) were taken during JGOFS-EqPac Survey II (http://www1.whoi.edu/jgofs.html; Figures 2.2A,B). Th_p was calculated as the difference between Th_t and Th_d (Figure 2.2C). Model output was evaluated by its ability to reproduce the following key features observed in the EqPac Survey II data: 1) uniformly low levels of Th_t in the mixed layer, 2) secular equilibrium levels of Th_t at 200-250 m, 3) Th_p levels approximately a third of the Th_d levels and 4) Th_p levels that have their maximum in or directly below the mixed layer and decrease at greater depth.

MODEL PARAMETERIZATION

We used a 2-dimensional steady state model with a meridional resolution of 1/8° and a vertical resolution of 10 m to evaluate the effect of a hypothetical advection and diffusion regime on distributions of ^{234}Th. Calculating model fluxes at steady state allowed us to obtain an exact solution without uncertainties due to numerical diffusion or dispersion. The numerical scheme was set up as a steady-state flux inventory using a staggered grid such that for any compartment, inventories of ^{234}Th were defined within the compartment and velocities at each corner. This scheme was chosen because it conserves fluxes in areas where diffusion coefficients change, such as at the base of the model's mixed layer. After all parameters were set, the matrix of equations was inverted to obtain distributions of dissolved and particulate ^{234}Th.

Our 2-dimensional advection stream function for meridional and vertical velocity was modeled after the work of Chai (1995) which used the modular ocean model (MOM) forced by the COADS winds observed during September-November of 1992 and after the work of Liu et al. (1994) which was forced by climatological winds. The stream function was a set of empirical, exponential functions combined to give streamlines of velocity. The empirical equations for meridional (v) and vertical (w) velocity are:

$$v = (1-e^{-0.35y})\cdot(5.125-y)\cdot(0.22\cdot(e^{-z/50}-e^{-290/50}-z/50\cdot e^{-z/50})-6.4\cdot(\pi/290\cdot\cos(z\cdot\pi/290)\cdot(e^{-z/120}-e^{-290/120})-\sin(z/290\cdot\pi)/120\cdot e(^{-z/120})))$$

$$w = (z\cdot(e^{-z/50}-e^{-290/50})\cdot 0.22-6.4\cdot\sin(\pi z/290))\cdot(e^{-z/120}-e^{-290/120})\cdot(0.35\cdot e^{(-0.35*y)}\cdot(5.125-y)-1-e^{(-0.35*y)})$$

where y and z are the meridional (° latitude) and vertical (meters) coordinates, respectively. Contour plots of v and w are shown in Figures 2.3A and B, respectively. Zonal advection was neglected in this model. Liu et al. (1994) gave a detailed climatological analysis of the relative features of equatorial and tropical circulation, showing that water upwelled at the equator was primarily associated with intense meridional recirculation rather than meridional export past 5°N and 5°S. Chai (1995) used a less detailed numerical model forced by actual winds to estimate upwelling conditions during EqPac Survey II. He found a upwelling velocity at the equator of 4 m d^{-1} at 50 m. Upwelling decreased to 1 m d^{-1} at

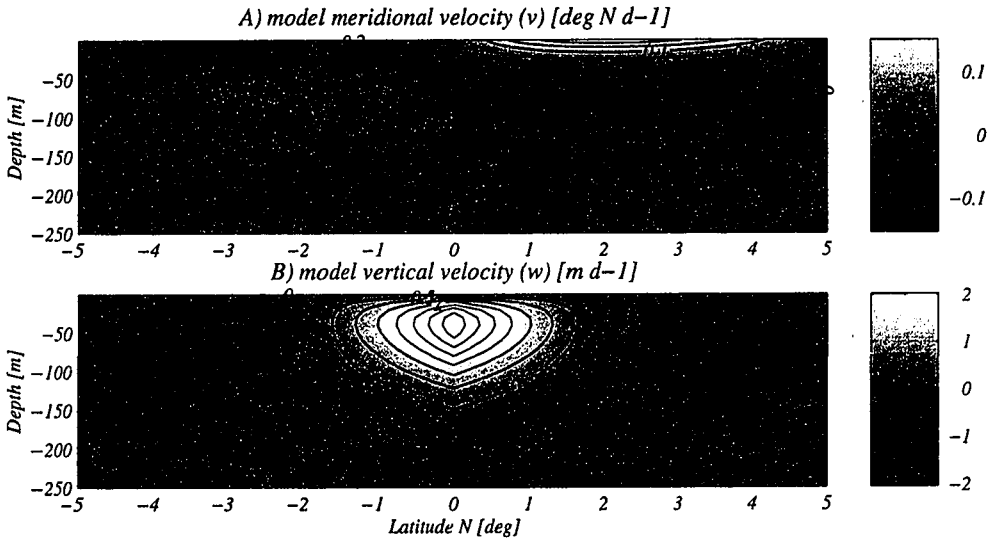

Figure 2.3: Contours of meridional velocity (2.3A; °N d^{-1}) and vertical velocity (2.3B; m d^{-1}) between 5°N and 5°S in the upper 250 m from the empirical stream function.

the base of the euphotic zone (120 m) and to zero vertically below 150 m and horizontally at 2°N and 2°S. For simplicity, the circulation was assumed to be symmetric about the equator and thus does not reflect the true meridional asymmetry observed in this region that is caused by the presence of the Inter-tropical Convergence Zone north of the equator (Philander, 1990). The shapes of the contours of upwelling velocity (Figure 2.3B) were tuned to reproduce the features in Chai (1995) described above. Circulation was also assumed to be closed between the equator and 5° north and south. The work of Liu et al. (1994) suggested that about 25% of the meridional flow along the surface escapes recirculation. More recent work by Lu et al. (1998) suggested that this flow could be as much as 70%. These studies imply that the model used here overestimates downwelling velocities between 2° and 5° by 25-70% relative to upwelling velocities at the equator. As our focus here is on the equator, not on the 2°-5° region, we do not consider this uncertainty a critical flaw in the model but note it as a word of caution.

Estimates of diffusion in the literature vary over a considerable range depending on the time and space scales (i.e. magnitudes of convection) that the measurements integrate over. Horizontal diffusion estimates range from 3 m^2 s^{-1} from a tracer release experiment in the south Pacific (Ledwell, 1993) to 5000 m^2 s^{-1} from a larger

scale helium-tritium mass balance in the tropical Pacific (Fine and Ostlund, 1980). Similarly, estimates of vertical diffusion in the literature vary over an order of magnitude between microscale and tracer release estimates of 0.1 $cm^2\ s^{-1}$ (e.g. Ledwell, 1993) and tracer budget estimates of 1-2 $cm^2\ s^{-1}$ (e.g. Munk, 1966). For this study we set K_h = 1000 $m^2\ s^{-1}$ (= 0.007 $°lat^2\ d^{-1}$) and K_z = 0.3 $cm^2\ s^{-1}$ (= 2.6 $m^2\ d^{-1}$) below the mixed layer consistent with Pacanowski and Philander (1981). A constant mixed layer with a depth of 70 m obtained from the EqPac Survey II average (using the density change of 0.125; Gardner et al., 1996) was set to mix once per day with a vertical diffusion coefficient of 0.028 $m^2\ s^{-1}$ (= 2450 $m^2\ d^{-1}$).

Estimates of particle concentration (P) were obtained from CTD beam attenuation (http://www1.whoi.edu/jgofs.html; Figure 2.4). To express P in more convenient units, beam attenuation was converted to particulate organic carbon concentration units using a factor of 18.5 mmol C m^{-2} calibrated from the Multiple Unit Large Volume Filtration System (MULVFS) data of J. H. Bishop (in press). The ^{234}Th decay constant (λ) was set to 0.02876 d^{-1}, and the desorption rate constant (k_{-1}) was set to 0.0068 d^{-1} after the compilation of Clegg and Whitfield (1993).

For the model to predict the distributions of ^{234}Th, the apparent adsorption rate constant (k'_1) had to be estimated for each grid cell. Though k'_1 can be calculated directly from the data for some cells and then interpolated for the others, the resulting field is extremely noisy due to analytical uncertainty. We chose to minimize these complications by parameterizing k'_1 in the model, taking advantage of the strong correlation observed here and elsewhere between k'_1 and P (Bacon and Anderson, 1982; Honeyman et al., 1988; Dunne et al., 1998). We assumed a first order relationship between k'_1 and P ($k'_1 = k_1 \cdot P$) to parameterize the adsorption field in the model using a three step process. In the first step, Equation 2.1 was re-arranged into Equation 2.3 to obtain estimates of k'_1 from the EqPac Survey II data using Th_d and Th_p shown in Figure 2.2 and U calculated from salinity and density ($U=0.0686 \cdot S \cdot (1+\sigma_t/1000)$; Murray et al., 1996). Estimates of v and w were taken from Chai (1995). As analytical uncertainty in Th_d was too high to estimate second derivatives, diffusion terms were neglected.

$$\mathbf{k'_1 = [\ \lambda \cdot (U - Th_d) + k_{-1} \cdot Th_p - v \cdot \partial Th_d/\partial y - w \cdot \partial Th_d/\partial z\ ] / Th_d} \qquad (2.3)$$

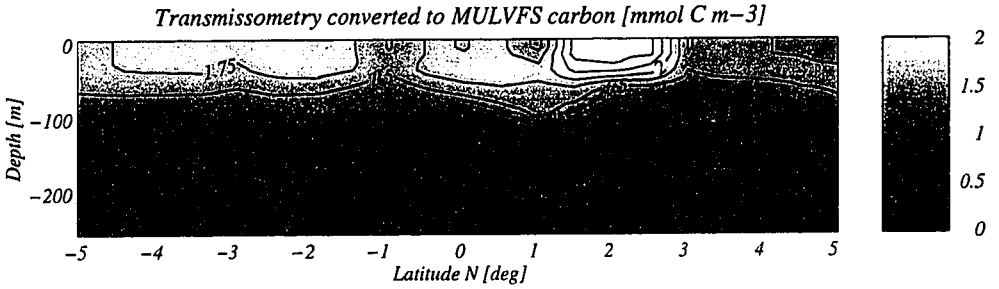

Figure 2.4: Data contour of beam attenuation (mmol C m^{-3}) between 5°N and 5°S in the upper 250 m during JGOFS-EQPAC Survey II normalized to particulate carbon from Bishop (in press).

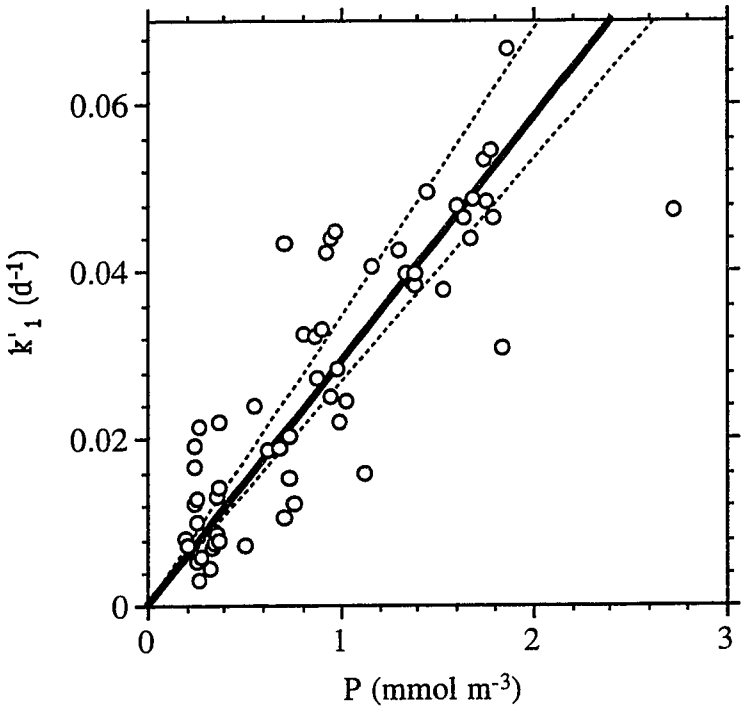

Figure 2.5: Estimates of the adsorption rate constant, k'_1 (day^{-1}), versus particle concentration, P (mmol C m^{-3}) from beam attenuation using the data from JGOFS EQPAC Survey II in Figures 2.2 and 2.4. Also shown is the fixed-intercept regression (solid line with slope = 0.02905 mmol C^{-1} m^3 day^{-1}; Mood, 1950) with its 95% confidence interval of 0.0266 - 0.0343 mmol C^{-1} m^3 day^{-1} (dotted lines). Assuming $k'_1 = k_1 \cdot P$, the slope gives the value for k_1.

In the second step, values of k'_1 were regressed against P (Figure 2.5) to obtain an inherent adsorption rate constant (k_1) from the slope. Variability in P was able to explain 73% of the variability in k'_1, giving us great confidence in the parameterization. We estimated the most probable slope (k_1 = 0.02905 mmol C^{-1} m^3 d^{-1}) and its 95% confidence intervals (0.0266 - 0.0343 mmol C^{-1} m^3 d^{-1}; n = 60) using Mood's non-parametric method (Mood, 1950). Mood's method has three advantages: 1) It weights ranks, eliminating biases due to extreme values. 2) It enables the straight-forward calculation of confidence intervals. 3) It allows the intercept to be fixed (to zero in this case). Thirdly, the model field of k'_1 was obtained through multiplying k_1 by P (Figure 2.4) in each grid cell.

Boundary conditions for the model were zero flux across all boundaries except along the bottom where Th_p was allowed to vary. The model activity field of ^{238}U was set everywhere to 2440 dpm m^{-3}. The model sinking velocity (S) was used as an adjustable parameter to minimize the difference between observed and modeled ^{234}Th deficiencies in the upper 120 m (Figure 2.9A). The 0-120 m depth interval was chosen as the criteria for this calculation to assure consistency with the JGOFS-EQPAC flux normalization protocol to a 120 m euphotic zone defined by the 0.1% light level (Murray et al., 1996). This minimization procedure gave a sinking velocity of S = 3.01 m d^{-1} with a 93% confidence interval of 2.51 - 3.59 m d^{-1}. At the chosen sinking velocity, the observed and modeled deficiencies agree within 10% on average. The value of S = 3.01 m d^{-1} was used for all model runs except in the sinking velocity sensitivity analysis.

RESULTS AND DISCUSSION

DISCUSSION OF MODELED ^{234}TH DISTRIBUTIONS

Our primary goal was to determine the effect of advection and diffusion on the ^{234}Th deficiency and thus the calculated ^{234}Th sinking flux. To this end we considered primarily distributions of total ^{234}Th (= dissolved + particulate) because the distribution of total ^{234}Th determines the ^{234}Th deficiency. Here we present model fields of total ^{234}Th, first from the chemical model alone without any physical terms and then with the inclusion of each term individually to illustrate its impact. Neglecting both advection and diffusion

gave the distributions shown in Figure 2.6A. ^{234}Th increased almost linearly with depth between the surface and 150 m to values in equilibrium with ^{238}U. This broad, linear increase in ^{234}Th with depth was unlike the sharp vertical front in ^{234}Th at the base of the mixed layer that was actually observed (Figure 2.2A). Adding horizontal and vertical diffusion without advection gave the contour plot shown in Figure 2.6B. In this case total ^{234}Th was uniformly low in the mixed layer and increased linearly between 70 and 150 m. The striking contrast between Figure 2.6A and Figure 2.6B in the upper 70 m illustrates the importance of the mixed layer in homogenizing upper ocean ^{234}Th activities in the central equatorial Pacific. Adding advection without diffusion produced contours of ^{234}Th that bowed upward at the equator and spread downward at higher latitudes (Figure 2.6C). In addition, the process of adsorption and sinking (and to a small degree subsequent desorption) at the equator had a focusing effect, creating extremely high values of ^{234}Th in the vertical zone where particulate ^{234}Th was high. This feature is further discussed below.

The combined effects of advection and diffusion are shown in Figure 2.6D. The addition of a mixed layer removed much of the vertical structure while horizontal mixing broadened and smoothed the meridional extent of high surface ^{234}Th due to upwelling. Mixed layer values near the equator were elevated while levels at high latitudes were depressed relative to the diffusion-alone case (Figure 2.6B). The strong subsurface maximum observed in Figure 2.6C at the equator was replaced by a much weaker subsurface maximum at 125 m which was displaced slightly to the north. This northward displacement of the maximum was because the highest particle concentrations observed at 2°N (Figure 2.4) led to the highest predicted values of k'_1(Equation 2.3). Diffusion smeared the features at the equator and at 2°N. The model results for total ^{234}Th in Figure 2.6D can be compared directly with the data for total ^{234}Th in Figure 2.2A for a qualitative assessment of the model. The model reproduced both the patterns and magnitudes observed in the data including the mixed layer levels, the equatorial surface maximum and the equatorial subsurface maximum. On average, modeled total ^{234}Th activities were within 11% of the data and reproduced 76% of the variability.

We compare each source and removal term in the ^{234}Th flux balance in the upper 120 m in Figure 2.7. The ^{234}Th deficiency, the difference between the U and Th_t decay fluxes, is shown instead of the absolute fluxes for ease in comparison with the other terms. Except at the equator, the deficiency and the sinking flux were of similar magnitude

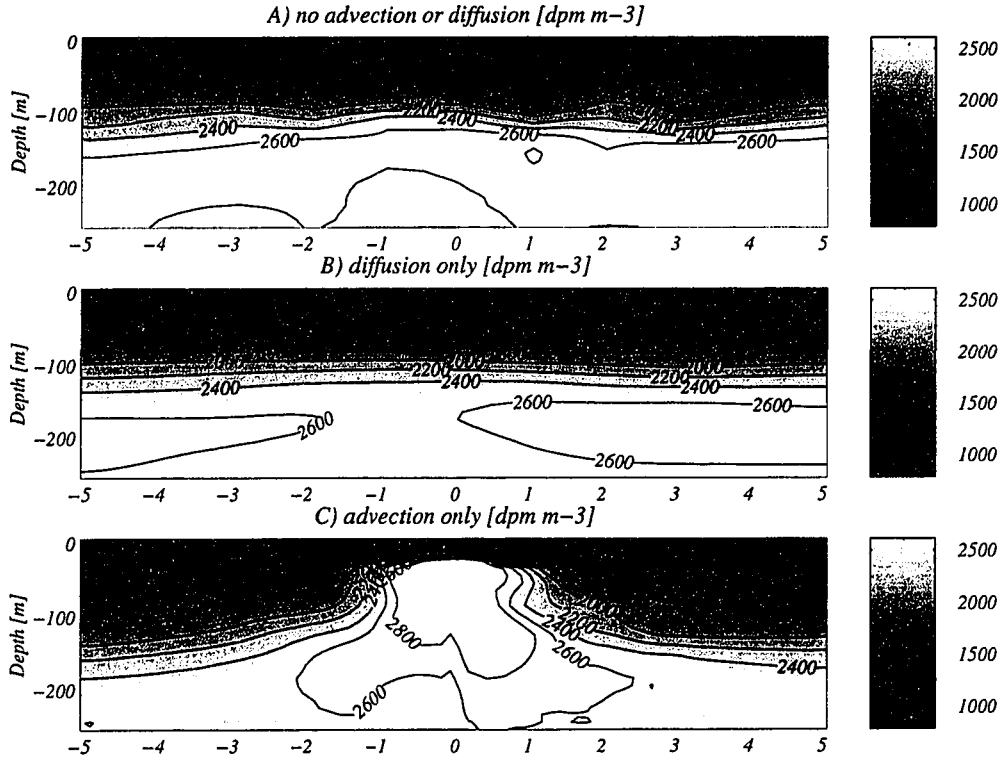

Figure 2.6: Model contours of total ^{234}Th (dpm m^{-3}) between 5°N and 5°S in the upper 250 m from the two dimensional model without advection or diffusion (2.6A), with diffusion but no advection (2.6B), with advection but no diffusion (2.6C) and with advection and diffusion (2.6D).

(opposite in sign). Upwelling at the equator input high ^{234}Th into the upper 120 m, making vertical advection a large positive flux and resulting in a smaller ^{234}Th deficiency from ^{238}U. Vertical advection was thus an important part of the ^{234}Th flux balance at the equator. This result confirms previous studies. Horizontal diffusion carried some of this high ^{234}Th away from the equator. The important role of horizontal diffusion on the ^{234}Th flux balance at the equator was not previously accounted for. Off the equator horizontal advection carried an additional amount further away. Vertical diffusion across the base of the euphotic zone (120 m) was everywhere a small factor and was not an important part of the ^{234}Th flux balance. This was also not previously known. It should be noted that this is only true in regions of the ocean such as the equatorial Pacific where the mixed layer is

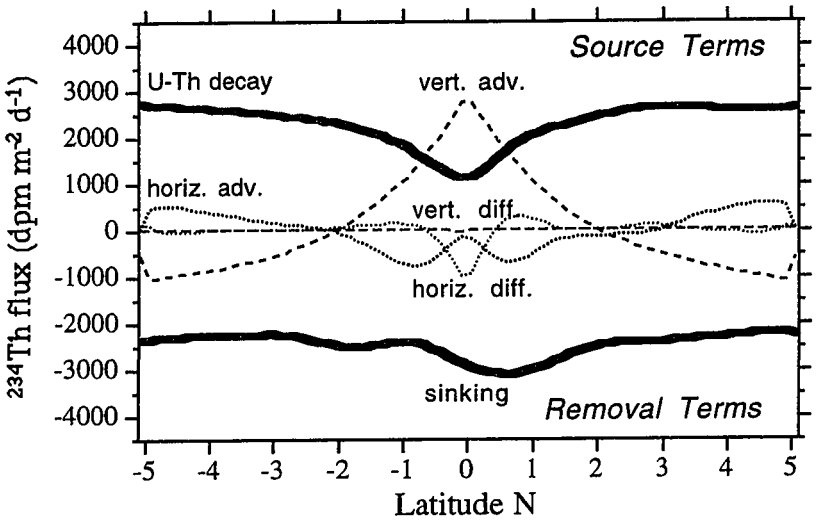

Figure 2.7: Model diagnostic summary of the ^{234}Th flux balance between 0 - 120 m versus latitude showing: the difference between ^{238}U and ^{234}Th decay (the deficiency; thick gray), particle sinking (thick black), vertical advection (dashed black), horizontal advection (dotted black), vertical diffusion (dashed gray) and horizontal diffusion (dotted gray).

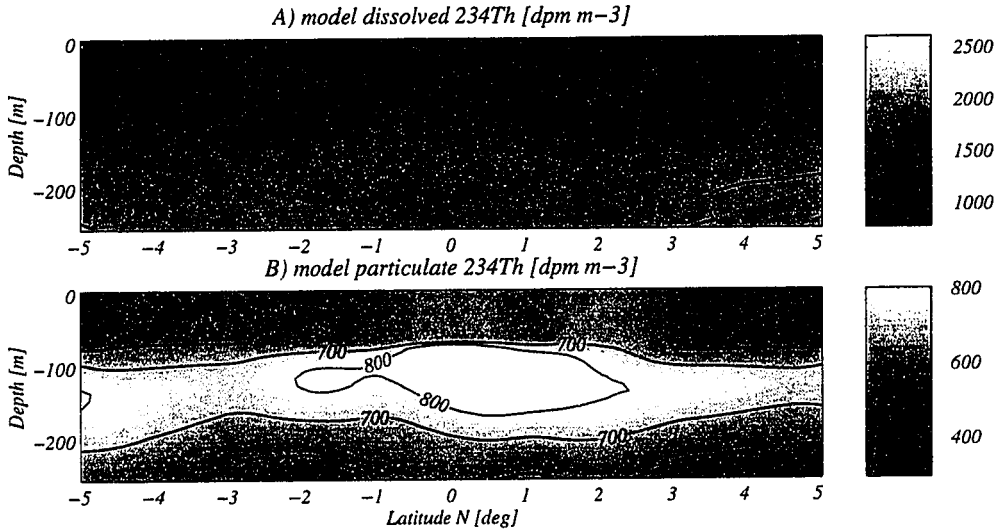

Figure 2.8: Model contours of dissolved (2.8A) and particulate (2.8B) ^{234}Th (dpm m^{-3}) between 5°N and 5°S in the upper 250 m from the two dimensional model with advection and diffusion.

shallower than the depth of the euphotic zone. The model gave significant negative advective fluxes between 2° and 5° due to downwelling. Because the model did not allow any water to leave at the surface to the north and south, it over-estimated downwelling at high latitudes relative to upwelling at the equator.

The model Th_d distribution (Figure 2.8A) compared well with the data (Figure 2.2B), reproducing the surface low and linear subsurface increase. It showed a similar overall pattern as for modeled Th_t (Figure 2.6D) except that the model Th_d lacked a subsurface maximum. On average, modeled Th_d activities were within 6.3% of the data and reproduced 85% of the variability.

The distribution of modeled Th_p (Figure 2.8B) compared less well with observed Th_p activities, averaging only within 27% relative error. Partly this was due to analytical noise in the differencing technique used to estimate Th_p in Figure 2.2B. The subsurface maximum in the distribution of modeled Th_t was the major feature of distribution of modeled Th_p. This subsurface maximum appeared in the data only at 2°S (Figure 2.2C). The model Th_p subsurface maximum extended across all latitudes but concentrated just north of the equator (0°-1°) between the maximum in w at the equator (Figure 2.3B) and the maximum in P at 2°N (Figure 2.4). The surface low in Th_p was a consequence of the combination of the zero flux boundary condition at the surface and the parameterization of uniform sinking of Th_p. Neglecting the effects of advection and diffusion, model Th_p increased with depth from the surface to the depth where adsorption balanced decay, desorption and sinking (Equation 2.2). The addition of vertical diffusion and a mixed layer removed much of the depth structure. The subsurface maximum did not completely disappear as adsorption exceeds decay, desorption and sinking in the upper 100 m.

Comparison of ^{234}Th in the water column and in sediment traps

In this section we evaluate the degree to which the measured ^{234}Th deficiency reflected the sinking flux of ^{234}Th during EqPac Survey II and discuss the usefulness of the ^{234}Th method for sediment trap calibration in the presence of strong upwelling. As was discussed above, it has been proposed that the ^{234}Th deficiency is an accurate, independent measure of the sinking flux of ^{234}Th and can be compared with the

measured ^{234}Th flux to calibrate sediment traps (Buesseler, 1991). The ^{234}Th fluxes expected from the observed (+) and modeled (O) ^{234}Th deficiencies alone in the upper 120 m are shown in Figure 2.9A. These estimates agreed quite well (averaging within 10%). We found this very encouraging considering that our simple model used only minimal adjustable parameters, a single adsorption rate constant and sinking velocity, to fit the data. In the model, upwelling transported high ^{234}Th from depth. This led to an intense equatorial minimum in the deficiency. That this minimum was well displayed in the data (Figure 2.9A) is supporting evidence that upwelling was indeed vigorous during EqPac Survey II.

Three estimates of the sinking flux of ^{234}Th at 120 m are shown in Figure 2.9B: the ^{234}Th flux collected in sediment traps (Δ; Murray et al., 1996), the observed deficiency of total ^{234}Th from ^{238}U corrected for vertical and meridional advective fluxes (+) using velocities from Chai (1995) (Murray et al., 1996) and the model-derived sinking flux of ^{234}Th (O) expressed as the product of the sinking rate times the particulate ^{234}Th activity at 120 m (= $S \cdot Th_{p120}$). The magnitude of the model sinking flux (O) and the observed ^{234}Th deficiency corrected for advective fluxes (+; Murray et al., 1996) were quite similar, averaging within 17% and showing no significant positive or negative bias between them (Mann-Whitney U-test, $P>0.10$; Sokal and Rohlf, 1995; Rohlf and Sokal, 1995). These two flux estimates showed similar meridional trends of broad maxima near the equator, roughly mirroring the minima observed in Figure 2.9A. The advection corrections made for the EqPac Survey II data (Murray et al., 1996) are thus consistent with their model predictions, suggesting that 1) advection can be estimated using observed ^{234}Th gradients and 2) that advection corresponds to a large fraction of the difference between the deficiency and the sinking flux.

The ^{234}Th method has shown that drifting sediment traps are often subject to intense biases (Buesseler, 1991). For the ^{234}Th method to be a useful calibrator of sediment traps, however, its own uncertainties must be less than the uncertainties in sediment trap fluxes alone. The observed deficiency corrected for advection (+) and the model sinking flux (O) compared well and contrast with the sediment trap fluxes (Δ) in Figure 2.9B. Sediment trap fluxes (Δ) were statistically higher than the model flux (O) by 27-59% (Mann-Whitney U-test, $P<0.05$), averaging 32% higher. Over the whole region (5°N - 5°S) Sediment trap fluxes (Δ) were also statistically higher than the deficiency

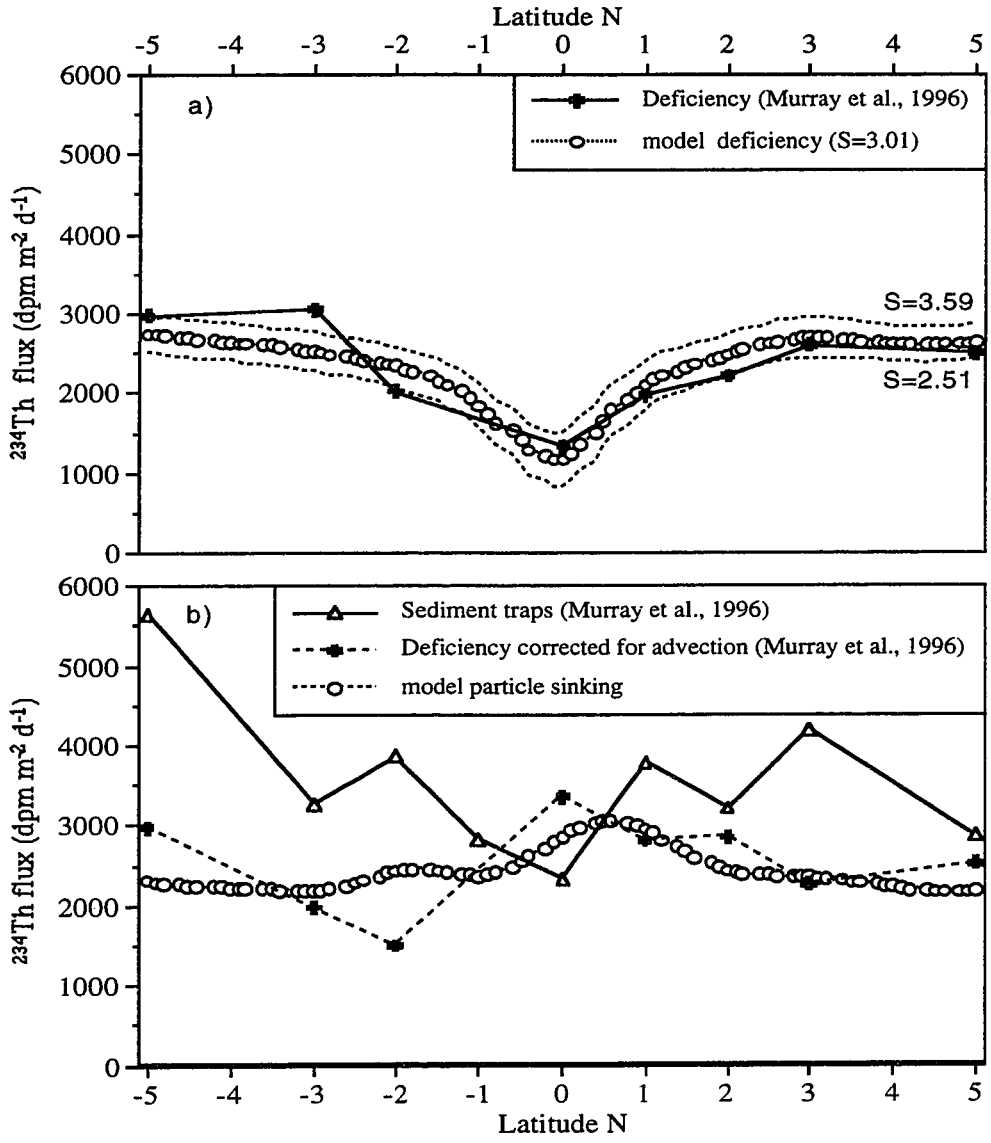

Figure 2.9: Comparisons at 120 m between data from Murray et al. (1996) and model output for the ^{234}Th deficiency (Figure 2.9A) and the ^{234}Th sinking flux (Figure 2.9B). Figure 2.9A compares the measured ^{234}Th deficency (filled crosses), model deficiency tuned to the observations (S=3.01 m d^{-1}; open circles) and 93% confidence interval for the sinking velocity (S=2.51 m d^{-1} to S=3.59 m d^{-1}; dotted lines). Figure 2.9B compares the measured ^{234}Th flux in sediment traps (100-150 m average;open triangles), measured ^{234}Th deficiency corrected for advection (filled crosses) and model sinking flux (open circles).

corrected for advection (+) by 12-89% (Mann-Whitney U-test, $P<0.05$), averaging 49% higher. Murray et al. (1996) used this comparison as evidence that Particle Interceptor Traps (PIT) over-collected ^{234}Th.

This consistency of the observed advection corrected ^{234}Th deficiency with the model ^{234}Th sinking flux, relative to the variability in the ^{234}Th trap fluxes, is support for calibrating trap fluxes using the ^{234}Th method. It suggests that processes behind ^{234}Th cycling were relatively homogenous over the entire EqPac Survey II transect and that the observed ^{234}Th deficiency can be adequately corrected for advection using observed gradients and estimates of v and w to give an accurate approximation of the true export of ^{234}Th. It should be noted that this is a necessary but not sufficient criterion for use of the ^{234}Th method for calibrating sediment traps. The other necessary criterion is that the ^{234}Th content of particles collected in sediment traps must be representative of the sinking material. This issue is discussed in detail elsewhere (e.g. Murray et al., 1996; Dunne et al., 1998).

Sensitivity of ^{234}Th fluxes to the physical model

To compare the relationship between the modeled ^{234}Th deficiency alone and the modeled sinking flux (the deficiency plus physical terms) in more detail, we present the ratio of deficiency flux: sinking flux at 120 m (R_{def}) as a function of latitude for a suite of model solutions using various combinations of advection and diffusion terms (Figure 2.10). As in Figure 2.6, results are for model runs in which combinations of advection and diffusion were switched on and off to illustrate their influence on calculated ^{234}Th fluxes given various hypothetical sets of conditions. Also shown is the ratio of the observed deficiency flux to the advection corrected deficiency flux for EqPac Survey II from Murray et al. (1996). R_{def} shows the coherence between the expected sinking flux of ^{234}Th and the ^{234}Th deficiency. Without advection or diffusion in the model (◊; same as Figure 2.6A), R_{def} was identical to unity. With diffusion alone in the model (●; same as Figure 2.6B), the deficiency still predicted the sinking flux within 2% at all latitudes. This is a situation characteristic of many areas of the open sea. With advection but no diffusion in the model (+, same as Figure 2.6C), the combination of high ^{234}Th water upwelling from below and desorption of ^{234}Th from sinking particles resulted in negative values of R_{def} at the equator. This implies that in the absence of diffusion, not only would the ^{234}Th

deficiency underestimate the sinking flux of ^{234}Th at the equator, but a super-equilibrium would exist. Model results with advection and either vertical diffusion (∇) or horizontal diffusion (Δ) suggested that both vertical and horizontal diffusion are important in mitigating this effect in the central equatorial Pacific. With all advection and diffusion processes incorporated into the model (+), R_{def} compared quite well with the ratio from Murray et al. (1996). The two estimates compared least well at 2-3°S where the advection correction in Murray et al. (1996) was highly influenced by the zonal transition between the south equatorial countercurrent and the south equatorial current. Given that the model horizontal diffusion flux away from the equator was such so large, it is surprising that the model and Murray et al. (1996) approximation agree so well at the equator. The uncertainty in the model advection and diffusion fluxes and their sensitivity to the scavenging model is further discussed below.

As shown in Figure 2.10, upwelling in the central equatorial Pacific can have a large effect on the accuracy of the ^{234}Th deficiency as an indicator of the ^{234}Th sinking flux. Because the strength of upwelling varies considerably in the central equatorial Pacific, we decided to assess the affect of this variability on the accuracy of the ^{234}Th method by varying the magnitude of the model advection field. We present model results for the ratio of the deficiency flux to the sinking flux (R_{def} ; Figure 2.11A) and the ratio of the deficiency flux corrected for advection to the sinking flux ($R_{def+adv}$; Figure 2.11B) versus latitude for a range of magnitudes of equatorial upwelling. In addition to the simulation for the conditions of EqPac Survey II with upwelling at the base of the euphotic zone (w_{120}) at 1 m d^{-1}, we show simulations with $w_{120} < 1$ m d^{-1} (thin, gray lines) to simulate weaker upwelling and $w_{120} > 1$ m d^{-1} (thin, black lines) to simulate stronger upwelling. Model results suggest that the ^{234}Th deficiency alone under-estimated ^{234}Th sinking flux by 144% at the equator (Figure 2.11A). Furthermore, model results suggest that the ^{234}Th deficiency corrected for advection over-estimated the ^{234}Th sinking flux by about 33% at the equator due to the important role of horizontal diffusion in transporting recently upwelled waters away from the equator. Figure 2.11 shows that during conditions of relative mild upwelling, the potential accuracy of the ^{234}Th method improves dramatically as there is better agreement between the ^{234}Th deficiency and the ^{234}Th sinking flux. Conversely, when upwelling is stronger than observed during EqPac Survey II, the ^{234}Th deficiency so drastically underestimates the sinking flux of ^{234}Th that the ^{234}Th method of

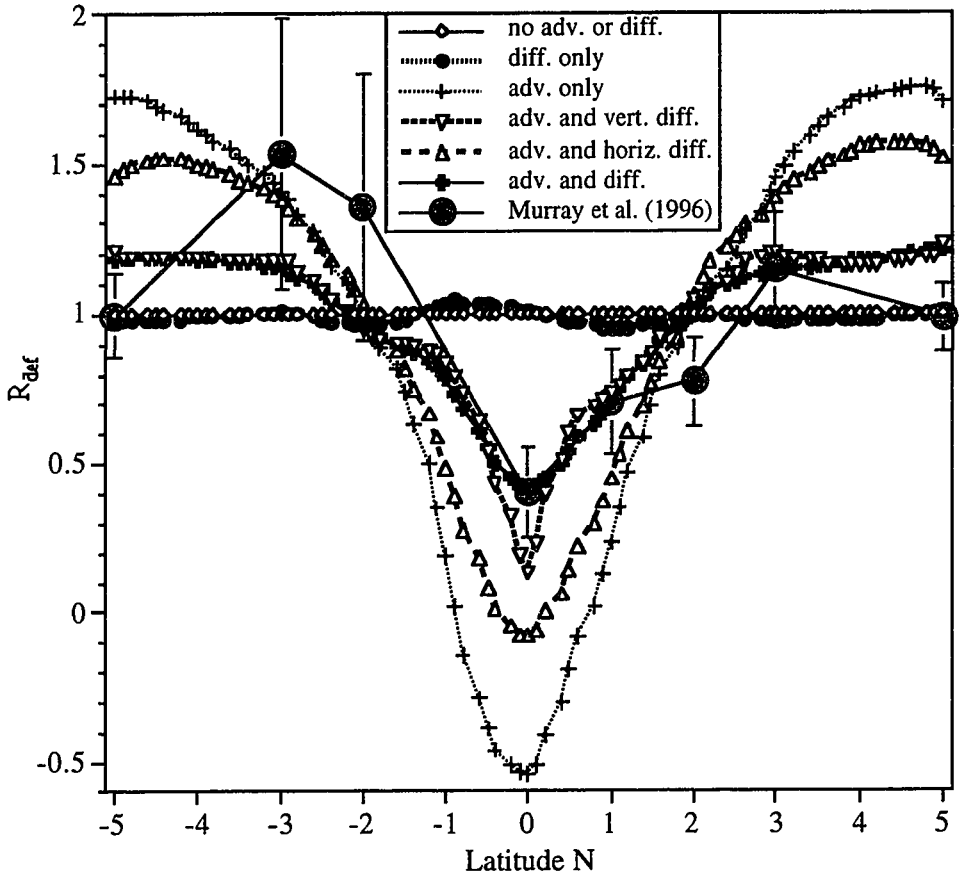

Figure 2.10: Estimates of R_{def} for various hypothetical circulation scenarios: no advection or diffusion (open diamonds), diffusion only (closed circles), advection only (crosses), advection and vertical diffusion only (down-turned, open triangles), advection and horizontal diffusion only (up-turned, open triangles), with advection and diffusion (closed crosses) and data from Murray et al. (1996) (large, filled circles).

calibrating sediment traps is based almost exclusively on the ^{234}Th advective and diffusive balance which is poorly constrained. Under these hypothetical conditions of vigorous upwelling, the ^{234}Th method has very limited utility. Using these results as a basis for evaluating the ^{234}Th method, we argue that the ^{234}Th method was successfully applied to calibrate sediment traps during EqPac Survey II, but that situations having upwelling velocities at the base of the euphotic zone greater than 1 m d^{-1} would prohibit use of the ^{234}Th method of estimating particle export within a reasonable uncertainty (factor of 2).

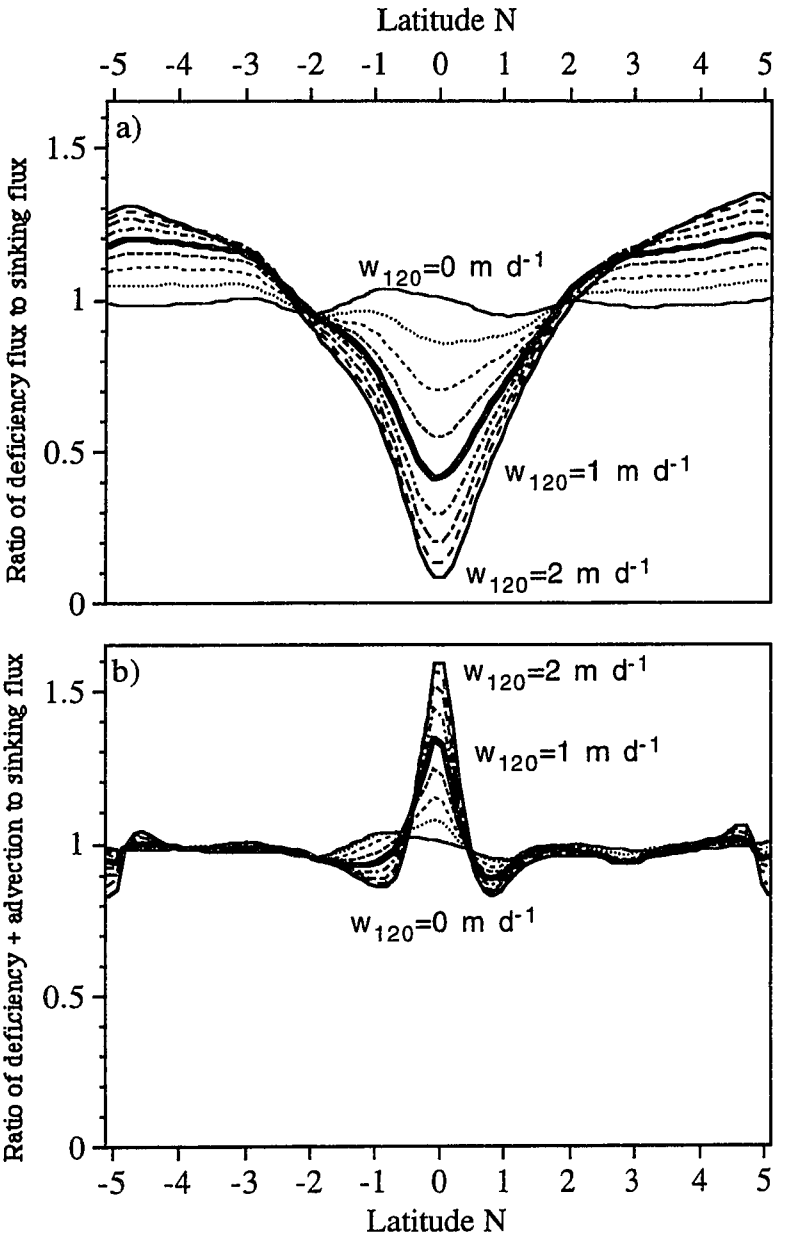

Figure 2.11: Model results for R_{def} (2.11A) and $R_{def+adv}$ (2.11B) versus latitude. Curves are results for relative strength of upwelling at the equator in 0.25 m d^{-1} increments from 0 m d^{-1} (gray) through the chosen 1 m d^{-1} (thick black) to twice the chosen value (2 md^{-1}; black).

SENSITIVITY TO THE SCAVENGING MODEL

We chose the chemical scavenging model of Bacon and Anderson (1982; Figure 2.1) for this analysis from the variety of models described in the literature (see comparison in Dunne et al., 1997) because of its simplicity. Circulation affects the ^{234}Th balance through the ^{234}Th gradients (Equations 2.1 and 2.2). As these gradients are a manifestation of particle scavenging, it is important to consider uncertainties in the scavenging model to understand the role of circulation on the ^{234}Th flux balance. Sources of potential variability lie in both the adsorption and sinking parameterizations.

Given the assumptions in the scavenging model of a first order inherent adsorption rate constant ($k'_1 = k_1 \cdot P$) and a homogeneously sinking particle pool, the data constrain estimates of k_1 and S quite well, resulting in little variability in R_{def} and $R_{def+adv}$ (Figure 12). Uncertainty in the magnitude of k_1 (Figure 2.5) had very little effect on R_{def} and $R_{def+adv}$. The 95% confidence limits on k_1 (0.0266 - 0.0343 m^3 mmol C^{-1} d^{-1}) translated into a negligible 1% relative uncertainty in R_{def} at the equator. Uncertainty in the sinking velocity parameterization translated to a larger variability in R_{def} and $R_{def+adv}$ and is shown in Figure 2.12. 95% confidence limits on S (2.51 - 3.59 m d^{-1}) translated to a 7% relative uncertainty in R_{def} at the equator. This uncertainty was slightly smaller than the uncertainty in the deficiency itself which averaged 9% during EqPac Survey II (Murray et al, 1996) and much less than the total uncertainty due to the uncertainty in the advective component.

The first mechanistic assumption of the scavenging mechanism (Figure 2.1) is that ^{234}Th adsorption to particles can be parameterized as a first order reaction between dissolved ^{234}Th and the particle concentration. There is some evidence that the order of the reaction is less than one due to a "particle concentration effect" (Honeyman et al., 1987). To understand the model sensitivity to the reaction order, we re-parameterized k'_1 using the reaction order (b) as a free parameter (i.e. $k'_1 = k_1 \cdot P^b$). We found that the data constrained the 95% confidence interval of the reaction order to between b = 0.68 (giving k_1 = 0.0321) and b = 1.27 (giving k_1 = 0.02925). This uncertainty in the adsorption parameterization translated to a 10% relative uncertainty in R_{def} at the equator. Again, this uncertainty was of similar magnitude to the uncertainty in the measured deficiency itself.

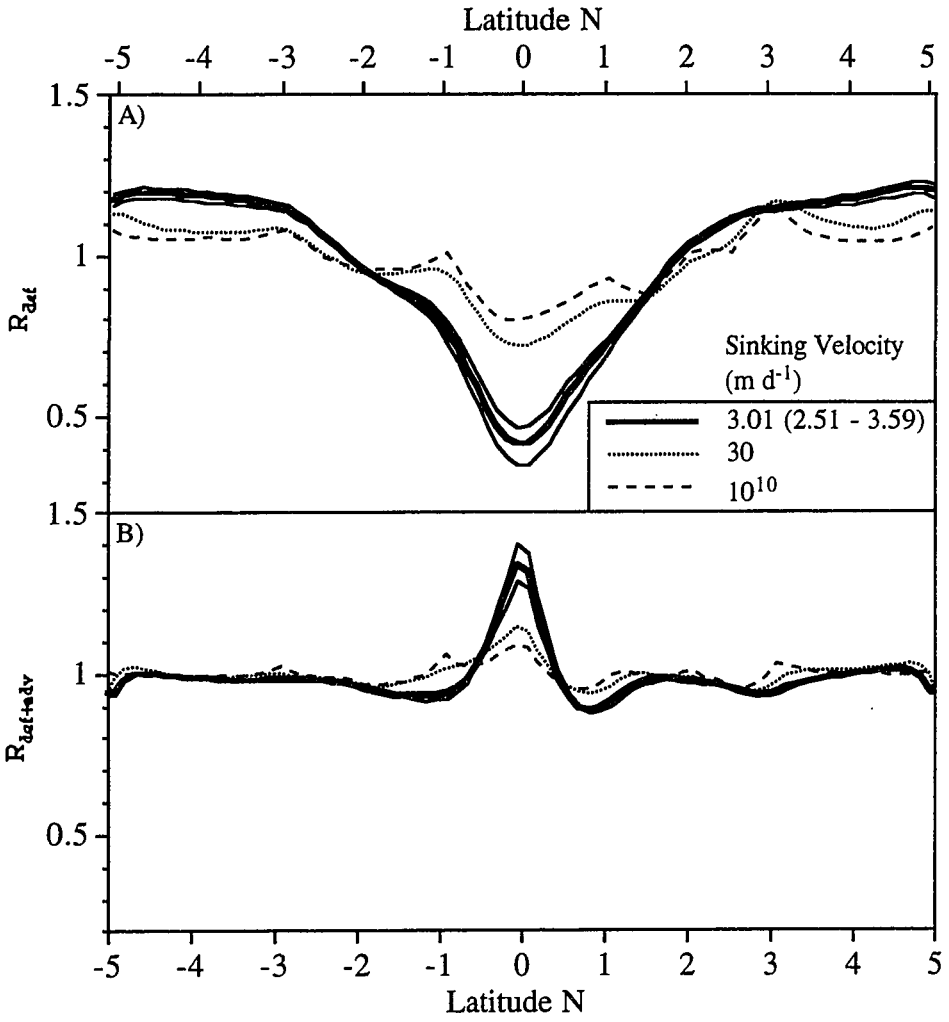

Figure 2.12: Model results for R_{def} (2.12A) and $R_{def+adv}$ (2.12B) under various scenarios: the sinking velocity tuned to the observed deficiency S = 3.01 m d^{-1} (thick, solid line) with it's upper (S=3.59 m d^{-1}; thin, solid line) and lower (S=2.51 m d^{-1}; thin, solid line) 93% confidence limits, the case of rapidly sinking particles of S = 30 m d^{-1} (dotted line) and with S approaching infinity (S = 10^{10} m d^{-1}; dashed line).

The second mechanistic assumption of the scavenging mechanism (Figure 2.1) is that ^{234}Th export is dominated by slow sinking of relatively common, small particles. Effectively, slow sinking velocity was used to parameterize particle processes

such as repackaging and aggregation that convert suspended particles into sinking ones. In addition, this assumption allowed us to constrain the model using the dissolved ^{234}Th data. Alternatively, if particle processes in the central equatorial Pacific were relatively instantaneous and ^{234}Th scavenging was limited by adsorption alone, ^{234}Th export would dominated by the rapid sinking of relatively rare, large particles (Dunne et al., 1997). We investigated this potential scavenging mechanism by re-parameterizing k_1 and S under the assumption that the sinking flux was dominated by rare, rapidly sinking particles. Data on total ^{234}Th was assumed to represent non-sinking ^{234}Th only ($Th_d \approx Th_t$) and the concentration of ^{234}Th on rapidly sinking particles was initially assumed negligible ($Th_p \approx 0$). We first re-calculated k'_1 values from the total ^{234}Th data using Equation 2.3. We then recalculated k_1 (= 0.0089 mmol C^{-1} m^3 d^{-1}) from the slope of k'_1 versus P as before using Mood's method. Finally, we recalculated S (= 30 m d^{-1}) as before from the observed deficiency.

This scavenging mechanism gave ^{234}Th distributions (Figure 2.13A) with dramatically different vertical and meridional structure than the mechanism. A diagnostic summary of the ^{234}Th flux balance between 0 - 120 m is shown in Figure 2.13B. Compared to the mechanism of slowly sinking particles, the mechanism of rapidly sinking particles gave activities of total ^{234}Th slightly closer to the data (on average within 8%) but reproduced slightly less of the variability in the data (73%). ^{234}Th activities were much lower at depth than before, well below equilibrium with ^{238}U. We attribute this to the relative efficiency of particle sinking relative to desorption and decay in this mechanism. The mechanism of rapidly sinking particles also showed much less little meridional structure in ^{234}Th near the surface than either the data or the mechanism of slowly sinking particles.

The scavenging mechanism of rapidly sinking particles gave values of R_{def} that clustered much more tightly about unity (gray, dotted line, Figure 2.12), implying that the ^{234}Th deficiency would be approximately twice as accurate a predictor of the ^{234}Th sinking flux if particle processes (e.g. aggregation and repackaging) were instantaneous and sinking was dominated by rare, rapidly sinking particles. In Figure 2.12, we also show the hypothetical case in which the sinking velocity approaches infinity ($S = 10^{10}$). As the sinking velocity approaches infinity, R_{def} approached not 1.00 but a value less than 1.00 limited by the rate of adsorption and circulation of Th_d.

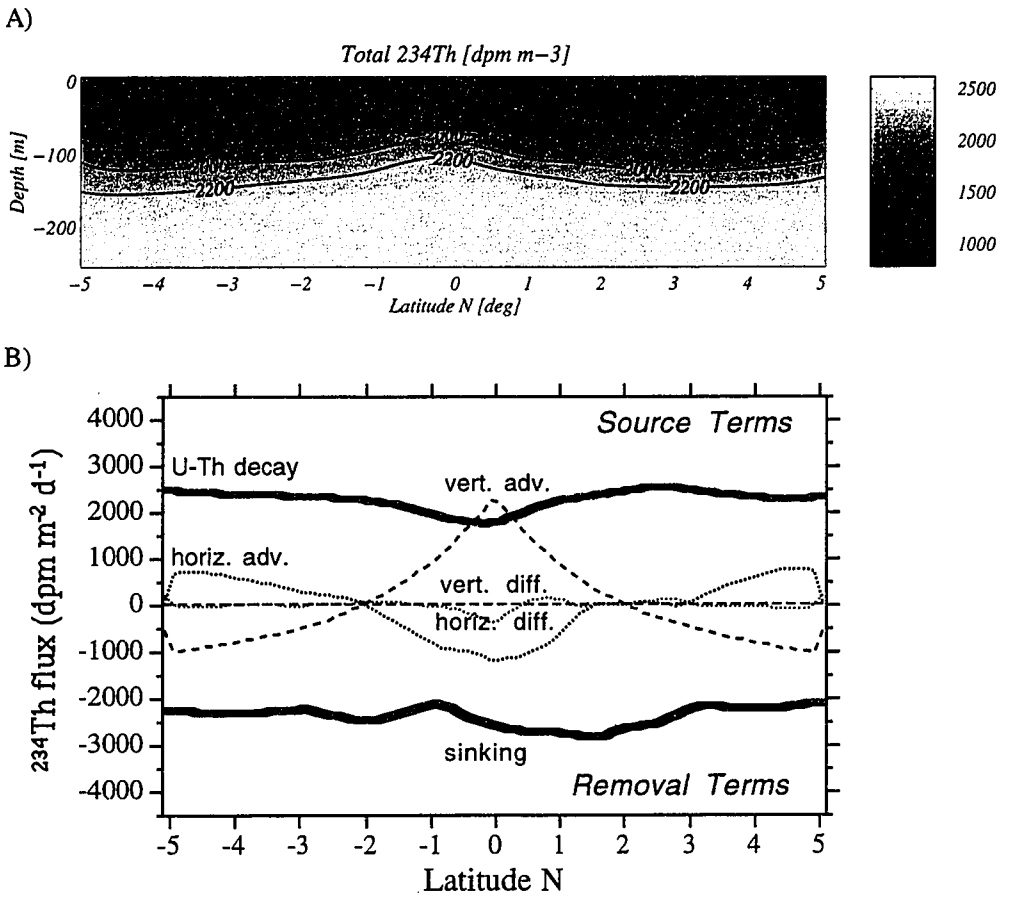

Figure 2.13: Model contours of total ^{234}Th (2.13A; dpm m^{-3}) between 5°N and 5°S in the upper 250 m using the scavenging mechanism of rapidly sinking particles (k_1 = 0.0089 mmol C^{-1} m^3 d^{-1}; S=30 m d^{-1}). Model diagnostic summary of the ^{234}Th flux balance between 0 - 120 m versus latitude (2.13B) using this same scavenging mechanism.

This sensitivity of R_{def} to the scavenging mechanism makes it important to distinguish which scavenging mechanism is more appropriate. Firstly, the mechanism of slowly sinking particles gave ^{234}Th deficiencies which were on average within 10% of the observed deficiency and within 12% at the equator. ^{234}Th deficiencies from the rapidly sinking particle model were on average within only 15% of the observed deficiency and

within only 35% at the equator. Secondly, meridional advection was a large term at the equator (-1187 dpm m^{-2} d^{-1}) for the scavenging mechanism of rapidly sinking particles (Figure 2.13B). This was much higher than the meridional fluxes of ^{234}Th at the equator calculated by Murray et al. (1996; -108 ± 65 dpm m^{-2} d^{-1}) and Buesseler et al. (1995; ~0 dpm m^{-2} d^{-1}) and in the model with slowly sinking particles (-158 dpm m^{-2} d^{-1}). The large meridional flux of ^{234}Th away from the equator at the surface in the model of rapidly sinking particles is not balanced by high ^{234}Th transported meridionally towards the equator near the base of the euphotic zone because the ^{234}Th activities at this depth are relatively low. Given these two pieces of evidence, we suggest that the scavenging model with slowly sinking particles was more representative of euphotic zone scavenging in the central equatorial Pacific, as it predicted only moderate meridional fluxes of ^{234}Th from the equator (Figure 2.7). It is important to note that these results suggest only that there is a timescale associated with particle processes (e.g. repackaging, aggregation) in the central equatorial Pacific and not that all particles necessarily sink slowly at all depths. Indeed, the good comparison of the data and the model with rapidly sinking particles at depths below the euphotic zone suggests that particle sinking may be dominated by rapidly sinking particles in this region. This analysis showed that R_{def} is very sensitive to the nature of the particle removal process and that the deficiency is a much more accurate predictor of the sinking flux under conditions of rapid particle processing and sinking.

Overall uncertainty in R_{DEF} and $R_{DEF+ADV}$

To gauge the overall accuracy of calculated ^{234}Th sinking fluxes during EqPac Survey II, we estimated the uncertainty in R_{def} and $R_{def+adv}$ using the Monte-Carlo Bootstrapping technique of error propagation (Bevington and Robinson, 1992; Press et al., 1992). Uncertainty in all input parameters was propagated through the model to obtain 95% confidence intervals on R_{def} and $R_{def+adv}$ (Figure 2.14). The error in k_1 and S was assumed to be normally distributed (σ_{k1} = 0.001925 mmol C m^{-3} day^{-1}; σ_S = 0.29 m day^{-1}). Relative standard deviation of 50% were assumed for the v and w fields (F. Chai, personal communication). We assumed the uncertainty in diffusion constants to be exponentially distributed about the chosen value to approximate the skew in the range of values in the literature discussed above. This assumption gave 95% confidence intervals of 0.04 - 2.22 cm^2 s^{-1} for K_z (below the euphotic zone only) and 135 - 7390 m^2 s^{-1} for K_h. The Monte-

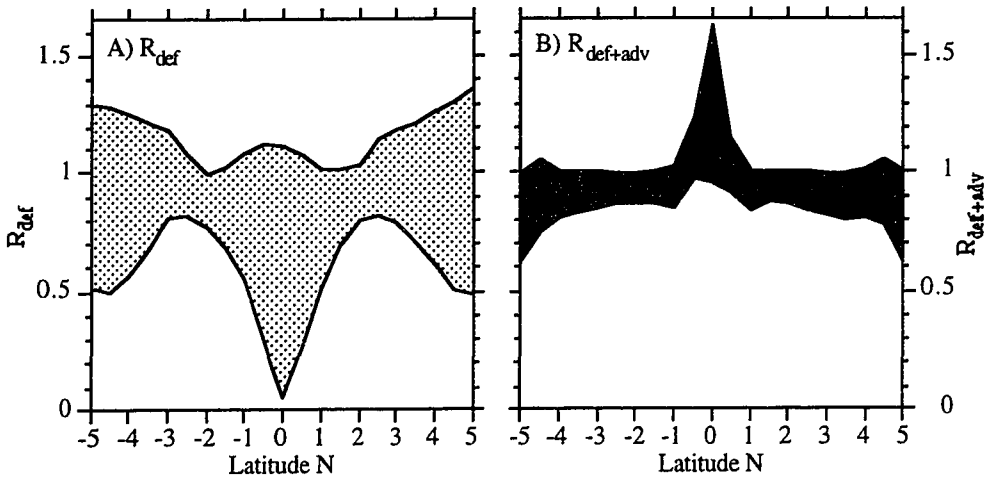

Figure 2.14: 95% confidence intervals on R_{def} (2.14A) and $R_{def+adv}$ (2.14B) from the Monte-Carlo Bootstrapping method (Bevington and Robinson, 1992; Press et al., 1992).

Carlo Bootstrapping routine then picked 5000 cases of input parameters based on these uncertainties to obtain 5000 estimates of R_{def} and $R_{def+adv}$.

Results of this analysis showed that uncertainty in both R_{def} and $R_{def+adv}$ was large at the equator. The 95% confidence intervals for both R_{def} (Figure 2.14A) and $R_{def+adv}$ (Figure 2.14B) spanned from unity to approximately twice the median value. This uncertainty was dominated by the uncertainty in the terms for advection and horizontal diffusion. At the equator, uncertainty in R_{def} suggests that the sinking flux may have been up to 5 times greater than the deficiency would predict. This uncertainty implies that the ^{234}Th method cannot be used to calibrate sediment traps at the equator without correcting the calculated ^{234}Th flux for advection. Uncertainty in $R_{def+adv}$ suggests that accounting for advection but not diffusion overestimates the sinking flux by up to 63% at the equator and underestimates the flux by 0-23% off the equator. When a similar analysis was performed using the scavenging mechanism of rapid particle sinking, 95% confidence intervals shrank considerably about unity but kept the same overall shape as in Figure 2.14. In general, this analysis confirmed the viability of using the ^{234}Th deficiency corrected for advection as a measure of the sinking flux of ^{234}Th and as a means of calibrating sediment traps. Within one degree of the equator, however, these estimates may have biases up to 50% due to the role of horizontal diffusion.

CONCLUSIONS

We coupled a chemical scavenging model with a simple physical model of equatorial circulation to investigate the impact of circulation on calculations of the ^{234}Th export flux. We assumed adsorption to be first order with respect to both dissolved ^{234}Th and particle concentration (k_1 = 0.2905 mmol C^{-1} m^3 d^{-1}). The sinking velocity was adjusted to a single value of 3.01 m d^{-1}. The model reproduced both the meridional trend in the observed ^{234}Th deficiency of relatively low ^{234}Th deficiencies near the equator and the depth structure observed for total and dissolved ^{234}Th. Model results illustrated the importance of a mixed layer in reproducing observed total ^{234}Th distributions.

The model sinking flux of ^{234}Th compared well with the observed ^{234}Th deficiency corrected for advection (Murray et al., 1996) relative to the measured sediment trap fluxes of ^{234}Th (Murray et al., 1996) which were found to be relatively erratic and high. This illustrated the high level of internal consistency in ^{234}Th method between predicted and observed fluxes necessary for its use to calibrate sediment traps.

Analysis of the model physics illustrated the importance of advection in the ^{234}Th flux balance in the equatorial surface layer. This study confirms that upwelling at the equator has a dramatic impact on the applicability of the ^{234}Th method for particle export calculation. However, our results point to a significant role of horizontal diffusion in mitigating the effect of vertical advection on ^{234}Th fluxes at the equator such that the ^{234}Th deficiency corrected for advection over-estimated the ^{234}Th sinking flux by 33% in neglecting horizontal diffusion. Nevertheless, this potential bias in the estimates of Buesseler et al. (1995), Murray et al. (1996), Bacon et al. (1996) is within the original published uncertainties of ~60%. Vertical mixing was shown to be a negligible ^{234}Th flux across 120 m. A model sensitivity analysis to the strength of equatorial upwelling showed that the ^{234}Th deficiency would be only a small component of the total ^{234}Th balance under conditions of upwelling stronger than those estimated for the EqPac Survey II, implying that uncertainty in the sinking flux of ^{234}Th would be very large under these conditions and application of the ^{234}Th method would be ill-advised.

A sensitivity analysis of the scavenging mechanism used in the model showed that the ratio of the ^{234}Th deficiency to the ^{234}Th sinking flux (R_{def}) was insensitive to the uncertainty of k_1 and S which are well constrained by the data. Investigation of other

potential sinking mechanisms suggested that if ^{234}Th export were governed by rare, rapidly sinking particles, it would have been only about half as sensitive to advection than if it were governed by slowly sinking particles. This suggested that the ^{234}Th deficiency would be an accurate predictor of the ^{234}Th sinking flux during particle aggregation and rapid sinking (e.g. phytoplankton blooms) even in fairly vigorous physical regimes. Because the scavenging mechanism of slowly sinking particles compared better with the observed ^{234}Th deficiency and calculated meridional ^{234}Th fluxes at the equator than the mechanism of rapidly sinking particles, we suggested that the slowly sinking particle mechanism was more appropriate for the central equatorial Pacific.

Propagation of uncertainty through the model further illustrated the large uncertainty in the ^{234}Th method at the equator. Results suggested that the ^{234}Th deficiency underestimated the ^{234}Th sinking flux by 1 - 612% (P=0.05) while advection corrected estimates overestimated the ^{234}Th sinking flux by 0 - 63% (P=0.05) because they neglected horizontal diffusion. In general, comparison of model results with observations from Murray et al. (1996) confirmed that in this dynamic regime, the ^{234}Th deficiency corrected for advection was successfully used to measure of the sinking flux of ^{234}Th and improved the accuracy of sediment traps.

CHAPTER 3: EXPORT PRODUCTION IN THE WESTERN AND CENTRAL EQUATORIAL PACIFIC: ZONAL AND TEMPORAL VARIABILITY

INTRODUCTION

New and export production from the equatorial Pacific upwelling zone is an important moderator of variability in the global carbon cycle. Chavez and Barber (1987) suggested that the Wyrtki box (90°E - 180°E, 5°N - 5°S), which corresponds to an aerial extent equal to 3% of the global ocean, contributes from 18 to 56% of global new production. Though a great deal has been learned since then about meridional and temporal variability in the central equatorial Pacific, little is known about export production in the western equatorial Pacific or about the relative role of wave-induced, seasonal and inter-annual temporal forcing of export.

Much of what we know about the equatorial Pacific comes from the US Joint Global Ocean Flux Study (JGOFS-EqPac) which set out to better characterize carbon fluxes in the high-nutrient low-chlorophyll (HNLC) region of the central equatorial Pacific in the eastern and central equatorial Pacific ocean (e.g. Murray et al., 1994). The EqPac study found that small phytoplankton (Bidigare and Ondrusek, 1996) were recycled by microzooplankton (Landry et al., 1995) in an efficient microbial loop. Primary production was largely based on recycled nutrients (McCarthy et al., 1996) and the sinking particulate flux was low (Murray et al, 1996). A great deal of temporal variability was observed, however. Between boreal spring, El Niño conditions of Survey I, and boreal fall, non-El Niño conditions of Survey II, surface nitrate concentrations, primary production and particulate organic carbon export doubled (3 to 6 μM, 62 to 112 mmol C m^{-2} d^{-1} and 5 to 12 mmol C m^{-2} d^{-1}, respectively) and mesozooplankton grazing quadrupled (5-24 mmol C m^{-2} d^{-1}) between 2°N and 2°S in the upper 100 m while the particle inventory only increased by 20%. Synthesis of the EqPac data showed that the HNLC condition persisted due to intense grazing control of small phytoplankton and iron limitation of large phytoplankton (Landry et al., 1997). Variability in the equatorial food web was accurately modeled as a response to variability in upwelled iron (Loukos et al., 1997).

One of the issues which remained unresolved after EqPac was the zonal extent of the high nitrate, highly productive central equatorial Pacific with respect to its contact with the western Pacific, a region devoid of nitrate in the upper euphotic zone. The extent to which particle export varies in the zonal extent is of great importance to global oceanic uptake of carbon dioxide. Primary production in the western equatorial Pacific (155°E) during the Australian JGOFS program varied over a considerable range, 20 to 50 mmol C m^{-2} d^{-1} (Mackey et al., 1997). Particle export in this region has never been reported. If the western equatorial Pacific were to resemble the oligotrophic gyres it would be expected to have primary production less than 35 mmol C m^{-2} d^{-1} with particle export being about 2 mmol C m^{-2} d^{-1} (Michaels et al., 1994; Karl et al., 1995) and total export production about 5 mmol C m^{-2} d^{-1} (Emerson et al., 1997). If this condition applies to the western equatorial Pacific, it would imply a large zonal gradient in particle flux along the equator.

Another issue that was unresolved after EqPac was the separation of seasonal, El Niño-Southern Oscillation (ENSO) and wave-induced variability as forcing functions on equatorial biogeochemistry. Carbon fluxes during the JGOFS EqPac study were found to vary dramatically between Survey I/Time-series I and Survey II/Time-series II. These differences may have been associated with seasonal increases in wind-driven upwelling during the boreal fall Survey II/Time-series II, inter-annual variability due to the strong El Niño condition during the Survey/Time-series I period, Kelvin waves during Survey I/Time-series I or tropical instability waves during Survey II/Time-series II. Analysis of only the two time periods was not enough to distinguish between these effects and ascertain which are the dominant sources of variability.

^{234}Th was extensively used to estimate particle export during the EqPac program (Buesseler et al., 1995; Murray et al., 1996; Bacon et al., 1996). The most basic particle-^{234}Th cycling model is a steady-state mass balance in which the vertical flux of ^{234}Th equals the difference between the rates of in-situ production of ^{234}Th ($t_{1/2}$ = 24.1 days) from its long-lived, conservative parent ^{238}U ($t_{1/2}$ = 4.47×10^9 years) and in-situ radioactive decay of ^{234}Th. The relationship between this calculation of ^{234}Th flux and the export flux of organic carbon depends on the mechanisms of particle cycling and on the organic carbon to ^{234}Th ratio of sinking particles. The ^{234}Th method consists of two parts: 1) estimation of the ^{234}Th sinking flux by measuring the radioactive deficiency of ^{234}Th

from its parent, ^{238}U, and any spatial or temporal gradients in ^{234}Th and 2) estimation of the ^{234}Th and carbon content of sinking particles to convert the ^{234}Th flux to a carbon flux.

The purpose of this paper is to present results from two zonal transect cruises along the equator between 165°E and 150°W: the French JGOFS FLUPAC study aboard the R/V l'Atalante in October, 1994 and the Zonal Flux study aboard the R/V Thomas G. Thompson in April, 1996 both from New Caledonia to Tahiti (Figure 3.1). These cruises took place under extremely different conditions: the FLUPAC cruise during a strong El Niño and the Zonal Flux during a mild La Niña. The FLUPAC cruise included intensive 7-day time series studies of the two endpoints while the Zonal Flux cruise included an extensive study at six two-day stations along the equator. The goals of this study are fourfold: 1) to measure zonal gradients in carbon fluxes in order to determine how far the zone of high productivity in the central equatorial Pacific propagates along the equator toward the west 2) to distinguish the sources of temporal variability of particle export in the equatorial upwelling zone through comparison with results from EqPac 3) to describe the role of total organic carbon accumulation as a sink for new production and 4) to evaluate the potential for silicate regulation of particle export in the equatorial upwelling zone.

SAMPLES AND METHODS

The FLUPAC cruise occupied two six-day time series stations at the equator, one at 167°E (TS-I) and another at 150°W (TS-II) aboard the R/V l'Atalante in October, 1994. The Zonal Flux cruise occupied two-day stations at 2°S, 0° and 2°N at 165°E and along the equator at 174°E, 177°W, 170°W, 160°W and 150°W aboard the R/V Thompson in April-May, 1996. Samples were collected for complete sets of hydrographic, chemical and biological parameters at these stations. Results for the FLUPAC cruise are described in Rodier and Le Borgne (1997) and are published in two data volumes (Le Borgne et al. 1995; Le Borgne and Gesbert, 1995).

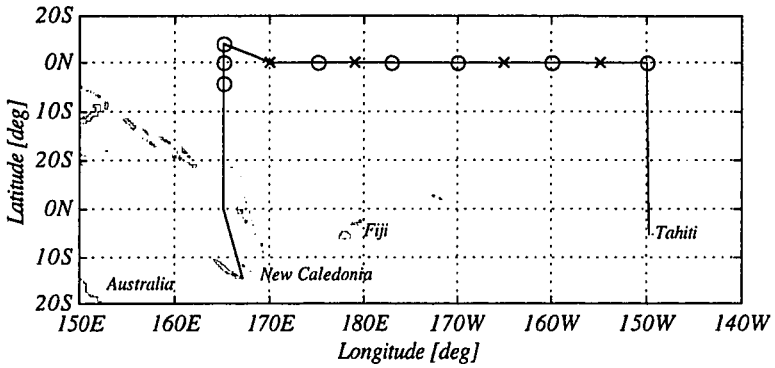

Figure 3.1: Map of the equatorial Pacific showing the cruise track for the Zonal Flux cruises with circles showing stations of 2-day trap deployments. The FLUPAC cruise track was similar to that during Zonal Flux with triplicate 2-day trap deployments at 167°E and 150°W.

Water column samples for total ^{234}Th were collected using an integrating sampling method from the surface to the trap depths using CTD-rosette mounted 10-l Niskin bottles in which equal volume samples at an even 15-20 m depth spacing were combined into a single, averaged ~18-l sample. Sampling was performed daily during each of the FLUPAC time series and once per station during Zonal Flux. Short, four hour stations were conducted every two degrees during FLUPAC and every three to five degrees during Zonal Flux along the equator. Twice during Zonal Flux, discrete profiles of ^{234}Th were taken every 20 m in the upper 200 m. Analyses of ^{234}Th were conducted following the combination of the procedures of Anderson and Fleer (1982) and Coale and Bruland (1985) given in Murray et al. (1996). The parent, ^{238}U was separated from ^{234}Th within two days aboard ship. Further purification, plating, beta and alpha counting were performed in Seattle. ^{234}Th activities were decay-corrected to the time of collection.

During FLUPAC, the background on the beta counters was about 0.3 counts per minute, and the efficiency about 60%. Alpha counting to determine the activity of the ^{230}Th yield tracer had negligible backgrounds and efficiencies of about 33%. Uncertainty (1σ) in the activity of ^{234}Th from least-squares propagation of error for each step in the analytical/counting process was 6.2%.

During Zonal Flux uncertainty in beta counting was higher and more variable due to two analytical problems: 1) a blockage in the gas line due to dust led to variability in carrier gas flow rate and 2) beta counters were contaminated by ^{232}Th samples being measured at the same time. Both factors resulted in variably-elevated background levels. We used weekly checks in the counter background constrain the uncertainty. In addition, three criteria were used for rejecting individual countings: counting performed less than three days after a ^{232}Th counting, ^{234}Th counts less than twice background and ^{232}Th counts more than half ^{234}Th counts. Uncertainty in the activity of ^{234}Th from the least-squares propagation of error for each step in the analytical/counting process averaged 11%, twice the normal value.

During both cruises, ^{234}Th activities were calibrated using deep (500 - 1000 m) samples assumed to be in equilibrium with ^{238}U and proportional to salinity. We used the relationship of (^{238}U dpm/l = $0.0686*\sigma_t$) obtained from the work of Ku et al. (1977) and Chen et al. (1986). This process raised ^{234}Th activities by 10.1% during FLUPAC and 9.4% during Zonal Flux.

Sinking particles were sampled using drifting sediment traps as described in Murray et al. (1996). Knauer et al. (1979) style particle interceptor traps (PIT) with an aspect ratio of 8:1 (length:width) were used for ^{234}Th and mass. The Rodier and Le Borgne (1997) traps, constructed of opaque plastic (Lorenzen et al., 1983) with a similar aspect ratio of 6.5:1 (length:width) and an automatic closing mechanism were used for carbon and mass. Traps were deployed at the base of the euphotic zone at 100 m, 160 m and 200 m during FLUPAC and at between 100 and 140 m and at 200 m during Zonal Flux. Mesozooplankton swimmers were carefully picked from all trap samples using forceps under the supervision of Robert Le Borgne first by naked eye, then under magnification, then again by naked eye. The swimmer component at FLUPAC TS I was small, averaging less than 5% of total mass. The FLUPAC TS-II site had a larger swimmer component. Total salt-corrected mass (swimmer-free) from three deployments of traps at 100 m and 160 m was 131 mg. Euphausiids and copepods removed from these traps weighed a total of 13 mg. Two large (2.5 cm) Caridae shrimp weighing a total 42 mg were also removed from the second FLUPAC TS-II trap deployment. Had swimmers not been picked, they would have contributed 42% to the total mass. Rodier trap filters were picked of foraminifera while PIT style trap filters were not. To account for inter-trap

variability in the total amount of material being analyzed, carbon and ^{234}Th data were normalized to mass for direct comparison.

Results for temperature, salinity, nutrients, chlorophyll, particulate organic carbon, primary production, ^{15}N new production (C. Navarette, A. Le Bouteiller and Z. Johnson, personal communication; Rodier and Le Borgne, 1997; Aufdenkampe et al., in preparation) and total organic carbon discussed here were taken using JGOFS protocols. Samples were taken for total organic carbon on both cruises. Data and interpretation for the FLUPAC cruise were given in Hansell et al. (1997b). Analyses for TOC from the Zonal Flux cruise were made at the Bermuda Biological Station using the same method (Hansell et al., 1997b).

This study uses estimates of upwelling to correct the model ^{234}Th sinking flux for advection. To this end, horizontal velocities were obtained from the general circulation model output of the National Centers for Environmental Prediction Pacific Ocean Hindcast Model. This model assimilates TOGA-TAO temperature and TOPEX/Poseidon sea surface height data to infer circulation on a horizontal resolution of 1° latitude by 1.5° longitude and a vertical resolution of 15 grid points in the upper 200 m (http://nic.fb4.noaa.gov:8000/research/cmb/climate_ocnanl.html). Vertical velocities were then estimated from divergence. We made use of temperature, dynamic height and meridional velocity data from the TOGA-TAO array and data on the Southern Oscillation Index (SOI), all courtesy of the National Oceanic and Atmospheric Administration (http://www.pmel.noaa.gov/toga-tao/home.html). All data can be found at the US Joint Global Ocean Flux Study home page (http://www1.whoi.edu/jgofs.html).

RESULTS

HYDROGRAPHY, NUTRIENTS, BIOMASS AND PRODUCTIVITY

The western Pacific warm pool was well established in October, 1994 as part of the El Niño conditions present almost continuously from late 1991 through early 1995 (Figure 3.2). The Southern Oscillation Index (SOI) averaged -1.7 for the three months before the FLUPAC cruise, indicating particularly strong El Niño conditions.

Conditions during the Zonal Flux cruise were drastically different. The SOI averaged 0.5 for the three months before the Zonal Flux cruise, indicating moderate La Niña conditions.

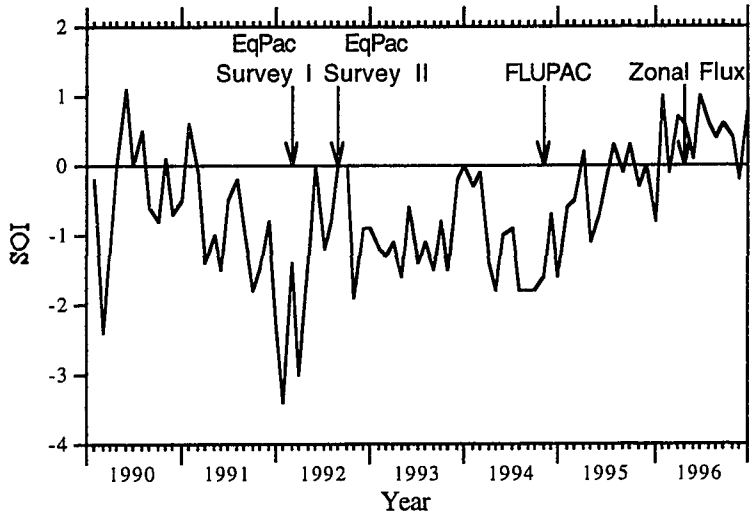

Figure 3.2: Southern Oscillation Index for the years 1990 through 1996 (courtesy National Oceanic and Atmospheric Administration).

Temperature and salinity for both zonal transects are shown in Figure 3.3. FLUPAC surface waters were 29-31°C in the warm pool. The warmest waters were centered near the date line, but 29°C water extended eastward all the way to 167°W. A strong thermocline was established at 100 m across the entire transect. Temperatures were much lower during Zonal Flux with the warm pool (defined by the 29°C isotherm) shifted over 37° westward relative to FLUPAC. Isotherms shoaled towards the east approximately 1 m per degree over 45° of longitude with the thermocline much shallower and more intense in the east. During FLUPAC the western equatorial Pacific warm pool was characteristically low in salinity (S = 34) with isohalines rising eastward from the base of the euphotic zone at 165°E to the surface near 175°W. During Zonal Flux, salinity was everywhere higher in the western Pacific than during FLUPAC, consistent with the lack of a warm pool at 165°E. During FLUPAC TS-I in the warm pool, variability in salinity determined variability in mixed layer depths (57 ± 32 m; $\Delta\rho_{0\text{-MLD}} > 0.125$; Gardner et al., 1995). Elsewhere, temperature determined the mixed layer depth which was deep at FLUPAC TS-II (91 ± 13) and shallow along the Zonal Flux transect (49 ± 15 m).

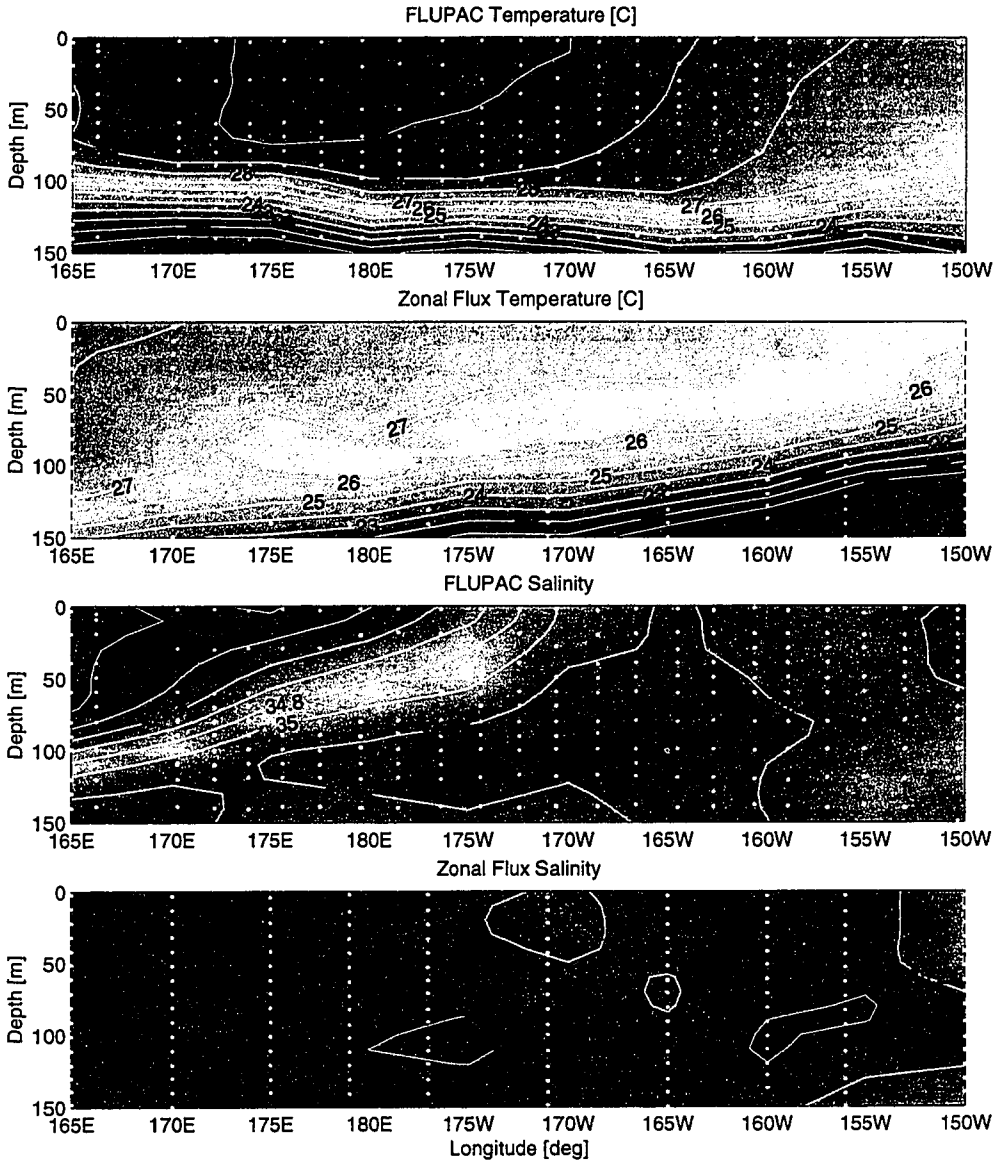

Figure 3.3: Longitude versus depth contours for temperature and salinity from the FLUPAC and Zonal Flux cruises.

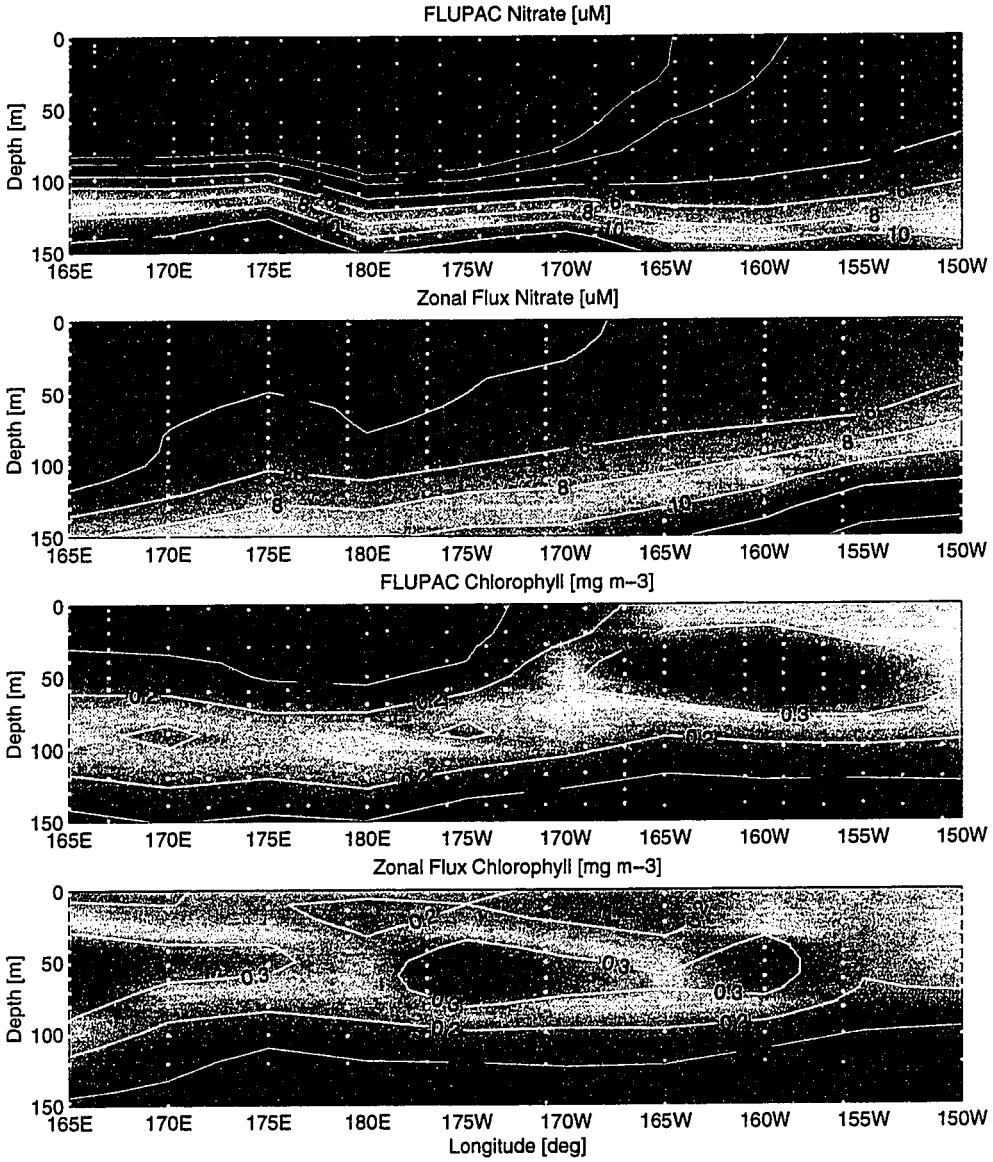

Figure 3.4: Longitude versus depth contours for nitrate (μM) and chlorophyll α (mg m^{-3}) from the FLUPAC and Zonal Flux cruises.

Nitrate and chlorophyll *a* for both zonal transects are shown in Figure 3.4. The warm pool was well defined by zero nitrate in the upper euphotic zone during FLUPAC. Elsewhere during both cruises, nitrate followed temperature (r^2 = 0.93; Figure

3.3). During Zonal Flux surface nitrate was almost 3 μM at 165°E and increased evenly towards the east. Chlorophyll *a* distributions followed similar patterns as nitrate with low surface values during FLUPAC in the warm pool. During FLUPAC there was a deep chlorophyll maximum at 80 - 100 m in the western equatorial Pacific which thickened and shoaled to 20 - 70 m in the east. During Zonal Flux chlorophyll a distributions had a subsurface maximum between 30 - 70 m with no zonal trend.

Total organic carbon (TOC) across both zonal transects are shown in Figure 3.5. As described in Hansell et al. (1997), high values of TOC during FLUPAC were observed in the warm pool with a strong front at 170°W and a strong, inverse relationship with nitrate ($r^2 = 0.78$). Observations of TOC during Zonal Flux were well in line with the rest of the observations demonstrating only minimal zonal gradients and following the same relationship observed between nitrate and TOC during FLUPAC.

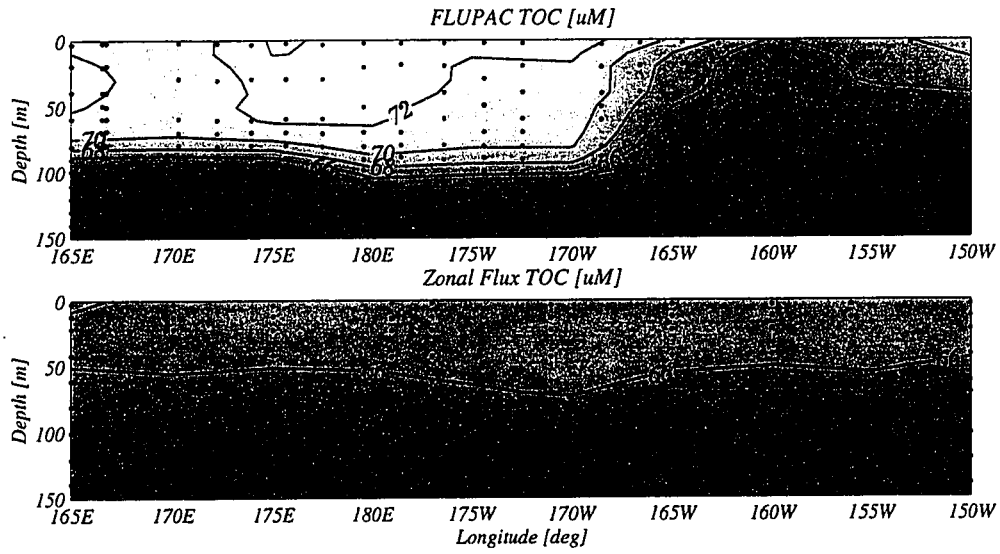

150°W at an intermediary level of 80 ± 7 mmol C m^{-2} d^{-1} (Le Borgne et al., in press; Z. Johnson, personal communication).

$^{15}NO_3$ new production measured during FLUPAC was 1.4 mmol N m^{-2} day^{-1} at TS-I and 2.1 mmol N m^{-2} day^{-1} at TS-II (C. Navarette, personal communication; Rodier and Le Borgne, 1997). New production during the Zonal Flux cruise was a relatively low 1.0 mmol N m^{-2} day^{-1} at 165°E, and increased steadily to 4.8 mmol N m^{-2} day^{-1} at 150°W (Aufdenkampe et al., in preparation).

^{234}TH ACTIVITIES

^{234}Th activities as a function of depth are shown for both cruises in Figure 3.6. At FLUPAC TS-I ^{234}Th activities were slightly deficient relative to ^{238}U in the upper 110 m (2.16 ± 0.10 dpm/l), in equilibrium with ^{238}U between 100 and 160 m (2.56 ± 0.13 dpm/l) and in slight excess of ^{238}U between 160 m and 210 m (2.64 ± 0.13 dpm/l). At FLUPAC TS-II ^{234}Th activities were more strongly and variably deficient from ^{238}U in the upper 100 m (2.03 ± 0.20 dpm/l) but again in equilibrium with ^{238}U between 100 and 160 m (2.46 ± 0.09 dpm/l) and in slight excess of ^{238}U between 160 m and 210 m of 2.69 ± 0.10 dpm/l. One 0-100 m ^{234}Th sample at FLUPAC TS-II was taken a day after the last 2-day trap deployment southward of the trap recovery (0.5°S). Though no particulate organic carbon or chlorophyll anomalies were observed in this cast, euphotic zone nitrate values were relatively deficient relative to temperature - evidence that a period of high export had recently occurred from this water mass. We suggest that this water mass was part of an approaching Tropical Instability Wave (see discussion) and do not include the ^{234}Th sample in the deficiency model.

During the Zonal Flux transect remarkably invariant ^{234}Th activities were observed in the upper 120 m (2.02 ± 0.316 dpm/l) with deeper ^{234}Th activities in equilibrium with ^{238}U between 120 and 200 m (2.47 ± 0.13 dpm/l). During Zonal Flux, discrete profiles of ^{234}Th were also obtained at 170°E and 155°W. ^{234}Th activities increased roughly linearly from the surface to 100 m in these profiles with to slight excess of ^{234}Th over ^{238}U below 100 m. Given the relatively high uncertainty in data from the Zonal Flux cruise (~11%), we do not consider the depth, dependency of these profiles

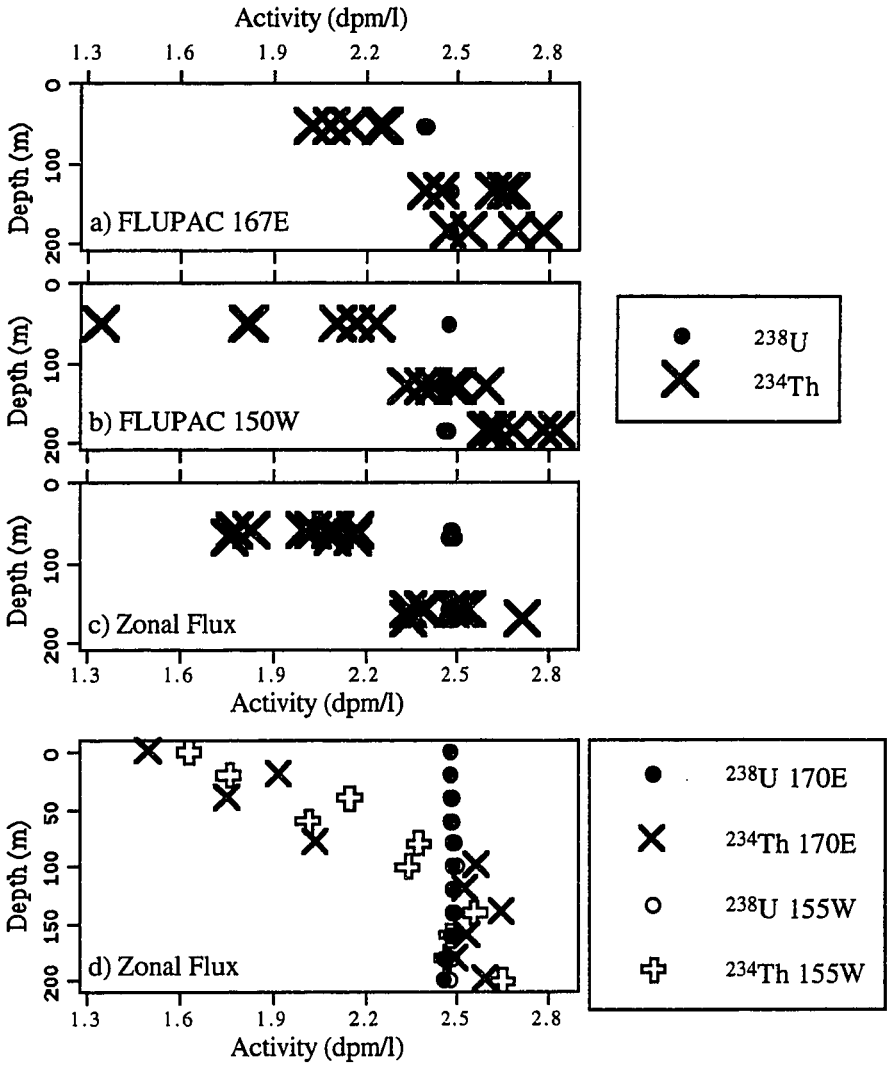

Figure 3.6: Total "integrated" ^{234}Th and ^{238}U water column activities (dpm/l) from FLUPAC TS-I (4.6A) and TS-II (4.6B) and Zonal Flux (4.6C) as well as "discrete" activites from Zonal Flux (4.6D).

significantly different and have averaged them to obtain a single ^{234}Th depth dependency in our advection calculations for both cruises.

SEDIMENT TRAP FLUXES

Sediment trap fluxes at the base of the euphotic zone (100-140 m) are shown in Figure 3.7. As stated in the previous section, ^{234}Th and mass fluxes were obtained from sediment traps of the Particle Interceptor Trap (PIT) design while organic carbon and mass fluxes (along with chlorophyll and other parameters, Rodier and Le Borgne, 1997) were obtained from traps of the Lorenzen design (with an extended aspect ratio). At FLUPAC TS-I and predominantly along Zonal Flux, PIT ^{234}Th (Figure 3.7A) fluxes agreed well with observations during EqPac. Relatively high and variable PIT ^{234}Th (Figure 3.7A) fluxes were observed at FLUPAC TS-II and slightly elevated fluxes at 160°W during Zonal Flux. Lorenzen trap organic carbon fluxes (Figure 3.7B) were much less variable, with low values at FLUPAC TS-I, high values at FLUPAC TS-II and intermediate values during Zonal Flux. PIT mass (Figure 3.7C) tracked PIT ^{234}Th fluxes extremely well, leading to a relatively small range in the ratio of ^{234}Th to mass in sinking material (5.0 ± 1.4 dpm/mg, Figure 3.7E) consistent with observations during EqPac (Murray et al., 1996). Lorenzen trap mass fluxes were low at FLUPAC TS-I and intermediate at FLUPAC TS-II and during Zonal Flux. Because of the high occasional variability observed in PITs which was not observed in the Lorenzen traps and the tight correlation observed between ^{234}Th and mass in PITs ($r^2 = 0.80$, $n = 50$, $P < 0.001$), mass was used to inter-calibrate between ^{234}Th and organic carbon to obtain the C:^{234}Th ratio in sinking particles ($C{:}^{234}Th_{Lor} = C_{Lor}/mass_{Lor} \cdot mass_{PIT}/^{234}Th_{PIT}$; Figure 3.7F). Estimated C:^{234}Th ratios of sinking material at the base of the euphotic zone had no zonal gradient during Zonal Flux. Differences in the C:^{234}Th ratio between FLUPAC TS-I (3.7 ± 0.9 μmol/dpm) and the entire Zonal Flux transect (3.1 ± 0.5 μmol/dpm) were insignificant ($P>0.1$) while the FLUPAC TS-II estimates (4.6 ± 0.4 μmol/dpm) were significantly higher at the $P=0.005$ level (Mann-Whitney U test; Sokal and Rohlf, 1995).

^{234}TH-BASED ESTIMATES OF TRAP ACCURACY AND PARTICLE EXPORT

^{234}Th deficiency fluxes and upwelling-corrected deficiency fluxes at the base of the euphotic zone (100-140 m) are shown in Figure 3.8. Variability in the ^{234}Th deficiency flux (Figure 3.8A) was minimal (± 40%) with the lowest values in the warm pool during FLUPAC TS-I and the highest value at 160°W during Zonal Flux. Values were very similar to those obtained during both EqPac cruises (Figure 3.8A). The vertical

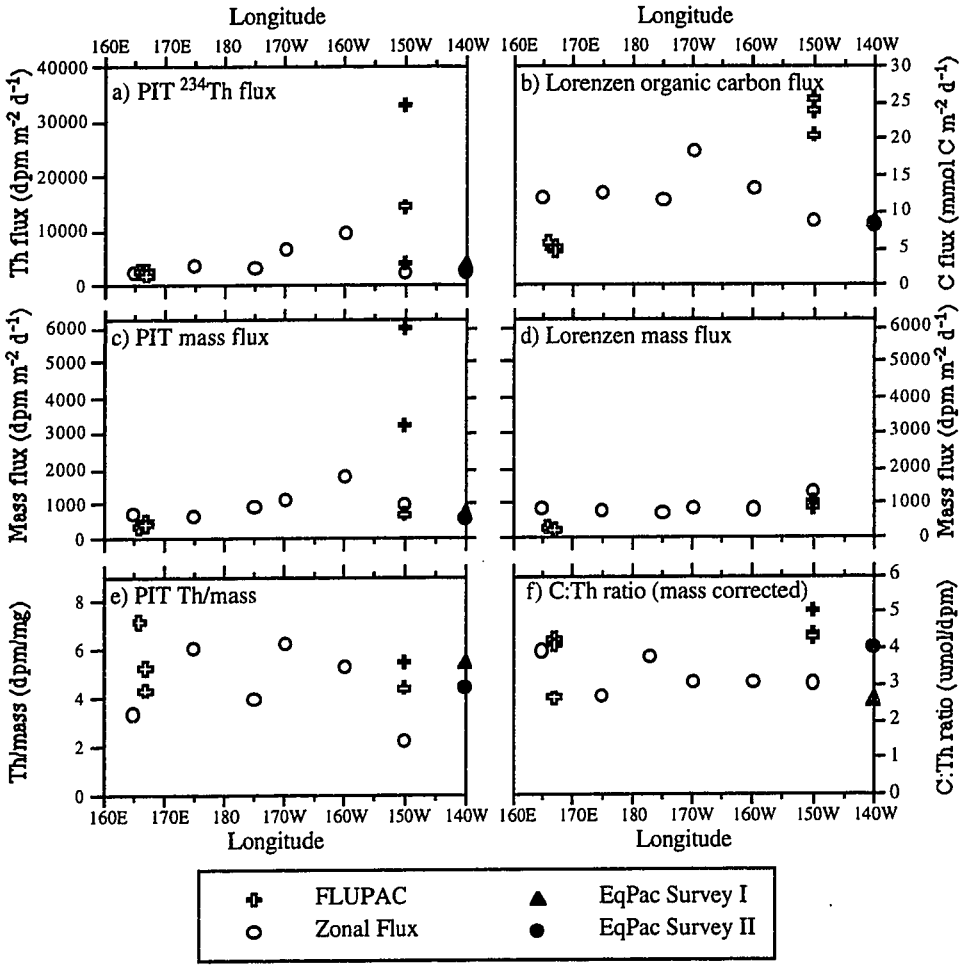

Figure 3.7: Sediment trap fluxes at the base of the euphotic zone versus longitude for PIT ^{234}Th (4.7A; dpm m^{-2} d^{-1}), Lorenzen organic carbon (4.7B; mmol C m^{-2} d^{-1}), PIT mass (4.7C; mg m^{-2} d^{-1}), Lorenzen mass (4.7D; mg m^{-2} d^{-1}), The PIT ^{234}Th:mass ratio (4.7E; dpm/mg) and the PIT ^{234}Th/Lorenzen organic carbon ratio (4.7F; µmol C/dpm) from the FLUPAC (open crosses) and Zonal Flux (open circles) cruises. Also shown are vertically averaged data from EqPac Survey I (1°N - 1°S; filled triangles) and EqPac Survey II (1°N - 1°S; filled circles). The ratio of PIT ^{234}Th:Lorenzen organic carbon is not corrected through mass for the EqPac cruises.

advection component of the ^{234}Th model increased the total estimated downward flux of ^{234}Th considerably (Figure 3.8B). The Zonal Flux deficiency flux estimates were raised on average by 107% due to the upwelling correction. This is slightly less than the corrections

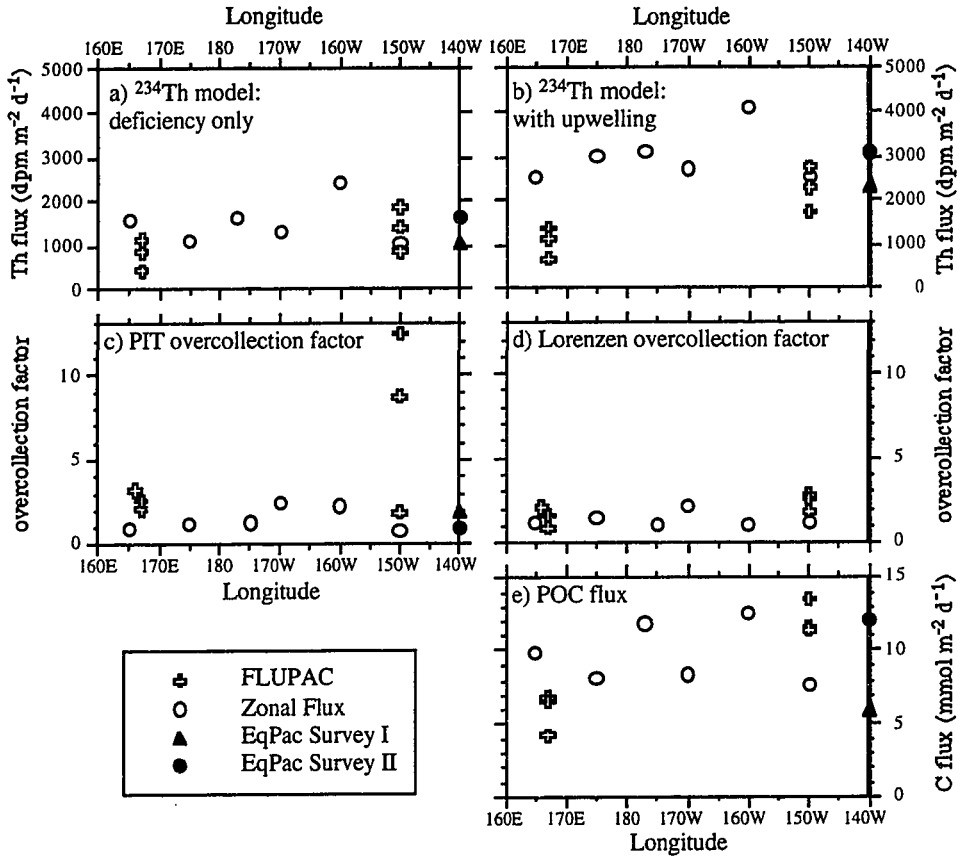

Figure 3.8: Model fluxes at the base of the euphotic zone versus longitude for the observed ^{234}Th deficiency (4.8A; dpm m^{-2} d^{-1}), ^{234}Th deficiency with upwelling correction (4.8B; dpm m^{-2} d^{-1}), model estimate of PIT overcollection (4.8C; PIT flux/model flux), model estimate of Lorenzen overcollection (4.8D; Lorenzen trap flux/model flux), and model particulate organic carbon flux (POC export; 4.8E; mmol C m^{-2} d^{-1}) from the FLUPAC (open crosses) and Zonal Flux (open circles) cruises. Also shown are data from EqPac Survey I (1°N - 1°S; filled triangles) and EqPac Survey II (1°N - 1°S; filled circles).

of 121% during EqPac Survey I and 145% in EqPac Survey II (Murray et al., 1996). FLUPAC TS-II was raised to a lesser degree (70%) while FLUPAC TS-I was raised the least (33%). Overall, the flux estimates during FLUPAC were 50% lower at TS-I than at TS-II. Deficiency fluxes during Zonal Flux averaged 34% higher than FLUPAC TS-II and, similarly to the ^{234}Th deficiency fluxes, had no zonal gradient.

Comparison of measured and modeled ^{234}Th fluxes in sediment traps gives an estimate of the degree of trap over-collection for ^{234}Th. Over-collection factors for PITs (= $(^{234}Th_{PIT})/(^{234}Th_{model})$) at the base of the euphotic zone (100-140 m) are shown in Figure 3.8C. At FLUPAC TS-I, PITs had over-collected ^{234}Th in the range of 2.1 - 2.7 times. At FLUPAC TS-II, PIT over-collection was much higher and more variable with ^{234}Th over-collection range of 1.8 - 12.0 times. During the Zonal Flux transect, PITs were relatively accurate with ^{234}Th over-collection in the range of between 0.9 - 2.7 times. Over-collection by Lorenzen traps (= $(Mass_{Lor} * {}^{234}Th_{PIT})/(Mass_{PIT} * {}^{234}Th_{model})$) at the base of the euphotic zone (100-140 m) was minimal with an over-collection range of 1.0 - 2.7 times the model flux as shown in Figure 3.8D. On average, flux correction using ^{234}Th decreased the Lorenzen trap flux by 32 ± 24% at the base of the euphotic zone.

^{234}Th-based particulate organic carbon fluxes at the base of the euphotic zone (POC export) were relatively invariant in the upwelling region as shown in Figure 3.8E. FLUPAC TS-I had the lowest fluxes (5.9 ± 1.4 mmol C m^{-2} d^{-1}), though only slightly lower than EqPac Survey I (6.1 mmol C m^{-2} d^{-1}, 1°N - 1°S). Both cruises took place during El Niño conditions. Fluxes at FLUPAC TS-II were 12.2 ± 1.1 mmol C m^{-2} d^{-1} which were not statistically different from those during Zonal Flux (9.8 ± 2.1 mmol C m^{-2} d^{-1}; P>0.1) which had no zonal gradient. These estimates compare well with estimates from EqPac Survey II (12.1 mmol C m^{-2} d^{-1}, 1°N - 1°S).

Uncertainty in ^{234}Th model flux estimates

Uncertainty in ^{234}Th-based particle export fluxes comes from the uncertainty in three components of the model: the ^{234}Th deficiency relative to ^{238}U, the C:^{234}Th ratio in sinking particles and effects of circulation on the ^{234}Th deficiency. Least squares propagated uncertainty in single measurements of the observed ^{234}Th deficiency averaged 55 ± 24% for both cruises. Since the FLUPAC cruise utilized two measurements of the ^{234}Th deficiency for each POC export estimate, the overall FLUPAC uncertainty in the deficiency was only 39%. The total observed variability in estimates from both cruises was 43%. Uncertainty in the C:^{234}Th ratio in sediment traps at the base of the euphotic zone can also be estimated from the total variability in the data. Without normalizing for mass, the C:^{234}Th ratio for both cruises was 2.8 ± 1.5 µmol/dpm giving a variability of 54%.

Normalizing for mass increased the mean by 32% to 3.7 ± 0.8 μmol/dpm and reduced the variability considerably to 21%.

Uncertainty in the upwelling flux of ^{234}Th was found to have a large impact on flux estimates from EqPac (Buesseler et al., 1995; Murray et al., 1996; Bacon et al., 1996). Least squares propagated uncertainty in the upwelling flux averaged 116 ± 4% during Zonal Flux assuming an uncertainty in w of 50% and the uncertainty in observed ^{234}Th gradients. This led to an overall uncertainty in the model ^{234}Th flux averaging 67 ± 12%. Because an average of two discrete ^{234}Th profiles obtained during the Zonal Flux was used to estimate vertical ^{234}Th gradients for the FLUPAC cruise, the uncertainty in the upwelling fluxes is higher than in the Zonal Flux cruise. To get a quantitative estimate of this uncertainty, we calculated upwelling fluxes using three hypothetical scenarios. A scenario of linear increase in ^{234}Th from the surface to 120 m gave upwelling fluxes that were 9 ± 8% lower than the estimated fluxes from the observations. A scenario of linear increase in ^{234}Th from the surface to 60 m (similar to the observations; Figure 3.6C) gave upwelling fluxes that were 8 ± 16% higher than the estimated fluxes from the observations. A scenario of linear increase in ^{234}Th from 60 m to 120 m (the opposite of what was observed) gave upwelling fluxes that were 56 ± 5% lower than the estimated fluxes from the observations. Overall, the uncertainty in the gradient in ^{234}Th contributed less to the overall uncertainty in the upwelling flux than did the uncertainty in w. Because the FLUPAC cruise took place during an extended period of diminished upwelling, however, the magnitude of the upwelling fluxes were lower (Figure 3.8B). Thus, the overall impact of the uncertainty in upwelling was smaller during the FLUPAC cruise.

Though upwelling is arguably the largest transport term in the ^{234}Th mass balance at the equator (Dunne et al., in press), the uncertainty in the other circulation terms also needs to be addressed. Buesseler et al. (1995) showed that zonal advection was a negligibly small flux in the central equatorial Pacific during the EqPac study. This result was confirmed here as no gradients in ^{234}Th could be observed along the Zonal Flux transect. Though a difference in ^{234}Th was observed between FLUPAC TS-I and TS-II, these sites were from water masses with very different densities that probably do not mix. Buesseler et al. (1995 and Murray et al. (1996) also showed that meridional advection was also a small flux at the equator during the EqPac study. The role of turbulent mixing is less well constrained. Dunne et al. (in press) suggested that ^{234}Th based particle export

estimates at the equator from EqPac Survey II overestimated the particle export by 33% by neglecting horizontal mixing. Because we have no discrete profiles of ^{234}Th off the equator, it is impossible for us to directly evaluate this potential source of variability in this study. Dunne et al. (in press) also showed however, that the role of horizontal mixing was very sensitive to the intensity of upwelling and thus was important only during periods of high upwelling. Upwelling velocities in the model were as high as 3.9 m d^{-1} at 40 m and 1.0 m d^{-1} at 120 m. Comparison in terms of relative upwelling suggests that estimates from FLUPAC were the least biased by horizontal mixing, since upwelling velocities estimated for that time period were low (2.1 m d^{-1} at 45 m and -0.6 m d^{-1} at 120 m). Upwelling velocities estimated for the Zonal Flux cruise (3.0 m d^{-1} at 45 m and 0.7 m d^{-1} at 120 m), however, were only slightly less than those estimated for EqPac Survey II (3.9 m d^{-1} at 50 m and 1.1 m d^{-1} at 120 m; Chai, 1995). While ^{234}Th-based estimates of the particulate organic carbon flux may by unaffected by horizontal mixing, the Zonal Flux estimates may be about 20% too high.

VARIABILITY IN TRAP COLLECTION EFFICIENCY

The same types of sediment traps were used to collect ^{234}Th and organic carbon in the EqPac program (Murray et al., 1996). As no inter-calibration using mass was possible during EqPac, it is important to ascertain whether the EqPac traps suffered inter-trap collection biases as observed at FLUPAC TS-II which would serve to alter the estimated C:^{234}Th ratio. If traps of the PIT design measured for ^{234}Th had indeed collected more material than those of the Lorenzen design measuring C, then C:^{234}Th values would have been artificially low. Fortunately, EqPac C:^{234}Th ratio estimates did not have spurious low values, leading us to conclude that this differential hydrodynamic bias between traps observed at FLUPAC TS-II was not an important factor during EqPac.

The source of variability in the flux of material caught in sediment traps of the PIT design at FLUPAC TS-II is also a matter of some concern. Swimmers, hydrodynamic biases and temporal variability in flux are all reasonable potential sources of variability to consider. The ^{234}Th:mass ratio measured for a variety of potential swimmer contaminants are shown in Table 3.1. These swimmers all have ^{234}Th:mass values much lower than the values obtained in traps. Because the ^{234}Th:mass ratio in sediment traps was invariant (Figure 3.7E), we reject the possibility of swimmer contamination. Because traps

of the Lorenzen design did not collect highly variable amounts of material, we reject the possibility of actual temporal variability in the sinking flux as well. This leaves hydrodynamic bias as the most probable source of PIT variability. Using l'Atalante's acoustic Doppler current profiler (ADCP) and the trajectory of the sediment traps, we calculated the average velocity of water across the top of the traps during FLUPAC. Most of the velocity across the traps was due to zonal shear between the surface and the eastward propagating equatorial undercurrent at the depth of the traps. At FLUPAC TS-I, average velocities of sediment traps relative to the flow were estimated to have been in a fairly small range between 17 and 21 cm s^{-1}. At FLUPAC TS-II, average velocities of sediment traps relative to the flow were twice that at TS-I, also in a fairly small range between 36 and 41 cm s^{-1}. These results suggest that the higher horizontal shear across the water-trap interface at FLUPAC TS-II served to increase the particles caught in the traps.

Table 3.1: ^{234}Th:mass ratios (mg/dpm) for swimmers and net tow material collected at the equator, 150°W during the FLUPAC cruise.

Sample type	**Length** (mm)	**^{234}Th/mass** (dpm/mg)
Phytoplankton aggregates	>2 (?)	1.67 ± 0.21
Foraminifera	1 - 2	1.16
200-500 μm net tow	0.2 - 0.5	0.55 ± 0.02
500-2000 μm net tow	0.5 - 2.0	0.53 ± 0.05
Copepods	2 - 3	0.31 ± 0.01
Euphausiids	6 - 9	0.084 ± 0.003
Chaectognaths	13 - 17	low (<0.02)
Caridae	25	low (<0.02)
Gelatinous material	>10 (?)	low (<0.02)

DISCUSSION

COMPARISON OF CONDITIONS IN OCTOBER 1994 AND APRIL-MAY 1996

One goal of this study was to establish variability in POC export both zonally between the western and central equatorial Pacific and temporally between season and El Niño-Southern Oscillation (ENSO) condition. Results from this study are summarized in Table 3.2. Relatively low POC export was observed in the warm pool at TS-I (5.9 ± 1.4 mmol C m^{-2} d^{-1}) consistent with the observation that the region was devoid

of nitrate in the upper 2/3 of the euphotic zone (Figure 3.4) and exhibited low inventories of particulate organic carbon and chlorophyll and low levels of integrated primary production (Table 3.2). High levels of POC export were observed at FLUPAC TS-II (12.2 ± 1.1 mmol C m^{-2} d^{-1}) consistent with the euphotic zone having 3-9 μM nitrate (Figure 3.4), higher inventories of particulate organic carbon and chlorophyll and extremely high integrated primary production (Table 3.2). Along the Zonal Flux transect POC export (9.8 ± 2.1 mmol C m^{-2} d^{-1}), nitrate concentrations and chlorophyll inventories were similar to values observed at FLUPAC TS-II. Integrated primary production was lower along the Zonal Flux than at FLUPAC TS-II while particulate organic carbon inventories were slightly higher. In general, the effect of El Niño was to change the geographic extent of the equatorial upwelling zone as defined by super-micromolar nitrate and, subsequently, the geographic extent of high POC export. Beyond this broad criteria, however, no deleterious effect of El Niño was observed during FLUPAC on primary production, new production or POC export.

Table 3.2: Sea surface temperature (SST; °C) and nitrate ($SSNO_3$; μM), 0-120 m inventories of total particulate carbon (∫PC; mmol C m^{-2}) and chlorophyll (∫Chl; mg Chl m^{-2}), integrated ^{14}C primary production (∫PP; mmol C m^{-2} d^{-1}; A. LeBouteiller, Z. Johnson, pers. comm.) and $^{15}NO_3$ new production*6.6 (∫NP; mmol N*6.6 m^{-2} d^{-1}; A. LeBoutelier, A. Aufdenkampe, pers. comm.) and POC export (mmol C m^{-2} d^{-1}) during FLUPAC and Zonal Flux as well as EqPac SST, $SSNO_3$, ∫PC, ∫Chl, ∫PP and ∫NP (JGOFS data base), POC export (Murray et al., 1996) for the EqPac Surveys and, POC export for the EqPac Time-series using ^{234}Th fluxes from Bacon et al. (1996) and sediment trap C:^{234}Th ratios from Murray et al. (1996) with Bacon et al. (1996) estimate given in parentheses.

Station	SST	$SSNO_3$	∫PC	∫Chl	∫PP	∫NP	POC export
FLUPAC							
TS I, 165E	29.3 ± 0.3	0.00 ± 0.00	313 ± 69	19 ± 3	60 ± 5	9.9 ± 1.0	5.9 ± 1.4
TS II, 150W	27.2 ± 0.1	2.85 ± 1.89	401 ± 72	25 ± 3	126 ± 4	13.9 ± 0.8	12.2 ± 1.1
Zonal Flux							
165E	28.2 ± 0.2	3.03 ± 0.07	561 ± 52	34 ± 3	71 ± 21	6.6	9.9
175E	27.8 ± 0.1	2.94 ± 0.08	493 ± 36	25 ± 4	87 ± 8	19.7	8.1
177W	27.4 ± 0.2	4.32 ± 0.05	600 ± 98	27 ± 6	80 ± 41	17.1	11.8
170W	27.3 ± 0.1	4.15 ± 0.08	555 ± 47	26 ± 4	89 ± 11	18.3	8.4
160W	27.0 ± 0.0	4.72 ± 0.06	455 ± 29	27 ± 7	82 ± 9	23.3	12.6
150W	26.3 ± 0.1	5.49	478	21 ± 2	75 ± 2	31.8	7.7
EqPac							
Survey I, 1N-1S	28.5 ± 0.1	2.83 ± 0.17	240 ± 46	25 ± 1	60 ± 8	3.8 ± 0.9	5.3 ± 1.6
Time-series I	28.5 ± 0.2	2.83 ± 0.25	468 ± 82	29 ± 1	90 ± 3	15 ± 7	*6.7 (1.9)*
Survey II, 1N-1S	25.1 ± 0.5	5.97 ± 0.38	320 ± 93	32 ± 2	101 ± 8	17.1 ± 7.2	12.1 ± 3.0
Time-series II	25.1 ± 0.3	5.76 ± 1.21	529 ± 79	33 ± 2	129 ± 6	22 ± 10	*12.8 (2.4)*

COMPARISON WITH RESULTS FROM THE EQPAC SURVEYS

Comparison with EqPac allows us to more fully explore the role of the seasonal cycle and ENSO condition in forcing POC export in the western and central equatorial Pacific. Whereas the EqPac program studied boreal spring El Niño conditions and boreal fall, non-El Niño conditions, the Zonal Flux cruise took place during boreal spring La Niña conditions and the FLUPAC cruise during boreal fall conditions of El Niño. POC export was low in EqPac Survey I and FLUPAC TS-I and high in EqPac Survey II, FLUPAC TS-II and the entire Zonal Flux transect. The observation of low POC export at FLUPAC TS-I (5.9 ± 1.4 mmol C m^{-2} d^{-1}) is consistent with nitrate limitation of the food web in the upper half of the euphotic zone due to the presence of the warm pool (Figures 4.3,4.4). POC export values were similar during EqPac Survey I and Survey II (Murray et al., 1996) at stations with the euphotic zone dominated by sub-micromolar nitrate (4.1 ± 2.1 mmol C m^{-2} d^{-1}; 12°N, 9°N, 7°N, 5°N, 12°S). At all other sites nitrate levels were super-micromolar throughout the euphotic zone and demonstrated higher POC export averaging 8.5 ± 4.5 mmol C m^{-2} d^{-1} for all 4 cruises.

Given the relatively invariant POC export observed near the equator (1°N-1°S) during Survey II, FLUPAC TS-II and Zonal Flux, we are left to explain only the low POC export observed in the HNLC region during EqPac Survey I (3.7 ± 1.8 mmol C m^{-2} d^{-1}) and the extremely high export during EqPac Survey II at 2°N (19.5 mmol C m^{-2} d^{-1}). Given the high POC export at FLUPAC TS-II (boreal fall, El Niño) and during Zonal Flux (boreal spring, non-El Niño), we conclude that the low POC export observed during the EqPac Survey I cruise (boreal spring, El Niño) was not solely the result of either seasonal or El Niño variability alone while the high POC export observed during the EqPac Survey II cruise (boreal fall, non-El Niño) is equally attributable to either seasonal or El Niño variability alone. Assuming that seasonal and El Nino forced variability are the dominant sources of POC export variability, these combined results suggest that only the combination of deleterious seasonal and El Niño effects on equatorial upwelling have an observable effect on POC export within the HNLC region. In addition to seasonal and ENSO condition however, equatorial waves provide another source of upwelling variability that may determine primary production, new production and POC export variability in the HNLC region.

THE ROLE OF EQUATORIAL WAVES

Two forms of equatorially-trapped waves provide for a significant portion of equatorial Pacific variability (Philander, 1990; Figure 3.9). The first of these, the equatorial Kelvin Wave, is formed by westerly wind bursts piling up water onto the equator while water on the equator gets pushed eastward and downward. The subsequent elevation sea surface height and corresponding depression in the thermocline is rapidly translated eastward at about 2.0-2.3 ° d^{-1} with intense downwelling and subsequent upwelling of the thermocline with a period of 1-2 months determined by the zonal and temporal extent of the wind burst (Figure 3.9A). The second type of wave, Tropical Instability Wave (a.k.a. TIW, long wave, Legeckis wave, 21-day wave, 28-day wave), takes the approximate form of Rossby Waves as variability in easterly winds pulls water westward and poleward, giving it an anticyclonic tendency. North of the equator, these waves are amplified by the shear between the South Equatorial Current and the North Equatorial Countercurrent horizontal advection, the meridional currents advecting cool equatorial surface water northward and warm NECC water southward while developing intense upwelling near the equator and intense downwelling at the northward leading edge (Figure 3.9B). While Kelvin waves tend to inhibit upwelling of nutrient-rich water into the euphotic zone, TIWs tend to enhance it.

We hypothesize that Kelvin wave and Tropical Instability Wave (TIW) activity, rather than large scale variability of season or El Niño may have caused the observed variability in POC export between the EqPac Survey I, EqPac Survey II, FLUPAC and Zonal Flux cruises. Kessler and McPhaden (1995) showed that the EqPac Survey I and Time-series I cruises took place under the influence of Kelvin waves while the EqPac Survey II and Time-series II cruises took place during a period of intense TIW activity.

Interpretation of data from the JGOFS EqPac Time-series II (Foley et al., 1997) and Survey II (Archer et al., 1997b) cruises showed that TIWs can have a potent impact on biogeochemistry of the equatorial Pacific. During most of EqPac Time-series II, primary production was $8 \pm 11\%$ higher that the EqPac Time-series I cruise (Barber et al., 1996). The passage of the TIW was characterized by positive meridional velocity, low temperature and high salinity, nutrients and chlorophyll (Foley et al., 1997). Rates of

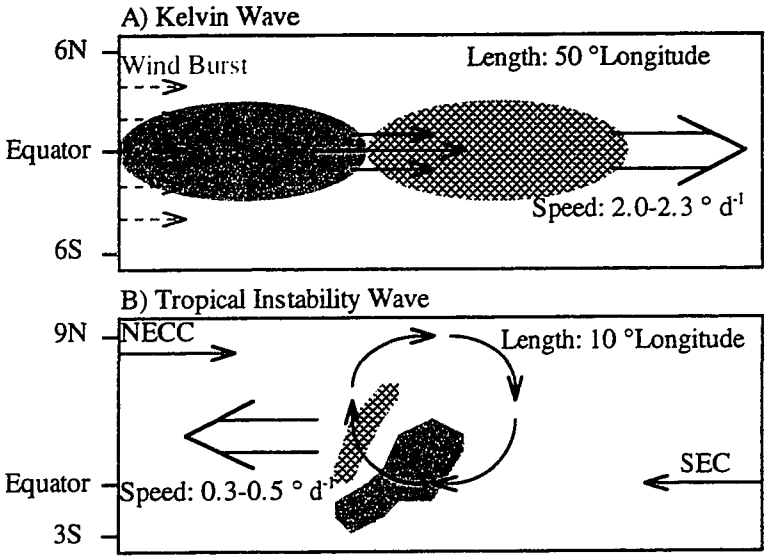

Figure 3.9: Schematic of propagation and advection associated with a Kelvin Wave (Philander, 1990; 4.9A) and a Tropical Instability Wave (Flament et al., 1997; Harrison, 1997; 4.9B). Propagation (double black arrows), horizontal water motions (single black arrows) and inferred downwelling (hatched areas) and upwelling (gray areas) are shown. Forcing by wind (4.9A; gray arrows) and the shear between the North Equatorial Counter Current (NECC) and the South Equatorial Current (SEC) are also illustrated.

primary production increased an additional 23 ± 14% over ambient values during the passage of a TIW. EqPac Survey II encountered a convergent front associated with a TIW at 2°N with an impressive accumulation of Rhizoselenia at the surface (Yoder et al., 1994; Archer et al., 1997) and increased biological activity all through the water column between 1-3°N (Dunne et al., submitted). New production and POC export at 2°N associated with the cold water south of the front was estimated at 33 mmol C m^{-2} d^{-1} (McCarthy et al., 1996) and 20 mmol C m^{-2} d^{-1} (Murray et al., 1996), respectively. At the equator, nutrients, particle concentrations and fluxes where similar to those observed during EqPac Time-Series II before and after the passage of the TIW (Table 3.2). A recent study showed that Kelvin Waves posed strong forcing on chlorophyll concentrations at a mooring at the equator, 155°W during the onset of the 1997-1998 El Niño (Chavez et al., 1998).

Though the FLUPAC cruise took place during a strong El Niño, export at FLUPAC TS-II was high relative to EqPac Survey I cruise. Eldin et al. (1997) showed that the FLUPAC cruise track followed the path of a Kelvin wave which preceded the

cruise by approximately 20 days. They also noted the presence of TIW activity at the equator, 155°W using dynamic height data from the TOGA-TAO array. Both Kelvin wave and TIW activity are evident in the TOGA-TAO data at 155°W (Figure 3.10A) and 140°W (Figure 3.10B) on the equator as shown in Figure 3.10. Two Kelvin waves are clearly seen in the variability of the dynamic height at both stations - one peaking in August and the other in October. Strong TIW activity is apparent in the variability in the meridional velocity at 140°W. Fourier analysis of the data gave a strong peak at a TIW-scale wavelength of 22 days. While Kelvin waves propagate rapidly eastward at approximately 1.8 degrees per day, TIWs propagate westward at only 0.5 degrees per day. Given these timescales of propagation, the strong northward meridional velocity signal during 9/16-9/22 (TIW-I in Figure 3.10B) would have passed the FLUPAC TS-II site around 10/9. FLUPAC TS-II took place two weeks later, 10/19-10/28. We suggest that the rise in dynamic height at the end of September (corresponding to an increased heat inventory in the upper ocean) was due to the Kelvin Wave, while the gradual lowering of dynamic height during October is a manifestation of the subsequent arrival of TIWs. The peak in northward meridional velocity at 10/10-10/13 (TIW-II in Figure 3.10B) would have reached 150°W at the end of FLUPAC TS-II. Though this TIW would have arrived too late to affect the beginning of TS-II, it is a possible explanation for the observation in the ^{234}Th data of decreased ^{234}Th and nitrate deficit at its end (Figure 3.6).

In contrast to FLUPAC, the Zonal Flux cruise took place during a period of neither Kelvin wave (characteristic of the La Niña condition) nor TIW activity (characteristic of the boreal spring). Results from Zonal Flux demonstrate that the presence of TIWs is not a necessary condition for POC export to be as high as it was during EqPac Survey II. However, it appears that TIWs serve to stimulate production both under conditions of diminished upwelling (FLUPAC TS-II relative to EqPac Survey I) and under non-El Niño conditions (EqPac Survey II north of the equator and EqPac Time Series II relative to Zonal Flux). The observation of slightly lower primary production and particle export estimates during Zonal Flux relative to FLUPAC TS-II suggests that during FLUPAC the TIW-effect of food web stimulation (EqPac Time Survey II) outweighed the Kelvin wave-effect of production suppression (EqPac Survey I).

As Kelvin wave activity is characteristic of El Niño, particularly during its onset (Kessler and McPhaden, 1995), there should be a correlation between the

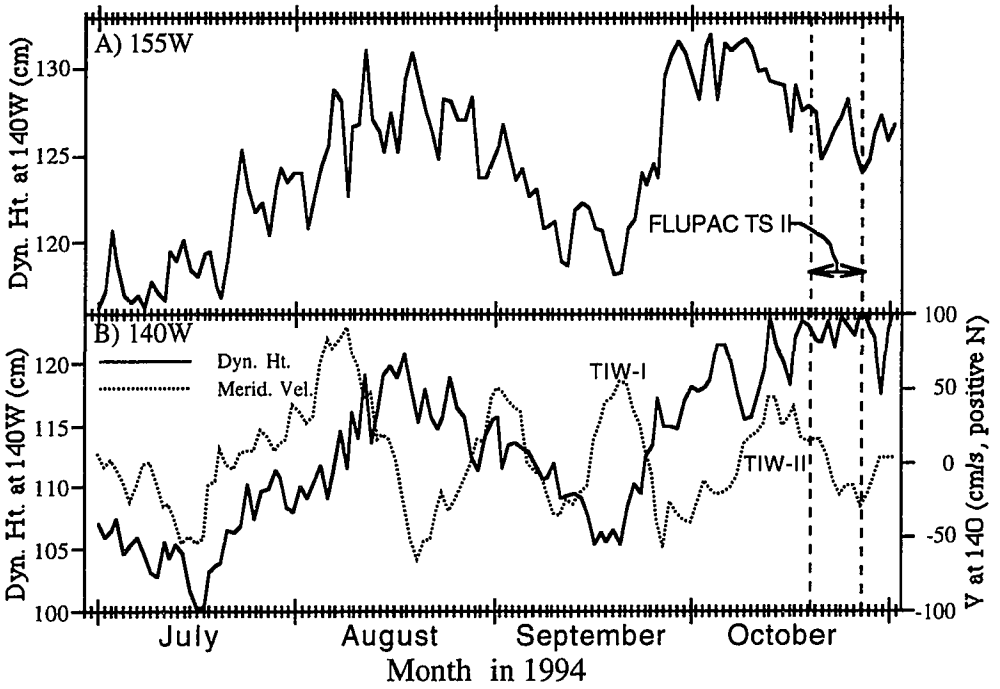

Figure 3.10: Data from TOGA-TAO buoys on the equator for July through October, 1994 showing dynamic height (cm) at 155°W (4.10A) and dynamic height (cm) along with surface meridional velocity (cm/s) at 140°W (4.10B).

suppression of new, total and export production and El Niño. We suggest that the suppression of production observed during EqPac Survey I as part of the overall El Niño condition was specifically a response to Kelvin wave activity rather than a general feature of the El Niño. We suggest that the correlation between season and production should prove to be more robust, however, through the strong seasonality of TIWs.

COMPARISON WITH ^{15}N NEW PRODUCTION AND TOTAL ORGANIC CARBON

^{234}Th-calibrated sediment trap carbon fluxes are not the only estimates of net biological production available for these cruises. Integrated ^{15}N new production from the FLUPAC (Rodier and Le Borgne, 1997) and Zonal Flux (Aufdenkampe et al., in preparation) cruises were generally greater than POC export (Table 3.2). The difference between these two estimates may either be due to either a recent temporal increase in new production (the ^{15}N estimate integrates only a day while the ^{234}Th estimate integrates over a

month) or a steady-state accumulation of total organic carbon (TOC). Assuming that ^{15}N new production should vary both above and below the monthly mean, we consider the data set of all four cruises as a whole to minimize the problem of non-steady state. Taking the difference between ^{15}N new production and POC export for the EqPac Survey Cruises (entire transect: 12°N - 12°S), FLUPAC and Zonal Flux gives a mean TOC accumulation of 22 ± 46% of new production (n = 35).

The role of accumulation and transport of total organic carbon (TOC) was evaluated directly using the regression of TOC against 6.6*NO_3 (6.6 = Redfield conversion from nitrogen to carbon) in the upper 120 m for EqPac Surveys I and II, FLUPAC and Zonal Flux (Table 3.3) using Model II analysis (principal axis or major axis; Sokal and Rolf, 1995). This analysis is very similar to that performed previously by Hansell et al (1997a,b) who found that approximately 20% of new production accumulated as TOC using Model I regression of TOC against total inorganic carbon and 6.6*NO_3 from NOAA-OACES and FLUPAC data. The range of slopes in our analysis was small, between 0.17 (Zonal Flux) and 0.27 (FLUPAC), implying that 17 - 27% of new production accumulates as TOC in the equatorial Pacific, consistent with the previous interpretation by Hansell et al. (1997b) using property-property regressions, Quay et al., (1997) using a mass-balance approach and Archer et al. (1997a) using an inverse model of TOC incorporated into the 3-D flow field from a high resolution equatorial Pacific general circulation model to estimate the grow-in timescale of TOC upon contact with the euphotic zone.

Table 3.3: Model II slopes, 95% confidence intervals of slopes and squared correlations for the regression of total organic carbon (TOC) versus 6.6*NO_3 for EqPac surveys I and II, FLUPAC and Zonal Flux using all data between 2°N and 2°S in the upper 120 m.

Cruise	Slope	Range (95% level)	r^2
EqPac Survey I	-0.22	-0.16, -0.28	0.62
EqPac Survey II	-0.24	-0.22, -0.26	0.92
FLUPAC	-0.27	-0.25, -0.29	0.74
Zonal Flux	-0.17	-0.13, -0.20	0.55

TOC ACCUMULATION MODEL

We independently estimated TOC accumulation using a 2-D steady-state inverse model of TOC circulation and accumulation tuned to observed TOC distributions.

We coupled a stream function of vertical and meridional velocity to a simple TOC accumulation function scaled to new production during EqPac Survey I and II estimated from ^{15}N new production (McCarthy et al., 1996; A factor of 6.6 was used to convert nitrogen new production to carbon new production) and ^{234}Th-based particle export (Murray et al., 1996; A factor of 1.22 was used to convert particle export to new production based on the property-property estimate of fractional TOC accumulation). We ignore the zonal component of the circulation, because zonal gradients in TOC during Zonal Flux were negligible (Figure 3.5). The stream function was established between 10°N and 10°S in the upper 300 m. Equatorial upwelling from two sets of flows were considered (Figure 3.11): 1) Large scale surface Ekman flow to the oligotrophic gyres with deeper geostrophic return (through the sides of the model) and 2) Small scale upwelling with meridional recirculation between 5°N and 5°S. The Ekman/geostrophic component was tuned to match the ^{14}C-based estimates of the zonally-averaged and vertically-integrated water flux (1.75 ± 0.53 m^2 s^{-1}; Quay et al., 1983) with an Ekman depth of 80 m. Overall, vertical velocity at the equator was shaped to match the maximum velocity of $w \approx 4$ m/d at 40 m and exponential attenuation towards no motion vertically with $w \approx 1$ m/d at 100 m and meridionally to $w \approx 0$ at 2°N and 2°S to match GCM results for vertical velocities during the EqPac Survey II study period (CPC; Chai, 1995). This resulted in 58% of upwelling being meridional recirculated, consistent with the range of model estimates of 68% (Liu et al., 1994) and 18% (Lu et al., 1998). Model mixing parameters were set to K_y = 1000 m^2 s^{-1} and K_z = 0.3 m^2 s^{-1} (Pacanowski and Philander, 1981). At the boundaries (10°N and 10°S), the TOC was set to the vertically-smoothed average of the two adjacent TOC data profiles (usually 9° and 12°) available from the EqPac Survey Cruises. The model was then run to optimize the accumulation flux of TOC as fraction of new production that best matched the observed TOC data of Peltzer et al. (1996) in the euphotic zone (0-120 m).

When the model was run with TOC boundaries and estimates of new production from EqPac Survey II, a best fit was obtained with TOC accumulation as 22% of new production. Without meridional recirculation, the model estimated TOC accumulation as 25% of new production, a result of the meridional cells recirculating recently upwelled water in the equatorial zone and increasing the average TOC concentration therein. Results were found to be most sensitive to the flux chosen for the

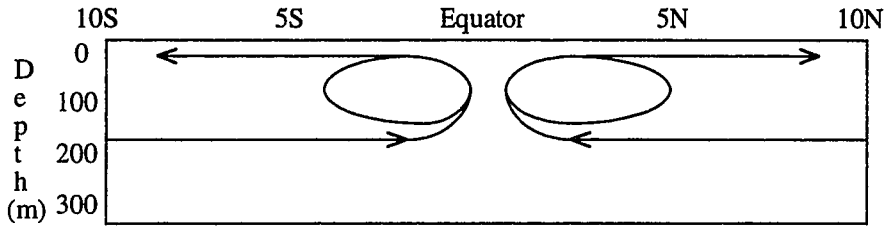

Figure 3.11: Schematic of equatorial Ekman/geostrophic flow and meridional recirculation used in the 2-D (meridional and vertical) model.

Ekman/geostrophic flow with the uncertainty values given in Quay et al. (1983) translating to a % TOC accumulation range of 15% of new production under weak circulation and 30% of new production under strong circulation. These results agree very well with the estimates of Hansell et al. (1997a,b) and those presented in this study (previous section).

When the model was run with EqPac Survey I TOC boundaries and estimates of new production, the model estimated TOC accumulation as 78% of new production. We suggest that this high value is a result not of high percentile accumulation of TOC but rather of the non-steady state mismatch between the TOC accumulation timescale of a year and the new production timescale of a day to a month. We interpret this mismatch as further evidence that the EqPac Survey I cruise occurred during an inordinately weak period of equatorial upwelling. In a second experiment, we reduced the Ekman/geostrophic component of the circulation to match the 22% TOC accumulation observation during EqPac Survey I (Table 3). This gave the flux across the boundaries as 0.58 $m^2 s^{-1}$, suggesting that the El Niño condition and associated Kelvin waves of late 1991 and early 1992 had reduced the effect of Ekman transport on TOC to approximately 33% of the mean.

In summary, inverse model results for EqPac Survey II confirm estimates based on four cruises from direct comparisons of ^{15}N new production with ^{234}Th-based particle export (22 ± 46% TOC accumulation) and property-property regression analyses (23 ± 4% TOC accumulation) with the conclusion that the equatorial Pacific upwelling zone is characterized by a dominance of particle export over TOC accumulation. Model results for EqPac Survey I suggest that large-scale Ekman circulation had slowed dramatically in response to the El Niño condition and associated Kelvin waves in late 1991 and early 1992. These results are essentially identical to those obtained by Archer et al. (1997a).

C:^{234}Th RATIOS IN SEDIMENT TRAPS

The choice of the C:^{234}Th ratio to convert the ^{234}Th model flux estimate to a POC export flux estimate has been a topic of great debate in the ^{234}Th community. Results from sediment trap studies have often been disputed because of the question of swimmer contamination, a process which would bias the data towards high C:Th ratios. Estimates based on in-situ filtration result in much lower C:^{234}Th ratios (0.5 - 2.5 µmol/dpm; Buesseler et al., 1995; Bacon et al., 1996; Murray et al., 1996; Charette et al., in press). C:^{234}Th ratios (µmol/dpm) based on drifting sediment trap samples near the base of the euphotic zone from various studies are shown in Table 3.4. Comparison of these studies shows remarkable consistency which is suggestive of three things: 1) sediment traps can be reproducibly picked of swimmers 2) the C:^{234}Th ratio of sinking particles has a relatively narrow range 3) the process of particle reprocessing and sinking has a relatively uniform timescale.

Table 3.4: C:^{234}Th ratios (µmol/dpm) and their variability (1 s.d.) from drifting sediment traps near the base of the euphotic zone from various studies.

Study	C:^{234}Th ratio (µmol/dpm)	Reference
FLUPAC TS-I	3.7 ± 0.9	this study
FLUPAC TS-II	4.6 ± 0.4	this study
Zonal Flux	3.1 ± 0.5	this study
EqPac Survey I	2.8 ± 1.1	Murray et al., (1996)
EqPac Survey II	3.6 ± 1.8	Murray et al., (1996)
North Atlantic Bloom Experiment	4.5 ± 1.8	Buesseler et al. (1992)
Bermuda Atlantic Time-series	7.0 ± 0.5	Buesseler et al. (1994)
subarctic northeast Pacific	3.3 ± 1.8	Charette et al. (in press)
Santa Barbara Channel	3.5 ± 0.8	Dunne et al. (in prep.)
Hawaii Ocean Time-series	5.6	Murray et al. (in prep.)

A second line of evidence in favor of sediment trap C:Th ratios over those based on in-situ filtration comes in comparison of the resulting POC export fluxes with other flux estimates for the equator during the boreal fall of 1992. Variability in C:Th ratios were largely responsible for variability in POC export fluxes. Those based on in-situ filtration by Buesseler et al. (1995) of 3-5 mmol C m^{-2} d^{-1} (4°N - 4°S) during the NOAA sponsored surveys and Bacon et al. (1996) of 2.4 ± 0.9 mmol C m^{-2} d^{-1} during EqPac Time-Series II were much lower than those based on sediment traps by Murray et al.

(1996) of 12.1 ± 3.0 mmol C m^{-2} d^{-1} (1°N - 1°S). Quay (1997) compiled all available estimates of carbon fluxes from EqPac to statistically evaluate the equatorial carbon mass balance show that estimates from Bacon et al. (1996) and Buesseler et al. (1995) are unreasonably low as they imply a large, unexplained carbon imbalance for this time period. We suggest a re-evaluation in the use of in-situ filtered material to obtain the C:^{234}Th ratio the POC export in favor of the use of sediment traps. Thus, we have revised the Bacon et al. (1996) POC export estimates for the EqPac time-series cruises using C:^{234}Th ratios from the respective EqPac Survey cruises (Table 3.2).

CONCLUSIONS: EXPORT ALONG THE EQUATOR IN THE PACIFIC

This study answered a number of important questions remaining after the JGOFS EqPac study and re-evaluated variability in equatorial Pacific export production as the expression of three features: surface nitrate, Kelvin waves (or the combination of seasonally low upwelling and El Nino low upwelling) and TIWs. The first order forcing function of equatorial export is the presence or absence of nitrate. Compared to POC export in the oligotrophic north Pacific at the Hawaii Ocean Time-series (HOT; 2 mmol C m^{-2} d^{-1}; Michaels et al., 1994; Karl et al., 1995), results from EqPac Survey I and Survey II (4 mmol C m^{-2} d^{-1}; Murray et al., 1996), showed that the presence of subsurface nitrate roughly doubled POC export. Within the HNLC region, POC export doubled once again to between 8 and 12 mmol m^{-2} d^{-1}. While export of dissolved organic carbon at HOT has been shown to account for a large portion of total export (Emerson et al., 1997), TOC accumulation accounts for only about 22% of total export in the equatorial Pacific HNLC region.

As has been a general observation in the equatorial Pacific HNLC region beginning with the work of Barber and Chavez (1991), biomass and production appear saturated with respect to nutrient concentration at the equator. This study found no direct evidence of export functionality on nutrient concentration beyond the condition of no surface nutrients resulting in low export during FLUPAC TS-II). EqPac observations of low export during Survey I (El Niño, boreal spring) and high export during Survey II (non-El Niño, boreal fall) were previously attributed to an unknown combination of seasonal and El Niño effects. Given the high export at the nitrate rich site of FLUPAC (El

Niño, boreal fall) and the entirely nitrate-rich site of Zonal Flux (La Niña, boreal spring) we conclude that neither the ENSO nor the seasonal condition alone is responsible for the level of export. While EqPac Survey I occurred directly after the passage of a Kelvin Wave but before the ecosystem had recovered, EqPac Time-series I took place a month later, after the ecosystem had recovered. The occurrence of Tropical Instability Waves during the EqPac Survey II and Times Series cruises was well documented. The observation of relatively high export at FLUPAC TS-II suggests that the effect of TIWs may overwhelm the effect of Kelvin waves. The low export during EqPac Survey I suggests that Kelvin Waves may be strong forcing functions. While Kelvin Waves appear to halve export, TIWs tend to double it.

Within the region of persistent surface nutrients - the equatorial upwelling zone - we suggest that variability in export is a function of balance in the equatorial food web (Chavez and Barber, 1991; Landry et al., 1997) which we consider primarily a function of equatorial waves. Through this work we have developed the following working hypotheses: 1) Kelvin waves depress the food web uniformly by downwelling surface waters and decreasing the average light level experienced by phytoplankton, thus increasing grazing pressure on all phytoplankton. 2) TIWs differentially stimulate the food web by rapidly upwelling iron-enhanced water to give those phytoplankton which are able quickly respond and out-compete grazing an advantage. It is these relationships between physics and biology which are most difficult to constrain using limited data sets, but which are likely the dominant factors determining biogeochemical fluxes in this region. Modeling of the explicit effects of Kelvin waves and TIWs on the equatorial food web and the resulting biogeochemical fluxes are the critical next step in validating these hypotheses.

CHAPTER 4: SILICON:NITROGEN COUPLING IN THE EQUATORIAL PACIFIC UPWELLING ZONE

INTRODUCTION

Diatoms are a group of phytoplankton which utilize silicate to form siliceous frustules. Their high excess density and often large size makes them prone to rapid sinking (Smith et al., 1996). Diatoms utilize nitrate readily and sometimes preferentially (Dugdale et al., 1995; Lomas and Glibert, 1998), thus feeding the ammonium-based microbial loop with new nitrogen. They have been shown to be a dominant part of the biological pump in open ocean phytoplankton blooms (e.g. Billet et al., 1983), coastal upwelling (e.g. Nelson and Goering, 1978) and the high nutrient low chlorophyll (HNLC) waters of the southern ocean (e.g. Gersonde and Wefer, 1987).

The HNLC region of the central equatorial Pacific upwelling zone (EUZ; Murray et al., 1994) is a regime of considerable interest to biogeochemists and one in which diatoms have been implicated to play a large role in the biological pump (Chavez et al., 1990). Interest in this area has arisen because of the importance of the EUZ to the global carbon budget. A process study in the central equatorial Pacific surveyed this region as part of the U. S. Joint Global Ocean Flux Study (EqPac; Murray et al, 1994). The goals of the EqPac Process Study were to characterize carbon fluxes in this region and better understand the inefficiency with which the HNLC food web is able to export nutrients out of the euphotic zone as sinking particles (Barber and Chavez, 1991). Previous work had suggested this was due to iron limitation (Martin, 1990), grazing control (Frost and Franzen, 1992) or a combination of both (Chavez et al., 1991).

Circulation in the central equatorial Pacific is complex but has been well characterized because of its coupling with the El Niño-Southern Oscillation (e.g. Philander 1990). Three aspects of equatorial circulation: the mean state, seasonal and El-Niño variability, and propagating Kelvin and Tropical Instability waves, all combine to control variability in nutrient concentrations and biogeochemical fluxes in this region. A schematic of the mean circulation is shown in Figure 4.1. On the equator easterly trade winds upwell

water and drive it both meridionally away from the equator and from east to west along the surface as part of the South Equatorial Current. Piling up of water in the west results in subsurface return flow in a tight jet called the Equatorial Undercurrent. In the western equatorial Pacific warm pool, a combination of slackening of the trade winds and highly variable westerly wind bursts drive downwelling. The seasonal cycle of wind stress drives seasonal variability in surface temperatures and upwelling between high temperatures/low upwelling in the boreal spring and low temperatures/high upwelling in the boreal fall. The El Niño-Southern Oscillation is an equally important source of long-term variability with a relaxation of upwelling during El Niño and an intensification during La Niña (Philander, 1990). Two equatorial surface waves, Kelvin waves and Tropical Instability Waves (TIWs), are the major sources of small time and space scale variability. Kelvin waves, stimulated by westerly wind bursts, propagate eastward as a bulge along the equator, (Kessler and McPhaden, 1995). TIWs are complex westward propagating anti-cyclonic vortices which edge on the equator, are more frequently found to the north than the south and are most prominent during the boreal fall (Flament et al., 1996).

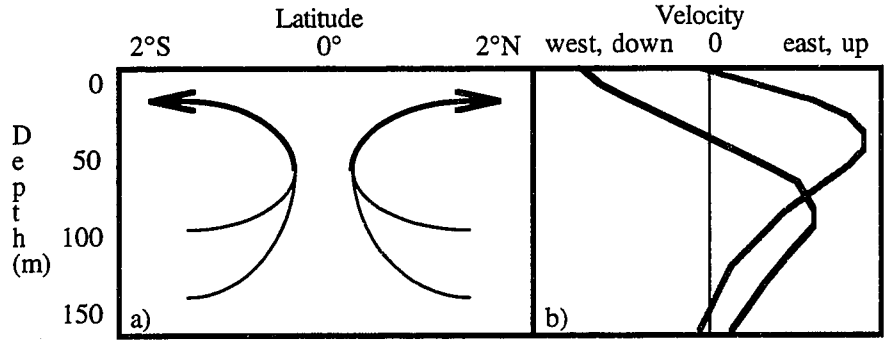

Figure 4.1: Schematic of the mean circulation in the central equatorial Pacific showing meridional and vertical velocity between 2°N and 2°S in the upper 150 m (4.1A) and schematic profiles of zonal (black) and vertical (grey) velocity at the equator (4.1B).

All of these circulation features come into play in the interpretation of the EqPac data towards describing the magnitudes and variability of carbon fluxes in this region and solving the riddle of the HNLC regime. Hernes et al. (1997) suggested that only dense, mineral-associated particles make it out of the euphotic zone in the equatorial Pacific, implicating the silica frustules of diatoms as a potential mode of sinking. Landry et al. (1997) synthesized the EqPac data and concluded that the presence of the HNLC

condition in the region was due to a combination of microzooplankton grazing control of the pico-plankton and limitation of larger phytoplankton because of lack of iron. In the absence of significant eolian inputs of iron to this region (Donaghay et al., 1991; Ku et al., 1995), the equatorial undercurrent (rather than the atmosphere) may be the dominant, though low level, source (Gordon et al., 1997).

While most work on equatorial production has pointed to iron and grazing as the important controls (e.g. Landry et al., 1997), the availability of silicate has also been invoked as a regulating force. Bender and McPhaden (1990) found a minimum in silicate at the equator, 135°W during 1988 which they inferred to be the signature of a recent diatom bloom. Ku et al. (1995) recognized that the disappearance ratio of silicate to nitrate in the EqPac data was much lower than in other ocean areas due to the dominance of local recycling relative to eolian input of nutrients in the central equatorial Pacific. They suggested that particle export from the equatorial Pacific upwelling zone might be regulated by the input of "new" silicate.

Dugdale and Wilkerson (1998) expanded this argument using two additional pieces of information: 1) The regression between silicate and nitrate between 1°S and 1°N in the upper 200 m during the US-JGOFS EqPac Survey II cruise (see methods) suggested that nitrate and silicate were taken up in a 1:1 ratio consistent with diatom growth requirements and 2) Average euphotic zone silicate concentrations during the WEC 88, EqPac Survey I and EqPac Survey II cruises (see methods) showed that silicate varied little between seasons relative to nitrate, consistent with the chemostat concept wherein only the limiting nutrient is drawn down to a constant low level while others vary dependent on the input concentrations. Dugdale and Wilkerson (1998) then used a food web model of silicon and nitrogen cycling based on Dugdale et al. (1995) to illustrate that this hypothesis is consistent with estimates of nitrogen cycling during the EqPac Survey II.

In this chapter, I investigate the degree to which diatoms control the biological pump in the equatorial upwelling zone. I utilize data from meridional and zonal equatorial transects during a suite of El Niño and normal, cold-tongue conditions to describe the extent of silicon limitation of particle export in the equatorial upwelling zone. I include particulate silica and organic nitrogen measurements in sediment traps and the water column and ^{15}N-new production from the US JGOFS EqPac Surveys, the France JGOFS

FLUPAC and the Zonal Flux cruises (see methods) as well as water column nutrient data from nineteen equatorial cruises. The comprehensive nature of this data set supports the notion of intense silicate utilization during EqPac Survey II but shows that this cruise occurred during a period of relatively strong upwelling compared to a climatological mean defined by this set of 19 equatorial cruises. Nutrient, particle concentration, new production and sediment trap data are presented which illustrate that silicon and nitrogen cycling in the central equatorial Pacific euphotic zone are sometimes tightly coupled but are in general described by preferential export of nitrogen over silicon. Potential mechanisms for this are discussed in a synthesis of this data with previous observations within the context of a conceptual model. This work suggests that diatom dominance of new production and particle export is controlled by size selectivity in grazing and iron limitation. Non-steady state conditions resulting from Kelvin and Tropical Instability waves are heavily implicated in driving changes in the equatorial food web.

DATA

Water column nutrient data from the upper 120 m, 2°N to 2°S were obtained from 19 equatorial cruises (Table 4.1): eight Hawaii-Tahiti Shuttle Experiment (HTSE) meridional transects along 150-158°W in 1979 and 1980 (D. Archer, personal communication; T. Takahashi, personal communication), National Oceanographic and Atmospheric Administration (NOAA) National Marine Fisheries Service cruises along 81-129°W from August to September 1986, 1987 and 1989 (Fiedler et al., 1991), the World Ocean Circulation Experiment (WOCE) P16C cruise along 150°W in September 1991 and P17C cruise along 120°W in June 1991 (ftp://nemo.ucsd.edu/woce/Data/Pacific/), US JGOFS EqPac Surveys along 140°W in February-March and August-September 1992, US JGOFS EqPac Time Series at the equator 140°W in March-April and October 1992 (http://www1.whoi.edu/jgofs.html), FRANCE JGOFS FLUPAC zonal transect along the equator between 165°E and 150°W in October of 1994 aboard the N/O l'Atalante (LeBorgne et al., 1995) and the Zonal Flux zonal transect along the equator between 165°E and 150°W in April-May of 1996 aboard the R/V Thomas G. Thompson. For the HTSE cruises nitrite and ammonia measurements were not available. For the WOCE and NOAA cruises ammonia measurements were not available.

Table 4.1: Summary of data from the HTSE, NOAA, WOCE P16 and P17, JGOFS EqPac, FRANCE JGOFS FLUPAC and Zonal Flux cruises between 2°N and 2°S showing the longitude of study, Southern Oscillation Index (SOI), the Niño 3.5 SST anomaly, the slope and intercept of the Model II least squares regression of silicate versus dissolved inorganic nitrogen as well as the squared Pearson product-moment coefficient (r^2). The longitude (-), SOI (+) and Niño 3.5 sea surface temperature anomaly (-) are indicators of the strength of upwelling, the slope an indicator of the relative consumption of silicate and nitrogen, the intercept an indicator of the extent of nitrogen limitation relative to silicate and the squared Pearson product-moment coefficient an indicator of the percent of the variability accounted for in the correlation.

Cruise	Long. W	SOI Index	Niño 3.5 anomaly	Slope	Intercept	r^2
HTSE 1	150-153 W	-0.07	0.08	0.33	1.67	0.84
HTSE 3	150-158 W	-0.03	0.31	0.86	-1.50	0.80
HTSE 5	150-158 W	0.67	0.36	0.62	-0.33	0.69
HTSE 7	150-158 W	0.37	0.05	0.21	1.25	0.32
HTSE 9	150-158 W	-0.30	0.53	0.22	1.66	0.50
HTSE 11	150-158 W	-0.43	0.79	0.20	1.44	0.42
HTSE 13	150-158 W	-0.30	0.2	0.51	0.47	0.72
HTSE 15	150-158 W	-0.83	0.43	0.35	1.31	0.69
NOAA-86	87-113 W	-0.37	1.13	0.69	1.01	0.96
NOAA-87	85-129 W	-0.67	1.73	0.62	1.01	0.94
NOAA-88	81-128 W	1.50	-1.58	0.70	-0.28	0.96
WOCE P17	120 W	-1.0	0.98	0.70	-0.96	0.68
WOCE P16	150 W	-1.0	0.64	0.42	1.65	0.74
Survey I	140 W	-2.6	1.99	0.27	1.63	0.37
Time Series I	140 W	-1.9	1.66	0.49	0.21	0.34
Survey II	140 W	-0.3	0.07	0.76	-2.49	0.93
Time-series II	140 W	-0.6	-0.05	0.83	-1.63	0.81
FLUPAC	163W- 150W	-1.7	0.93	0.40	0.75	0.71
Zonal Flux	165E- 150W	0.5	-0.20	0.41	0.63	0.66
Average	142 W	-0.48	0.53	0.51	+0.39	0.69
Sum N ≤ 7.62	-	-		0.28	+1.54	0.29
Sum N > 7.62	-	-		0.85	-2.83	0.90

US JGOFS EqPac Survey I took place in the boreal spring during the passage of a series of Kelvin Waves associated with El Niño conditions while Survey II took place in the fall during a temporary abatement of El Niño (Kessler and McPhaden, 1995). Carbon fluxes (e.g. new production, primary production, particle export) all increased dramatically from Survey I to Survey II (Murray et al., 1994) as a consequence of this physical forcing. EqPac Survey II encountered a convergent front associated with a TIW (Yoder et al., 1994), observing both an intense accumulation of Rhizoselenia at this "Great Front" and dramatic changes in the biogeochemistry of the euphotic zone (Archer et al, 1998). During the FRANCE JGOFS FLUPAC cruise, a boreal fall El Niño condition had displaced the warm pool east of the date line to 170°W. Because the warm pool is a water mass distinct from the EUZ, only FLUPAC nutrient data taken east of the western

Pacific warm pool were considered in this analysis. During the Zonal Flux cruise, a boreal spring La Niña had displaced the warm pool over 25° westward, past 165°E. Consequently, equatorial nutrient data along the entire Zonal Flux transect were considered in this analysis. Southern Oscillation Indices (SOI) shown in Table 4.1 are averages for the three months before each cruise while temperature anomalies in the Niño 3.5 region of 5°N - 5°S, 170°W - 120°W (Table 4.1) are monthly averages for each cruise (http://www.pmel.noaa.gov/toga-tao/el-nino/home.html). All regressions between nutrients were made using Model II (principal axis or major axis; Sokal and Rohlf, 1995) which treats both variables as being subject to error and thus avoids biasing the regression towards the x-axis.

Silica was measured as both water column particulate concentrations and sinking fluxes during EqPac. Silica flux samples were collected on 0.4 μm Nuclepore filters in drifting sediment traps of the Particle Interceptor Trap (PIT) design (Murray et al., 1996) during EqPac Survey I between 12°N and 1°N (until the array was lost at the equator) and Survey II between 12°N and 12°S. Samples for water column particulate silica concentration were collected during EqPac Survey II between 9°N and 5°S by filtration of 2.36 l samples from 10 l Niskin bottles onto 1 μm Nuclepore filters. All EqPac silica samples were processed in Seattle using the soda-hydrolysis method of Paasche (1980) and measured spectrophotometrically using a Bausch and Lomb spectronic 100. All Zonal Flux and FLUPAC silica samples were processed in Brest, France using the method of Paasche (1973) (Blain et al., 1997).

I utilize data for on-deck $^{15}NO_3$ new production (McCarthy et al., 1996), drifting sediment trap nitrogen fluxes from the EqPac Survey Cruises (available at http://www1.whoi.edu/jgofs.html), water column particulate silica concentrations (Blain et al., 1997), in-situ $^{15}NO_3$ new production (Navarette, 1998), drifting sediment trap nitrogen (Rodier and LeBorgne, 1998) and silica fluxes from the French FLUPAC cruise and in-situ $^{15}NO_3$ new production (Aufdenkampe, in preparation), drifting sediment trap nitrogen and silica fluxes from the Zonal Flux cruise.

All sediment trap fluxes for EqPac (Murray et al., 1996) and for FLUPAC and Zonal Flux (Dunne et al., in preparation) were calibrated using ^{234}Th in traps and advection-corrected ^{234}Th deficiencies. Sediment trap nitrogen and silica estimates for all

cruises shown here are averages of all trap samples collected between 100-150 m. As eolian inputs are thought to be extremely low in this region (Donaghay et al., 1991; Ku et al., 1995), particulate silica is assumed to be 100% biogenic.

RESULTS

First considered is the relationship between dissolved silicate and dissolved inorganic nitrogen (DIN), defined as the sum of NO_3^-, NO_2^- and NH_4^+, in the upper 120 m of the water column. Nutrient data are presented in Figure 4.2 for the EUZ between 2°N and 2°S for cruises from which particulate silica data are available. The 2°N and 2°S interval was chosen to be consistent with the EqPac designation of the equatorial upwelling zone (Murray et al., 1996) and with model results for the meridional extent of equatorial upwelling (Liu et al., 1994). This analysis was limited to the upper 120 m in order to focus only on the zone where new production takes place, using the EqPac designation of the euphotic zone's 0.1% light level at 120 m (Murray et al., 1994). Restricting the vertical analysis to the euphotic zone minimizes complications in silicon and nitrogen due to: 1) differential remineralization of organic nitrogen and dissolution of particulate silica beneath the euphotic zone and 2) complexities of equatorial circulation (Figure 4.1), specifically the combination of the shallowness of equatorial upwelling and the strength of the equatorial undercurrent, both tending to de-couple processes from distributions in the vertical extent. NO_2^- and NH_4^+ were included in the analysis to enable comparison of nutrient mass balances with sediment trap fluxes. This analysis for EqPac Survey II (Figure 4.2b) gives a significantly lower slope (0.76; Table 4.1) than the value of 1.00 in Dugdale and Wilkerson (1998). The difference in slope is due to a combination of factors. Model II regression of nitrate in the 0-200 m, 1°N to 1°S domain of Dugdale and Wilkerson (1998) gives a slope of 0.923. Increasing the latitudinal extent of the domain to 2°N and 2°S decreases the slope to 0.865. Decreasing the vertical extent of the domain to 0-120 m further decreases the slope to 0.763. Adding NO_2 and NH_3 into the analysis decreases the slope only slightly, to 0.759. As discussed below, these differences are small relative to the differences observed between cruises.

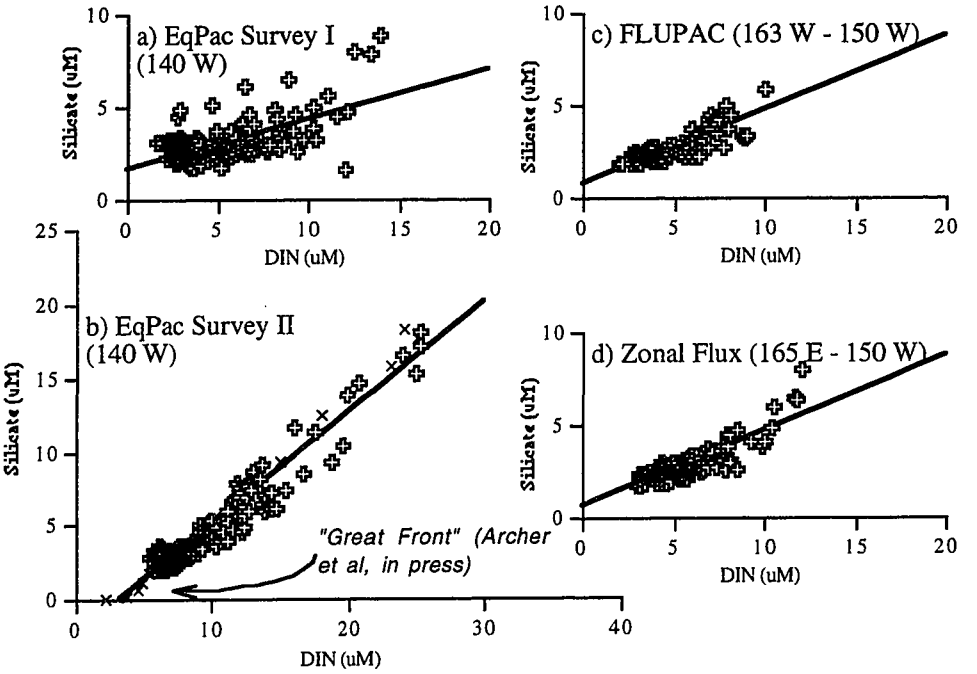

Figure 4.2: Dissolved inorganic nitrogen (NO_3 + NO_2 + NH_4) versus silicate in the upper 120 m between 2°N and 2°S for four cruises: 4.2a,b) US JGOFS EqPac Survey cruises along 140°W in Feb-March and August-September 1992, 4.2c) the France JGOFS FLUPAC cruise along the equator between 163°W and 150°W in October 1994 and 4.2d) the Zonal Flux cruise along the equator between 165°E and 150°W April-May 1996. Also shown are the Model II least squares regressions for each cruise given in Table 4.1.

A key assumption is the Si:N ratio for nutrient uptake in diatoms. Brzezinski (1985) found the Si:N ratio to be 1.05 mol/mol (total range: 0.41 - 4.38 mol/mol) in laboratory experiments with 27 species of coastal and open ocean diatoms. This ratio has been shown to vary considerably under limitation by light, temperature and other nutrients (Paasche, 1980; Brzezinski, 1985). Recent work suggests that this ratio may double under limitation by iron (Hutchins and Bruland, 1998; Takeda, 1998). Here the classic Brzezinski (1985) value of 1.05 (mol Si)/(mol N) is used in lieu of direct measurements. Comparing this value with the slope for Survey II (0.76) suggests that the silicon and nitrogen cycles were strongly coupled at the time, in agreement with Dugdale and Wilkerson (1998). The negative intercept of this regression (-2.5; Table 4.1) implies that, given a continuation of the observed trend in silicate and DIN, silicate would be

exhausted before DIN. However, neither nutrient falls below 2 μM in the analysis (except at the "Great Front") prohibiting the general conclusion that either nutrient was absolutely limiting. At the predicted rate silicate would be exhausted when DIN reached about 3.3 μM. As shown in Figure 4.2, the only instance where silicate was taken to zero coincided with the subsurface diatom bloom and surface biomass accumulation that was associated with the passage of the instability wave at 2°N ("The Great Front"; Archer et al., 1998). During this event diatoms were apparently able to consume silicate and nitrogen and completely remove silicate.

The results from the other three cruises (EqPac Survey I, FLUPAC and Zonal Flux) shown in Figure 4.2 were quite different. Maximum silicate and nitrate concentrations reached only half those found during EqPac Survey II. The slopes of these regressions (see Table 4.1) range between 0.27 - 0.41. The intercepts are all positive and imply that DIN would be exhausted first while silicate still remained at 0.6 - 1.6 μM. Clearly, something was special about the ocean biogeochemistry or physics during EqPac Survey II.

Table 4.2: Summary of the Pearson product-moment coefficient (r) for the silicate:DIN regression slope with: average concentration, maximum concentration, month away from January (maximum = July), longitude W, Niño 3.5 SST anomaly and SOI. Only values of $r \geq 0.43$ are significant at the P = 0.05 level (Rohlf and Sokal, 1995).

Parameter correlated with slope (Table 1)	**r**
mean DIN	0.72
mean Si	0.66
maximum DIN	0.80
maximum Si	0.91
longitude W	-0.49
month (July max.)	0.30
SOI	0.23
Niño 3.5 anomaly	-0.21

A more comprehensive analysis of all available cruise data shows the wide range of conditions observed in the EUZ. Characterizations by Longitude W, Southern Oscillation Index (SOI), Niño 3.5 SST anomaly and Model II (principal axis) least squares regression are shown for all 19 cruises in Table 4.I. Silicate:DIN slopes range between 0.20 - 0.83. Pearson product-moment correlations between cruises for the silicate:DIN

slope with other parameters are given in Table 4.2. The slopes are highly correlated ($P \leq 0.01$, $r \geq 0.56$, $n = 19$; Rohlf and Sokal, 1995) with the mean DIN and silicate concentrations as well as the maximum DIN and silicate concentrations for each cruise. Because nutrient concentrations tend to increase with the strength of upwelling, one might expect the slopes to increase seasonally towards the months of maximum trade winds (positive at maximum in July; Philander et al., 1990), geographically towards the eastern Pacific (negative westward) and climatologically with the Niño 3.5 SST anomaly (negative with temperature) and SOI (positive). Though the correlations for these four parameters with the silicate:DIN slope were all in the correct direction, only the longitude correlation was significant at the 95% confidence level (Table 4.2). These cruises have average longitudes (mean = 142°W) west of the Dugdale and Wilkerson (1998) study and SOI and Niño 3.5 SST anomaly values (-0.48 ± 0.95 and 0.53 ± 0.81, respectively) skewed towards El Niño-like conditions. Though no significant correlations were observed between the silicate:DIN ratio and either SOI index or Niño 3.5 SST anomaly, it is reasonable that one does indeed exist beyond the scatter in the data. If so, these factors would tend to weight this analysis to a small degree towards lower DIN and silicate values indicative of milder upwelling. However, it should be noted that the conditions sampled during these cruises were representative of EUZ climatology since 1979 which has been dominated by the El Niño condition (SOI = -0.51 ± 1.12; mean Niño 3.5 SST anomaly = 0.37 ± 0.95).

To describe the overall relationship between DIN and silicate in the euphotic zone of the equatorial upwelling zone, data are shown from all 19 equatorial cruises together in Figure 4.3. The data in Figure 4.3 are distributed such that the slope is low (0.28) at low DIN and silicate concentrations and high (0.85) at high DIN and silicate concentrations with an inflection near 7.6 μM DIN and 3.7 μM silicate. At high DIN and silicate concentrations, changes in DIN are accompanied by approximately equal changes in silicate. However, the data from the euphotic zone predominantly occupy the region of lower slope. Of the 2313 data points in Figure 4.3, 1534 (66%) have DIN ≤ 7.62 μM. The average DIN concentration in the upper 120 m for each cruise was 6.9 ± 3.4, indicating that the euphotic zone is dominated by the low-slope signature. As discussed below, the break in slope is an important clue for underlying controls on the biological pump in the EUZ.

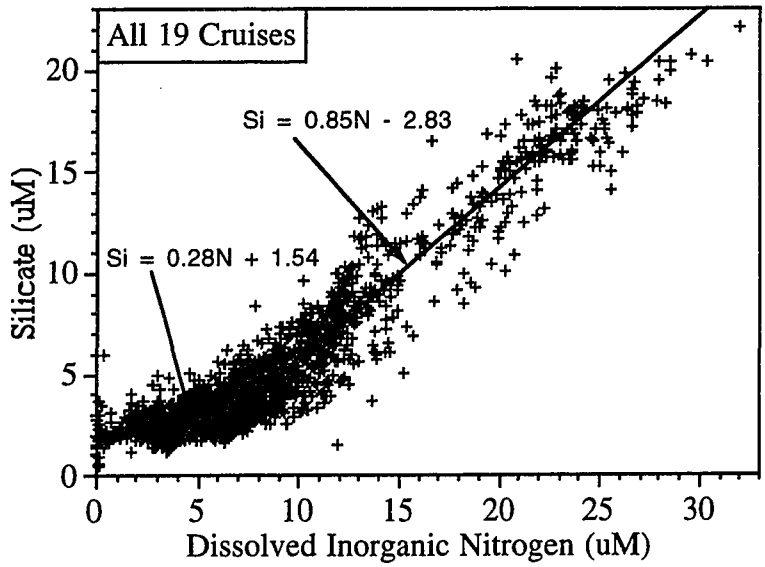

Figure 4.3: The composite relationship between dissolved inorganic nitrogen (NO_3 + NO_2 + NH_4) and silicate in the upper 120 m between 2°N and 2°S for the HTSE, NOAA, WOCE P16C and P17C, JGOFS EqPac, FLUPAC and Zonal Flux cruises in Table 4.1. The data were ranked by nitrogen and fitted using least squares regressions from each end. The break in slope was determined as the point where each of the two regressions predicted the same silicate value at the nitrogen midpoint (fixed nitrogen = 7.26, silicate = 3.32).

The important role of diatoms during EqPac Survey II is clearly evident in the water column particulate silica results from that cruise (Figure 4.4). The distribution of water column particulate silica shows strong maxima north and (less so) south of the equator. The intense northern maximum coincides with the location of "The Great Front" at 2°N (Archer et al., in press). The maximum value of 413 nM at the equator, 140°W during the Non-El Niño EqPac Survey II cruise is approximately twice the maximum value of 201 nM at 155°W observed during the El Niño FLUPAC cruise (Blain et al., 1997) and four times the maximum value of 102 nM at 155°W during the La Niña Zonal Flux cruise. The relatively high concentrations observed during EqPac Survey II are consistent with the cruise's relatively westward longitude (140°W). More surprising was the lack of change in water column particulate silica between FLUPAC (El Niño) and Zonal Flux (La Niña). As discussed below, this observation is consistent with a suite of other biogeochemical biomass and rate measurements showing a lack of variability between these two cruises (LeBorgne et al., in press; Dunne et al., in prep.). The Si:N mole ratio in bottle-filtered

particulate matter was 0.2 at 150°W on the equator during both FLUPAC and Zonal Flux. During EqPac Survey II at 140°W on the equator, this ratio was much higher, at 0.8. In contrast to the constancy of other planktonic forms (Bidigare and Ondrusek, 1996) and the total carbon biomass (Murray et al., 1996) in the central equatorial Pacific, siliceous organisms are evidently highly variable contributors to the total particle concentration in this region.

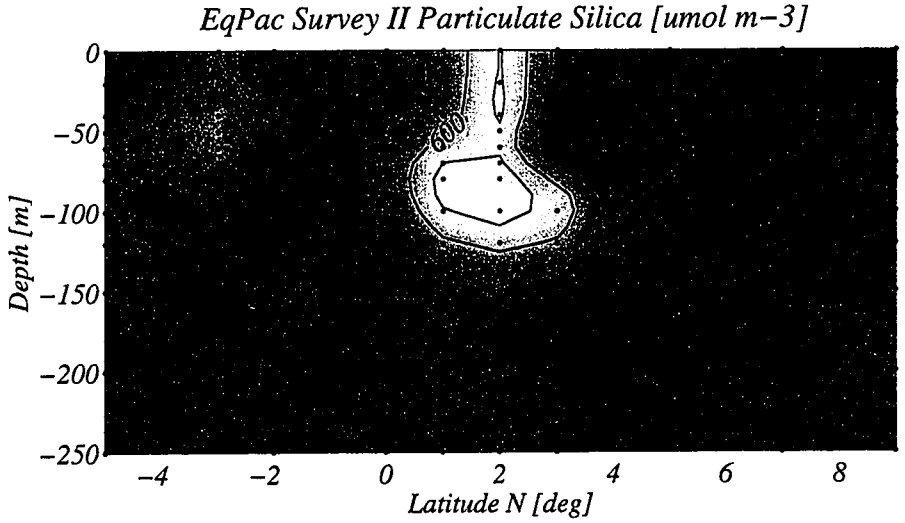

Figure 4.4: Latitude-depth section of water column particulate silica concentrations during US JGOFS EqPac Survey II. Contours are in μM.

^{15}N new production (McCarthy et al., 1996; Navarette, 1998; Aufdenkampe et al., in preparation) and ^{234}Th-calibrated sediment trap nitrogen and silica fluxes are shown for EqPac Surveys I and II, FLUPAC and Zonal Flux in Figure 4.5. EqPac nitrogen uptake and sediment flux data are discussed in McCarthy et al. (1996) and Murray et al. (1996). FLUPAC nitrogen uptake and sediment flux data are discussed in Rodier and LeBorgne (1998). FLUPAC silica data are discussed in Blain et al. (submitted). Values of all three parameters are uniformly low during EqPac Survey I but relatively high between 5°N and 5°S during EqPac Survey II. Highly significant correlations ($P<0.1$) exist between nitrogen and silica sediment trap fluxes ($r^2 = 0.88$) and between each of these and new production ($r^2 = 0.51$ and 0.73, respectively) for the EqPac Surveys. Sediment trap data during the FLUPAC short time series at 150°W show similar magnitudes and

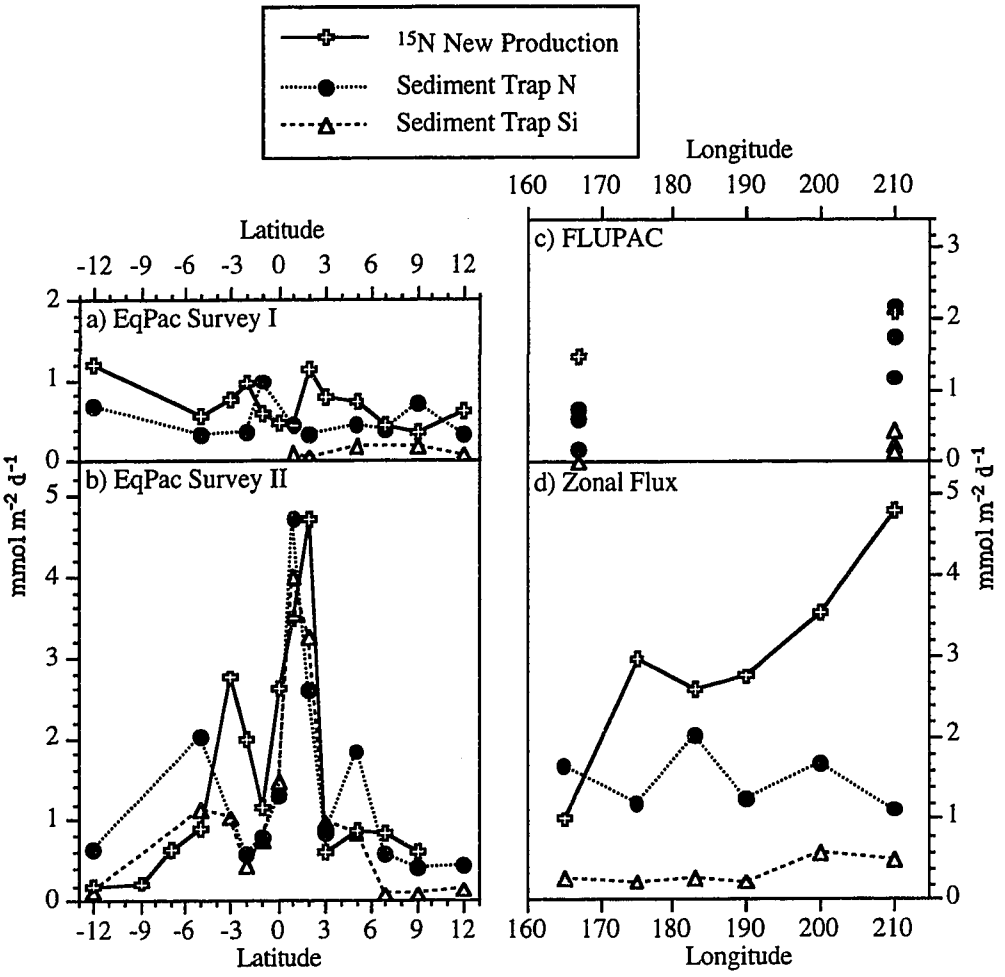

Figure 4.5: Integrated ^{15}N new production (McCarthy et al., 1995) and sediment trap fluxes of nitrogen and silicon versus latitude for EqPac Survey I (4a), EqPac Survey II (4b), FLUPAC (4c) and Zonal Flux (4d) cruises, all in mmol m^{-2} d^{-1}. All sediment trap fluxes were corrected using ^{234}Th as described in Murray et al. (1996).

variability as the entire Zonal Flux transect between 165°E and 150°W, consistent with observations of biomass, primary production and grazing estimates (LeBorgne et al., in press; Dunne et al., in preparation). This lack of variability is impressive considering the relatively strong upwelling inferred for Zonal Flux from the La Niña conditions prevalent at the time. The FLUPAC and Zonal Flux cruises alone give only weak correlations (0.02 <

$P < 0.05$) between nitrogen and silica fluxes ($r^2 = 0.44$). No correlation was observed between new production and either nitrogen or silica sediment trap fluxes during these cruises. The range of new production and particulate organic nitrogen sinking flux during the FLUPAC site at 150°W and the Zonal Flux cruise (0.5 - 4.8 mmol N m^{-2} d^{-1}) were of similar magnitude to the EqPac Survey II cruise between 2°N and 2°S (0.6 - 4.7 mmol N m^{-2} d^{-1}). This similarity contrasts to the dissimilarity in the relatively high subsurface nutrient concentrations in EqPac Survey II.

DISCUSSION

SILICON TO NITROGEN RATIOS

The distributions of nutrients, water column particulate matter and sediment trap fluxes provide important clues about the relative cycling of nitrogen and silicon in the highly variable upwelling conditions of the EUZ. As shown in Figure 4.3, the silicate:DIN nutrient slope is dependent on nutrient concentration. The mole ratio of silicate to DIN disappearance from the nutrient pool $([SiO_3]_{120} - [SiO_3]_0)/([N]_{120} - [N]_0)$ and the Si:N ratio in sediment trap material are shown in meridional sections for EqPac Survey I and EqPac Survey II and in zonal sections for FLUPAC and Zonal Flux in Figure 4.6a-d. Assuming that: 1) the particle concentration is at steady state, 2) the production of dissolved organic nitrogen is negligible and 3) nutrients are predominantly supplied vertically, then the ratio of silicate to DIN disappearance from the nutrient pool (ΔSi:ΔDIN ratio) should equal the Si:N ratio in sinking particles. The good comparison near the equator between the Si:N ratio of vertical disappearance and the sinking flux in Figure 4.6 gives us confidence in the validity of the above assumptions of particle steady state, vertical particle export and vertical nutrient supply during these cruises. Off the equator the ratio of vertical Δsilicate:ΔDIN ratio differed from the sediment trap Si:N ratio. This difference likely reflects meridional or zonal differences in Δsilicate:ΔDIN ratios and the dominance of horizontal processes over vertical ones off the equator.

Further analysis of sediment trap material, the vertical Δsilicate:ΔDIN ratio and the silicate:DIN slope in the 2°N to 2°S band in Table 4.3 shows striking intra-cruise consistency. During EqPac Surveys I and II between 2°N and 2°S, the ranges in the Si:N

ratio in trap material agreed well with the disappearance ratio of ΔSilicate:ΔDIN in the water column and the slope of the silicate:DIN regression from Table 4.1. During FLUPAC the range of Si:N ratio in trap material was at the low end of the disappearance ratio of ΔSilicate:ΔDIN in the water column and the slope of the silicate:DIN regression from Table 4.1. During Zonal Flux, the range in Si:N ratios in trap material spanned the range in the disappearance ratio of Si:N in the water column. The good agreement between the nutrient and trap data suggests that any of the three parameters listed in Table 4.3 can be used to estimate the silicate:DIN utilization ratio in the biological pump.

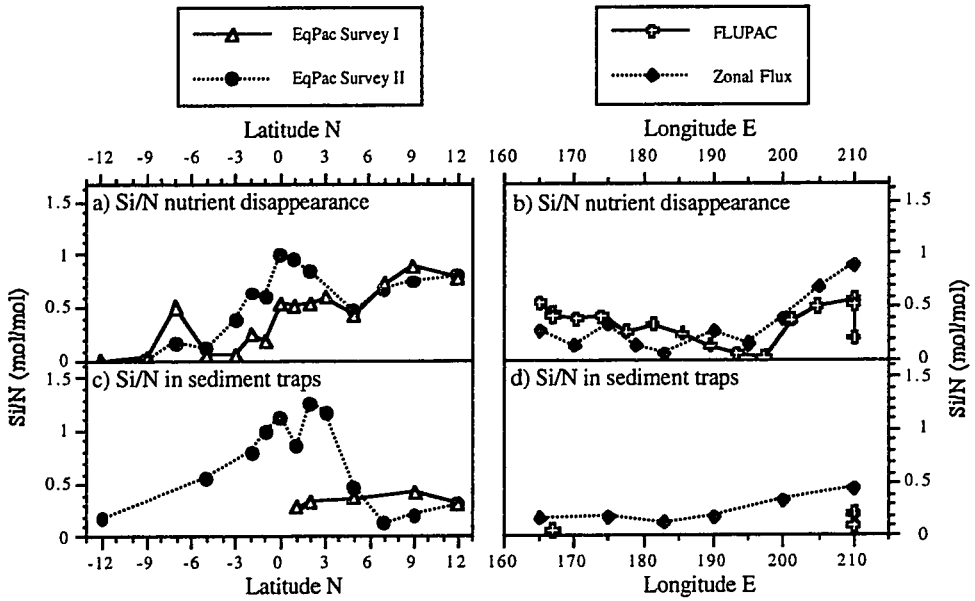

Figure 4.6: The disappearance ratio of silicate over dissolved inorganic nitrogen between 120 m and the surface $([SiO_3]_{120} - [SiO_3]_0)/([N]_{120} - [N]_0)$ (4.6a, 4.6b) and the average ratio of silicon to nitrogen in sediment traps between 100 and 150 m (4.6c, 4.6d) both mol/mol versus latitude for EqPac Survey I (open triangles) and EqPac Survey II (filled circles) cruises (4.6a, 4.6c) and versus longitude for the FLUPAC (open crosses) and Zonal Flux (filled diamonds) cruises.

Given the nutrient data alone, the high slope in EqPac Survey II could be interpreted simply as an artifact of horizontal advection or of recent upwelling of waters characterized by remineralization/dissolution processes. Results from sediment traps corroborate the apparent nutrient uptake, however, and suggest that the nutrient data are

indeed a signature of biological pumping from the euphotic zone. Thus, biogeochemical coupling between nitrogen and silicon is temporally variable - the data confirms the Dugdale and Wilkerson (1998) argument for EqPac Survey II but not for the other three cruises. The low utilization and export of silicon relative to nitrogen during EqPac Survey I, FLUPAC and Zonal Flux suggests that the biological pump in the equatorial upwelling zone is more complex than suggested by the model of Dugdale and Wilkerson (1998). Particulate silica is apparently only exported from the EUZ euphotic layer only during high-nutrient and high-flux periods of very strong upwelling such as in EqPac Survey II.

Table 4.3: Summary of the mole ratio of silicon to nitrogen utilization using three methods: the range of sediment trap Si:N, the range in the vertical Δsilicate:ΔDIN ratio between the surface and 120 m and the model II regression slope from Table I for the four cruises.

Cruise	Sediment trap Si/N	Vertical Δsilicate/ΔDIN	silicate:DIN slope
EqPac Survey I	0.29 - 0.34	0.19 - 0.54	0.27
EqPac Survey II	0.79 - 1.25	0.60 - 1.00	0.76
FLUPAC	0.10 - 0.23	0.03 - 0.59	0.40
Zonal Flux	0.14 - 0.45	0.07 - 0.89	0.41

Comparison of particulate fluxes with the water column inventory of particulate silica provides additional insight into the temporally variable relationship between the role of silicon (diatoms) in the biological pump. The average sediment trap silica flux between 100 and 150 m and integrated ^{15}N new production in the euphotic zone are both highly correlated ($P<0.005$) with the particulate silica inventory in the upper 120 m during EqPac Survey II (Figure 4.7a,b). 71% of the variability in silica flux (Figure 4.7a) and 77% of the variability in new production (Figure 4.7b) during EqPac Survey II can be explained through changes in the inventory of particulate silica. The regression with silica trap flux for EqPac Survey II has a slope corresponding to a single residence time (τ_{Si}) of 30 ± 7 days for particulate silica sinking out of the upper 120 m. The fact that the regression goes through the origin is strong evidence for a single timescale for the sinking of particulate silica. In addition, data from FLUPAC at 150°W (τ_{Si} = 31 ± 13 days) and the entire Zonal Flux transect (τ_{Si} = 18 ± 5 days) (Figure 4.7a) compare well with EqPac Survey II, giving us even greater confidence in the robustness of this timescale. The EqPac Survey II regression for new production has a positive intercept, suggesting either that a small amount of new production occurs independent of the particulate silica inventory (i.e. by non-Si requiring phytoplankton) or that diatoms were more efficient under

conditions of low abundance. It is important to note that this plot utilizes all data from EqPac Survey II and that the low new production values are from outside the designated 2°N to 2°S equatorial upwelling zone.

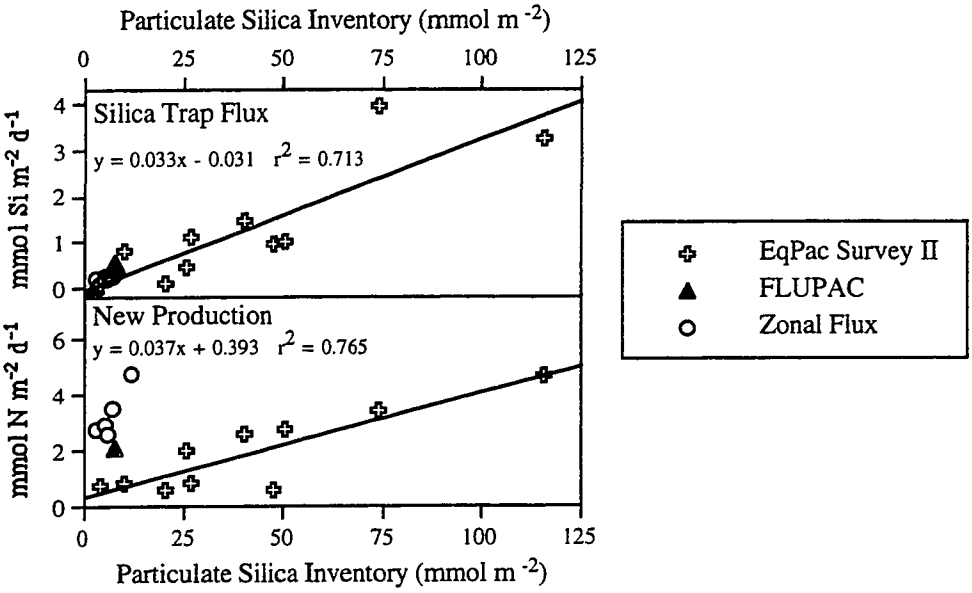

Figure 4.7: ^{234}Th-corrected silica flux in sediment traps (4.7a) and ^{15}N new production (4.7b) versus the inventory of particulate silica in the upper 120 m for the EqPac Survey II (open crosses), FLUPAC (filled triangles) and Zonal Flux (open circles) cruises.

Data from FLUPAC and Zonal Flux have a very different relationship between new production and particulate silica concentration than observed during EqPac Survey II (Figure 4.7b). During these cruises, particulate silica concentrations and silica fluxes were low while new production remained high. This implies that diatoms were either extremely efficient at utilizing nitrate or that another phytoplankton group was dominating new production. In summary, while particulate silica concentration has a relatively direct link with sinking flux (Figure 4.7a), its link with new production is strong only when upwelling is either strong or non-steady state (Figure 4.7b).

COMPARISON WITH OTHER DATA ON DIATOMS

Estimates of diatom concentrations in the water column vary considerably depending on the approach used to measure them. There were a three methods used to estimate diatom abundance during the JGOFS EqPac Survey II: particulate silica obtained by 1 μm filtration of bottle samples (this study), particulate silica by in-situ 53 μm filtration (J. Bishop, personal communication) and photosynthetic pigments determined on 0.7 μm filtration of bottle samples (Bidigare and Ondrusek, 1996). In addition, enumeration of diatoms in > 20 μm particles (Iriarte and Fryxell, 1995) was performed on the EqPac Time Series II cruise. Water column silica concentrations in >53 μm particles measured using the Multiple Unit Large Volume Filtration System (MULVFS) of J. Bishop (personal communication) show the same trends during EqPac Survey II as >1μm particulate silica concentrations from Niskin bottles (Figure 4.4). The MULVFS values, however, are consistently 15-20% of the >1μm bottle results - e.g. the MULVFS "Great Front" values at 2°N do not exceed 300 nM while the >1μm bottle values are greater than 800 nM. This difference suggests that only 15-20% of the water column particulate silica concentration is >53 μm. Biomass of diatoms estimated using the pigment marker fucoxanthin gave a 0-120 m inventory of diatom Chl *a* from fucoxanthin averaging 2.7 mg Chl *a* m^{-2}. This value was 12% of total Chl *a* during EqPac Survey II between 3°N - 3°S (Bidigare and Ondrusek, 1996). Assuming a C:Chl *a* ratio of 58 (g/g; Eppley et al., 1992) and a Si:C ratio of 0.13 (mol/mol; Brzezinski, 1985), gives an estimate of silica associated with living diatoms at 1.6 mmol Si m^{-2}, which is equivalent to only 3% of the total measured water column particulate silica concentration. Considering that fucoxanthin-based diatom Chl *a* and particulate silica inventories during EqPac Survey II agree extremely well ($r = 0.94$, $n = 10$), the Si:Chl*a* conversion use here is probably an under-estimate such that the living fraction of diatoms is much greater than 3%.

A higher fraction of living diatoms is also evident in comparison particle enumeration and epifluorescence based estimates. Enumeration of >20 μm particles during the EqPac Time-series II cruise (Iriarte and Fryxell, 1995) gives an estimate of large diatom biomass of 9.8 ± 4.7 mmol C m^{-2} - also equivalent to 3% of total particulate silica. However, epifluorescence based estimates of the size distribution of living diatoms suggest that as much as 95% of the diatom population in this region is < 20 μm (Chavez et al., 1990). The combination of particle enumeration (Iriarte and Fryxell, 1995) and

epifluorescence (Chavez et al., 1990) data suggests that the total biomass of living diatoms could be similar to the bottle water column particulate silica estimates. Zooplankton biomass estimates from EqPac Time Series cruises suggest that radiolarians composed less than 1% of the zooplankton community with a total inventory of 0.2 mmol C m^{-2} during EqPac Time Series II (Verity et al., 1996) and 1.9 mmol C m^{-2} during FLUPAC (LeBorgne, personal communication) and so do not account for an appreciable fraction of particulate silica. Given the great deficiency of iron in the equatorial Pacific, these comparisons are also consistent with recent studies (Hutchins and Bruland, 1998; Takeda, 1998) suggesting that the Si:N ratio in diatoms is much ggreater than 1.0 under iron limitation.

Growth rates of diatoms estimated from fucoxanthin changes in dilution experiments between 3°N and 3°S during EqPac Surveys I and II averaged approximately 0.89 ± 0.05 d^{-1} in the euphotic zone with a strong depth dependency from 1.7 d^{-1} at 10-20 m to 0.5 d^{-1} at 70-80 m (Latasa et al., 1997) with little variability between cruises. Combined with the fucoxanthin concentration data and the Si:N ratio of Brzezinski (1985), this gives estimated total diatom nitrogen and silica production rates of 1.5 mmol m^{-2} d^{-1} for EqPac Survey II. These diatom production estimates are similar in magnitude to estimates of ^{15}N new production (2.6 mmol N m^{-2} d^{-1}; McCarthy et al., 1996) and ^{234}Th-calibrated sediment trap fluxes (1.8 mmol N m^{-2} d^{-1}, 1.7 mmol Si m^{-2} d^{-1}; this study) for this latitude band during EqPac Survey II - further evidence for tight coupling between silicon and nitrogen at this time. In light of the mis-match between fucoxanthin- and silica-based diatoms estimates, a large, dissolution-resistant, detrital particulate silica pool during Eqpac Survey II is inferred. This hypothesis is consistent with the diatom assemblage being much larger during EqPac Survey II (Landry et al., 1997).

During EqPac Survey II, water column particulate silica concentrations were much higher than during FLUPAC and Zonal Flux, though residence times with respect to sinking were equivalent at approximately 30 days (Figure 4.7a). I suggest that diatoms were relatively large during EqPac Survey II, leading to low dissolution rates and increased export efficiency of particles. This hypothesis is consistent with Landry et al. (1997), who described a general shift in the food web during EqPac Survey II towards larger size structure stimulated by partial release of iron stress. The observation that residence times were invariant between cruises implies that sinking rates of opal were invariant and is

inconsistent with the direct sinking of diatom tests as the dominant removal mechanism, as there is a strong dependence of sinking velocity on size (Smayda, 1970; Komar et al., 1981; Alldredge and Gotschalk, 1988). However, the constancy of sinking velocities of opal is consistent with the process of the fecal pellet sinking such that the size of fecal pellets remained constant between cruises.

CONCEPTUAL MODEL OF NITROGEN AND SILICON CYCLING

To understand the source of variability in new and export production in this region, it is crucial to understand the nature of the coupling between the particulate nitrogen and silicon mass balances. Utilizing the following conceptual model of nitrogen and silicon cycling in the equatorial Pacific upwelling zone, I evaluate potential constraints on the uptake and removal processes which control these particle mass balances. In the model (Figure 4.8) nitrate upwells and is taken up by phytoplankton which convert it to particulate organic nitrogen (PON). PON is then subject to conversion to dissolved organic nitrogen (DON), remineralization to ammonium and nitrite (which are subsequently re-incorporated into diatom and non-diatom PON) and loss through a pool of sinking detritus. Silicate also upwells into the euphotic zone and is taken up by a subset of phytoplankton, diatoms, which convert it to silica. Silica is subject to dissolution back to silicate and loss through a pool of sinking detritus. According to the model,the nitrogen and silicon cycles can be de-coupled in five ways (Figure 4.8): 1) Silicate can be taken up both during new (nitrate) and regenerated (ammonia and nitrite) diatom production. 2) Non-diatom phytoplankton may utilize nitrate. 3) PON and DON can be remineralized (either to the relatively utilizable forms of ammonium and nitrite or to nitrate) while silica cannot. 4) Organic nitrogen can cycle biologically between PON and DON phases, providing for significant horizontal export of a large, refractory nitrogen pool (DON), while silica cannot. 5) Diatom silica is subject to chemical dissolution while PON is not.

Given these factors, the strong correlation between the distributions and fluxes of silicon and nitrogen is impressive. Analysis of EqPac Survey II suggests that nitrogen and silicon were tightly coupled because regenerated diatom production, new production by other phytoplankton, DON production and silica dissolution were negligible. Evidence from the other cruises discussed above and from previous studies, however, suggests that at least some of the processes of decoupling shown in Figure 4.8 are

important. Here each of these processes are discussed in the context of the conceptual model.

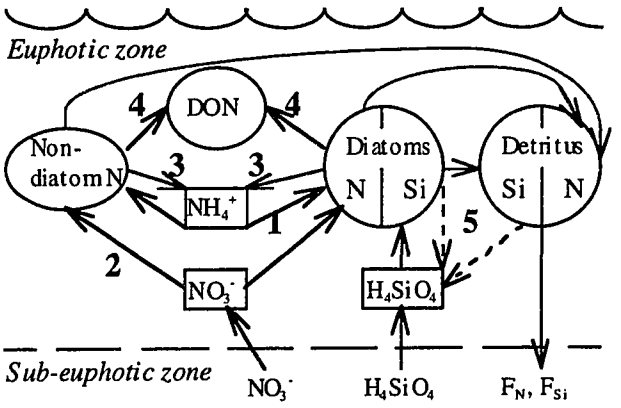

Figure 4.8: Flow diagram of the conceptual model. Boxes, nutrient reservoirs; circles, particle reservoirs; arrows, fluxes; grazing fluxes, gray arrows; dissolution fluxes, dotted arrows; all other fluxes, solid black arrows. Numbers refer to diatom regenerated production (1), non-diatom new production (2), remineralization of PON (3), removal to DON (4) and silica dissolution (5).

Diatom regenerated production (1) and non-diatom new production (2) - The link between diatoms and new production in the equatorial Pacific is extremely variable suggesting that the size structure of the diatom community determines its role in new production. During EqPac Survey II the strong, linear correlation between water column particulate silica and new production (Figure 4.7b), the nearly equal losses of silicate and DIN (Figure 4.2b) and fluxes to sediment traps (Figures 4.5,4.6) are all evidence of the strong link between diatoms and new production. During FLUPAC and Zonal Flux, however, water column particulate silica levels were low while new production levels remained high; silica biomass varied widely between cruises while new production was relatively invariant (Figure 4.7). Silica uptake rates from ^{32}Si incubations (Blain et al., 1997) also remained high during FLUPAC, approximately equal to rates of new production. Assuming a 1:1 ratio of silicon and nitrogen incorporation into diatoms, diatom silica production was high enough to accommodate all new production during FLUPAC. This possibility makes it important to determine whether only diatoms determined nitrate-based production during EqPac Survey I, FLUPAC and Zonal Flux. Evidence from Price et al. (1994) suggests otherwise. Price et al. (1994) performed

experiments on nitrate and ammonia uptake near 140°W at the equator during August, 1991 and found that the <3 μm size class was responsible for 85% of the nitrate uptake and that even the <1 μm size class took up significant levels of nitrate. Since the <3 μm size class excludes diatoms (e.g. Blain et al., 1997; Chavez et al., 1990), it is improbable the diatoms were the dominant group taking up nitrate during the Price et al. (1994) study and, by inference, during the EqPac Survey I, FLUPAC and Zonal Flux cruises.

Total rates of new production exhibit little variability between the EqPac Survey II, FLUPAC and Zonal Flux cruises (Figure 4.5) while diatom new production appeared extremely variable. Though it is reasonable that diatoms should have high rates of new production at high nutrient conditions due to a dominance of larger species, it is unclear why non-diatoms had higher rates of new production at low nutrient conditions. One possibility would be inhibition of non-diatom nitrate uptake by ammonium at high nutrient conditions. This is not supported by the data, however, as average ammonium concentrations during EqPac Survey II (0.18 μM) were not higher than average ammonium concentrations during EqPac Survey I (0.21 μM), FLUPAC (0.22 μM) and Zonal Flux (0.13 μM). This issue cannot be resolved at this time. Nonetheless, the uptake data and Si:DIN nutrient slopes are consistent with a switch in the equatorial Pacific between a food web with large, nitrate-utilizing diatoms at high concentrations of silicate and DIN and a small, more complex food web at low concentrations of silicate and DIN.

PON remineralization (3) - PON removal is another potentially strong source of de-coupling between the nitrogen and silicon cycles. The dominant mechanism of PON removal is remineralization to DIN as part of the tight microbial loop in the central equatorial Pacific. Microzooplankton grazing converts most PON to ammonium. Diatom specific mortality rates due to microzooplankton grazing were estimated to be quite high during EqPac, 0.53 ± 0.21 d^{-1} during Survey I and 0.44 ± 0.13 d^{-1} during Survey II (Latasa et al., 1997). These high specific mortality rates are typical for this region and imply that diatom PON is recycled on the timescale of 2 days. Specific mortality rates for non-diatoms were estimated to be higher than for diatoms (Landry et al., 1995; Latasa et al., 1997), suggesting that the recycling of diatom PON was less efficient than for non-diatom PON. PON remineralization to DIN serves to increase the Si:N nutrient slope over the uptake ratio because DIN is preferentially retained relative to particulate silica while silicate is lost as particulate silica. As the loss of silicate thus overestimates of the role of

diatoms in the nitrogen cycle, the observed high loss of DIN relative to silicate reflected by the low Si:DIN nutrient slopes under the low nutrient condition (Table 4.1) implies an even more dominant role of non-diatoms.

DON removal (4) - Another potential mechanism of PON removal is accumulation and horizontal advective export of total organic nitrogen (TON = PON + DON). Hansell et al. (1997) estimated accumulation and horizontal advection of TON as 27% of the total elemental draw-down of DIN during the NOAA OACES cruises along 110°W, 125°W and 140°W. This extra loss term for nitrogen would lead to a slight lowering of the disappearance ratio of Si:N in the water column nutrients below the sediment trap ratio but could not be observed because of the scatter in the data (Table 4.3).

Silica dissolution (5) - The similarity in the rates of diatom production from fucoxanthin and silica export in ^{234}Th-calibrated sediment traps leaves room for little particulate silica dissolution, a flux which was neglected in Dugdale and Wilkerson (1998). Measurements of particulate silica dissolution in surface waters are available from other studies. Paasche (1973) first suggested that dissolution of diatoms plays an important role in the silica cycle. Silica in small, centric diatoms has been shown to dissolve with specific rates of 0.05-0.2 d^{-1} at 20°C (Nelson et al., 1976). Kamatani (1982) measured particulate silica dissolution for a variety of diatom species. He found a strong species effect on the absolute rate and a strong temperature effect such that the rate constant increased by a factor of 2.3 for each 10°C rise in temperature independent of the species studied. He also found that the rate constant increased by a factor of 4 to 5 after acid cleaning - simulating passage through a gut. The relationship of Kamatani (1982) suggests that the 3.8 °C average euphotic zone temperature difference between FLUPAC (27.3 °C) and EqPac Survey II (23.5 °C) can account for a ~0.1 d^{-1} difference in specific dissolution rate. Nelson and Goering (1978) found dissolution rates equal to diatom growth rates in the Baja California and northwest African upwelling systems. Brzezinski and Nelson (1995) measured specific rates of particulate silica dissolution in sediment traps (~19°C) at the Bermuda Atlantic Time-series Site (BATS) of 0.07 ± 0.03 d^{-1}. Blain et al. (submitted) estimated a specific rate of particulate silica dissolution of 0.4 d^{-1} (~27 °C) during the FLUPAC cruise from the mass balance between ^{32}Si silicate uptake and the flux of silica in sediment traps, suggesting that 92% of biogenic silica produced in the euphotic zone re-dissolved. These studies suggest that dissolution can be a major part of the silica cycle in the euphotic zone,

and imply that diatom growth rates had to exceed 0.2-0.4 d^{-1} in the equatorial Pacific upwelling zone during FLUPAC solely to overcome losses by dissolution before silica can be exported vertically.

Dissolution, the potentially dominant loss term for particulate silica (Brzezinski and Nelson, 1995; Blain et al., 1997), may be the source of the large observed variability between cruises. The evidence is strong that large, dissolution-resistant diatoms were responsible for nitrate-based production during EqPac Survey II. On the other hand, Blain et al. (1997; in press) concluded that 92% of particulate silica produced during FLUPAC dissolved in the euphotic zone. If loss of particulate silica by dissolution is a general feature of the low nutrient condition in the equatorial Pacific, diatom dissolution has a crucial control on the biological pump in this region. It has well documented that dissolution occurs only to non-living diatoms (Lewin, 1961). At present, controls on silica dissolution and removal are poorly constrained. Clearly there is a need to better understanding controls on silica dissolution rand removal in order to correctly model silica cycling.

In this hypothetical scenario of the EUZ biological pump, dissolution loss of diatoms maintains silicate at 1-2 μM levels in two modes of biogeochemical cycling. In the first mode (cold-tongue conditions) nutrients are high and diatom new production is an efficient particle export mechanism. In the second mode (El Niño/warm conditions) nutrients are low, diatom populations have low abundances - presumably because of loss of living biomass through grazing and dissolution - such that silicate levels are maintained at 1 - 2 μM levels with diatoms contributing only a fraction of the new production. This analysis of the EUZ supports the Dugdale and Wilkerson (1998) conclusion that diatoms can dominate the biological pump during conditions of vigorous upwelling (Murray et al., 1994), but also suggests that a second situation of non-diatom pumping may account for the majority of nitrate disappearance (Table 4.1, Figure 4.3). Whereas Dugdale and Wilkerson (1998) concluded that the constancy of silicate concentrations in the equatorial Pacific indicated silicate limitation of total production, I suggest as an alternate view that this constancy may be due to dissolution limitation of particulate silica removal.

ROLE OF IRON AND A NON-STEADY STATE FOOD WEB

The crucial factor for determining the role of diatoms in the biological pump is what controls diatom net specific growth. The relationship between new production and water column and sediment trap silica (Figures 5 and 7) suggests that in situations where specific growth rates of diatom populations are much greater than loss by silica dissolution and grazing, new production by diatoms rises dramatically. The sharp change in nutrient utilization ratio inferred from Figure 4.3 implies a severe change in food web dynamics due to depletion of one of the two macronutrients (DIN or silicate) or a third nutrient such as iron. Uptake limitation of diatoms by silicate has been observed elsewhere in the Sargasso Sea (Brzezinski and Nelson, 1996). Results from Blain et al (1997) from FLUPAC, however, showed no dependency of silicate uptake on silicate concentration, suggesting that silicate uptake limitation is not the crucial factor in the equatorial Pacific. This was further illustrated in the EqPac Survey II data for the "Great Front" in which diatoms were able to draw down silicate completely, evidencing the lack of an absolute concentration threshold for uptake.

There is a wealth of evidence for iron limitation in this region. DiTullio et al. (1993) presented results from incubation experiments in the tropical north Pacific showing co-limitation of specific phytoplankton growth rates by both macro-nutrients and iron. Addition of macronutrients alone had no effect on the diatom population, strong evidence against macro-nutrient limitation. Results from the Feline, EqPac and PlumEx cruises all showed low levels of iron in the EUZ (Johnson et al., 1997) suggesting that iron is exclusively limiting in this region because major nutrients are seemingly plentiful. In addition, during FLUPAC the diatom growth (division) rate was both independent of silicate concentrations and severely depressed (Blain et al., 1997; 0.6 d^{-1} compared to the maximum of 3.7 d^{-1}) implying that some factor other than silicate, such as iron, was limiting diatom specific growth (division).

One method of evaluating the role of iron in this system is to compare observed variability in diatom production with the amount of variability that would be predicted through variability in iron. If iron was the controlling factor on diatom production and the diatom community can be considered homogeneously limited by iron, then variability in diatom production (and biomass) would have been controlled by the

diatom specific growth (division) rate. Diatom community specific growth rates did not change significantly between EqPac Survey I and Survey II. Specific diatom mortality by grazing, however, was lower by about ~0.1 d^{-1} during EqPac Survey II compared to EqPac Survey I (from 0.52 to 0.43 d^{-1}; Latasa et al., 1997), suggesting that variability in grazing, rather than in nutrients, was the dominant controlling factor.

As I have suggested, the change in net nutrient utilization may have been due a shift in the size spectrum of phytoplankton rather than a shift in the specific growth rate. The species composition and size distributions changed dramatically between these time periods (Iriarte and Fryxell, 1995). Landry et al. (1997) provide the convincing argument that differences observed between the two EqPac Surveys were due to the combination of selective increase in growth rates of large phytoplankton (including diatoms) through selective grazing control of smaller phytoplankton (including diatoms). In this scenario, small diatoms grow at their maximum growth rates all times, but large diatoms only match these rates during periods of high iron input. This hypothesis is consistent with the high particulate silica concentrations observed during the EqPac Survey II cruise as larger diatoms are slower to dissolve (Kamatani, 1982). If this hypothesis is correct, then variability in the ratio of Si:N utilization and particle export in the equatorial Pacific is controlled by the variability in the food web structure induced by changes in the intensity of iron limitation.

An ensemble of data types from the EqPac Surveys and Time-series point to the potentially large role of Kelvin Waves and TIWs in changing food web structure in the EUZ. During EqPac Survey I, the euphotic zone was only beginning to rebound from the passage of a series of Kelvin waves which had depressed the thermocline (Kessler and McPhaden, 1995). Consequently, EqPac Survey I had the lowest levels of new production and particle export observed. TIWs serve to lift normally deep (and presumably iron-rich) isopycnals into the euphotic layer for a short period, allowing large diatoms to flourish temporarily. The very nature of variable upwelling may exert a strong influence on the observed variability in production.

The role of non-steady state has long been considered an important factor for polar to subtropical regions, but has been previously thought to be unimportant for the EUZ. Observation of the "Great Front" and comparisons between cruises illustrated the

potential role of Kelvin waves and TIWs in driving diatom control of production and variability in equatorial biogeochemistry. While the frequency, geographical extent and total impact of Kelvin waves and TIWs remains uncertain, the concept of non-steady state is an important area for future efforts in understanding equatorial biogeochemical cycles. Landry et al. (1997) provided a two-fold explanation for the increase in large diatom biomass based on iron and grazing selectivity. The propagation of these waves may also provide an important push towards changing food web structure.

CONCLUSIONS

In summary, evidence in nutrients and sediment traps is strong for diatom control of new production in the equatorial Pacific for some episodes of intense upwelling such as EqPac Survey II. On average, however, the role of diatoms in the biological pump is limited. The presense of high silicate and nitrate concentrations during episodes of high diatom activity are suggested to be a response to iron availability. The limited capacity of diatoms in the biological pump is because the small varieties which are able to grow under the lowest silicate and iron concentrations are only partial contributors to total new production are subject to intense silica dissolution. I suggest that the conditions that determine diatom control of the biological pump are the combination of size-selectivity in iron, grazing (Landry et al., 1998) and dissolution limitation of diatom abundance and the presence of non-steady state conditions such as Tropical Instability Waves which bring high nitrate, silicate and iron waters from depth and allow to flourish the larger, dissolution-resistant, nitrate-utilizing, diatoms prone to sinking.

CHAPTER 5: ^{234}TH-BASED PARTICLE CYCLING IN THE SANTA BARBARA CHANNEL

INTRODUCTION

Coastal areas of the world's oceans are regions of complex circulation, biology and biogeochemistry and the regions most tightly connected to human activities. Intense seasonality of particle export due to phytoplankton blooms are common. These areas probably have a large impact on global carbon cycling, but this is still poorly quantified. In addition, these regions are critical ecosystems for human activities because they support the majority of the world's fisheries (e.g. Ryther, 1969).

In contrast to the High Nitrate-Low Chlorophyll (HNLC) regions of the open ocean where upwelled major nutrients have residence times of many months in the euphotic zone, nutrients are utilized in coastal regions in a matter of weeks. This difference has been proposed to be a consequence of the abundance of the micro-nutrient iron (Martin et al. 1990) and the persistence of seed populations of large, rapidly reproducing phytoplankton such as diatoms, the high sinking velocities of these large phytoplankton, and the high fecal pellet sinking velocities of the large zooplankton which consume them (Alldredge and Silver, 1988). Eppley and Peterson (1979) estimated that neritic and inshore waters, which comprise 3% and 11% of the world's oceans, contribute 46% and 30% of global new production. Chavez and Toggweiler (1995) used physical estimates of nitrogen budgets to estimate that coastal upwelling regions, which comprise 1% of the ocean area, account for 11% of global new production.

The Southern California Bight in general, and the Santa Barbara Channel in particular, are extremely well studied coastal upwelling areas for four reasons: 1) proximity to the immense industrial region of Santa Barbara, Los Angeles and San Diego has stimulated a great deal of research related to the pollution potential, 2) the numerous fisheries have spawned studies on the controls on fish populations, 3) the petroleum industry has stimulated both exploratory geoscience and ecological impact studies and 4)

close proximity to numerous oceanographic institutions has made this region a testing bed for research.

The Santa Barbara Channel is a coastal upwelling region whose biogeochemistry has a variety of important scientific and societal implications. The focus of this study is to describe the mechanism of particle cycling and export from the Santa Barbara Channel using ^{234}Th as an indicator of particle sinking. In particular this work will describe the ^{234}Th content of the spectrum of conventionally measured particles including those collected by bottles, large-volume in-situ filtration, sediment traps, SCUBA diving and colloidal extraction and attempts to better characterize the role of marine snow as a sinking particle phase.

BACKGROUND ON THE SANTA BARBARA CHANNEL

CIRCULATION IN THE SANTA BARBARA CHANNEL

The Santa Barbara Channel (SBC) is a basin off the southwestern coast of the United States that is primarily east-west oriented. The SBC is 100 km long, 45 km wide and 500 m deep. It constitutes the northern end of the Southern California Bight (Figure 5.1). The SBC is bordered by the mainland US to the north and east and the Channel Islands to the south. It is a region of major petroleum production and the site of three large offshore drilling platforms. The surface circulation in the SBC has received a great deal of attention in recent years, because of the ever present risk of oil spills from these platforms.

The surface circulation in the SBC is derived from both the large scale California Current and the variable and intense westerly winds which redirect flow and promote local upwelling. The California Current is a relatively broad (300 km), slow-moving (~10 cm s^{-1}), large transport (10 Sv) southward current along the US west coast (Hickey, 1979). At the northern edge of the Southern California Bight at Point Conception, the coastline jogs abruptly eastward while the California Current continues roughly southward, essentially making the Southern California Bight a backwater. South of the Channel islands, part of the California Current turns eastward and returns northward as the California Counter Current in a large scale anticyclonic eddy. This eddy rejoins the

California Current at Point Conception (Hickey, 1993) and forms a second, cyclonic eddy in the western-half of the SBC.

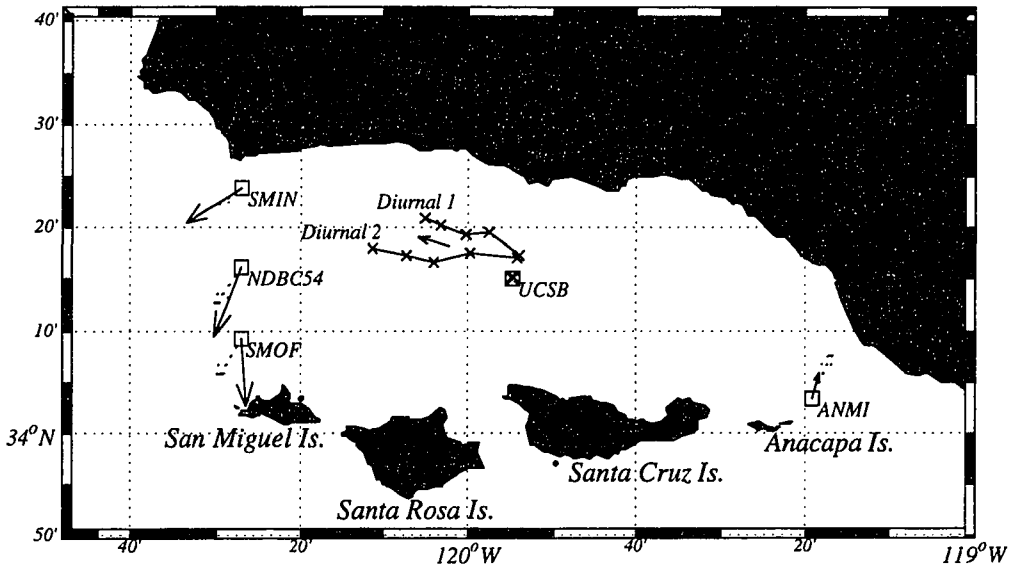

Figure 5.1: Map of the Santa Barbara Channel with position of moorings and cruise stations. Average surface current velocities from two weeks before (dotted arrows) and during (solid arrows) the cruise are shown for San Miguel Inshore (SMIN), San Miguel Offshore (SMOF) and Anacapa middle (ANMI) moored current meters [courtesy of Clinton Winant] and from the National Data Buoy Center 46054 buoy (NDBC54) [courtesy of NDBC]. Positions of ^{234}Th stations are shown in crosses with lines connecting samples taken as the ship followed the drifting traps (Diurnal I, Diurnal II). The position of the University of California at Santa Barbara mooring (UCSB) and the average surface currents determined from the ship ADCP during the cruise are also shown.

Circulation within the SBC has been described in terms of six synoptic states resulting from the tenuous balance between wind stress and pressure gradient across the SBC (Henderschott and Winant, 1996; Harms and Winant, 1998; Figure 5.2). Strong and variable easterly winds promote intense upwelling in March through mid-May (Figure 5.1a). From May through October, the circulation undergoes a 16-day cycle between the upwelling, cyclonic, relaxation and quiescent states (Harms and Winant, 1998). During the late fall and winter, the combination of variable wind stress and pressure gradients produces short-duration unidirectional flow through the channel alternating from east to west.

Upwelling within the channel has generally been considered to be confined to the area near Point Conception and close to the coast (B. Hickey and D. Siegal, personal communication) as a response to the along shore winds. Recent work has suggested, however, that Ekman upwelling within the main basin of the SBC itself may be nearly as strong due to the weak wind field along the coast joining with the intense wind field offshore (Morawitz and Bray, submitted). In either case, springtime upwelling has a remarkably strong effect within the channel, lifting isopycnals approximately 100 m over the course of March and April with upwelling velocities averaging 1.8 m d^{-1} over these months and reaching maximum sustained rates of 3.5 m d^{-1} over periods of a week or more (Morawitz and Bray, submitted).

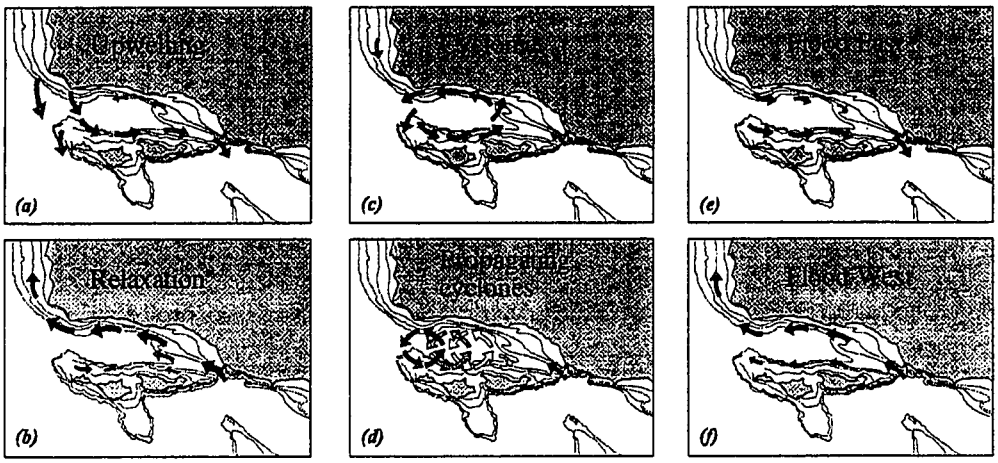

Figure 5.2: Schematic diagram of the six synoptic views of circulation in the Santa Barbara Channel. (a) Upwelling, (b) Relaxation, (c) Cyclonic, (d) Propagating Cyclones, (e) Flood East and (f) Flood West (Modified from Harms and Winant, 1998).

The 1983 *Organization of Persistent Upwelling Structures* (OPUS) study of the Point Conception upwelling system used drifters to study the upwelling center between Point Conception and Point Arguello (Dugdale and Wilkerson, 1989). Drifter deployments showed that water upwelled between Point Arguello and Point Conception moves either in an cyclonic loop westward before turning south and east into the Santa Barbara Channel or travels directly into the Santa Barbara Channel (termed anticyclonic). In either case, upwelled water eventually makes it into the Santa Barbara Channel. Using their estimates of probable drifter tracks to the UCSB mooring in the center of the Santa Barbara Channel

(Figure 1; about 130 km) combined with drifter velocities during the upwelling events (about 20 km/d), gives an average travel time of 7 days for upwelled water to make it from Pt. Conception to the UCSB mooring.

PARTICLE SEDIMENTATION IN THE SANTA BARBARA CHANNEL

Sporadic input of minerals in flood events is the main process filling the inner basins of the Southern California Borderlands. Emery (1960) used ^{14}C accumulation rates to show that sites on the shelves and banks are non-depositional and erosional ($\approx$60 mg m^{-2} d^{-1}). There is low deposition on the slopes ($\approx$200 mg m^{-2} d^{-1}) and high deposition on the basin floors ($\approx$1200 mg m^{-2} d^{-1} on average; $\approx$2500 mg m^{-2} d^{-1} for the Santa Barbara Basin). Sedimentation on the basin floors is thought to involve a combination of direct biogenic and terrigenous input combined with re-deposition of sediment suspended in nepheloid layers from the shelves and slopes.

The Santa Barbara Basin Trap Intercomparison Study took place March 2 - April 19, 1978. Traps were deployed for a month and a half at depths between 162 and 381 m. All traps collected about the same amount and quality of material (1639 $\pm$ 473 mg m^{-2} d^{-1}; Dymond et al., 1981). This mass flux was low relative to ^{210}Pb- and ^{14}C- based sediment accumulation rates (2521 mg m^{-2} d^{-1}; Bruland et al., 1981; Krishnaswami et al., 1973; Emery, 1960). These results suggested that there was a significant horizontal augmentation of flux near the bottom through nepheloid layers. Because the 1978 winter was particularly wet, they suggest that their trap fluxes might be unusually high.

Fleischer (1972) compared the mineralogy of river sediments near the Santa Barbara Basin with sediments at the basin floor and concluded that the sediments were composed primarily of minerals illite, montmorillonite, quartz and kaolinite. The Santa Clara River was the dominant source. Fleischer (1972) also showed that the median mineral grain size was about 2 μm with a mode of about 8 μm. The size distribution had a long tail in what would be the colloidal fraction. The flux and mineralogical data suggested that approximately half of the trap flux was mineral material.

There are thus three main sources of terrestrial material to the basin floor of the Santa Barbara Channel: 1) suspended sediment input at the surface from sporadic,

flood-derived river plumes, 2) shallow re-suspended sediment in nepheloid layers generated by internal waves and the high shear encountered between the California Countercurrent and the coastal shelves and 3) deep nepheloid layers also probably a consequence of internal waves. A combination of processes 1) and 2) appear to augment the trap mass flux by about 100%. Processes 1) and 3) appear to augment sediment accumulation rates by an additional 40%.

THE SANTA BARBARA CHANNEL ECOSYSTEM

There have been numerous ecosystem studies of the Santa Barbara Channel and the Southern California Bight. Ongoing studies include the California Cooperative Oceanic and Fisheries Investigations (CalCOFI; 1949-present) which make large scale surveys of the Southern California Bight (http://www-mlrg.ucsd.edu/calcofi.html). The University of California at Santa Barbara has recently completed a five year time series at the UCSB mooring in the center of the basin (http://www.crseo.ucsb.edu/sbmooring/) and is now continuing the time-series work in the "Plumes and Blooms" Project including transects from Santa Rosa Island to the mainland near Santa Barbara (http://www.icess.ucsb.edu/PnB/PnB.html). There are several books dedicated to the subject of ecosystems in the Southern California Bight (Emery, 1960; Eppley et al., 1986; Dailey et al., 1993).

The Southern California Bight is generally characterized by a two-layer ecosystem consisting of an oligotrophic surface layer (generally the upper 20 m) and a sub-surface productive layer (to 30-60 m) at and below the nitricline within the euphotic zone. Phytoplankton blooms are common in the winter and spring throughout the Southern California Bight due to an intensification of upwelling. The Santa Barbara Channel is in general more eutrophic than the rest of the Southern California Bight due to its relationship to the Point Conception upwelling center.

The Santa Barbara Basin Trap Intercomparison Study (March-April, 1978) - This study estimated POC export at 5.4 mmol C m^{-2} d^{-1} from three types of traps moored almost two months in the center of the Channel at depths between 162 and 341 m. The allochthonous component can be accounted for by assuming the mineral component of the traps had the organic carbon content of shelf sediment (1.2%; Emery, 1960 - Figure 178).

This lowers the flux to 4.4 mmol C m^{-2} d^{-1}. Dunbar and Berger (1981) show that 60-90% of the trap flux was in the form of fecal pellets, which were also composed of >83% fine-grained clays and quartz. This composition was indistinguishable from that determined by Fleischer et al. (1972). $CaCO_3$ and SiO_2 contributed little to the flux (3% for $CaCO_3$ and 6% for SiO_2 by mass). Sinking velocities in fecal pellets were estimated to be rapid (71-1694 m d^{-1}). They suggested that the reason for the high flux is due to the mineral component and that the clays increase the export efficiency of the biological pump (e ratios).

OPUS (April-May, 1983) - New production was studied in the OPUS program (April - May, 1983) using time series at the upwelling center, drifters deployed from the upwelling center and transects between Point Conception and Anacapa (Dugdale and Wilkerson, 1989). They showed that the combination of biomass accumulation and optimization of phytoplankton physiological state both serve to escalate, accelerate or "shift up" new production in newly-upwelled waters and suggested that the acceleration was proportional to the concentration of nitrate in the upwelled water. Their results showed that the intense observed variability in new production was related spatially to the advective regime and temporally to wind-driven upwelling events and phytoplankton physiological processes. Their drifter deployments showed that water upwelled between Point Arguello and Point Conception moves either in an cyclonic loop westward before turning south and east into the Santa Barbara Channel or travel directly into the Santa Barbara Channel (termed anticyclonic). They estimated that it took 9-10 days for the water mass to achieve maximum new production over which the water mass traveled 36 to 595 km with apparent velocities of 8.6 to 43.3 cm/s. Blooms arising from these events thus often reached their maximum in biomass within the Santa Barbara Channel.

CaBS (1983-1990) - This study (Jackson et al., 1989; 1992) took place in the Santa Monica and San Pedro Basins. These basins are in general farther away from upwelling centers and consequently more oligotrophic than the Santa Barbara Basin. They obtained a tight carbon budget for May, 1986 as summarized in Table 5.1. Primary production, new production and particle export were all high with an f-ratio of 0.15 (new production/primary production) and an e-ratio of 0.21 (POC export/primary production). Macrozooplankton and bacteria grazing consumed 29% and 55% of the primary production, respectively. The microzooplankton component of grazing was not measured.

The carbon budget observed during the May 1986 CaBS revealed an important role for macrozooplankton, consistent with the general oceanographic paradigm that coastal areas regions of relatively large-sized ecosystems with high new production and particle export (e.g. Eppley and Peterson, 1979).

Table 5.1: Summary of organic carbon inventory and flux results of Jackson et al. (1989) from the CaBS in Santa Monica Basin.

Biomass ($mmol\ m^{-2}\ d^{-1}$)	Above Nitracline (0 - 16 m)	Within Nitracline (16 - 39 m)	Associate flux ($mmol\ C\ m^{-2}\ d^{-1}$)	Above Nitracline (0 - 16 m)	Within Nitracline (16 - 39 m)
Phytoplankton	106	88	Primary production	53	52
			New production	3.3	12.4
Microflagellates	1.3	1.3			
Mesozooplankton	12	12	Grazing	11	19
			Fecal pellet prod.	3.3	5.8
Bacteria	180	82	Bacterial intake	34	24
Total particles	336	396			
Detritus (by diff)	36	203	Particle Export		22
			Deep sediment trap flux		3.9
			Sediment oxidation		2.4
			Burial		1.4

Augmentation of the deep sinking flux through downslope transport as suggested by Emery (1960) was confirmed during CaBS in Santa Monica Basin using ^{14}C (Williams et al., 1992). Interpretation of this work relies on the historical record of atmospheric ^{14}C which increased from 0 per mil before 1957 to a maximum in the 1960s due to nuclear weapons testing and decreased to +200 per mil by 1986. This signal is reflected in the Dissolved Inorganic Carbon (DIC) of surface seawater and the particulate organic carbon (POC) and dissolved organic carbon (DOC) produced from it. Comparison between the various DIC, POC and DOC components shows a number of salient features of Southern California Bight biogeochemistry (Table 5.2). Most important of these to this study is that DOC is of the order 1000 years old and that while surface POC is "new" (less than 30 years old), deep POC is a mixture of "old and new".

Bacterial dynamics during CaBS (Azam et al., 1992) showed that: 1) Bacterial carbon in the euphotic zone was 0.5-2.0 times the phytoplankton carbon. 2)

Bacterial carbon demand in the euphotic zone was equivalent to 30-60% of primary production. 3) Below the euphotic zone bacterial carbon demand was equivalent to ≥80% of the attenuation of sinking carbon. 4) Bacteria provide 95% of biogenic particle surface area while phytoplankton provide only 1% with the remainder in microflagellates and viruses. Azam et al. (1992) suggested that since bacteria provide so much of the surface area available for ^{234}Th adsorption, phytoplankton sinking alone cannot account for the observed ^{234}Th sinking flux.

Table 5.2: Summary of ^{14}C results of Williams et al. (1992) from the CaBS in Santa Monica Basin as well as each result's implications for the cycling of organic matter in the Southern California Bight.

Sample	^{14}C (per mil)	Implication
DIC (5 m)	+94	DIC is a mixture of "old" and "new"
Suspended POC (5 m)	+110	surface POC is "new"
Trap POC (100 m)	+77	trap POC is mostly "new"/post-bomb
Suspended POC (80, 100 m)	+106	trap POC is older than suspended POC - due to the lateral POC component
Suspended POC (510 m)	+27	deep POC is reworked and old
DOC (5 m)	-197	surface DOC is old, 1760 yr.
DOC (100 m)	-314	deep DOC is older, 2605 yr.

ROLE OF MARINE SNOW

Large (>1 mm) aggregates are thought to provide a major contribution to the particle export flux. Much of particle export out of the euphotic zone can be in the form of these large, rapidly-sinking aggregates (Fowler and Knauer, 1986). Aggregation also serves as a concentration mechanism that enhances grazing (Alldredge and Silver, 1988) and bacterial consumption (Alldredge et al., 1986). Aggregation also promotes sheltering and highly reducing micro-environments (Alldredge, 1989). Studies have shown that 20 ± 13% of particulate mass and 21 ± 15% of total particulate carbon (Alldredge, 1979) as well as 16 ± 11% of chlorophyll and 2.3 ± 3.2% of primary production (Alldredge and Cox, 1982) in the Santa Barbara Channel can occur in this form of large aggregate. Alldredge and Gotschalk (1988) characterized the sinking rates of these large aggregates using SCUBA at 74 ± 39 m d^{-1}. Using an average concentration of aggregate carbon of 2.7 μM (Alldredge, 1979), the sinking flux of aggregates was estimated to be 197 ± 185 mmol C m^{-2} d^{-1} for the Santa Barbara Channel. Even the lower limit of this range, 12 mmol m^{-2} d^{-1}, is more than double the estimated sinking flux in sediment traps from the Santa Barbara

Basin Trap Intercomparison Study. Clearly, marine snow has the potential to account for most of the export flux. Comparison of the trap and marine snow estimates suggests that sediment traps do not effectively measure the sinking flux of marine snow.

The role of marine snow is expected to be highly variable both because the aggregates themselves are extremely patchy spatially and because their production, which appears to occur specifically at the termination of a phytoplankton bloom, is episodic. The patchiness of marine snow has been documented using in-situ camera studies (A. Alldredge, personal communication). A blooms was simulated in a mesocosm tank as part of the Significant Interactions Governing Marine Aggregation (SIGMA, 1993) study. After 8 - 12 days a phytoplankton bloom, mass aggregation and settling event resulted (Alldredge et al., 1995). This timescale is identical to that predicted by the "shift-up" hypothesis for this region (Dugdale and Wilkerson, 1989) and illustrates that marine snow production and sinking can be intensely episodic. The biogeochemical significance of marine snow is thus extremely difficult to ascertain by direct measurement. One of the goals of this study was to use ^{234}Th as an independent tracer of particle sinking to evaluate the significance of marine snow to particle export.

Use of ^{234}Th in the Southern California Bight

Moore et al. (1981) conducted radionuclide measurements during the Santa Barbara Basin Trap Intercomparison Study. They calculated the flux of ^{210}Pb, ^{210}Po and ^{228}Th from their water column deficiencies and measured flux to sediment traps. Because the trap flux was greater than the deficiency flux, they argued that there is "transient stripping" occurring. This means that waters advected into the basin are stripped of radionuclides. They suggested that the half-live of ^{210}Po (106 days) was too long for that isotope to accurately represent scavenging within the basin as its efficiency integrates over too long a time scale. They suggested that the half life of ^{234}Th (24 days) was short enough to represent local process. They made the first attempt to calibrate the accuracy of sediment traps using ^{234}Th. They measured a ^{234}Th:^{238}U ratio of 0.55 at 25 m and used a single profile of ^{234}Th from 50 miles to the southwest in the California Current where ^{234}Th:^{238}U = 0.56 at 25 and averaged 0.72 in the upper 150 m (Knauss et al., 1978) to estimate the ^{234}Th deficiency. From this they concluded that there was no significant difference between the ^{234}Th trap flux (3836 dpm m^{-2} d^{-1}) and the ^{234}Th deficiency (3014 dpm m^{-2} d^{-1}).

During the first CaBS in the Santa Monica Basin (October 1985), Huh and Beasley (1987) measured profiles of dissolved and particulate thorium isotopes. Particulate ^{234}Th activities were quite low (0.10 - 0.21 dpm/l) throughout the water column. Dissolved ^{234}Th activities were about 1.2 dpm/l in the upper 50 m. The sum of dissolved plus particulate ^{234}Th came into equilibrium with ^{238}U (2.4 dpm/l) near 150 m resulting in a ^{234}Th deficiency in the upper 150 m of 2092 - 2496 dpm m^{-2} d^{-1}.

GOALS OF THIS STUDY

Previous work has suggested that the Santa Barbara Channel is a region of intense and sporadic particle export (Dugdale and Wilkerson, 1989) in which marine snow may play an important role (Alldredge and Silver, 1988). It had been suggested that the marine snow component of particle export was not accurately estimated from sediment traps (Alldredge, pers. comm.). Furthermore, early ^{234}Th studies suggested that this isotope could be a sensitive tracer of marine snow as an additional component of the particle flux (Bruland et al., 1981). The combination of these factors lead me to undertake the present study. The primary goals of this study were to establish the magnitude and mechanism of particle sinking in this coastal upwelling regime, specifically to quantitatively evaluate the role of marine snow in the particle flux.

A secondary goal of this study was motivated by my early work with the EqPac program. As discussed in Chapter 3, two methods of estimating the C:^{234}Th ratio sinking particles were used during EqPac: sediment traps and large volume filtration. These methods gave very different C:^{234}Th ratios for sinking material and subsequently very different particle export estimates (Buesseler et al., 1995; Murray et al., 1996; Bacon et al., 1996). I decided to compare the results of these two techniques with a third, independent method of estimating the C:^{234}Th ratio of sinking particles, marine snow.

Finally, I have been able to take advantage of a parallel study of colloids that was also undertaken during this cruise to describe the ^{234}Th content of particles across the entire size spectrum of particles in the marine environment. The Santa Barbara Channel was chosen because of its: well-characterized circulation patterns, characteristic spring upwelling and phytoplankton blooms, history of marine snow and sediment trap research and proximity to the laboratories at the University of California at Santa Barbara (UCSB).

METHODS

CRUISE DESCRIPTION

Sampling took place April 1-9, 1997 aboard the R/V Point Sur. High winds and rough seas prevented most water column sampling on April 1, 8 and 9. The sampling scheme centered around two diurnal studies of biological abundance and production that began just north of the UCSB mooring (Diurnal I - April 4-6; Diurnal II - April 7-9; Figure 1). Each Diurnal study initiated with a hydrocast for the primary production array at 0400. An array of drifting sediment traps was deployed at 0500 to be recovered after 51 hours. A second drifting array was then deployed pre-dawn at 0600 on the first day of each Diurnal study for primary (^{13}C), new ($^{15}NO_3$) and silicon (^{32}Si) production (Shipe et al., in prep) and net and gross oxygen production. This array was recovered after sunset at 2100. Water column sampling was performed along the track of the drifting sediment trap array. The ship's CTD rosette of 30 l Niskin bottles was fitted with sensors for temperature, salinity, beam attenuation and fluorescence. Nutrients (NO_3, PO_4 and H_4SiO_4) and particulate chlorophyll, phaeopigments and organic carbon (POC and nitrogen (PON) measurements in bottles were performed at UCSB. Biogenic and lithogenic silica in bottle and trap samples were measured at UCSB (Shipe et al., in prep.).

WATER COLUMN ^{234}TH

Measurements of ^{234}Th were made using the combination described in Chapter 3 (Dunne et al., submitted-a) of an integrated sample approach and vertical profiles of discrete samples. The integrated sampling technique was used to measure the average ^{234}Th activity in the 0-75 m and 75-150 m intervals in order to estimate the ^{234}Th deficiency over the traps at 75 m and 150 m depths. Station locations for this sampling are shown in Figure 1. For the integrated approach 3.6 l samples of seawater were taken at 15 m intervals (0, 15, 30, 45, 60 and 75 for 0 - 75 m samples; 75, 90, 105, 120, 135 and 150 m for 75 - 150 m samples) and combined into a single sample. Three discrete profiles of total and dissolved ^{234}Th were taken in the upper 100 m (0, 20, 40, 55, 75 and 100 m) using a CTD rosette with 30 l Niskin bottles. The first cast was at the UCSB mooring (April 2), the second was at the recovery point of the traps after the conclusion of Diurnal I (April 6) and the third was before recovery of the traps during Diurnal 2 (April 8). Approximately

10 l of seawater were taken for total ^{234}Th before the 30 l Niskin bottles were pressure filtered through a 1 μm Nuclepore filter for collection of approximately 15 l of dissolved ^{234}Th. Particulate ^{234}Th was measured on the 1 μm Nuclepore filters from the April 6 and April 8 profiles. Samples were processed using the analytical methods described in Chapter 3 (Dunne et al., submitted-a) and Murray et al. (1996). The efficiency of ^{234}Th recovery was determined using a ^{230}Th yield tracer with subsequent beta and alpha counting. Analytical uncertainty in ^{234}Th was 0.12 dpm/l or 6% of the total.

Sediment Traps

Two similar but slightly different Particle Interceptor Traps (PIT) were used. The UW-PITs were described in Chapter 3. The UCSB-PITs were of a similar design but had slightly smaller dimensions. Both types of traps were deployed at 75 m and 150 m for 51 hours on 4/4 and 4/7 using the methods described in Murray et al. (1996) and Chapter 3. Meticulous visual scans by both naked eye and microscope revealed surprisingly few zooplankton swimmers (<3 each) which were subsequently picked. UW-PITs were analyzed for ^{234}Th and total mass as described in Chapter 3 (Dunne et al., submitted-a). Chloride was analyzed to correct for the mass of seasalt. UW-PITs were also analyzed for Al by flame atomic absorption spectrometry. Particulate organic carbon was measured on UW-PIT trap samples from Diurnal I and UCSB-PIT samples from Diurnal II at UCSB. Total mass and biogenic and lithogenic silica were also measured on UCSB-PITs (Shipe et al., in prep). Some UCSB-PITs (75 m during Diurnal I and a trap at each of the 75 and 150 m depths during Diurnal II) were fitted with a dish of acrylamide gel that was photographed and used to estimate the size distribution of particles caught in the traps (after Alldredge, 1998).

Large Volume Filtration

A single large volume in-situ filtration system (LVFS) was borrowed from J. Bishop at the University of Victoria (now at Lawrence Berkeley Laboratories). The LVFS consisted of a baffling system, a 53 μm Nitex screen pre-filter, two 1 μm quartz filters, a large volume pump and a flow meter connected in series. All sample handling at sea and for the measurement of mass were performed using the methods of Bishop (1999). The system was deployed on the hydrowire to the prescribed depth and turned on for 1

hour using power from a secondary cable attached to the hydrowire. The LVFS was then recovered and vacuum pumped to remove the excess seawater within the system. The filter assembly was then detached, taken into the lab and disassembled. The filters were placed on a vacuum pump assembly, rinsed with 30 ml of weak (1%) $NaHCO_3$ solution to remove salt and vacuumed to dryness. Filters were then dried in a 50°C oven for 24 hours before storage in plastic bags. Samples were analyzed for mass at the University of Victoria. Subsamples of the 1 µm quartz filters were analyzed for organic carbon, nitrogen, ^{234}Th, Aluminum and chloride (for salt). The 53 µm Nitex pre-filters were analyzed for N, ^{234}Th, Al and chloride (for salt).

Marine Snow

Seven mid-morning SCUBA dives were performed on April 3, 4, 5, 7 and 8 for collection of marine snow between depths of 10 m and 20 m. Samples of marine snow were taken using syringes into three size fractions: small (nominal diameter 1 mm - 3 mm), medium (nominal diameter 3 mm - 5 mm) and large (nominal diameter 5 mm - 10 mm) as described in Alldredge (1991). Splits of between 30 and 234 aggregates of each size class were filtered onto pre-weighed 1 µm Nuclepore filters for measurement of mass, ^{234}Th and chloride (for salt). Splits were also analyzed for mass, particulate organic carbon and particulate organic nitrogen at UCSB.

Colloids

Samples were taken mid-morning at 15 m on April 2, 3, 4, 6, 7 and 8 for analysis of colloids using six 30 l Niskin bottles. Bottles were pressure filtered sequentially through a 1 µm Nuclepore filter and a 0.2 µm Millipore filter into 20 l polyethylene cubitainers. Single water samples for the <1 µm and <0.2 µm fractions were also taken during this process. The remaining 80 l were transferred to a polycarbonate tank. Colloidal separation proceeded over approximately 6 hours as the <0.2 µm filtered water was pumped across either a 1 KD or 3 KD (on alternate days) cross-flow ultra-filtration cartridge. The "truly dissolved" (<1 KD or <3 KD) filtered water was collected in a second polycarbonate tank. When the colloidal fraction (>1 KD or >3 KD, <0.2 µm) was concentrated down to approximately 2-3 liters, cross-flow filtration was terminated. Triplicates of the "truly dissolved" fraction, a single colloidal fraction and a three sequential

acid rinses of the two tanks and the cross-flow filtration system (1 N HCl in artificial seawater) were taken. Dissolved organic carbon and ^{234}Th were measured on all fractions.

OXYGEN PRODUCTION

In-situ dissolved O_2 was measured during each production array deployment in light, dark and $HgCl_2$-killed 125 ml glass bottles of the standard type used for Winkler titration. Samples were collected using conventional techniques under low illumination (<0.2 μmol photons m^{-2} s^{-1}). "Killed" samples were spiked with 100 μl of saturated $HgCl_2$ solution. All samples were kept in the dark before deployment. "Dark" and "killed" bottles were placed in black, plastic bags. All bottles were hung on the production array using plastic netting. During recovery of the production array, samples were taken aboard, kept in the dark and immediately measured for O_2 using the Winkler method. Analytical precision was estimated from replicates to be 0.3 μM O_2 (0.3%).

RESULTS

CURRENTS

Winds at the NDBC54 mooring (Figure 5.1) were steady from the Southwest averaging 13 knots for the two weeks before the cruise and 19 knots during the cruise. Winds within the channel were extremely variable in magnitude but always upwelling favorable (e.g. from the west). The winds measured on the ship averaged 12 knots from the west with sustained winds averaging over 20 knots on the evenings of April 3, 6, 7 and 8 and reaching 30 knots on the April 8. Observations of surface mean flow from current meter moorings (ANMI, SMIN and SMOF, C. Winant, pers. comm.; NDBC54, courtesy of the National Data Buoy Center) are shown in Figure 5.1 for the two weeks before the cruise (dashed arrows) and for during the cruise (solid arrows). The average surface current measured using the Pt. Sur's ADCP (relative to 119 m) is also shown. The presence of westward flow between the UCSB mooring and the mainland and at the eastern (ANMI) and western (SMIN) mouths of the Channel are indicative of a strong California Countercurrent during the cruise. The strong southward velocity component along the western mouth of the Channel (SMIN, NDBC54 and SMOF) is indicative of the upwelling that characterizes this season and reflects the westerly winds that

were prevalent during the cruise. The slightly eastward velocity at SMOF is consistent with counterclockwise gyre circulation in the western half of the channel during the cruise (but not during the previous two weeks). Overall, the observed circulation pattern was consistent with the Upwelling/Relaxation synoptic states characteristic of the season (Figure 5.2a,b; Harms and Winant, 1998). Subsurface velocities from the ship ADCP were constant in the upper 25 m (10-20 cm/s) and decreased roughly linearly with depth below 25 m to approximately half the surface value (5-10 cm/s) by 100 m at NDBC54. Tidal cycles and wind-induced oscillations in currents were both observed to be of slightly greater magnitude than each of the arrows. The strong cyclonic eddy structure characteristic of the western half of the SBC was apparent in satellite temperature during the cruise (Figure 5.3).

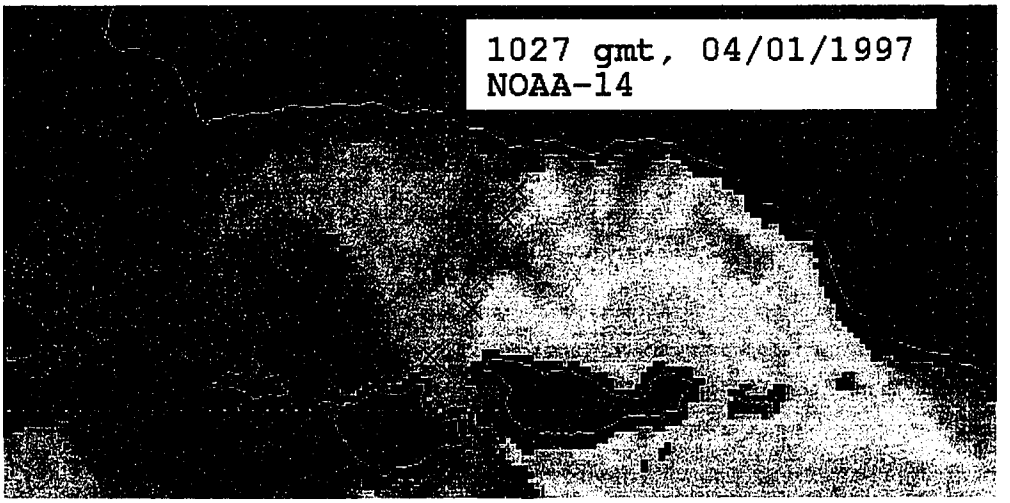

Figure 5.3: AVHRR surface temperature in the Santa Barbara Channel from the NOAA-14 Satellite. The color scale is such that blue indicates 12°C and green indicates 15°C. Red x-marks indicate stations along the Institute for Computational Earth System Science - Plumes and Blooms project. Courtesy of NOAA and ICESS.

HYDROGRAPHY, NUTRIENTS AND BIOMASS

Contours of temperature (Figure 5.4A,B), nitrate (Figure 5.4C,D), chlorophyll (Figure 5.4E,F; from fluorescence calibrated from discrete bottle measurements; [Chl (μg/l)] = 2.624·[flour (m^{-1})] - 0.039, r^2 = 0.82) and particulate mass (Figure 5.4G,H; from beam attenuation calibrated from Hall et al., in press; C_p (μg/l) =

1596·[beam (m^{-1})] - 573) are shown as a function of time for Diurnal I and II in Figure 5.4. During Diurnal I, the surface warmed from 13.8°C to 14.7°C while the 10°C isotherm rose from about 86 m to about 66 m as the sediment trap array drifted northwest (Figure 5.4a; Figure 5.1). During Diurnal II, the surface cooled from 14.9°C to 13.3°C while the 10°C isotherm rose from about 89 m to about 52 m as the sediment trap array drifted west (Figure 5.4B; Figure 5.1). Mixed layer depths ($\Delta\rho$ = 0.125; Gardner et al., 1995) averaged 20 ± 6 m. Isopleths of nitrate were relatively stable during Diurnal I (Figure 5.4C) whereas during Diurnal II, the 21 μM isopleth rose from 75 m to 45 m (Figure 5.4D). Surface values of nitrate were lowest at the beginning of Diurnal II (2.6 μM) and highest at its end (7.5 μM).

With 1% light levels at 45 m and 0.1% light levels at 60 m, the euphotic zone was approximately half as deep as in the typical open ocean. The subsurface chlorophyll maximum averaged 0.9 μg/l at 14 m (Figure 5.4E,F). A maximum value of 1.7 μg/l was observed at 8 m near the UCSB mooring the evening of April 6 between Diurnal I and Diurnal II. Chlorophyll inventories in the euphotic zone (0-60 m) varied between 20 mg m^{-2} and 45 mg m^{-2}, averaging 31 mg m^{-2}. They increased from 22 mg m^{-2} to 37 mg m^{-2} during Diurnal I and from 32 mg m^{-2} to 39 mg m^{-2} during Diurnal II. Beam attenuation based particle concentration in the upper 45 m closely followed fluorescence-based chlorophyll (Figure 5.4G,H). A persistent intermediate nepheloid layer between the depths of 50 m and 90 m was also apparent in beam attenuation. Particulate concentrations at this depth were approximately twice that at depths above and below. This layer followed the 10°C isotherm (equivalent to the σ = 26.1 isopycnal). Wind forcing was an important contribution to biomass variability, accounting for a majority (61%) of the variability in the beam attenuation-based particle inventory. The correlation between wind speed and chlorophyll inventory was lower, though still significant at the 5% level, and accounted for 18% of the variability.

The most impressive feature of Figure 5.4 is the High Nitrate-Low Chlorophyll (HNLC) quality of the data. In some regions this is a permanent feature (e.g. Landry et al., 1997). In the discussion section, I show that the low biomass condition observed during the cruise was a temporary consequence of non-steady state upwelling too recent to have completely "shifted-up" (Dugdale and Wilkerson, 1989) and accumulated biomass.

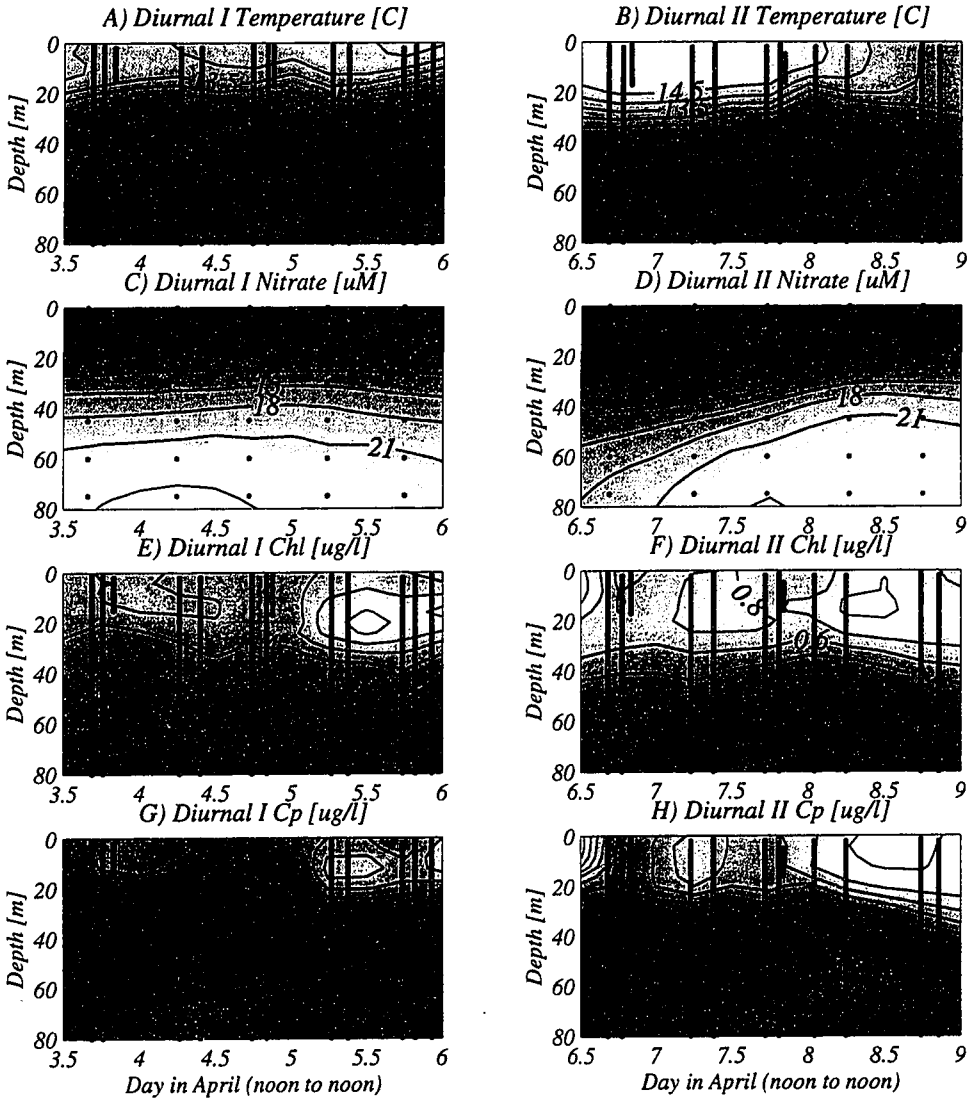

Figure 5.4: Contours of temperature (°C; 5.4A,B), nitrate (μM; 5.4C,D), chlorophyll (μg/l; 5.4E,F) and particle mass (μg/l; 5.4G,H) from hydrocasts during Diurnal I and Diurnal II versus depth in the upper 80 m. X-axis refer to days in April, 1997 with noon as whole numbers. Black points indicate hydrocast data.

From the variability in all four parameters in Figure 5.4, it is clear that neither Diurnal I nor Diurnal II achieved the goal of tracking the evolution of a single water mass. It is thus impossible to make the Lagrangian approximation of spatial independence.

Given the variability observed near the UCSB mooring and along the westward track of each Diurnal study, it is also inappropriate to make a steady-state approximation for this data set. The Diurnal studies appear to have tracked the variable process of mixing between California Countercurrent water and either recently upwelled Point Conception water which subsequently rounded the cyclonic gyre or water upwelled directly within the basin.

WATER COLUMN ^{234}TH

The variability and HNLC qualities of the core data (Figure 5.4) are also apparent in the water column ^{234}Th data. Integrated estimates of average total ^{234}Th activities and associated ^{234}Th deficiency relative to ^{238}U in the upper 75 m are shown in Figure 5.5. ^{234}Th was close to equilibrium before Diurnal I, decreased steadily during Diurnal I and then was erratic during Diurnal II. The average 0-75 m ^{234}Th of 2.04 ± 0.26 dpm/l (n=12). Because the activities were generally high, near the equilibrium value of 2.37 dpm/l, the moderate variability in the activity (12%) translated into large variability in the ^{234}Th deficiency (76%). Integrated estimates of total ^{234}Th activities between 75 m and 150 m averaged 2.32 ± 0.29 dpm/l (n=9) and demonstrated no significant deficiency.

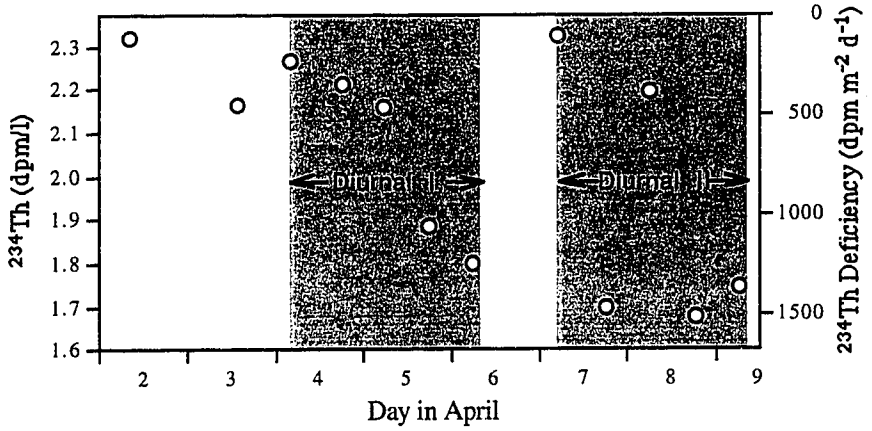

Figure 5.5: Average ^{234}Th activities (dpm/l) and associated ^{234}Th deficiencies relative to ^{238}U (dpm m^{-2} d^{-1}) for 0 - 75 m using the integrated method. X-axis refer to days in April, 1997 with noon as whole numbers. Gray areas designate Diurnal studies. Background ^{238}U activities averaged 2.37 dpm/l for 0 - 75 m.

Profiles of discrete total, dissolved and particulate ^{234}Th are shown in Figure 5.6. Total ^{234}Th activities (Figure 5.6A) were strongly deficient relative to ^{238}U in

the mixed layer. Below the mixed layer, ^{234}Th activities came to equilibrium with ^{238}U. Dissolved ^{234}Th activities (Figure 5.6B) were constant through the upper 100 m. Particulate ^{234}Th activities (Figure 5.6C) were extremely low at the surface and increased to a subsurface maximum between 50 and 80 m. This subsurface maximum was co-incident with the intermediate nepheloid layer shown in beam attenuation (Figure 5.4G,H) and lithogenic particle distributions from silica (R. Shipe, in prep.) and aluminum (Figure 5.9).

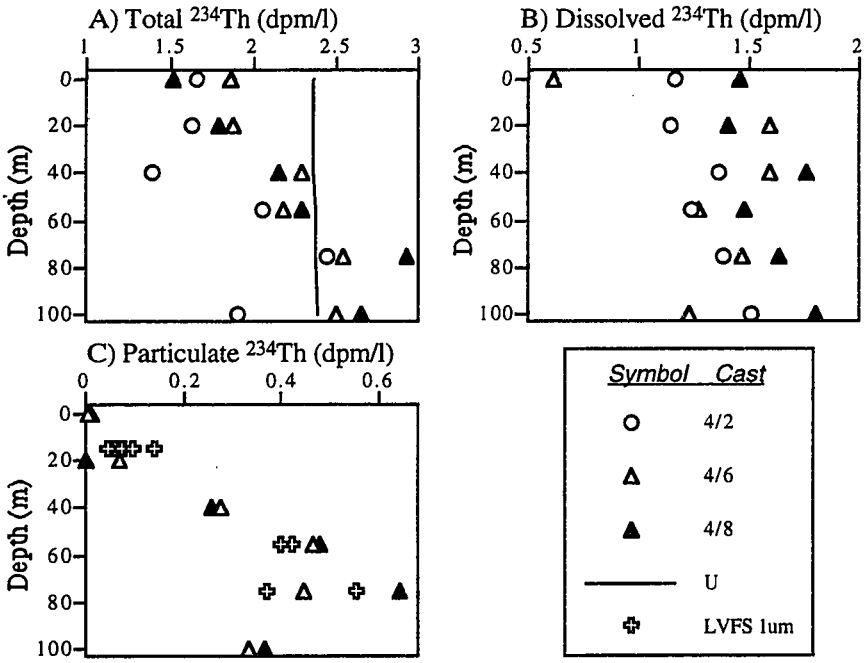

Figure 5.6: ^{234}Th activities (dpm/l) versus depth in the upper 100 m from bottle and LVFS samples. Three profiles of total ^{234}Th (5.6A) and dissolved ^{234}Th (5.6B) taken April 2, 6 and 8 as well as two profiles of particulate ^{234}Th taken April 6 and 8 and 1-53 μm LVFS samples (5.6C) are shown.

SEDIMENT TRAPS

Average sediment trap fluxes of mass, carbon, ^{234}Th, aluminum and calcium and their uncertainties (from triplicate traps) are shown in Table 5.3. Trap fluxes increased with depth between 75 m and 150 m during Diurnal I. No significant difference in trap flux was observed during Diurnal II. Salt correction reduced UW-PIT mass estimates by 8 ± 3%. UCSB-PIT mass estimates were not corrected for salt.

Table 5.3: Summary of sediment trap results for salt-corrected mass (mg m^{-2} d^{-1}), ^{234}Th (dpm m^{-2} d^{-1}), organic carbon (mmol m^{-2} d^{-1}), aluminum (mmol m^{-2} d^{-1}) and calcium (mmol m^{-2} d^{-1}) fluxes. Posted uncertainties are standard deviations of replicate analyses.

Deployment	UW-PIT mass (mg m^{-2} d^{-1})	UCSB-PIT mass (mg m^{-2} d^{-1})	UW-PIT ^{234}Th (dpm m^{-2} d^{-1})	UW-PIT carbon (mmol m^{-2} d^{-1})	UCSB-PIT carbon (mmol m^{-2} d^{-1})	UW-PIT Al (mmol m^{-2} d^{-1})	UW-PIT Ca (mmol m^{-2} d^{-1})
Diurnal I - 75 m	1678 ± 101	3113 ± 504	2442 ± 163	13.1 ± 2.5	----------	2.95	1.12
Diurnal I - 150 m	3122 ± 43	4356 ± 120	4513 ± 294	14.7 ± 3.9	----------	6.57	2.16
Diurnal II - 75 m	2334 ± 82	3211 ± 277	3537 ± 227	----------	19.9 ± 1.6	5.03	1.64
Diurnal II - 150 m	2393 ± 106	2885 ± 148	3185 ± 51	----------	16.0 ± 1.3	4.60	1.47

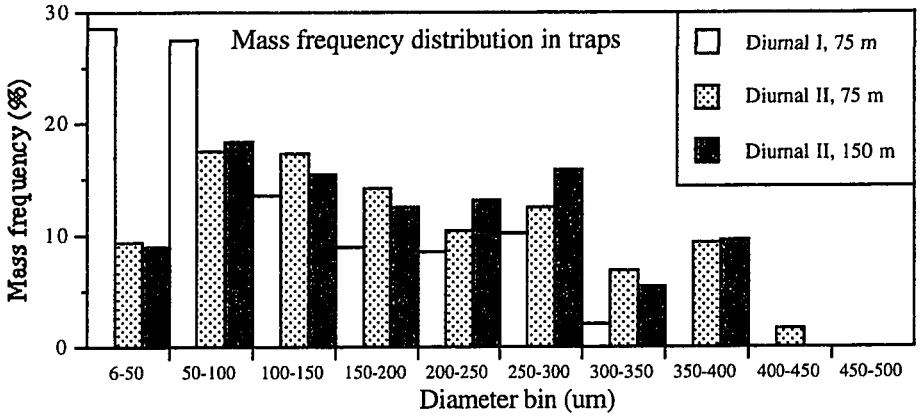

Figure 5.7: Percentile mass frequency of the size distribution (μm) of material in sediment traps using an acrylamide gel method (Alldredge et al., 1997; A. Alldredge, pers. comm.).

The size distribution of material was analyzed using a single sediment trap fitted with an acrylamide gel plate. Sizes were measured using digital, optical methods and converted to mass units (Alldredge et al., 1997; Figure 5.7). Particles caught in sediment traps were predominantly >50 μm in size (61-91%). No particles greater than 450 μm were observed in the traps. Trap particles were larger than ambient particles, smaller than marine snow particles but similar in size to particles caught using 53 μm large volume filtration. This is consistent with two competing hypotheses: 1) the biggest particles (marine snow) aren't a significant component of the sinking flux or 2) traps do not catch sinking material (marine snow). Sediment trap material was also analyzed visually under the microscope. Visually, the material appeared to be composed of approximately 30% fecal pellets, 10% lithogenic material and 60% aggregates of algae, bacteria and detritus.

LARGE VOLUME FILTRATION

Concentrations of mass, carbon, ^{234}Th, aluminum and calcium measured using the Large Volume Filtration System (LVFS) are shown in Table 5.4. Mass and carbon in >53 μm LVFS samples at 15 m were extremely variable. Though significant correlations were observed between the absolute values, the strongest correlations were observed when normalized to ^{234}Th. 66% and 80% of variability in the C:^{234}Th and ^{234}Th:mass ratios, respectively, in >53 μm LVFS samples at 15 m can be accounted for in the correlation with longitude (60% and 63%, respectively, can be accounted for with time).

Table 5.4: Mass (μg/l), organic carbon (μM), ^{234}Th (dpm/l), aluminum (nM) and calcium (μM) data from the Large Volume Filtration System >53 μm and 1-53 μm fractions.

Date/time	Depth (m)	mass (μg l^{-1})	carbon (μM)	^{234}Th (dpm l^{-1})	aluminum (nM)	calcium (μM)
>53 μm						
4/4 8:00	15	251	3.54	0.026		
4/4 20:00	15	127	2.53	0.025		
4/5 9:00	15	77	1.55	0.022	9.0	
4/5 12:00	15	43	0.84	0.017		
4/5 20:00	15	39	0.48	0.014		
4/6 9:00	15	29	0.60	0.019		
4/7 8:00	15	49	0.72	0.012		
4/7 20:00	15	31	0.65	0.016	4.0	
4/8 8:00	15	48	0.15	0.022	4.3	
4/8 19:00	15	27	0.62	0.020		
4/9 8:00	15	20	0.35	0.027		
4/2 16:00	55	10	0.24	0.020	8.8	
4/9 6:00	55	9	0.02	0.028	8.3	
4/4 14:00	75	14	0.32	0.044	10.3	
4/7 11:00	75	23	0.05	0.034	23.8	
1-53 μm						
4/4 8:00	15	219	4.41	0.060		
4/4 20:00	15	114	2.23	0.059		
4/5 9:00	15	86	1.07	0.042	5.2	0.14
4/5 12:00	15	103	1.32	0.042		
4/5 20:00	15	141	2.46	0.043		
4/6 9:00	15	156	1.99	0.077		
4/7 8:00	15	170	1.82	0.075		
4/7 20:00	15	182	2.75	0.071	9.6	0.32
4/8 8:00	15	149	2.69	0.070	15.0	0.21
4/8 19:00	15	168	2.53	0.095		
4/9 8:00	15	212	3.28	0.139		
4/2 16:00	55	143	0.94	0.423	6.5	0.20
4/9 6:00	55	145	0.96	0.396	5.7	0.21
4/4 14:00	75	117	0.66	0.372	10.7	0.19
4/7 11:00	75	215	0.91	0.553	10.8	0.22

The second 1 μm quartz filter collected about 1/3 the mass and carbon as the first 1 μm quartz filter, consistent with previous observations (J. Bishop, pers. comm.).

As observed previously (Altabet et al., 1992; Dunne et al., 1997), large volume filtration estimates of particulate organic carbon (sum of all three fractions) are consistently 2.5-times lower than bottle particulate organic carbon estimates. This has previously been interpreted as a combination of aggregation of sub-micron particles into filtered particles in bottle sampling (Altabet et al., 1992) and the difference in filter pore sizes between these techniques (Dunne et al., 1997).

Estimates of particulate ^{234}Th activities from 1 μm quartz filtered LVFS samples agree well with 1 μm Nuclepore filtered bottle samples (Figure 5.6C). At 15 m, the second 1 μm quartz filter caught approximately the same amount of ^{234}Th as the first (approximately 0.1 dpm/l), while at 55 m and 75 m the second 1 μm quartz filter caught a quantitatively smaller amount and only a small fraction of what was caught on the first filter (approximately 0.03 dpm/l). The observation that so many of the particles which passed through the first 1 μm filter were caught on the second 1 μm filter suggests that at 15 m the (few) particles bearing ^{234}Th were approximately 1 μm in size.

Marine Snow

Results for the mass, carbon and ^{234}Th content in marine snow are presented in Table 5.5. Mass and ^{234}Th in marine snow were extremely well correlated (r^2 = 0.85) with an average ^{234}Th:mass ratio of 0.93 ± 0.31 dpm/mg. No significant size dependency of the marine snow ^{234}Th:mass ratio was observed. Marine snow was also analyzed visually under the microscope and was found to be qualitatively identical to trap material in terms of composition. This is remarkable considering that marine snow aggregates were in general much bigger than sediment trap aggregates (10 mm rather than 0.1 mm). The only difference apparent visually between them was that marine snow occasionally contained dinoflagellates while trap material did not.

Colloids

Summary data from six ultra-filtrations using water samples from 15 m are given in Table 5.6. The directly measured colloidal fraction was quite small for both organic carbon (6% of total) and ^{234}Th (3% of total). A small fraction of the organic carbon (4% of total) and a large fraction of ^{234}Th (42% of total) adhered onto the walls of the ultra-

filtration system and containers and was subsequently recovered in the acid rinses. The low ^{234}Th content of colloidal material corresponds to an upper limit of 0.036 dpm/l for the colloidal ^{234}Th in the acid rinses. This implies that >92% of the ^{234}Th in the acid rinses belonged in the ultrafiltered fraction.

Table 5.5: Summary of results for the volume (ml/agg.), mass (µg/l), organic carbon (µmol/l), ^{234}Th (dpm/aggx10^3) and ^{234}Th:mass ratio (dpm/mg) in marine snow aggregates in small (1 mm - 3 mm), medium (3 mm - 5 mm) and large (5 mm - 10 mm) size classes. Volume and carbon estimates were determined at UCSB.

Date	Size	volume (ml/agg)	mass (µg/agg)	carbon (µmol/agg)	^{234}Th (dpm/aggx10^3)	^{234}Th:mass (dpm/mg)
4/3	small	8.7 ± 6.3	7.0 ± 0.1	0.32 ± 0.17	5.7 ± 2.1	0.81 ± 0.29
	medium	32.6 ± 8.3	21.5 ± 1.6	0.99 ± 0.17	21.1 ± 2.3	0.99 ± 0.18
	large	71.8 ± 21.8	26.3 ± 0.3	1.42 ± 0.12	34.2 ± 6.5	1.30 ± 0.26
4/4	small	22.6 ± 15.0	11.5	0.40 ± 0.08	9.2	0.80
	large	132.0 ± 55.5	53.3	1.48 ± 0.04	45.2	0.85
4/5	small	8.5 ± 5.1	6.3	0.33 ± 0.05	9.3	1.48
	medium	40.6 ± 24.4	58.8	0.70 ± 0.14	43.7	0.74
	large	119.3 ± 52.3	40.7	1.31 ± 0.34	42.0	1.03
4/7	small	13.2 ± 7.5	7.7	0.25 ± 0.20	7.1	0.92
	medium	30.3 ± 11.2	24.0	0.44 ± 0.13	12.0	0.50
	large	59.8 ± 26.6	45.8	1.11	43.8	0.96
4/8	small	9.7 ± 3.8	12.5	0.23 ± 0.04	5.3	0.42

When comparing the various fractions, three inconsistencies are observed in the ^{234}Th mass balance: 1) ^{234}Th in the >1 µm particulate fraction (0.05 ± 0.02 dpm/l) is lower than difference of the <1 µm fraction subtracted from the total (1.72 - 1.32 = 0.40 ± 0.26 dpm/l), 2) ^{234}Th in the 0.2-1.0 µm particulate fraction (0.03 ± 0.01 dpm/l) is less than the <0.2 µm fraction subtracted from the <1 µm fraction (0.25 ± 0.27 dpm/l) and 3) ^{234}Th in the colloid fraction (0.05 ± 0.05) is lower than the ultrafiltered and acid rinse fractions subtracted from the <0.2 µm fraction (0.12 ± 0.28).

As has been observed previously (e.g. Dunne et al., 1997), bottle dissolved and particulate ^{234}Th activities are typically found not to sum to the directly measured total ^{234}Th activity. In this data set, the sum of dissolved and particulate ^{234}Th averaged 0.37 dpm/l less than total ^{234}Th. During colloidal filtration experiments, approximately 0.45 dpm/l of ^{234}Th - 42% of the ^{234}Th filtered- adsorbed onto the container and was subsequently removed by the three sequential acid rinses. Only a minor component (5%) of organic carbon adsorbed onto the container and was subsequently removed by the three

sequential acid rinses. This implies that the ^{234}Th adsorbed onto the walls of the container during the colloidal filtrations was from the truly dissolved phase rather than the colloidal phase. Given this tendency for dissolved ^{234}Th to adsorb on filtration surfaces, we suggest that the difference between total ^{234}Th activity and the sum of dissolved and particulate ^{234}Th activities is due to adsorption of dissolved ^{234}Th during filtration.

Table 5.6: Summary of average organic carbon (μM) and ^{234}Th (dpm/l) results from different size fractions analyzed using bottle and ultra-filtration separations conducted daily during the cruise. Water samples were from 15 m depth.

Size fraction	Organic Carbon (μM)	^{234}Th (dpm/l)
total	116.1 ± 10.6	1.72 ± 0.13
dissolved (<1 μm)	114.5 ± 4.5	1.32 ± 0.22
particulate (>1 μm)	----------	0.054 ± 0.023
dissolved (<0.2 μm)	113.6 ± 4.8	1.07 ± 0.16
particulate (>0.2 μm;<1 μm)	----------	0.029 ± 0.010
colloids (>3KD/10KD; <0.2 μm)	7.0 ± 1.2	0.052 ± 0.054
ultrafiltered (<3KD/10KD)	99.9 ± 7.2	0.45 ± 0.19
Acid rinse	4.9 ± 2.8	0.45 ± 0.13

CARBON AND ^{234}TH CONTENT OF PARTICLES

The percent organic carbon by mass and ^{234}Th:mass ratio in the various particle types measured during this cruise are shown in Table 5.7. Samples of marine snow, LVFS and bottle particles in the mixed layer (near 15 m) had similarly high %C and C:^{234}Th ratios. The ^{234}Th:mass ratio of sediment trap material was a factor of ten higher than marine snow. Colloidal material contained almost no ^{234}Th. The extremely low ^{234}Th content of all size classes of particles in the mixed layer (0-25 m) suggests that either: 1) marine snow, LVFS and bottle particles in the mixed layer have a low adsorptive affinity for ^{234}Th or 2) mixed layer particles were too recently-formed to have adsorbed levels of ^{234}Th characteristic of particles in other marine environments. The large discrepancy in ^{234}Th content between sediment trap material at 75 m and 150 m and all size classes of particles in the mixed layer (0-25 m) suggests the residence time of particles in the surface layer was much shorter than the timescale of ^{234}Th adsorption (1-2 weeks; Dunne et al., 1997) and that either: 1) Particles in the mixed layer were highly altered during their downward passage to the 75 m sediment traps and/or 2) there was a large horizontal input of ^{234}Th-rich material to the sediment traps. LVFS samples at 55 m and 75 m (both 1 μm and 53 μm) had %C and C:^{234}Th ratios similar to sediment trap material.

Table 5.7: Summary of the quality of different particle types in terms of organic carbon (% by mass) C:N ratio (mol/mol), ^{234}Th:mass (dpm/mg) and C:^{234}Th (µmol/dpm) and the number of samples (n). Posted uncertainties are standard deviations of the mean. Range given in parentheses for colloids is the total range. Organic carbon for the LVFS >53 mm fraction was obtained from nitrogen assuming C/N = 6.6.

*+Average of direct (>1 µm) and differenced (total-dissolved,<1 µm) estimates.

Particle Type	%C (g/g*100)	C/N (mol/mol)	^{234}Th/mass (dpm/mg)	C/^{234}Th (µmol/dpm)	n
Marine Snow	43.4 ± 16.8	7.4 ± 0.7	0.93 ± 0.31	36.9 ± 10.3	10
Sediment traps	6.1 ± 1.3	8.9 ± 1.7	1.61 ± 0.14	3.5 ± 0.8	12
1 µm LVFS					
15 m	14.1 ± 2.9	6.0 ± 0.5	0.80 ± 0.17	21.7 ± 7.0	11
55 m	9.3 ± 1.7	6.4 ± 0.3	2.65 ± 0.14	3.1 ± 0.4	2
75 m	6.2 ± 1.8	6.2 ± 0.2	2.92 ± 0.91	1.9 ± 0.04	2
53 µm LVFS					
15 m	18.3 ± 6.3+		0.48 ± 0.35	52 ± 39*+	11
55 m	9.3 ± 1.7+		2.51 ± 0.69	6.2 ± 7.9+	2
75 m	6.2 ± 1.8+		2.35 ± 1.22	4.4 ± 4.1+	2
Net Tow			0.01	3000	1
1 µm bottles*+					
0-20 m		6.7 ± 1.8		182 ± 125	9
40 m		7.5 ± 3.0		18 ± 14	3
60 m		6.6 ± 1.4		9 ± 5	3
75 m		7.8 ± 2.3		5 ± 2	3
100 m		8.9 ± 3.3		8 ± 6	3
Colloids				197 (54-3067)	6

Oxygen Incubations

Results of the oxygen incubation experiments are shown in Figure 5.8. The difference between light and killed samples is an estimate of net O_2 production (Figure 5.8A) while the difference between dark and killed samples measures O_2 respiration (Figure 5.8B). Samples kept in the light of the upper 15 m during Diurnal I and the upper 30 m during Diurnal-II showed significant increases in oxygen concentration over the incubation suggesting relatively high rates of net production (see summary in Table 5.8). Uncertainty in the data makes it impossible to make a quantitative estimate of respiration rates. However, assuming that respiration was constant in the upper 75 m, it is possible to estimate an upper limit of the average respiration rate given the data in Figure 5.8B using the Mann-Whitney U-test. This test suggests that the respiration rate was lower than 0.59 mmol O_2 m^{-3} d^{-1}. Assuming a photosynthetic quotient of 1.25 (Emerson et al., 1997), gives an upper bound for carbon remineralization during the cruise of 35 mmol C m^{-2} d^{-1}.

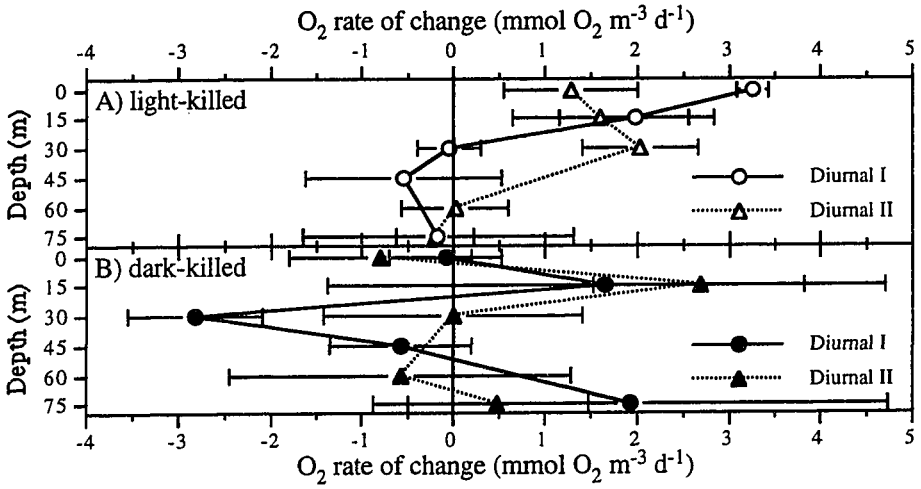

Figure 5.8: Summary of Oxygen incubation results versus depth for the two Diurnal studies. Estimated rates of production minus respiration, or net production (A) and total respiration (B) are shown. Posted uncertainty levels are standard deviations from triplicates. Dark-killed changes are multiplied by 24 and divided by 14 to convert from the incubation period (morning to evening) to a full day.

DISCUSSION

GENERAL ECOSYSTEM STATE

The large variability in nutrient and particle concentrations observed during the cruise is indicative of strong upwelling characteristic of this region in the spring. While nutrient concentrations were high, chlorophyll concentrations rarely exceeded 1 µg/l. These chlorophyll concentrations are only slightly higher than values characteristic of the equatorial Pacific, a classic High Nitrate-Low Chlorophyll (HNLC) region. However, comparisons with CalCOFI data taken after the cruise and ADEOS ocean color data through the month of April show that these conditions did not last for long as the intense upwelling before and during the cruise set the ecosystem for a phytoplankton bloom which realized its production and biomass potential the following week.

Though nutrients were plentiful during the cruise, the euphotic zone was characterized by modest total production as estimated by ^{13}C (Shipe et al., in prep.) with

almost all of it being attributable to new production estimated using ^{15}N (Shipe et al., in prep.) and net O_2 production (Table 5.8). Visual inspection revealed that the marine snow particles were primarily debris-based rather than phytoplankton-based, characteristic of a heavily degraded biomass (Alldredge, pers. comm.). The concentration of particulate organic carbon was high, averaging 12 μmol m^{-3}. Concentration of particulate organic carbon in marine snow was also quite high averaging 0.5 μM with a strong diurnal periodicity. The concentration of organic carbon on >53 μm particles by Large Volume Filtration was not significantly greater than concentration estimates of marine snow. During this initial stage of production "acceleration" (Dugdale and Wilkerson, 1989), the biomass and ^{234}Th budget were characterized by the pre-bloom, non-productive state.

Table 5.8: Summary of integrated production estimates in the upper 75 converted to organic carbon units of (mmol C m^{-2} d^{-1}). Gross primary production estimates by $DI^{13}C$ incorporation (Shipe et al., in prep), sediment trap flux from drifting cylindrical traps, new production by $^{15}NO_3$ incorporation (Shipe et al., in prep.), net production by O_2 change (Figure 5.8A) and remineralization by O_2 change (Figure 5.8A) are shown. Nitrogen estimate of new production was converted to carbon assuming C:N=6.6. Oxygen estimates are converted to C assuming O_2:C = 1.25 (Emerson et al., 1997).

mmol C m^{-2} d^{-1}	Total Production ($DI^{13}C$)	Sediment Trap Flux	New Production ($^{15}NO3$*6.6)	Net Production ($O_{2light\text{-}kill}$/1.25)	Remineralization ($O_{2dark\text{-}kill}$/1.25)
Diurnal-I	71	14 ± 1	71	31 ± 24	≤35
Diurnal-II	66	18 ± 3	111	63 ± 15	

INITIATION OF A PHYTOPLANKTON BLOOM

Measured production estimates indicated new (^{15}N) and net (O_2) production values similar to measured total production - much higher than the measured particle export in sediment traps. The observation of minimal O_2 respiration suggests that part of this difference may be attributed to additional particle export in marine snow. As I will show in the following sections, however, modeling of particle and ^{234}Th distributions during the cruise, however, indicate that remineralization was appreciable and that particle export could not explain all of the difference. The combination of these flux estimates suggests a strong non-steady state condition during the cruise.

Observed variability in chlorophyll and beam attenuation suggest only weak temporal gradients during the cruise. Measured variability in chlorophyll biomass in the

upper 45 m correlated significantly with time, suggesting that the 0-45 m chlorophyll inventory increased at a rate of 9.3 ± 1.6 % d^{-1}. Similarly, beam attenuation increased at a rate of 6.7 ± 2.0 % d^{-1}. Observations after the cruise, however, show intense variability consistent with a phytoplankton bloom.

Comparison between our cruise data and California Cooperative Oceanic and Fisheries Investigations (CalCOFI) data taken at the middle of the Pt. Sur transects (Figure 5.1) indicates the phytoplankton bloom which followed our cruise. The CalCOFI survey on April 16 observed depleted surface nitrate and extremely high subsurface chlorophyll (10 μg Chl/l) concentrations (Figure 5.9). On April 30, a UC Santa Barbara Plumes and Blooms survey found once again elevated surface nitrate (7 μM) and moderately high subsurface chlorophyll (2 μg Chl/l) concentrations at the UCSB mooring (Figure 5.1). Comparison between these three surveys suggests that the intense upwelling provided for an intense phytoplankton bloom immediately after the Pt Sur cruise which subsequently dissipated before the Plumes and Blooms cruise. Comparison of ship observations with ADEOS ocean color data taken during the month of April, 1997 confirmed this sequence of events (Figure 5.10).

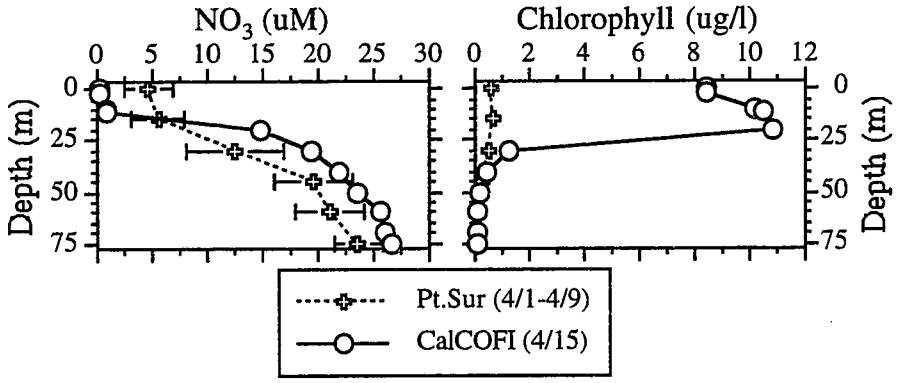

Figure 5.9: Comparison of nitrate (μM) and chlorophyll (μg/l) data from the Pt. Sur cruise between 4/1 and 4/9 (averages with standard deviation uncertainties) and CalCOFI station 82.47 on 4/16. Chlorophyll uncertainties are hidden in the symbol.

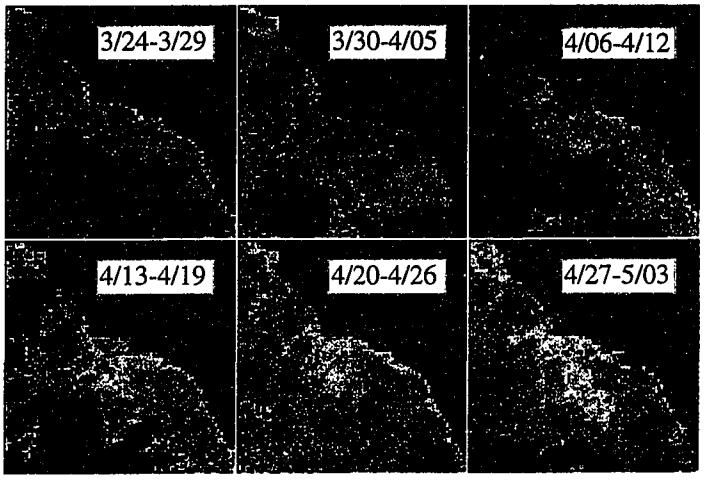

Figure 5.10: Weekly time series maps of ocean color from 3/24-5/3, 1997 from the ADEOS satellite. Each panel shows ocean color off the southern California coast from Monterey Bay (upper left) to the US-Mexico border (lower right) and centered on the Santa Barbara Channel. The color scale is logarithmic from blue (0.1 μg Chl/l) through green (0.8 μg Chl/l) to red (5 μg Chl/l). Data courtesy of the National Space Development Agency of Japan (http://www.eoc.nasda.go.jp/guide/).

The contrasting nitrate and chlorophyll concentrations observed between the Pt. Sur and CalCOFI cruises allows a crude estimate of net production. Over the 7 days between the Pt. Sur and CalCOFI cruises, chlorophyll-based phytoplankton abundance increased by 11 times (138 % d^{-1}) equivalent to a net production of 76 mmol C m^{-2} d^{-1} (assuming C:Chl = 30; Eppley, 1968), equal to the new and total production estimates during the Pt. Sur cruise. Analysis of nitrate change gave similar results. The nitrate decrease in the upper 11 m between the Pt. Sur and CalCOFI cruises corresponded to a net production of 47 mmol C m^{-2} d^{-1}. Below that depth, nitrate increased between the Pt. Sur and CalCOFI sampling periods as a result of the upwelling occurring which occurred sporadically over the months of March and April (see below; Figure 5.12). Including an estimate of upwelling during this time period from the change in temperature at the UCSB mooring (4 m d^{-1}) increases the nitrate-based net production to 78 mmol C m^{-2} d^{-1} in the upper 20 m.

THE TERRIGENOUS COMPONENT

During the Santa Barbara Trap Intercomparison Study high levels of aluminum were observed in sediment trap material. The terrigenous mineral component accounted for 53% of the sinking mass flux (Dymond et al., 1981; Fleischer, 1972). Analysis of fecal pellets suggested that repackaging of mineral material with marine-derived organic material into fecal pellets increased the efficiency of pellet sinking (Dunbar and Berger, 1981).

In this study I estimated the % terrigenous mineral component in sediment traps were obtained based on Si:mass and Al:mass ratios from the mineralogy of Fleischer (1972) for the Santa Barbara Basin. This provided for both aluminum (47%) and lithogenic silica (52%; Shipe et al., in prep.) based estimates of % terrigenous mineral in sediment traps. Our data are consistent with previous estimates (Dymond et al., 1981) that half of the particle export flux at this site is mineral material.

A compilation of the composition of suspended particulate material is given in Figure 5.11. Estimates of particulate organic carbon (μM C and μg/l organic matter) and lithogenic silica(Shipe et al., in prep.) from bottle samples converted to total mineral mass (μg/l) as well as biogenic silica (Shipe et al., in prep.) and $CaCO_3$ (based on the percentage in the 1-53 μm LVFS fraction) are shown (Figure 5.11). Particulate organic carbon was highest in the mixed layer and decreased rapidly below while mineral concentration increased with depth. The 1-53 μm LVFS fraction (Table 5.4) was 17% $CaCO_3$ at 15 m, 41% at 55 m and 13% at 75 m. The mineral mass divided by the sum of all four masses (mineral, particulate organic material, $CaCO_3$ and biogenic silica) gave an upper estimate of the % mineral in bottle material. Mineral material accounted for 4% of total mass in bottles in the mixed layer and increased to a maximum of 29% at 75m. The >53 μm LVFS samples were 2.4% mineral at 15 m and 19% at 55 m and 75 m. The 1-53 μm LVFS samples were slightly lower with 1.5% mineral at 15 m, 9% at 55 m and 15% at 75 m.

Comparison of sediment trap fluxes with particle concentrations gives an estimate of the sinking velocity of mineral material of 13 m d^{-1}, much faster than the equivalent sinking velocity of particulate organic carbon of 3.3 m d^{-1}. This high sinking velocity puts a strong constraint on the horizontal propagation of nepheloid layers. This sinking velocity implies that mineral material at 75 m was input to a nepheloid layer less

than six days previously. It is impressive that mineral material should be observed so close to the surface 10 km offshore. The pervasiveness of the nepheloid layer in the beam attenuation data (Figure 5.4G,H) suggests a nearly continuous generation mechanism, possibly driven by a combination of shear between the California Countercurrent or tidal flows and the sediments and subsequent lateral dispersal by tidal mixing.

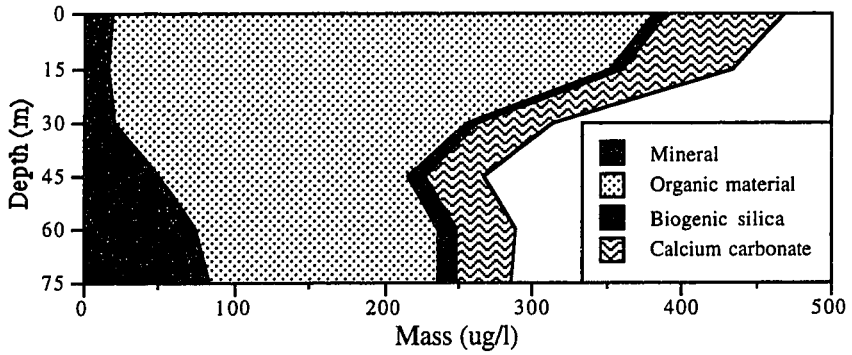

Figure 5.11: Sum of mineral, organic material, biogenic silica and calcium carbonate contributions to total mass (μg/l) in suspended matter versus depth. Mineral is based on lithogenic silica (Shipe et al., in prep.) and mineralogy from Fleischer (1972). Organic material is from bottle samples for particulate organic carbon. Biogenic silica is from Shipe et al. (in prep.). Calcium carbonate was estimated from %calcium carbonate in LVFS 1 μm samples (Table 5.4).

Horizontal input of particulate ^{234}Th from re-suspended sediments to sediment traps is of large concern. If re-suspended sediments equilibrate with respect to ^{234}Th sorption with the surrounding water, then horizontal input of mass should not effect the ^{234}Th budget. However, the timescale of re-suspension and sinking appears to be quite short relative to ^{234}Th sorption and decay. Thus, one would not predict significant exchange between sediment-derived nepheloid layers along their <6 day transit from the sediments to the sediment traps. Unfortunately, the ^{234}Th:mass ratio of shelf sediments in the Santa Barbara Channel is unknown. Assuming ^{234}Th:mass ratio in these sediments equal to the sediment trap ratio, the observation of half the total sediment trap mass flux was mineral suggests that approximately half of the ^{234}Th flux was also derived from re-suspended sediments. This estimate is highly uncertain, however, due to the uncertainty in the residence time of re-suspended sediments in the water column and the ^{234}Th:mass ratio of shelf sediments.

MODELED ^{234}TH EXPORT IN SINKING PARTICLES

The ^{234}Th method of estimating particle export uses the deficiency of ^{234}Th relative to ^{238}U. Observed ^{234}Th activities in the upper 75 m were high and near equilibrium with ^{238}U and quite variable with an average deficiency of 723 ± 313 dpm m^{-2} d^{-1}. Both of these features tend to increase uncertainty in the ^{234}Th deficiency. The high levels of ^{234}Th in the upper 75 m (Figure 5.5) are probably a response to spring upwelling. Observed variability in ^{234}Th in the upper 75 m probably reflects a combination of 1) direct upwelling of high ^{234}Th water 2) mixing between recently upwelled, high ^{234}Th water from Point Conception (which had subsequently made a counter-clockwise loop within the Santa Barbara Channel) and relatively low ^{234}Th California Countercurrent water and 3) "acceleration" of production (and scavenging) in recently upwelled water (Dugdale and Wilkerson, 1989). Because the ^{234}Th budget has multiple sources at non-steady-state, it is difficult to interpret the ^{234}Th data set in the context of a simple model of horizontal or vertical advection or temporal change. Variability in ^{234}Th activities in the upper 75 m significantly correlated with time, longitude (highly significant), wind speed, wind direction, meridional water velocity, salinity, fluorescence (highly significant) and beam attenuation (highly significant). The correlation with longitude was the most significant, accounting for 61% of the variability. When multiple linear regression was attempted to account for additional variance, only wind velocity significant increased the percentage of the variance explained. The combination of longitude and wind accounted for 76% of the variance.

It is tempting to interpret the variability in ^{234}Th as a manifestation of non-steady state particle scavenging. Because the duration of the cruise (8 days) was short relative to the half-life of ^{234}Th (24 days) and characteristic timescales of ^{234}Th scavenging (25-100 days; Dunne et al., 1997), interpretation of ^{234}Th variability as a manifestation of temporal change in the ^{234}Th budget is ill-advised. The generally high ^{234}Th activities at the beginning of the cruise and often lower activities later on during the cruise corresponds to a significant (P=0.03) temporal trend of -75 dpm m^{-3} d^{-1} and a flux of 5597 dpm m^{-2} d^{-1} which is greater than the observed deficiency by a factor of 8. As the variability in temperature, nutrients, chlorophyll and particle concentration showed that the Diurnal studies did not trace a single water mass, the inferred non-steady state component is likely the result of longitudinal gradients and temporally variable winds. Due to the relative

strength of the horizontal gradients relative to the temporal gradients, I have chosen to neglect the temporal component and interpret the variability in terms of horizontal and vertical advection and wind-induced variability.

Estimates of the horizontal advective fluxes driven zonally by the California Current and meridionally by the wind are easily calculated from the data. Least squares regression showed that ^{234}Th activities in the upper 75 m decreased towards the west at 2.1 $\pm$ 0.5 dpm m^{-3} d^{-1} ($P < 0.01$). The average zonal velocity of the drifting traps and the zonal velocity measured by the ship's ADCP was westward at 10 cm s^{-1}. The resultant zonal advective flux was 1216 $\pm$ 434 dpm m^{-2} d^{-1}, giving a sum of deficiency and advective fluxes of 1939 $\pm$ 535 dpm m^{-2} d^{-1}. The combination of longitudinal and wind-driven advective fluxes was 830 $\pm$ 366 dpm m^{-2} d^{-1}, giving a sum of all three modeled fluxes of 1584 $\pm$ 482 dpm m^{-2} d^{-1}. Additionally, the upwelled ^{234}Th flux must be considered.

During March and April, isopycnals were progressively lifted, as shown in moored temperature at the UCSB mooring (Figure 5.12). Upwelling velocities can be estimated from the temporal gradient in temperature multiplied by the vertical gradient over temperature ($w = dz/dt = dT/dt * dz/dT$; Morawitz and Bray, submitted). Using the average vertical thermal structure during the cruise (Figure 5.5) and the vertical gradient in temperature between 3/11 and 5/1 gives average upwelling velocities of 0.6, 1.3 and 2.6 m d^{-1} at 30 m, 50 m and 75 m, respectively. Combined with observed ^{234}Th activities (Figure 5.6), this results in an inferred vertical advection flux of 1125 $\pm$ 1509 dpm m^{-2} d^{-1} (assuming 50% uncertainty in w). Assuming the seasonal average upwelling velocity of 2 m d^{-1} (Morawitz and Bray, submitted), results in a similar vertical advection flux of 1500 dpm m^{-2} d^{-1}. The vertical advection flux increases the total model ^{234}Th sinking flux to 2709 $\pm$ 1526 dpm m^{-2} d^{-1} which is only 21% lower than the average sinking flux of ^{234}Th directly measured in sediment traps (3420 $\pm$ 797 dpm m^{-2} d^{-1}). Horizontal augmentation of flux by terrigenous component can easily account for the difference between the modeled and observed ^{234}Th sinking fluxes. Because of the large uncertainty in the model ^{234}Th sinking flux, no ^{234}Th correction has been made to the sediment trap fluxes such that the collection efficiency of sediment traps is essentially assumed to be equal to one.

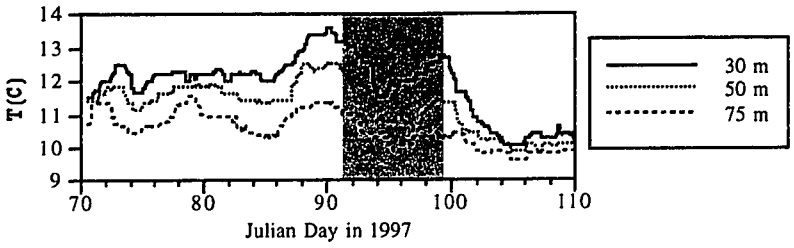

Figure 5.12: Temperature (C) records at 30 m, 50 m and 75 m at the UCSB mooring during March and April, 1997 (courtesy of Alison Murray). The shaded region specifies the time period of the cruise.

One of the original goals of this study was to constrain particle export in the Santa Barbara Channel using the total ^{234}Th budget. There are two reasons why this was unsuccessful. Firstly, the total ^{234}Th budget for the cruise was difficult to constrain. Assuming steady-state, the modeled ^{234}Th sinking flux was estimated to be 2709 ± 1526 dpm m^{-2} d^{-1} which compared well with the ^{234}Th flux observed in sediment traps of 3420 ± 797 dpm m^{-2} d^{-1}. Given that only 27% of the modeled ^{234}Th flux was due to the observed deficiency from ^{238}U, however, the ^{234}Th model was primarily based on the advection terms, the uncertainties of which are difficult to constrain. Secondly, the C:^{234}Th ratio in marine snow collected at 15 m averaged over 10-fold higher than the C:^{234}Th ratio in sediment trap material collected at 75 m and 150 m. This implies that the efficiency by which ^{234}Th would track the sinking of marine snow ^{234}Th was less than 10% of the efficiency that it tracked average particles in sediment traps. Thus, the sinking flux of marine snow is better constrained by the ^{13}C estimate of primary production (69 mmol m^{-2} d^{-1}; Table 5.6) than by the total ^{234}Th budget.

Clearly, this study is one example of the condition discussed hypothetically in Chapter 2 in which uncertainties in the total ^{234}Th budget prevent the use of total ^{234}Th scavenging as a reliable means of estimate particle export. Because the timescale of ^{234}Th adsorption is well known, however (e.g. Dunne et. al. 1997), the dissolved and particulate ^{234}Th budgets still provide a valuable constraint on the mechanism of particle sinking.

MECHANISM OF PARTICLE EXPORT - OBSERVATIONS

One goal of this study was to evaluate the role of marine snow and colloids in particle export using ^{234}Th. Alldredge and Silver (1988) suggested that marine snow might be the dominant sinking particle-type in this coastal upwelling setting. As discussed in the introduction, in-situ and laboratory estimates of velocities for marine snow sinking are as high as 50-100 m d^{-1} (Alldredge and Gotschalk, 1988; Silver and Alldredge, 1981). In-situ estimates of marine snow concentrations from camera profiles during the cruise averaged 0.71 ± 0.65 µM organic carbon and 28 ± 26 µg/l total mass in the upper 75 m (A. Alldredge, pers. comm.). Because these concentrations are similar in magnitude to concentrations of >53 µm LVFS, we suggest that the >53 µm LVFS filter and the camera observed the same size class of particles. This also implies that the >53 µm particles were also >0.5 mm. Comparison of the ^{13}C primary production and the marine snow concentration gives in an upper limit for the sinking velocity of marine snow of 96 m d^{-1}. Assuming that sediment traps are capable of efficiently collecting sinking marine snow and give representative estimates of the sinking particle flux results in an upper limit to the sinking velocity of marine snow of 23 m d^{-1}.

Marine snow concentrations derived from in-situ camera work (A. Alldredge, pers. comm.) showed intense diurnal periodicity during the cruise. Median noon and evening concentrations were 7-fold higher than night and morning concentrations, consistent with previous work (Dilling, 1997). This diurnal cycle may be result of periodicity in either the source or removal terms in the mass balance for marine snow. Dilling (1997) suggested that this periodicity was a result of the diurnal vertical migration cycle of zooplankton. Marine snow was either broken up or grazed at night when the zooplankton migrate up to the upper 75 m to feed. An alternate hypothesis (A. Alldredge, pers. comm.) is that marine snow is produced during the day through primary production and is exported through its high sinking velocities in the afternoon and evening. The latter hypothesis implies that the vertical sinking flux is much higher than estimated by sediment traps. Fortunately, ^{234}Th can be used to distinguish between these hypotheses.

While the total ^{234}Th budget itself does not constrain the role of marine snow in particle export, three features of the ^{234}Th-particle cycle observed during this cruise do have important implications for particle cycling and export in the Santa Barbara

Channel. 1) C:^{234}Th ratios of marine snow at 15 m are extremely high (37 ± 10) relative to sediment traps at 75 m and 150 m (3.5 ± 0.8). 2) The C:^{234}Th ratios in >1 μm-filtered particles from both bottles and the Large Volume Filtration System (LVFS) and >53 μm-filtered LVFS particles decrease from values near those of marine snow values at 15 m (47 ± 56, 22 ± 7 and 52 ± 39, respectively) to values similar to the sediment trap values at 75 m (8 ± 6, 1.9 ± 0.1 and 4 ± 4, respectively). 3) Colloidal particles have almost no ^{234}Th and consequently have extremely high C:^{234}Th ratios. 4) Particulate ^{234}Th activities are extremely low at the surface (<0.2 dpm/l) and increase with depth below the mixed layer to a maximum (0.6 dpm/l) at 75 m.

MECHANISM OF PARTICLE EXPORT - MODELING

To estimate the dominant mechanism of particle sinking, four separate one dimensional models were developed. These models include production, alteration and sinking of particles in coordination with ^{234}Th adsorption, desorption and decay. The first model - called the simple model - included only a single, passively-sinking and slowly-remineralizing particle pool. The second model - called the phyto. model - divided particles into two pools in terms of lability - rapidly-remineralizing phytoplankton and non-remineralizing, passively-sinking particles. The third - the agg. model - and fourth - the agg.-disagg. model - divided particles into two slowly-remineralizing pools in terms of size - small non-sinking particle and large, rapidly-sinking particles. All of these particle models are described in detail in Dunne et al. (1997) and in Chapter 2. A ^{234}Th scavenging model was coupled to each model in the same way - dissolved ^{234}Th produced from ^{238}U decay which either decays or adsorbs onto particles with second-order adsorption (adsorption rate = k_1*P*Th_d where k_1 =0.0083 μM^{-1} d^{-1} is the adsorption rate constant from Chapter 2 re-tuned for bottle particulate organic carbon, P is the particle concentration and Th_d is the dissolved ^{234}Th activity). Particulate ^{234}Th then follows the particle cycle, desorbs back to the dissolved phase (k_{-1} = 0.0068 d^{-1}) or decays (λ = 0.02876 d^{-1}).

Each model was forced with the same vertically dependent primary production flux of 67 mmol C m^{-2} d^{-1} and average ^{238}U activity of 2373 dpm m^{-3}. All of these models were constrained by the same flow field of zero upwelling at the surface and upwelling increasing linearly to a maximum of 2.6 m d^{-1} at 75 m with constant upwelling between 75 m and 100 m. The upper 30m was set to mix once per day with a vertical eddy

diffusion coefficient of K_z = 0.3 cm^2 s^{-1} below 30 m. Particle concentrations in the upwelling water at the base of the model (100 m) were specified as 4 μM for particles, 0.15 dpm m^{-3} for particulate ^{234}Th (from a deep ^{234}Th profile in the Santa Monica Basin; Huh and Beasley, 1987) and 2223 dpm m^{-3} for dissolved ^{234}Th (assuming equilibrium with ^{238}U).

Two sets of model runs were performed:

Set 1) Remineralization was assumed to be negligible and sinking velocities were optimized to reproduce the observed particle concentrations. This assumes that particle export equals primary production and models the effect of severe under-collection by sediment traps.

Set 2) Rate constants, and sinking velocities were optimized to reproduce both the observed particle concentrations and the observed sinking particle flux at 75 m (15.9 mmol C m^{-2} d^{-1}). This assumes that the sediment traps were perfect collectors and implies that either the measured new production (^{15}N) and net production (O_2) rates are over-estimates while the upper-limit remineralization (O_2) rate is an under-estimate (Table 5.8), or that a severely non-steady state ecosystem existed during the cruise.

The optimization routine found the minimum value of chi - the sum of differences between the model and average depth-dependent particle concentrations normalized to their data average as well as the difference between the model particle export and 15.9 mmol C m^{-2} d^{-1} normalized to 15.9 mmol C m^{-2} d^{-1} (Set 2 only). This was done by solving the model over a spectrum of rate constants in sinking velocities for chi in up to three dimensions and then finding the minimum. Due to computational constraints, this was done first in coarse resolution in order to find the general region of low chi and then in high resolution centered around the coarse resolution minimum.

Results using the simple model are shown in Figure 5.13. Without remineralization (Figures 5.13A-C) particle concentrations must increase with depth (Figure 5.13A) in contrast to the observations. With remineralization (Figures 5.13D-F), the simple model reproduces the observed depth trend (Figure 5.13D) though it underestimates the magnitude of this trend. The model reproduces that observed trend of increasing particulate ^{234}Th and decreasing C:^{234}Th with depth both with and without remineralization (Figures 5.13B, 5.13E). Only with remineralization does the simple

model reproduce total ^{234}Th activities which come into equilibrium with ^{238}U below the euphotic zone. On the whole, the simple model with remineralization reproduces the observations quite well.

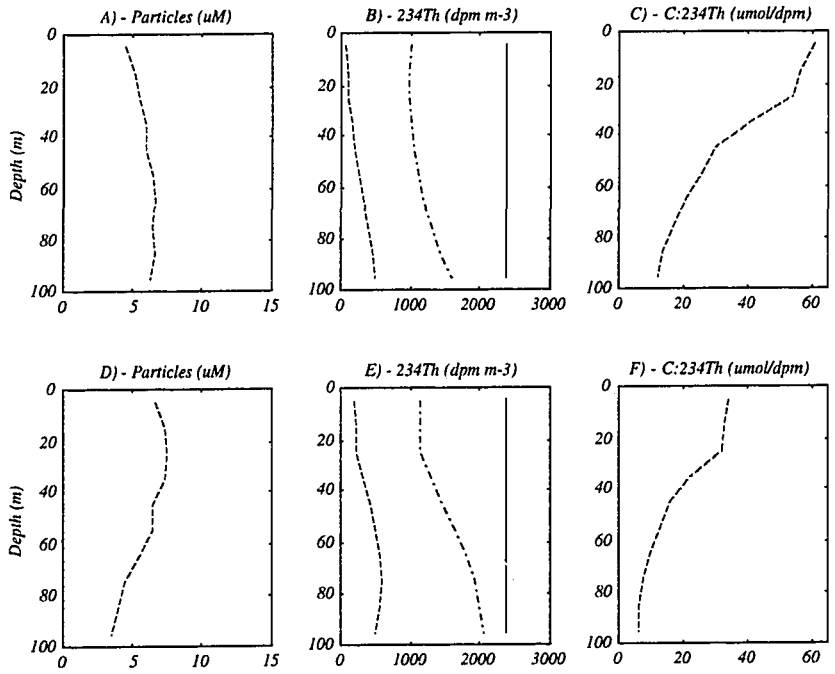

Figure 5.13: Results of the simple model for cases of particle export equaling total production (5.13A-C) and particle export equaling the sediment trap flux (5.13D-F). Shown are results for concentrations in μM of particles (dashed) (5.13A,D), activities in dpm m^{-3} of ^{238}U (solid black) and total (solid gray), dissolved (dash-dot) and particulate (dashed) ^{234}Th (5.13B,E) and the C:^{234}Th ratio in dpm/μmol of particles (dashed) (5.13C,F).

The phyto. model (Figure 5.14) distinguishes between rapidly remineralizing phytoplankton and degradation-resistant particles. The model was optimized to both the observed bottle particulate organic carbon and chlorophyll data converted to carbon units using C:Chl = 30 g/g (Eppley et al., 1968). Results from this model were similar from the simple model in terms of the surface particle concentrations, the gradient in ^{234}Th with depth and the C:^{234}Th ratio. Strong differences between these two models, however were also apparent. Including remineralization in this model did not produce the observed gradient in particle concentration with depth (Figure 5.14A, 5.14C). Because of

the high particle concentrations at depth, ^{234}Th did not come into equilibrium with ^{238}U below the mixed layer and resulted in a highly overestimated deficiency regardless of the inclusion of remineralization.

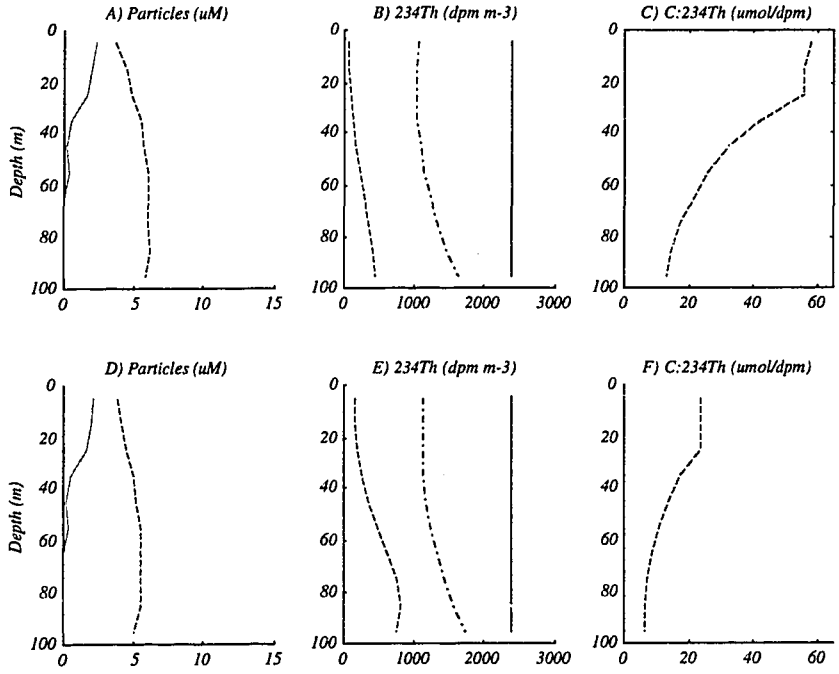

Figure 5.14: Results of the phytoplankton model for cases of particle export equaling total production (5.14A-C) and particle export equaling the sediment trap flux (5.14D-F). Shown are results for concentrations in μM of phytoplankton (solid) and other (dashed) and large particles (5.14A,D), activities in dpm m^{-3} of ^{238}U (solid black) and total (solid gray), dissolved (dash-dot) and particulate (dashed) ^{234}Th (5.14B,E) and C:^{234}Th ratios in dpm/μmol of particles (dashed) (5.14C,F).

The similarity between results of these two models contrast strongly to results from the central equatorial Pacific (Dunne et al., 1997). In the equatorial Pacific, phytoplankton comprised 50% of total particles. Incorporation of rapidly-remineralizing phytoplankton into the particle cycling model in Dunne et al. (1997) was essential to reconcile the co-occurrence of high mixed layer activities of particulate ^{234}Th (0.4 dpm/l) with high remineralization rate constants ($\gamma = 0.4$ for total particles). Since phytoplankton were only a small component (17%) of total particulate organic carbon in this study, the explicit incorporation of phytoplankton is unnecessary to explain ^{234}Th distributions.

The differences between these models however, illustrate the large impact that a high concentration of particles below the mixed layer would have on ^{234}Th distributions. This mechanism of ^{234}Th removal may be responsible for the two spuriously low subsurface total ^{234}Th values in Figure 5.6. However, the prevalence of high subsurface total ^{234}Th, suggests that high particle concentrations below the mixed layer were not common. This implies that either remineralization below the mixed layer was strong as modeled in Figure5.13D-F, or alternately, that particles did not sinking uniformly out of the mixed layer. I test this latter hypothesis through an aggregation model.

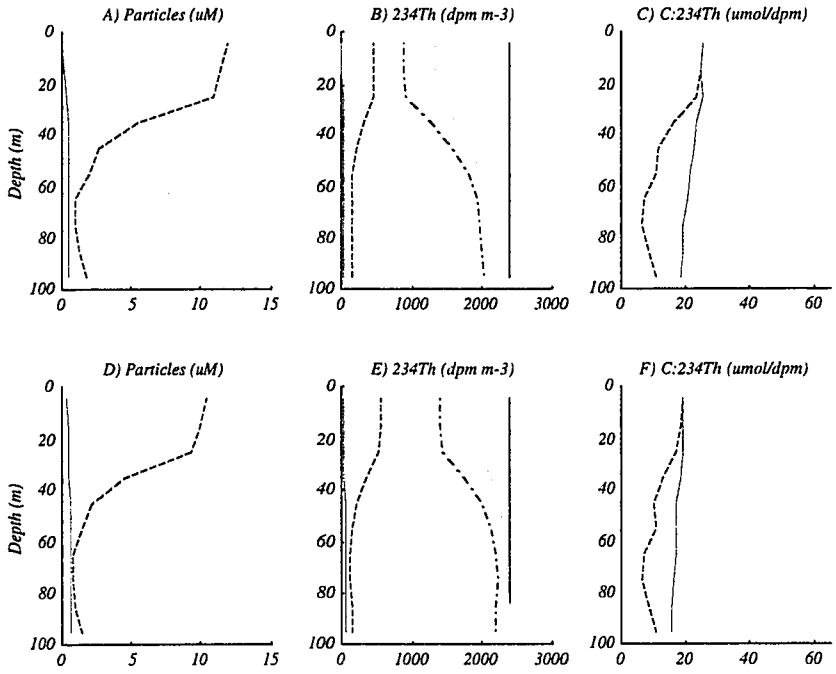

Figure 5.15: Results of the aggregation model for cases of particle export equaling total production (5.15A-C) and particle export equaling the sediment trap flux (5.15D-F). Shown are results for concentrations in μM of small (dashed) and large (solid) particles (5.15A,D), activities in dpm m^{-3} of ^{238}U (solid black) and total (solid gray), dissolved (dash-dot), small particulate (dashed) and large particulate (solid gray) ^{234}Th (5.15B,E) and C:^{234}Th ratios in dpm/μmol for small (dashed) and large (solid) particles (5.15C,F).

In the aggregation model (Figure 5.15), the sinking velocities of particles were estimated using the comparisons between flux and marine snow concentration estimated from camera work (A. Alldredge, pers. comm.). Results from this model

showed significant deviations from the data. Attenuation of particles with depth was extreme. Particle concentrations near the bottom boundary were supported exclusively by the upwelling boundary condition. Comparison between the high sinking velocity (Figure 5.15A-C) and low sinking velocity (Figure 5.15D-F) illustrates the extreme insensitivity of ^{234}Th scavenging in this model. As a consequence of the high relative particle concentrations at the surface, particulate ^{234}Th activities were highest at the surface.

Including disaggregation (Figure 5.16) reconciled much of the dissimilarities between the aggregation model and the observations. Rate constants in the agg.-disagg. model were optimized after a disaggregation rate constant was set to 5 d^{-1}. This value was chosen after the work of Clegg and Whitfield (1994) who estimated particle aggregation during the North Atlantic Bloom experiment. Though both sets of model runs reproduced the observed increase in particulate ^{234}Th with depth, only the model which included remineralization (Figure 5.16D-F) reproduced the observed variability in particulate ^{234}Th with depth. Disaggregation rate constants less than 2 d^{-1} had little effect on the particulate ^{234}Th profile. Parameter values used in all four models (Figures 5.13-5.16) are summarized in Table 5.9 along with the results of each model in terms of the ^{234}Th deficiency and the ^{234}Th sinking flux.

Overall, model results illustrated the importance of the residence time of particles as the determining factor in both the C:^{234}Th ratio of particles and the vertical structure of particulate ^{234}Th. Results of the simple model suggest that lifetimes of particles in the mixed layer (0-30 m) were extremely short (less than 30/3.4 = 9 days). Lifetimes of particles increased with depth, however. Lifetimes of particles from the simple model reached 22 days at 75 m. The subsurface concentration of particles was shown to play an important role in the persistence of the sub-surface deficiency of ^{234}Th from ^{238}U. Of the models without remineralization (wherein particle export equals primary production; 5.13-5.16,A-C), only the aggregation model reproduced reasonably low ^{234}Th deficiencies (Table 5.9). This model is rejected, however, due to its strong surface maximum in particulate ^{234}Th. Only the simple and aggreg.-disag. models which include remineralization adequately reproduce the particle and ^{234}Th observations. Efforts to obtain a precise estimate of particle export and remineralization remain inconclusive, however, because of the uncertainties in 1) the existence of steady-state, 2) the impact of horizontal

inputs of particulate ^{234}Th from re-suspended sediments and 3) the magnitude of the ^{234}Th deficiency accounting for advection.

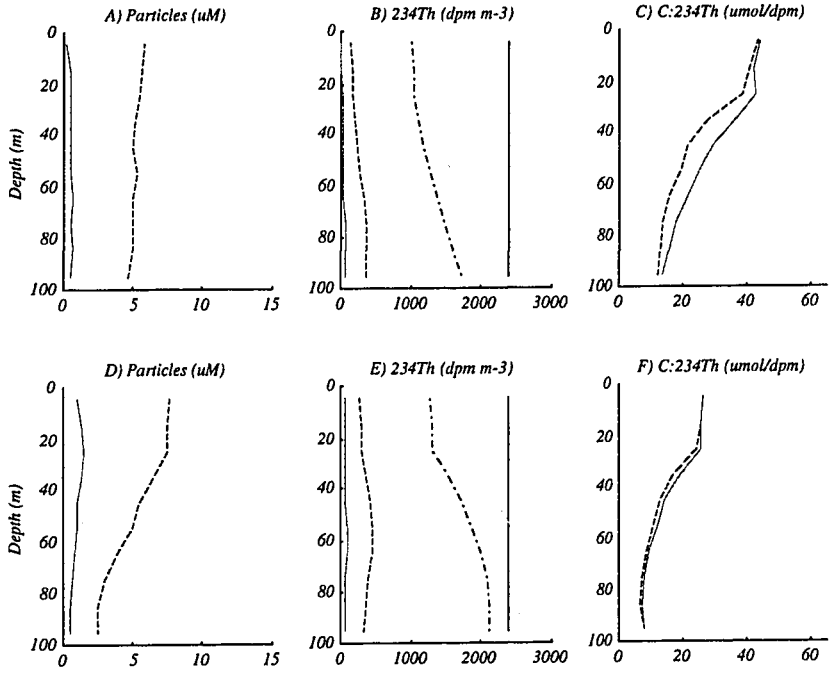

Figure 5.16: Results of the agg.-disagg. model for cases of particle export equaling total production (5.16A-C) and particle export equaling the sediment trap flux (5.16D-F). Shown are results for concentrations in μM of small (dashed) and large (solid) particles (5.16A,D), activities in dpm m^{-3} of ^{238}U (solid black) and total (solid gray), dissolved (dash-dot), small particulate (dashed) and large particulate (solid gray) ^{234}Th (5.16B,E) and C:^{234}Th ratios in dpm/μmol of small (dashed) and large (solid) particles (5.16C,F).

Table 5.9: Summary of model remineralization and aggregation rate constants (d^{-1}) and sinking velocity (m d^{-1}) inputs and ^{234}Th deficiency and sinking flux (dpm m^{-2} d^{-1}) outputs.

Model	Remineralization rate constant (d^{-1})	Aggregation rate constant (d^{-1})	Sinking velocity (m d^{-1})	^{234}Th deficiency (dpm m^{-2} d^{-1})	^{234}Th sinking flux (dpm m^{-2} d^{-1})
Simple	----------	----------	8.0	2429	3104
	0.0675	----------	3.4	1290	2018
Phyto	----------	0.9	8.5	2341	2991
	0.53	0.4	2.8	1763	2129
Agg.	----------	0.12	96	1469	2743
	0.09	0.055	23	448	963
Agg.-disagg.	----------	0.69	96	2106	3616
disagg = 5 d^{-1}	0.074	1.02	23	717	1920

CONCLUSIONS

In summary, the Santa Barbara Channel is a region of intense variability due to complex upwelling patterns and sedimentology. Given the difficulty experienced in this study of constraining the ^{234}Th budget in the upper 75 m, I reject the preliminary conclusion of Moore et al. (1981) that the residence time of ^{234}Th in Santa Barbara Channel surface waters is long enough to ignore advection and time dependencies. Other than the colloidal fraction being extremely low in ^{234}Th, this data set of the ^{234}Th content of different sized particles in the Santa Barbara Channel illustrated no clear size-dependency. These ubiquitously high C:^{234}Th values (i.e. low ^{234}Th) imply extremely short lifetimes of particles in the mixed layer. There was a strong depth dependence in the ^{234}Th content of particles interpreted in part to an increasing residence time of biologically-generated particles with depth, and in part to an horizontal re-suspended sediment input in nepheloid layers.

A large imbalance in favor of biological production over removal was observed during the cruise. Comparison with CalCOFI and ADEOS ocean color data taken after the cruise shows that the production-removal imbalance observed during the cruise continue through in the following week as a spring phytoplankton bloom. The Pt. Sur cruise thus observed the initiation of the phytoplankton bloom, the part of the bloom which was unsampled during the US JGOFS North Atlantic Bloom Experiment (NABE).

There are two major conclusions to be made from the observed trends in C:^{234}Th ratios of particles: 1) Colloidal particles are not a source of ^{234}Th (containing almost none of it) and are very different from sediment trap material. Thus, colloids can be ignored in the particle-^{234}Th model. 2) Observed variability in the C/^{234}Th of large/sinking particles and observed increase in particulate ^{234}Th with depth are inconsistent with direct aggregation and sinking. These ratios are consistent with both slow, passive sinking or repeated aggregation and disaggregation. Both these processes increase the residence time of particles with depth. Only the rapid aggregation-disaggregation mechanism, however, explains the observed lack of variability in the C:^{234}Th ratios between particle size classes. This work suggests that the dominant removal term in the marine snow budget is disaggregation. This removal is probably a result of zooplankton grazing as originally

suggested by Dilling (1997). As a result, sinking marine snow is created and destroyed repeatedly on it's passage from the mixed layer to the depths of sediment traps, steadily being grazed and gaining mineral material until it's excess density and sinking velocity increases enough to export it efficiently.

CHAPTER 6: BIOGEOCHEMICAL IMPLICATIONS OF A TWO-STATE ECOSYSTEM

INTRODUCTION

Physical flux constraints and assumptions of steady state are widely used by chemical oceanographers in order to understand biological and biogeochemical cycles. The two-state ecosystem hypothesis is separate from these traditional hypotheses of chemical and physical mass balance, implicating biology itself as a control of biogeochemical variability. The basis of this hypothesis is that ecosystem structure exerts a primary control on chemical fluxes. This chapter describes this hypothesis, illustrates supporting evidence both in the literature and through this dissertation and points out some potential implications of ecosystem control on biogeochemistry.

THE CONCEPT OF THE TWO STATE ECOSYSTEM

The simplest ocean ecosystem is based on phytoplankton production and zooplankton grazing. Primary production is thought to be limited by light and nutrients, while grazing is thought to be limited by temperature, prey concentration, prey type and zooplankton life cycle. Ecosystem state in some regions, such as coastal upwelling and open ocean regimes subject to variable stratification, is characterized by variable and often extremely high biomass, new production and particle export. Ecosystem state in other regions, such as High-Nitrate, Low-Chlorophyll (HNLC) and oligotrophic regimes, is characterized by invariantly low biomass, new production and particle export (e.g. Karl et al., 1995; Carlson et al., 1994; et al., McCarthy et al., 1996). This distinction between stable and dynamic ecosystems is the basis of the two-state ecosystem hypothesis which has been extensively described in terms of regional variability in new production (Dugdale and Goering, 1967; Eppley and Peterson, 1979; Chavez and Smith, 1995).

As the two-state hypothesis now stands, steady-state, low level new and export production by the microbial loop (the State I, or non-bloom scenario) is supplemented under non-steady state by the highly productive, larger food web (the State II, or bloom scenario). While the State I ecosystem is balanced and unchanging, the State

II ecosystem is episodic and dynamic. While the State I ecosystem is composed of efficiently grazed phytoplankton which do not sink, the State II system is composed of phytoplankton which can out-compete their grazers and rapidly sink, either directly or as zooplankton fecal pellets. Ecosystem state is primarily a function of light and nutrient availability and variability. The state has a great effect on the concentrations of living biomass in the ecosystem, the sinking particle flux and the residence time of nutrients in the surface ocean. Criteria for distinguishing between balanced and perturbed states are summarized in Table 6.1:

Criteria	**State I**	**State II**
Temporal Forcing (e.g. irradiance, wind, stratification, upwelling, iron deposition)	constant	episodic
Dominant Phytoplankton	small - nano/picoplankton	large - diatom/coccolith
Dominant Grazer	microzooplankton/protist	mesoplankton
Food Web Function	coupled	uncoupled
Specific Rates	growth = mortality	first growth > mortality, then growth < mortality
Particle export	low	high
Nutrient residence time	year(s)	days to weeks

In a fundamental sense, the State I ecosystem is composed of phytoplankton and zooplankton which are small and therefore produce non-sinking material, while the State II ecosystem is the opposite. In a mechanistic sense, phytoplankton in the two state ecosystem model are divided into two groups in terms of size, Michaelis-Menton nutrient uptake kinetics, and sinking velocities. Zooplankton are also divided into two groups with respect to specific growth rate and food preference. State I phytoplankton have low Michaelis-Menton half-saturation constants while large phytoplankton have high values. This difference allows small phytoplankton to flourish under low nutrient (iron) conditions. Maximum specific growth rates of State I zooplankton are greater than those of State I phytoplankton. Thus, phytoplankton are kept under grazing control in State I regardless of nutrient or light limitation. In State II, initial phytoplankton-specific grazing rates of zooplankton are lower than specific growth rates of phytoplankton. This may be due to low zooplankton concentrations, long zooplankton life cycles or negative food preference

(Evans and Parslow, 1985; B. Frost, pers. comm.) The lag in the response time of the grazing community allows State II phytoplankton to rapidly increase their biomass under the appropriate light and nutrient conditions. Because State II phytoplankton are relatively large and at high concentrations, they may spontaneously aggregate and rapidly sink (e.g. Jackson, 1990) in addition to becoming rapidly sinking fecal pellets.

Factors that influence the evolution from a State I to state II ecosystem include: the relationship between the depths of the euphotic zone and the mixed layer (Evans and Parslow, 1985), the abundance of the micro-nutrient iron (Martin et al., 1990), persistence of seed populations of large phytoplankton such as diatoms, phytoplankton and fecal pellet sinking velocities, the propensity for decoupling between high phytoplankton growth rates and either low zooplankton grazing rates, low zooplankton specific growth rates or long zooplankton life cycles.

Various incarnations of the two state hypothesis have been described in conceptual models of ecosystem structure and function beginning with Margalef's (1978) "mandala" of phytoplankton species succession across physical regimes from turbulent upwelling to stratified conditions and work to synthesize information on plankton cycles of inshore seasonal cycles (Smetacek et al., 1984) and in general (Smetacek, 1988). One quantitative attempt to describe the duality of ecosystems is the 'shift up' hypothesis of non-steady state new production after an upwelling event (Dugdale and Wilkerson, 1989). In this model, "acceleration" of nitrate utilization "shifts-up" an ecosystem, effectively from State I into State II. The magnitude of "acceleration" was shown to be a function of the initial nitrate concentration. "Acceleration" determined the ability of the State II ecosystem to increase both biomass and the physiological ability of phytoplankton to take up nutrients.

The most fundamental principles of the phytoplankton-zooplankton ecosystem have been successfully incorporated into mathematical models of ecosystem structure and function (e.g. Evans and Parslow, 1985). Incorporation of the two-state hypothesis into mathematical models, however, has traditionally been frustrated both intellectually by lack of understanding of causality behind the HNLC condition and logistically by difficulties associated with the overall objective of simulating ecosystem variability and the dispersive and chaotic mathematics which often result.

The production of biomass and its transport to depth (the biological pump) is a basic driving force of biogeochemistry in which nutrients and inorganic carbon are transformed into sinking particulate matter. This process has a large impact on carbonate chemistry, resulting in lowering of pCO_2 in the surface ocean and atmosphere. Partially as a consequence of the nature of time-averaging tracer techniques, chemical oceanographers have generally ignored the duality of ecosystems which is near dogma in biological oceanography. Most chemical tracer studies assume steady-state (State I) in the mass balances of elements. Recent studies have shown, however, that the non-steady state condition (State II) may be extremely important in the determination of the overall biogeochemical cycling of nutrients. Here I address the biogeochemical significance of ecosystem duality.

EVIDENCE OF A TWO-STATE ECOSYSTEM FROM THE LITERATURE

IRON EXPERIMENTS

Iron incubation experiments have been conducted in the subpolar north Pacific (Martin and Fitzwater, 1988), oligotrophic tropical Pacific (Price et al., 1994) and HNLC equatorial Pacific (Zettler et al., 1996). Two mesoscale Iron-Ex fertilization studies were conducted in the eastern equatorial Pacific (Coale et al., 1996). These studies conclusively showed that the growth rate of phytoplankton is limited by iron and that sporadic inputs of iron fuel rapid growth of large phytoplankton that can out-compete grazing and accumulate biomass. This impressive response implies that variable iron inputs from atmospheric deposition and upwelling in areas replete with other nutrients may result in a shift to the State II ecosystem in those areas. Iron input may therefore be an important factor controlling the variability of natural ocean ecosystems. All of these experiments of iron addition have taken place under non-steady-state conditions. Thus, the importance of grazing under steady-state release of iron stress could not be addressed. Such steady-state studies would greatly augment our understanding of the relative importance of grazing and iron limitation as controls in State II.

NORTH ATLANTIC BLOOM EXPERIMENT (NABE)

The first process study of the US Joint Global Ocean Flux Study (JGOFS) was a time series conducted in the North Atlantic during spring of 1989. This region is characterized by deep winter mixed layers in winter. As light levels and stratification increase in the spring, this region exhibits a characteristic phytoplankton bloom. NABE cruises followed the course of the spring phytoplankton bloom soon after it's inception, before nutrients had been extensively utilized (Bender et al., 1992). New production in the upper 50 m was found to be 40% of total production (Bender et al., 1992) from two independent estimates: temporal gradients in nitrate and nitrite inventories and the combination of particle export and accumulated biomass. This relatively high efficiency of nutrient utilization, biomass accumulation and particle export during NABE was described as characteristic of the State II ecosystem.

EQUATORIAL PACIFIC (EQPAC)

The equatorial Pacific was also the focus of a major JGOFS process study of carbon cycling (EqPac). The goals of EqPac were to characterize carbon fluxes in this region and better understand the inefficiency with which the HNLC food web is able to export nutrients out of the euphotic zone as sinking particles (Barber and Chavez, 1991). In general this study found primary production in the central equatorial Pacific to be similar to rates during NABE but dominated by small cells tightly coupled in a microbial loop rather than large cells accumulating biomass. The efficient recycling of organic matter by microzooplankton and the small size of the food web during EqPac was concluded to be a manifestation of iron limitation (Landry et al., 1997). Particle export was a relatively low, varying between 5% and 10% of primary production between the El Nino (boreal spring) and normal upwelling (boreal fall) conditions (Murray et al, 1996). EqPac data was synthesized to show that HNLC conditions persisted due to intense grazing control of small phytoplankton (State I) and iron limitation of large phytoplankton (Landry et al., 1997).

A great deal of temporal variability was observed. Between boreal spring, El Niño conditions of Survey I, and boreal fall, non-El Niño conditions of Survey II, surface nitrate concentrations, primary production and particulate organic carbon export each doubled (3 to 6 μM, 62 to 112 mmol m^{-2} d^{-1} and 5 to 12 mmol m^{-2} d^{-1}, respectively) and mesozooplankton grazing quadrupled (5 to 24 mmol m^{-2} d^{-1}) between 2°N and 2°S.

This variability was interpreted as a response to seasonal increases in upwelled iron flux (Loukos et al., 1997).

Tropical Instability Waves (TIWs) played a dramatic but uncertain role in moderating food web structure and biogeochemical fluxes during the boreal fall, normal upwelling EqPac Survey II and Time Series II cruises. TIWs are westward propagating anticyclonic vortices which take their energy from the shear between the South Equatorial Current and the North Equatorial Countercurrent. In addition to horizontal transport, they induce intense upwelling at the equator and downwelling at their northward, leading edge (Harrison, 1996). In general, TIWs have the effect of mixing nitrate and CO_2 rich equatorial waters with nitrate poor waters north of the equator and of upwelling normally deep, nitrate and CO_2 rich isopycnals into the euphotic layer. The exciting and unexpected observation during EqPac of a convergent front associated with a TIW (Archer et al., 1997) showed that TIWs could provide a non-steady state environment which allowed diatoms to grow rapidly and accumulate visibly at the surface. Moored time series observations compared well with shipboard observations supporting the argument that TIWs and Kelvin Waves control variability in biomass and production in the central equatorial Pacific (Foley et al., 1997; Chavez et al., 1998).

OTHER SYNTHESIS

Buesseler (1998) summarized ^{234}Th-based particle export results from a variety of State I (e.g. oligotrophic and HNLC) and State II (e.g. NABE, North Sea polyna and Arabian Sea monsoon) oceanic regimes. He showed that under State I conditions, ^{234}Th-based particle export was low, varying within 5-10% of primary production. In contrast, State II ecosystems -those undergoing perturbations through seasonal changes in irradiance, wind-mixing, pulsed inputs of nutrients (including iron) or stratification - resulted in accumulation of biomass with particle export between 25 and 50% of primary production.

EVIDENCE OF A TWO-STATE ECOSYSTEM FROM THIS WORK

Much of my work has illustrated ways in which ecosystem structure effects biogeochemistry. Specifically, the studies described in Dunne et al. (1997) and in Chapters

3, 4 and 5 observed situations in which the data could only be explained through a combination of the State I and State II ecosystem structure.

Differential lability of particles inferred from ^{234}Th during EqPac

In my earlier work, mechanisms of ^{234}Th scavenging by particles were investigated using particulate organic carbon and ^{234}Th data obtained during the JGOFS EqPac study incorporated into a variety of particle cycling models in Dunne et al. (1997). Though particulate organic carbon concentrations were low and remineralization rates were quite high, particulate ^{234}Th activities were moderate and deficiencies of ^{234}Th relative to ^{238}U were appreciable. A model of ^{234}Th scavenging which neglected remineralization gave adsorption rate constants consistent with previous work. Models which included homogenous remineralization of particles (inferred from the observed difference between primary production and particle export) and low observed particle concentrations gave adsorption rate constants nearly an order of magnitude higher than previous work. In order to reconcile the observed ^{234}Th distributions with previously quantified rates of particle-specific ^{234}Th adsorption, particulate organic carbon was compartmentalized into rapidly remineralizing and refractory pools. In this model, ^{234}Th adsorbed onto labile/phytoplankton particles was rapidly remineralized while ^{234}Th adsorbed onto the refractory particles accumulated in slowly sinking particles. Simply put, ^{234}Th distributions and known ^{234}Th chemistry were inconsistent with models of homogeneously remineralizing particles.

These models illustrated that the rapidly remineralizing microbial loop (State I) of the equatorial Pacific - which accounts for the vast majority of production in the region - contributes little to the vertical transport of carbon, nutrients and trace elements in particles. Simple comparison of production and biomass showed that recycling rates were high. Inferred rates of ^{234}Th cycling suggested that recycling was only occurring for half of the biomass. Refractory particles, indicative of State II, did not readily sink in this environment, probably because of their small size and low concentrations which prevent aggregation (Jackson et al., 1990). Particles produced from State II were more resistant to remineralization. Given any particular state of iron stress, particle export in the equatorial system was inferred to be essentially loss (top-down) controlled and highly indicative of State II.

PARTICLE EXPORT VARIABILITY BETWEEN EQPAC, FLUPAC AND ZONAL FLUX

Particle export was estimated during the FLUPAC and Zonal Flux zonal survey cruises and compared with results from EqPac in Chapter 3. Variability in particle export was interpreted to be a function of Kelvin Wave and TIW activity. While both Kelvin Wave and TIW activities were present during the FLUPAC cruise, neither wave type was present during Zonal Flux. Similar levels of new production, total production and particle export were observed in the HNLC region during these zonal surveys. A Kelvin Wave propagated along the equator immediately prior to EqPac Survey I. In Chapter 3 I suggest that this was the cause of the low levels of new production, total production and particle export observed during that cruise. A month later during EqPac Time-series I, much higher levels of new and total production were observed, but modest particle export remained low. TIW activity was evident during both EqPac Survey II and Time Series II. These cruises were characterized by the highest levels of new production, total production and particle export with all three reaching record highs at 2°N near the leading edge of a TIW.

Comparison of FLUPAC and Zonal Flux results with results from the US JGOFS EqPac cruises suggested that high nitrate (>1 μM) was the major forcing for new production and particle export near the equator, accounting for a doubling of each. Within the high nitrate zone, new production and particle export were both found to be enhanced (~doubled) during TIW activity and diminished (~halved) during Kelvin Wave activity. While the geographical extent of surface nutrients and associated enhanced production is clearly a strong function of season and ENSO, this work suggested that equatorially-trapped waves - rather than long-term variability in upwelling velocity - are the dominant sources of variability within the equatorial upwelling zone through modulation of the State II ecosystem.

VARIABLE SILICON:NITROGEN COUPLING IN THE EQUATORIAL PACIFIC

Contrary to the Landry et al. (1997) synthesis implicating a two-state ecosystem for the equatorial Pacific, Dugdale and Wilkerson (1998) presented a relatively simple proposal that the equatorial Pacific ecosystem was regulated by silicate flux. In Chapter 4, I evaluated this proposal using a more extensive data set for nutrients (silicate and nitrate), sediment trap material, water column particulate silica and new production.

The relationship between silicon and nitrogen cycling supported a strong role for the State II ecosystem in the equatorial Pacific. Relative utilization and export of silicate and nitrate in the equatorial Pacific euphotic zone was found to vary as a function of nutrient concentration. Nutrient regressions and sediment trap data showed that under high nutrient conditions (NO_3 > 7.6 μM), diatoms utilized and exported both nutrients at similar rates, suggesting that large, slowly dissolving, rapidly sinking diatoms were able to effectively utilize nutrients and export particulate material. This is one of the characteristics of State II. Under lower nutrient conditions (NO_3 < 7.6 μM), diatoms played a much smaller role, suggesting that small, rapidly dissolving and slowly sinking diatoms were more prevalent (State I). I suggested that the State I condition of low relative silicate utilization efficiency was a consequence of iron limitation, steady state upwelling and high temperature such that even though macro-nutrient concentrations (nitrate, silicate) were high, their utilization was low. This was consistent with the previous conclusion of Landry et al. (1997). Enhanced upwelling of relatively iron-rich waters leads to a State II response which is a consequence of seasonal and ENSO variability and mesoscale circulation associated with Tropical Instability Waves. Indeed, the only observation of complete silicate draw down in this HNLC system was at the convergent TIW front observed at 2°N during EqPac Survey II (Archer et al., 1997). In this instance, non-steady state conditions allowed a temporary acceleration of diatom production which resulted in accumulation of un-grazed diatoms at the surface and an increase in particulate silica throughout the euphotic zone from 1°N to 3°N.

INITIATION OF A PHYTOPLANKTON BLOOM IN A COASTAL UPWELLING REGIME.

In contrast to the relatively continuous, iron-poor upwelling characteristic the equatorial Pacific which leads to a dominance of State I, coastal upwelling conditions are generally episodic and iron-rich which leads to a dominance of State II. In Chapter 5, I presented results from a cruise in the Santa Barbara Channel that took place during the spring upwelling period of 1997 (April 1-9) aboard the R/V Pt. Sur. Though surface nutrients were high (~5 μM nitrate with presumably sufficient iron), phytoplankton biomass was moderately low (~0.7 μg Chl/l). Measured production estimates indicated new (^{15}N) and net (O_2) production values similar to measured total production - much higher than the measured particle export in sediment traps. This suggested a strong non-

steady state condition, though only small temporal gradients in biomass were observed. Comparison with California Cooperative Oceanic and Fisheries Investigations (CalCOFI) data taken at the middle of the Pt. Sur transects (Figure 5.1) showed that a phytoplankton bloom followed. Comparison of ship observations with ADEOS ocean color data taken during the month of April, 1997 confirmed this sequence of events. The contrasting nitrate and chlorophyll concentrations observed between the Pt. Sur and CalCOFI cruises allowed an approximate estimate of net production consistent with the new and total production estimates during the cruise.

This analysis showed that the Pt. Sur cruise occurred during the onset of a phytoplankton bloom as the system was in the process of shifting from State I to State II. These results are consistent with the "shift-up" hypothesis of Dugdale and Wilkerson (1989) developed to interpret new production during the Organization of Persistent Upwelling Structures (OPUS) at the Pt. Conception upwelling center. The increase in biomass as a consequence of the transition from State I to State II implied both that phytoplankton were physiologically-released from iron limitation and that zooplankton could not respond on the appropriate timescale in order to suppress the increase. In general, this study illustrated the impact of the State II ecosystem on biogeochemical cycling by increasing and (presumably) exporting biomass. As the Pt. Sur cruise served to sample the part of the bloom which NABE missed but missed the part of the bloom that NABE sampled, the combination of the two may provide a more comprehensive understanding of bloom dynamics.

IMPLICATIONS FOR PARTICLE EXPORT, NITRATE AND PCO_2

It is clear that the physical input of nutrients is the major controlling factor for global new production and particle export. For example, the flux of phosphate into the surface ocean determines the maximum vertical export flux of phosphate. Biogeochemists have tended to ignore ecosystem controls on biogeochemical cycles in favor of this type of time-averaged, mass-balance constraints. This is an over-simplification, however. Duality of ecosystem state - driven by variability in physics, light or iron input - has many potential implications for biogeochemistry. These include residence time of nutrients, particles, and particle-scavenged elements in the surface ocean, the excess partial pressure of CO_2

between the ocean and atmosphere (ΔpCO_2) and the geographical distribution of areas of low oxygen in the ocean interior. These hypothesized biogeochemical implications of a two-state ecosystem are summarized in Figure 6.1.

NUTRIENT RESIDENCE TIMES

The most basic distinction between ecosystem states is in the magnitude of new production which determines the residence time of nitrate in the surface ocean. As a consequence, nutrients (nitrate, ammonia, silicate) persist in the euphotic zone much longer and have much higher ambient concentrations under State I than under State II. As described in Chapter 4, loss of silicate from the equatorial euphotic zone was found to be even more sensitive to ecosystem state than nitrate.

ATMOSPHERIC pCO_2

The ambient concentration of nitrate and phosphate in the surface ocean corresponds to an heightening of oceanic pCO_2. The propensity of the surface ocean to outgas CO_2 before nutrients are utilized has important implications for atmospheric CO_2 and climate change. It is well known that the biological pump has an intense effect on atmospheric pCO_2. Along this line, it has been suggested that the toggling between State I and State II ecosystems may modulate atmospheric CO_2 on glacial to interglacial timescales through variability in iron limitation (Martin, 1990) and stratification. Martin (1990) went so far as to suggest that fertilization of the Southern Ocean could reverse the current anthropogenic atmospheric increase in CO_2. Following this suggestion, global ocean circulation models were used to evaluate the potential for iron fertilization to sequester CO_2 (Peng and Broecker, 1991; Joos et al., 1991; Kurz and Maier-Reimer., 1993). These studies considered the effect of fertilizing the Southern Ocean with iron so as to consume all surface phosphate along with stoichiometric amounts of inorganic carbon. They estimated that iron fertilization had the potential to lower pCO_2 by 17-107 ppm depending on the character of circulation and the rate of atmospheric pCO_2 increase. Considering that only the upper limit of this effect was considered, implimentation of iron addition would assumedly be much less effective. These results suggest that ecosystem structure could drive pCO_2 variability of the seasonal scale (5 ppm) but not at the magnitude of glacial-interglacial or anthropogenic change scales (100 ppm).

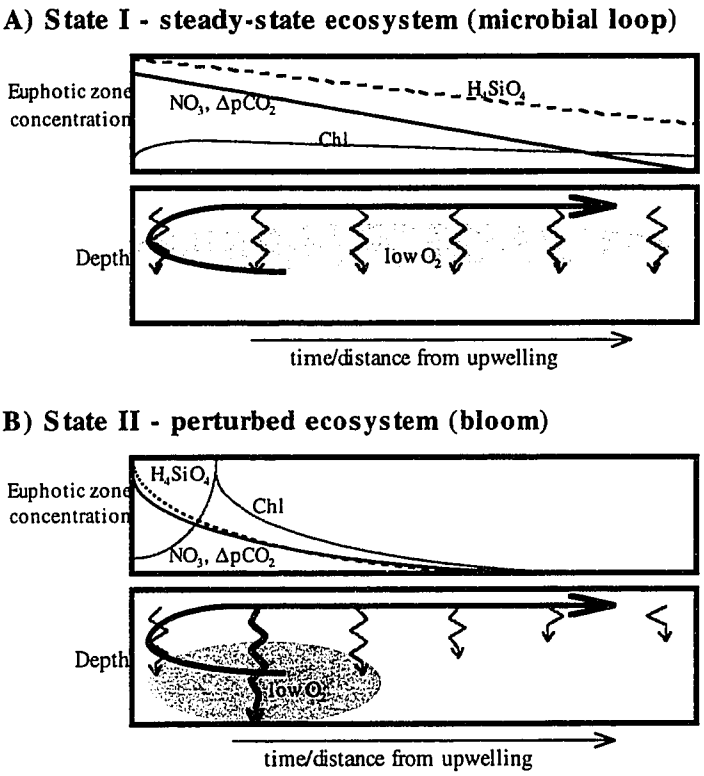

Figure 6.1: Schematic of biogeochemical implications of a two-state ecosystem. The upper two panels represent the State I, steady-state ecosystem of the microbial loop (6.1A) while the lower two panels represent the State II, perturbed ecosystem. For each state, the upper panel shows the progression of euphotic zone nitrate (black), silicate (dashed) and chlorophyll/phytoplankton biomass (gray) concentrations versus time or distance from upwelling. Also for each state, the lower panel illustrates circulation (thick black arrows), particle export (waved gray arrows) and areas of low oxygen in the interior versus depth. The thickness and length of the particle export arrows indicates the magnitude and depth of penetration of particle export.

GEOGRAPHICAL DISTRIBUTION OF PARTICLE EXPORT

The geographic distribution of particle export is extremely sensitive to ecosystem state. Particle export is more uniform under State I as nutrients are transported farther from upwelling centers (such as the equator or coasts) before being utilized. Under State II, intensification of new production is magnified in terms of particle export. These two effects tend to keep particle export focused closer to upwelling centers under State II.

THE COMPOSITION OF PARTICLE EXPORT - BIOTA AND SCAVENGING

The composition of material transported out of the euphotic zone to the ocean interior and sea floor is another important consequence of ecosystem state. In chapter 4, it was shown that silicon:nitrogen ratios in particle export were approximately 2-5 times higher in response to an increase in State II conditions. This effect is exemplified at the termination of diatom blooms (State II), when particulate silica is exported extremely efficiently. The role of ecosystem state in exporting calcium carbonate is unknown.

Elemental scavenging is a second feature of particle export which is highly sensitive to ecosystem state. State II particles can readily aggregate and be exported quickly due to the high particle concentrations that are associated with a bloom (Jackson, 1990). Because of the subsequently short residence times of these particles, they do not come into adsorptive equilibrium with the surrounding seawater and thus tend to scavenge elements much less efficiently. Comparison of the ^{234}Th content of particles between the predominantly State I conditions of the equatorial Pacific (Murray et al., 1996) with those from the North Atlantic Bloom Experiment (Buesseler et al., 1992) and Santa Barbara Channel (Chapter 5, Table 5.7) illustrates that much higher C:^{234}Th ratios are observed in the coastal, State II environment.

THE REMINERALIZATION DEPTH SCALE

The size spectrum of sinking particles in the State II ecosystem is predicted to be much larger than in State I. This is due to the large size of bloom-forming phytoplankton, the large size of the fecal pellets of zooplankton which consume these phytoplankton and the propensity of bloom-forming phytoplankton to aggregate. Because sinking velocity is a function of size, large particles sink much faster than small ones given similar excess densities over seawater. Furthermore, rapidly-sinking particles should be exported to depth more efficiently than slowly-sinking particles, given similar labilities of sinking particles. The combination of these features imply a much greater length scale for particle remineralization in State II than in State I. The magnitude of this effect is currently unknown but has major implications for the timescale of CO_2 sequestration in the ocean interior.

AREAS OF LOW OXYGEN IN THE OCEAN INTERIOR

Two features of the two-state ecosystem affect the maintenance of low oxygen regions in the ocean's interior. First, focusing of particle export geographically near upwelling centers in State II may maintain limited areas of intense oxygen depletion beneath upwelling centers. Second, the deeper remineralization scale hypothesized in State II would tend to maintain regions of low oxygen deeper in the water column than would occur in State I. In the state I ecosystem, shallow regions of low oxygen would be readily re-ventilated with high oxygen waters in recent contact with the atmosphere. Because the deeper regions of low oxygen in the State II ecosystem are relatively isolated from atmospheric ventilation, these low oxygen regions would presumable be that much more intense.

CONCLUSIONS

My work has illustrated some of the implications of the duality of ocean ecosystem state. Three separate lines of evidence were provided for the validity of the two-state food web as a conceptual approach for understanding biogeochemical cycling in the surface ocean. Specifically, it has shown that the State II ecosystem has marked biogeochemical signatures in trace metal scavenging, the relative utilization of nutrients and particle export and has a profound effect on particle concentrations and nutrient residence times. The major biogeochemical implication of the two-state food web addressed here is on the residence time of nutrients in the surface ocean and subsequently on oceanic ΔpCO_2. Ecosystem state also has implications for the quality of particles exported, the remineralization depth scale, the geographical distribution of export, and the maintenance of low-oxygen regions in the ocean's interior. In terms of fisheries, the persistence of the State II ecosystem has important implications for most coastal fisheries (including shellfish, cod and herring) which are derived from perturbed, or State II production.

WHAT'S NEXT? - FRONTIERS IN BIOGEOCHEMISTRY

The field of ecosystem modeling has taken great strides in the last few years. Recent work on the role of iron limitation of phytoplankton production has led to improved descriptions of the equatorial and sub-tropical Pacific HNLC conditions. At the

same time, recent mathematical descriptions of ecosystems in terms of power laws (so called allometric equations; Hurtt and Armstrong, 1999) have shown great promise in balancing numerical stability with ecosystem flexibility. With these advances, it seems inevitable that future technological advances in iron measurement will afford the development of new ecosystem models to more adequately reproduce observed ocean variability.

The role of eddies, fronts, internal waves and other mesoscale physical processes on ocean biogeochemistry is fascinating but not well understood. Biogeochemical studies of mesoscale processes have included those of eddies (McGillicuddy et al., 1998), filaments (Jones et al., 1996), fronts (Archer et al., 1997) and equatorial waves (Foley et al., 1997; Chavez et al., 1998). Observations of these processes have been classically limited to ship-board surveys using bottle casts. The limited temporal and spatial resolution of these techniques has strongly impaired scientific understanding of these phenomenon. Recently, however, technological advances in drifters, moorings and ship-towed packages have given chemical oceanographers new access to these phenomena by affording near-continuous spatial and temporal resolution of these phenomena.

Biogeochemistry has been aggressively applied to the question of global change over the two decades. Application of biogeochemistry to local and regional anthropogenic change has in the past been sporadic or isolated, but has recently become a topic of scientific and social urgency as anthropogenic pressure on natural ecosystems and human quality-of-life has intensified. Characterization and monitoring of natural systems potentially stressed by humanity are challenging and socially compelling areas for systematic research.

The current state of chemical oceanography includes basic descriptions of the biogeochemical processes relating to most of the individual elements. The next step is to generate a holistic understanding of how all these processes interact on diverse scales from global ocean circulation to the chemical reactions occurring in the micro-environments of individual particles. The global scale has recently become tractable using revolutionary computational advances and their applications of inverse theory to oceanography. This has allowed researchers to incorporate oceanographic data taken all

over the world into mathematical models of ocean circulation and biogeochemical cycling to gain a truly global perspective on particle sinking and remineralization in the ocean (e.g. Schlitzer, 1998). In principle, these global ocean inverse models (a.k.a. global adjoint models) allow probably the most highly constrained estimate of elemental (e.g. organic and inorganic carbon, nitrogen, phosphorous, silicon) export from the surface ocean and subsurface remineralization depth scales on a spatially explicit grid. These models are still in their infancy, but will ultimately provide a much better understanding of the ocean's capacity to sequester carbon and better allow scientists to assess the interaction between the ocean and climate change. The challenge will be to combine these description with mechanistic understanding of the chemical reactions occurring on the microscale to the mesoscale in order to evaluate the causality behind global biogeochemistry.

BIBLIOGRAPHY

Alldredge, A. L. (1979) The chemical composition of macroscopic aggregates in two neritic seas. *Limnol. Oceanogr.*, **24**, 855-866.

Alldredge, A. L. and J. L. Cox (1982) Primary productivity and chemical composition of marine snow in surface waters of the Southern California Bight. *J. Mar. Res.*, **40**, 517-527.

Alldredge, A. L., J. J. Cole and D. A. Caron (1986) Production of heterotrophic bacteria inhabiting macroscopic marine aggregates (marine snow) from surface waters. *Limnol. Oceanogr.*, **31**, 68-78.

Alldredge, A. L., and C. Gotschalk (1988) In situ behavior of marine snow, *Limnol. Oceanogr*, **33**, 339-351.

Alldredge, A. L., and M. W. Silver (1988) Characteristics, dynamics and significance of marine snow, *Prog. in Oceanogr.*, **20**, 41-82.

Alldredge, A. L. (1989) The significance of suspended detrital aggregates of marine snow as microhabitats in the pelagic zone of the ocean. In: *Recent Advances in microbial ecology, Proceedings of the 5th International Symposium on Microbial Ecology*, T. Hattori, Y. Ishida, Y. Maruyama, R. Morita and A. Uchida eds. Japan Scientific Societies Press.

Alldredge, A. L., C. Gotschalk, U. Passow and U. Riebesell (1995) Aggregation of a diatom bloom in a mesocosm: Bulk and individual particle optical measurements. *Deep-Sea Res. II*, **42**, 9-27.

Alldredge, A. L. (1998) The carbon, nitrogen and mass content of marine snow as a function of aggregate size. *Deep-Sea Res. I*, **45**, 529-541.

Anderson, R. F. and A. P. Fleer (1982) Determination of natural activities of thorium and plutonium in marine particle material. *Anal. Chem.*, **54**, 1142-1147.

Archer, D. E., T. Takahashi, S. Sutherland, J. Goddard, D. Chipman, K. Rodgers and H. Ogura (1996) Daily, seasonal and interannual variability of seasurface carbon and nutrient concentration in the equatorial Pacific Ocean, *Deep-Sea Res. Part II*, **43**, 779-808.

Archer, D., E. T. Peltzer and D. Kirchman (1997a) A timescale for dissolved organic carbon production in equatorial Pacific surface waters. *Global Biogeochemical Cycles*, **11**, 435-452.

Archer, D. and 16 others (1997b) Shipboard observations of a convergent front at 2°N during JGOFS Survey II Expedition in August, 1992. *Deep-Sea Res. II*, **44**, 1827-1849.

Aufdenkampe, A. K., J. J. McCarthy, J. P Dunne, M. Rodier and J. W. Murray (in preparation) New production along the equator in the central Pacific. *Deep-Sea Res. I.*

Azam, F., D. C. Smith and A. F. Carlucci (1992) Bacterial transformation and transport of organic matter in the Southern California Bight. *Prog. Oceanogr.*, **30**, 151-166.

Bacon, M. P. and R. F. Anderson (1982) Distributions of thorium isotopes between dissolved and particulate forms in the deep sea. *J. Geophys. Res.*, **87**, No. C3, 2045-2056.

Bacon, M. P., J. K. Cochran, D. Hirshberg, T. R. Hammar and A. P. Fleer (1996) Export fluxes of carbon at the equator during the EqPac time-series cruises estimated from ^{234}Th measurements. *Deep Sea Res. II*, **43**, 1133-1154.

Barber, R. T. and J. E. Kogelschatz (1990) Nutrients and productivity during the 1982/83 El Niño. In *Global Consequences of the 1982/83 El Niño-Southern Oscillation Event*, P. W. Glynn, ed., Elsevier.

Barber, R. T., and F. P. Chavez (1991) Regulation of primary productivity rate in the equatorial Pacific, *Limnol. Oceanogr.*, **36**, 1803-1815.

Barber, R. T., M. P. Sanderson, S. T. Lindley, F. Chai, J. Newton, C. C. Trees, D. G. Foley and F. P. Chavez (1996) Primary productivity and its regulation in the equatorial Pacific during and following the 1991-1992 El Niño. *Deep-Sea Res. II*, **43**, 933-969.

Barber, R. T. (1998) Diatoms, blooms and the regulation of community structure. Presentation at the 1998 meeting of the U. S. Joint Global Ocean Flux Study Synthesis and Modeling Project., Durham, N. H..

Bender, M. L., and M. J. McPhaden (1990) Anomalous nutrient distribution in the equatorial Pacific in April 1988: evidence for rapid biological uptake, *Deep-Sea Res.*, **37**, 1075-1084.

Bender, M. L., H. Ducklow, J. Kiddon, J. Marra and J. Martin (1992) The carbon balance during the 1989 spring bloom in the North Atlantic Ocean, 47N, 20W. *Deep-Sea Res.*, **39**, 1707-1725.

Bevington, P. R. and D. K. Robinson (1992) *Data Reduction and Error Analysis for the Physical Sciences, Second Edition*, McGraw-Hill Inc., pp.75-83.

Bidigare, R. R., and M. E. Ondrusek (1996) Spatial and temporal variability of phytoplankton pigment distributions in the central equatorial Pacific Ocean, *Deep-Sea Res. II*, **43**, 809-834.

Billet, D. S. M., R. S. Lampitt, A. L. Rice, and R. F. C. Mantoura (1983) Seasonal sedimentation of phytoplankton to the deep-sea benthos, *Nature*, **302**, 520-522.

Bishop, J. K. B. (in press) Particulate organic carbon/particulate dry weight and beam attenuation coefficient measurements, *Deep-Sea Res. I.*

Blain, S., A. Leynaert, P. Treguer, M.-J. Chretiennot-Dinet, and M. Rodier (1997) Biomass, growth rates and limitation of equatorial Pacific diatoms, *Deep-Sea Res. I*, **44**, 1255-1275, 1983.

Blain, S., P. Treguer, and M. Rodier (submitted) The silica cycle in the western equatorial Pacific: short-term and mesoscale variability, *J. Geophys. Res.*.

Broecker, W. S. and T.-H. Peng (1982) *Tracers in the Sea*, Eldigio Press, 690 pp.

Bruland, K. W., R. P. Franks, W. M. Landing and A. Soutar (1981) Southern California inner basin sediment trap intercalibration. *Earth Planet Sci. Lett.*, **53**, 400-408.

Brzezinski, M. A., The Si:C:N ratio in marine diatoms: Interspecific variability and the effect of some environmental variables, *J. Phycol.*, **21**, 347-357, 1985.

Brzezinski, M. A., and D. M. Nelson (1995) The annual silica cycle in the Sargasso Sea near Bermuda, *Deep-Sea Res. I*, **42**, 1215-1237.

Brzezinski, M. A., and D. M. Nelson (1996) Chronic substrate limitation of silicic acid uptake rates in the western Sargasso Sea, *Deep-Sea Res. II*, **43**, 437-453.

Buesseler, K. O. (1991) Do upper-ocean sediment traps provide an accurate indicator of particle flux?, *Nature*, **353**, 420-423.

Buesseler, K. O., M. Bacon, J. K. Cochran and H. Livingston (1992) Carbon and nitrogen export during the JGOFS North Atlantic Bloom Experiment estimated from ^{234}Th:^{238}U disequilibria. *Deep-Sea Res.*, **39**, 1115-1137.

Buesseler, K. O., A. F. Michaels, D. A. Siegel and A. H. Knap (1994) A three dimensional time-dependent approach to calibrating sediment trap fluxes. *Global Biogeochemical Cycles*, **8**, 179-193.

Buesseler, K. O., J. Andrews, M. Hartman, R. Belastock and F. Chai (1995) Regional estimates of the export flux of particulate organic carbon derived from thorium-234 during the JGOFS EQPAC program, *Deep-Sea Res. II,* **42**, 777-804.

Carlson, C. A., H. W. Ducklow and A. F. Michaels (1995) Annual flux of dissolved organic carbon from the euphotic zone in the northwestern Sargasso Sea. *Nature*, **371**, 405-408.

Chai, F. (1995) Origin and Maintenance of High Nitrate Condition in the Equatorial Pacific, a biological-physical model study. Ph.D. dissertation, Duke University, Durham, NC, 170 pp.

Charette, M. A, S. B. Moran and J. K. B. Bishop (in press) ^{234}Th as a tracer of particulate organic carbon export in the subarctic northeast Pacific Ocean. *Deep-Sea Res. I.*

Chavez, F. P. and R. T Barber (1987) An estimate of new production in the equatorial Pacific. *Deep-Sea Res.*, **34**, 1229-1243.

Chavez, F. P., K. R. Buck, and R. T. Barber (1990) Phytoplankton taxa in relation to primary production in the equatorial Pacific, *Deep-Sea Res.*, **37**, 1733-1752.

Chavez, F. P., K. R. Buck, K. K. Coale, J. H. Martin, G. R DiTullio, N. A. Welschmeyer, A. C. Jacobson, and R. T. Barber (1991) Growth rates, grazing, sinking and iron limitation of equatorial Pacific diatoms, *Limnol. Oceanogr.*, **36**, 1816-1834.

Chavez, F. P. and J. R. Toggweiler (1995) Physical estimates of global new production: the upwelling contribution. In *Upwelling in the Ocean: Modern Processes and Ancient Records*, Summerhayes, Emeis, Angel, Smith and Zeitschel eds., John Wiley and Sons Ltd.337-360.

Chavez, F. P. and S. L. Smith (1995) Biological and chemical consequences of open ocean upwelling. In *Upwelling in the Ocean: Modern Processes and Ancient Records*, Summerhayes, Emeis, Angel, Smith and Zeitschel eds., John Wiley and Sons Ltd., 149-170.

Chavez, F. P., P. G. Strutton and M. J. McPhaden (1998) Biological-physical coupling in the central equatorial Pacific during the onset of the 1997-98 El Niño. *Geophys. Res. Lett.*, **25**, 3543-3546.

Chen, J. H., R. L Edwards and G. J. Wasserburg (1986) ^{238}U, ^{234}U and ^{232}Th in seawater, *Earth Planet. Sci.Lett.*, **80**, 241-251.

Clegg, S. L. and M. Whitfield (1993) Application of a generalized scavenging model to time series ^{234}Th and particle data obtained during the JGOFS North Atlantic Bloom Experiment, *Deep-Sea Res.*, **40**, 1529-1545.

Coale, K. H. and K. W. Bruland (1985) ^{234}Th:^{238}U disequilibria within the California Current. *Limnol. Oceanogr.*, **30**, 22-33.

Coale, K. H. and 14 others (1996) A massive phytoplankton bloom induced by an ecosystem-scale iron fertilization experiment in the Equatorial Pacific Ocean. *Nature*, **383**, 495-501.

Dailey, M., D. Reish and J. Anderson eds. (1993) *Ecology of the Southern California Bight*, University of California Press, 926 pp.

Dilling, L. (1997) Consumption and Fragmentation of Marine Snow By Euphausiids and Copepods. Ph.D. Dissertation., University of California, Santa Barbara, 161 pp.

DiTullio, G. R., D. A. Hutchins, and K. W. Bruland (1993) Interaction of iron and major nutrients controls phytoplankton growth and species composition in the tropical North Pacific Ocean, *Limnol. Oceanogr.*, **38**, 495-508.

Donaghay, P. L., and 7 others (1991) The role of episodic atmospheric nutrient inputs in the chemical and biological dynamics of oceanic ecosystems, *Oceanogr.*, **4**, 62-70.

Dugdale, R. C., and J. J. Goering (1967) Uptake of new and regenerated forms of nitrogen in primary productivity, *Limnol. Oceanogr.*, **12**, 196-206.

Dugdale, R. C., and F. P. Wilkerson (1989) New production in the upwelling center at Point Conception, California: temporal and spatail patterns. *Deep-Sea Res.*, **36**, 985-1007.

Dugdale, R. C., F. P. Wilkerson, and H. J. Minas (1995) The role of the silicate pump in driving new production, *Deep-sea Res. I*, **42**, 697-719.

Dugdale, R. C., and F. P. Wilkerson (1998) Silicate regulation of new production in the eastern equatorial Pacific Ocean, *Nature*, **391**, 270-273.

Dunbar, R. B. and W. H. Berger (1981) Fecal pellet flux to modern bottom sediment of Santa Barbara Basin (California) based on sediment trapping. *Geol. Soc. Am. Bull.*, **92**, 212-218.

Dunne, J. P., J. W. Murray, J. Young, L. Balistrieri and J. K. B. Bishop (1997) ^{234}Th and particle cycling in the central equatorial Pacific, *Deep Sea Res. II*, **44**, 2049-2083.

Dunne, J. P. and J. W. Murray (in press) Sensitivity of ^{234}Th export to physical processes in the central equatorial Pacific, *Deep-Sea Res. I.*

Dunne, J. P., J. W. Murray, and M. Rodier (submitted-a) Particle export in the western and central equatorial Pacific, *Deep-Sea Res. I.*

Dunne, J. P., J. W. Murray, A. Aufdenkampe and M. Rodier (submitted-b) Diatom control of new production and particle export in the equatorial Pacific upwelling zone. *Global Biogeochemical Cycles.*

Dunne, J. P., J. W. Murray, L. S. Balistrieri and A. L. Alldredge (in preparation) ^{234}Th-based particle cycling and export in the Santa Barbara Channel. *Deep-Sea Res. I.*

Dymond, J. K. Fischer, M. Clauson, R. Cobler, W. Gardner, M. J. Richardson, W. Berger, A. Soutar and R. Dunbar (1981) A sediment trap intercomparison study in the Santa Barbara Basin. *Earth Planet Sci Lett.*, **53**, 409-418.

Eldin, G., M Rodier and M.-H. Radenac (1997) Physical and nutrient variability in the upper equatorial Pacific associated with westerly wind forcing and wave activity in October 1994. *Deep-Sea Res. II*, **44**, 1783-1800.

Emerson, S., P. Quay, D. Karl, C. Winn, L. Tupas and M. Landry (1997) Experimental determination of organic carbon flux from open-ocean waters. *Nature*, **389**, 951-954.

Emery (1960) *The Sea Off Southern California: a modern habitat for petroleum*, John Wiley and Sons Inc..

Eppley, R. W. (1968) An incubation method for estimating the carbon content of phytoplankton in natural samples. *Limnol. Oceanogr.*, **13**, 574-582.

Eppley, R. W. and B. J. Peterson (1979) Particulate organic matter flux and planktonic new production in the deep ocean. *Nature*, **282**, 677-680.

Eppley, R. W. ed. (1986) *Plankton Dynamics of the Southern California Bight*, Springer Verlag New York, Inc..

Eppley, R. W., F. P. Chavez, and R. T. Barber (1992) Standing stocks of particulate carbon and nitrogen in the equatorial Pacific at 150°W, *J. Geophys. Res.*, 97, 655-661.

Evans, J. T. and J. S. Parslow (1985) A model of annual plankton cycles. *Biol. Oceanogr.*, **3**, 327-347.

Fiedler, P. C., V. Philbrick, and F. P. Chavez (1991) Oceanic upwelling and productivity in the eastern tropical Pacific, *Limnol. Oceanogr.*, **36**, 1834-1850.

Fine R. A. and H. G. Ostlund (1980) Exchange times in the Pacific equatorial current system, *Earth Planet. Res. Lett.*, **49**, 447-452.

Flament, P. J., S. C. Kennan, R. A. Knox, P. P. Niiler, and R. L. Bernstein (1996) The three-dimensional structure of an upper ocean vortex in the tropical Pacific ocean, *Nature*, **383**, 610-613.

Fleischer, P. (1972) Mineralogy and sedimentation history, Santa Barbara Basin, California. *J. Sed. Petr.*, **42**, 49-58.

Foley, D. G., T. D. Dickey, M. J. McPhaden, R. R. Bidigare, M. R. Lewis, R. T. Barber, S. T. Lindley, C. Garside, D. V. Manov and J. D. McNeil (1997) Longwaves and primary productivity variations in the equatorial Pacific at 0°, 140°W. *Deep-Sea Res. II*, **44**, 1801-1826.

Fowler, S. W., and G. A. Knauer (1986) Role of large particles in the transport of elements and organic compounds through the oceanic water column, *Prog. in Oceanogr.*, **16**, 147-194.

Frost, B., and N. C. Franzen (1992) Grazing and iron limitation in the control of phytoplankton stock and nutrient concentration: a chemostat analogue of the Pacific equatorial upwelling zone, *Mar. Ecol. Prog. Ser.*, **83**, 291-303.

Gardner, W.D, S. P. Chung, M. J. Richardson and I. D. Walsh (1995) The oceanic mixed layer pump, *Deep-Sea Res. II*, **42**, 757-776.

Gersonde, R., and G. Wefer (1987) Sedimentation of biogenic siliceous particles in Antarctic waters from the Atlantic sector, *Mar. Micropaleontol.*, **11**, 311-332.

Gordon, R. M., K. H. Coale, and K. S. Johnson (1997) Iron distributions in the equatorial Pacific: Implications for new production, *Limnol. Oceanogr.*, **42**, 419-431.

Hansell, D. A., N. Bates, and C. A. Carlson (1997a) Predominance of vertical loss of carbon from surface waters of the equatorial Pacific Ocean, *Nature*, **386**, 59-61.

Hansell, D. A., C. A. Carlson, N. A. Bates and A. Poisson (1997b) Horizontal and vertical removal of organic carbon in the equatorial Pacific Ocean: a mass balance assessment. *Deep-Sea Res. II*, **44**, 2115-2130.

Harms, S. and C. D. Winant (1998) Characteristic patterns of the circulation in the Santa Barbara Channel. *J. Geophys. Res.*, **103**, 3041-3065.

Harrison, D. E. (1996) Vertical velocity in the central equatorial Pacific: a circulation model perspective for JGOFS. *Deep-Sea Res. II*, **43**, 687-705.

Henderschott, M. C. and C. D. Winant (1996) Surface circulation in the Santa Barbara Channel. *Oceanogr.*, **9**, 114-121.

Hernes, P. J., M. L. Peterson, J. W. Murray, S. G. Wakeham, C. Lee, and J. I. Hedges (1998) Particulate carbon and nitrogen fluxes and compositions in the central equatorial Pacific, *Deep Sea Res. II.*

Hickey, B. M. (1979) The California Current system - hypotheses and facts. *Prog. in Oceanogr.*, **8**, 191-279.

Hickey, B. M. (1993) Physical oceanography. in *Ecology of the Southern California Bight*, M. Dailey, D. Reish, J. Anderson eds., University of California Press, 19-70.

Honeyman, B. D., L. S. Balistrieri, and J. W. Murray (1988) Oceanic trace metal scavenging: the importance of particle concentration, *Deep-Sea Res.*, **35**, 227-246.

Huh, C.-A. and T. M. Beasley (1987) Profiles of dissolved and particulate thorium isotopes in the water column of coastal California. *Earth Planet. Sci. Lett.*, **85**, 1-10.

Hurtt, G. C. and R. A. Armstrong (1999) A pelagic ecosystem model calibrated with BATS and OWSI data, *Deep-Sea Res. I*, **46**, 27-61.

Hutchins, D. A., and K. W. Bruland (1998) Iron limitation and the silicate pump in the California upwelling region, AGU/ASLO Ocean Sciences Conference, San Diego, USA.

Iriarte, J. L., and G. A. Fryxell (1995) Micro-phytoplankton at the equatorial Pacific (140°W) during the JGOFS EqPac Time Series studies: March to April and October 1992, *Deep-Sea Res. II*, **42**, 559-584.

Jackson, J. A., F. Azam, A. F. Carlucci, R. W. Eppley and P. M. Williams (1989) Elemental cycling and fluxes off southern California. *Eos*, **70**, 146-149, 154-155.

Jackson, J. A. (1990) A model of the formation of marine algal flocs by physical coagulation processes. *Deep-Sea Res.*, **37**, 1197-1211.

Johnson, K. S., R. M. Gordon, and K. H. Coale (1997) What controls dissolved iron concentrations in the world ocean?, *Mar. Chem.*, **57**, 137-161.

Kamatani, A. (1982) Dissolution rates of silica from diatoms decomposing at various temperatures, *Mar. Biol.*, **68**, 91-96.

Karl, D. M., J. R. Christian, J E. Dore, D. V. Hebel, R. M Letelier, L. M. Tupas and C. D. Winn (1996) Seasonal and interannual variability in primary production and particle flux at station ALOHA, *Deep-Sea Res. II*, **43**, 539-568.

Karl, D. M., R. Letelier, L. Tupas, J. Dore, J. Christian and D. Hebel (1997) The role of nitrogen fixation in biogeochemical cycling in the subtropical North Pacific Ocean. *Nature*, **388**, 533-538.

Kessler, W. S., and M. J. McPhaden (1995) The 1991-1993 El Niño in the central Pacific, *Deep-Sea Res. II*, **42**, 295-334.

Knauer, G. A., J. H. Martin and K. W. Bruland (1979) Fluxes of particulate carbon, nitrogen and phosphorous in the upper water column of the northeast Pacific. *Deep-Sea Res.*, **26**, 97-108.

Knauss, K. G., T.-L. Ku and W. S. Moore (1978) Radium and thorium isotopes in the surface waters of the east Pacific and coastal southern California. *Earth Planet. Sci. Lett.*, **39**, 235-249.

Komar, P. D., Morse, A. P., Small., L. F., and S. W. Fowler (1981) An analysis of sinking rates of natural copepod and euphausiid fecal pellets, *Limnol. Oceanogr.*, **26**, 172-180.

Krishnaswami, S., D. Lal and B. S. Amin (1973) Geochronological studies in the Santa Barbara Basin: ^{55}Fe as a unique tracer for particle settling. *Limnol. Oceanogr.*, **18**, 763-770.

Ku, T.-L., K. G. Knauss and G. G. Matieu (1977) Uranium in open ocean: concentration and isotopic composition, *Deep-Sea Res.*, **24**, 1005-1017.

Ku, T.-L., S. Luo, M. Kusakabe, and J. K. B. Bishop (1995) ^{228}Ra-derived nutrient budgets in the upper equatorial Pacific and the role of "new" silicate in limiting productivity, *Deep-Sea Res. II*, **42**, 479-498.

Kurz, K. D. and E. Maier-Reimer (1993) Iron fertilization of the Austral Ocean - the Hamburg model assessment. *Global Biogeochemical Cycles*, **7**, 229-244.

Landry, M. R., J. Constantinou, and J. Kirshtein (1995) Microzooplankton grazing in the central equatorial Pacific during February and August, 1992, *Deep-Sea Res. II*, **42**, 657-672.

Landry, M. R., and 12 others (1997) Iron and grazing constraints on primary production in the central equatorial Pacific: an EqPac synthesis, *Limnol. Oceanogr.*, **42**, 405-418.

Latasa, M., M. R. Landry, L. Schluter, and R. R. Bidigare (1997) Pigment-specific growth and grazing rates of phytoplankton in the central equatorial Pacific, *Limnol. Oceanogr.*, **42**, 289-298.

LeBorgne, R., M. Rodier, A. LeBouteiller, and J. W. Murray (in press) Zonal variability of biological features and particle export flux in the pacific equatorial upwelling between 165°E and 150°W (April-May, 1996), *Oceanol. Acta.*

LeBorgne, R., C. Brunet, G. Eldin, M.-H. Radenac, and M. Rodier (1995) Campagne Oceanographique FLUPAC a bord du N.O. l'ATALANTE (23 septembre au 29 octobre 1994). Recueil des donnees. Tome 1: meteo, courantologie, hyrologie, donnees de surface, ORSTOM, *Noumea Archives Sciences de la Mer, Oceanographique*, **1**, 1-340.

LeBorgne, R and H. Gesbert (1995) Campagne Oceanographique FLUPAC a bord du N.O. l'ATALANTE (23 septembre au 29 octobre 1994). Recueil des donnees. Tome 2: optique marine, matiere organic dissoute, pigments photosynthetiques, observations microscopiques, production primaire, "broutage", zooplancton, sedimentation. ORSTOM. *Noumea Archives Sciences de la Mer, Oceanographique*, **2**, 1-303.

Ledwell, J. R., A. J. Watson and C. S. Law (1993) Evidence for slow mixing across the pycnocline from an open-ocean tracer-release experiment, Nature, 364, 701-703.

Lewin, J. C. (1961) The dissolution of silica from diatom walls. *Geochimica et Cosmochimica Acta*, **21**, 182-198.

Liu, Z., S. G. H. Philander, and R. C. Pacanowski (1994) A GCM study of tropical-subtropical upper-ocean water exchange, *J. Phys. Oceanogr.*, **24**, 2606-2623.

Lomas, M. W., and P. M. Glibert (1998) Temperature regulation of nitrogen uptake: a novel hypothesis about nitrite biogeochemistry in cold water diatoms, AGU-ASLO Ocean Sciences Meeting, San Diego, USA, Feb. 9-13.

Longhurst, A. R. (1991) Role of the marine biosphere in the global carbon cycle, *Limnol. Oceanogr.*, **36**, 1507-1526.

Lorenzen, C. J., N. A. Welschmeyer, A. E. Copping and M. Vernet (1983) Sinking rates of organic particles. *Limnol. Oceanogr.*, **28**, 766-769.

Loukos, H., B. Frost, D. E. Harrison and J. W. Murray (1997) Ecosystem model with iron limitation of primary production in the equatorial Pacific at 140°W. *Deep-Sea Res. II*, **44**, 2221-2249.

Lu, P., J. P. McCready JR., and B. A. Klinger (1998) Meridional circulation cells and the source waters of the Pacific Equatorial Undercurrent, *J. Phys.Oceanogr.*, **28**, 62-84.

Mackey, D. J., J. S. Parslow, F. B. Griffiths, H. W. Higgins an dB. Tillbrook (1997) Phytoplankton productivity and the carbon cycle in the western equatorial Pacific under El Niño and non-El Niño conditions. *Deep-Sea Res. II*, **44**, 1951-1978.

Margalef, R. (1973) Life-forms of phytoplankton as survival alternatives in an unstable environment. *Oceanologica Acta*, **1**, 493-509.

Martin, J. H. and S. E. Fitzwater (1988) Iron deficiency limits phytoplankton growth in the northeast Pacific subarctic, *Nature*, **331**, 341-343.

Martin, J. H. (1990) Glacial-interglacial CO_2 change: The iron hypothesis, *Paleoceanogr.*, **5**, 1-13.

McCarthy, J. J., C. Garside, J. L. Nevins, and R. T. Barber (1996) New production along 140°W in the equatorial Pacific during and following the 1992 El Niño event, *Deep-Sea Res. II*, **43**, 1065-1094.

Michaels, A. F., and M. W. Silver (1988) Primary production, sinking fluxes and the microbial food web, *Deep-Sea Res.*, **35**, 473-490.

Mood, A. M. (1950) *Introduction to the theory of statistics*, McGraw-Hill, N.Y.

Moore, W. S., K. W. Bruland and J. Michel (1981) Fluxes of uranium and thorium series isotopes in the Santa Barbara Basin. *Earth Planet. Sci. Lett.*, **53**, 391-399.

Morawitz, W. M. L and N. Bray (submitted) Local wind forcing and vertical velocities in the Santa Barbara Channel. *J. Geophys. Res.*.

Munk, W. H. (1966) Abyssal Recipes, *Deep-Sea Res.*, **13**, 707-730.

Murray, J. W., R. T. Barber, M. R. Roman, M. P. Bacon, and R. A. Feely (1994) Physical and biological controls on carbon cycling in the equatorial Pacific, *Science*, **266**, 58-65.

Murray, J. W., J. Young, J. Newton, J. Dunne T. Chapin, B. Paul, and J. J. McCarthy (1996) Export flux of particulate organic carbon from the central equatorial Pacific determined using a combined drifting trap-^{234}Th approach, *Deep-Sea Res. II*, **43**, 1095-1132.

Nelson, D. M., and J. J. Goering (1978) Assimilation of silicic acid by phytoplankton in the Baja California and northwest Africa upwelling systems, *Limnol. Oceanogr.*, **23**, 508-517.

Nelson, D. M., J. J. Goering, S. S. Kilham, and R. R. Guillard (1976) Kinetics of silicic acid uptake rates of silica dissolution in the marine diatom *Thalassiosira Pseudonana*, *J. Phycol.*, **12**, 246-269.

Paasche, E. (1973) Silicon and the ecology of marine planktonic diatoms. I. *Thalassiosira pseudonana* (*Cyclotella nana*) grown in a chemostat with silicate as limiting nutrient, *Mar. Biol.*, **19**, 117-126.

Paasche, E. (1980) Silicon content of five marine plankton diatom species measured with a rapid filter method, *Limnol. Oceanogr.*, **25**, 474-480.

Pacanowski, R. C. and S. G. H. Philander (1981) Parameterization of vertical mixing in numerical models of tropical oceans, *J. Phys. Oceanogr.*, **11**, 1443-1451.

Philander, S. G. (1990) *El Niño, La Niña, and the Southern Oscillation*, R. Dmowska and J. R. Holton eds., Academic Press.

Press, W. H., S. A. Teukosky, W. T. Vetterling, B. P. Flannery (1992) *Numerical Recipes in FORTRAN, Second Edition*, Cambridge University Press.

Price, N. M., B. A. Ahner, and F. M. M. Morel (1994) The Equatorial Pacific Ocean: Grazer-controlled phytoplankton populations in an iron-limited ecosystem, *Limnol. Oceanogr.*, **39**, 520-534.

Quay, P. (1997) Was a carbon balance measured in the equatorial Pacific during JGOFS?. *Deep-Sea Res. II*, **44**, 1765-1781.

Rodier, M., and R. LeBorgne (1997) Export flux of particles at the equator in the western and central Pacific Ocean, *Deep-Sea Res. II*, **44**, 2085-2113.

Rohlf, F. J. and R. R. Sokal (1995) *Statistical Tables*, 3rd edition, W. H. Freeman and Co., New York, NY.

Schlitzer, R. (1998) Silicon, carbon and nutrient budgets in the Southern Ocean derived from historical data, AGU/ASLO Ocean Sciences Conference, San Diego, USA.

Shipe, R., M. Brzezinski and A. L. Alldredge (in prep.) A time series of carbon, nitrogen and silicon cycling in the Santa Barbara Channel, *Cont. Shelf. Res.*.

Silver, M. W. and A. L. Alldredge (1981) Bathypelagic marine snow: deep-sea algal and detrital community. *J. Mar. Res.*, **39**, 501-530.

Smayda, T. J. (1970) The suspension and sinking of phytoplankton in the sea. *Oceanography and Mar. Biol. Ann. Rev.*, **8**, 353-414.

Smetacek, V., B. von Bodungen, B. Knoppers, R. Peinert, F. Pollehne, P. Stegmann, and B. Zeitschel (1984) Seasonal stages characterizing the annual cycle of an inshore pelagic system. *Rapp. P.-v. Reun. Cons. int. Eplor. Mer*, **183**, 126-135.

Smetacek, V., B. (1988) Plankton Characteristic, *Cont. Shelves*, **27**, 93-130.

Smith, C. R., D. J. Hoover, S. E. Doan, R. H. Pope, D. J. Demaster, F. C. Dobbs, and M. A. Altabet (1996) Phytodetritus at the abyssal seafloor across 10° of latitude in the central equatorial Pacific, *Deep-Sea Res. II*, **43**, 1309-1338.

Sokal, R. R., and F. J. Rohlf (1995) *Biometry: the principles and practice of statistics in biological research*, 3d ed., W. H. Freedman and Company.

Verity, P. G., D. K. Stoecker, M. E. Sieracki, and J. R. Nelson (1996) Microzooplankton grazing of primary production at 140°W in the equatorial Pacific, *Deep-Sea Res. II*, **43**, 1227-1282.

Williams, P. M., K. J. Robertson, A. Soutar, S. M. Griffin and E. R. M. Druffel (1992) Isotopic signatures (^{14}C, ^{13}C, ^{15}N) as tracers of sources and cycling of soluble and particulate organic matter in the Santa Monica Basin, California. *Prog. Oceanogr.*, **30**, 253-290.

Wyrtki, K. and B. Kilonsky (1984) Mean water and current structure during the Hawaii-Tahiti Shuttle Experiment, *J. Phys. Oceanogr.*, **14**, 242-254.

Yoder, J. A., S. G. Ackleson, R. T. Barber, P. Flament and W. M. Balch (1994) A line in the sea. *Nature*, **371**, 689-692.

Zettler, E. R., R. J. Olson, B. J. Binder, S. W. Chisholm, S. E. Fitzwater and R. T. Barber (1996) Iron-enrichment bottle experiments in the equatorial Pacific: responses of individual phytoplankton cells. *Deep-Sea Res. II*, **43**, 1017-1029.

VITA

John P. Dunne

University of Washington

1999

Education:

Ph.D. Winter, 1999. University of Washington, Seattle, WA
Field: Oceanography, Thesis: Measured and Modeled Particle export in the equatorial and coastal oceans

M.S. June 1996. University of Washington, Seattle, WA
Field: Oceanography, Thesis: ^{234}Th and particle cycling in the central equatorial Pacific, GPA: 3.55

B.S. June 1993. The University of California at San Diego
Major: Chemistry; Minor: Writing, GPA: 3.23

Professional Experience:

Graduate Researcher, Oceanography, University of Washington, Seattle, WA. Performed research, gave presentations, wrote papers, attended conferences and workshops, served as graduate rep. to faculty (*Advisor: James Murray*). Sept. 1993-Mar. 1999

Research Assistant, Marine Physical Laboratory, Scripps Institution of Oceanography, La Jolla, CA. Built automated pH and alkalinity systems, prepared CO_2 standards (*Advisor: Andrew Dickson*). June 1992-June 1993

Research Technician, Biophysica Corporation, La Jolla, CA. Performed UV spectroscopy and chromatography, prepared solutions, tended to laboratory animals (*Director: Milos Sovak*). Sept. 1990-June 1992

Analytical Technician, North State Environmental, South San Francisco, CA. Cataloged and re-organized and disposed of chemicals for an analytical laboratory (*Director: Frank Balistreri*). July, 1990

Research Assistant, UCSD Biology, La Jolla, CA. Dissected geckos and prepared gut and blood slides for analysis of diet and genetic diversity (*Advisor: Theodore Case*). March 1990 -June 1990

Field Experience:

Soap Lake, WA. *R/V Realander*, May, 1997. Chief Sci.: Laurie Balistrieri.

Santa Barbara Channel, CA. *R/V Point Sur*, April 1997. Chief Scientists: James Murray and Alice Alldredge

Equatorial Pacific. *R/V Thomas G. Thompson*, April-May 1996. Chief Sci.: James Murray

Hawaii Ocean Time-series. *R/V Moana Wave*, Oct.-Nov. 1995. Chief Sci.: Louis Tupas

Equatorial Pacific. *N/O l'Atalante*, Oct.-Nov. 1994. Chief Sci.: Robert LeBorgne

Puget Sound. *R/V Clifford Barnes*, five days between Mar., 1993 - Sept. 1994. Chief Sci.: James Murray

Teaching Experience:

Instructor: Washington Initiative for Science Education - Science Teacher Enhancement Program. Guided grade school teachers on field trips of scientific discovery. Summers of 1995 and 1996

Coordinator and Lecturer: University of Washington Outreach Program. Designed and gave lectures at middle and secondary schools and community groups in Seattle on topics in oceanography. Fall, 1994 - Winter, 1995

Teaching Assistant, UW Oceanography, Seattle, WA. Organized and led cooperative learning sessions, held office hours, performed grading. Phys. Ocean. - Winter 1994. Chem. Ocean. - Spring, 1994

Teaching Assistant, UCSD Chemistry, La Jolla, CA. Held discussions, problem sessions and office hours, performed grading. General Chem.: Winter, 1991 - Spring, 1992. Organic Chem.: Fall, 1992. General Chem. Lab.: Winter, 1993

Special Skills:

Analysis of trace metals, stable isotopes, radioisotopes, chlorophyll, carbon/nitrogen, oxygen, chloride, pH and alkalinity; experimental design; data management, statistical analysis and numerical modeling on UNIX and Macintosh computer platforms in Fortran, C, Matlab and Excel; research SCUBA; carpentry.

Honors:

NASA Earth System Science Fellow. 1995-1998

Scripps Undergraduate Research Fellow. Summer, 1992

Howard Hughes Undergraduate Research Fellow. Summer, 1992

Howard Hughes Scientific Enrichment Fellow. Spring, 1989

Publications:

Dunne, J. P., J. W. Murray, R. Shipe and A. Alldredge (in preparation) ^{234}Th-based particle cycling in the Santa Barbara Channel, *Deep Sea Research I.*

Aufdenkampe, A. K., J. McCarthy, J. Dunne, M. Rodier and J. Murray, (in preparation) New production along the equator in the Pacific, *Deep-Sea Research I.*

Dunne, J. P., J. Murray, M. Rodier and D. Hansell (submitted) Particle export in the western and central equatorial Pacific: zonal and temporal variability, *Deep-Sea Research I.*

Dunne, J. P., J. W. Murray, A. Aufdenkampe, S. Blain and M. Rodier, (submitted) Silicon:nitrogen coupling in the equatorial Pacific upwelling zone. *Global Biogeochemical Cycles.*

Dunne, J. P., and J. W. Murray (in press) Sensitivity of ^{234}Th export to physical processes in the central equatorial Pacific, *Deep-Sea Research I.*

Dunne, J. P., J. W. Murray, J. Young, L. Balistrieri and J. K. B. Bishop (1997) ^{234}Th and particle cycling in the central equatorial Pacific, *Deep Sea Research II*, 44, 2049-2083.

Archer, D., R. C. Barber, J. P. Dunne and 14 others (1997) A meeting place of great ocean currents: Shipboard observations of a convergent front at 2°N in the Pacific, *Deep Sea Research II*, 44, 1827-1849.

Murray, J. W., J. Young, J. Newton, J. Dunne, T. Chapin and B. Paul (1996) Export production determined using ^{234}Th: ^{238}U disequilibria, *Deep-Sea Research II*, 43, 1095-1132.

Presentations:

Ph.D. defense/Chemical Oceanography Departmental Seminar. Biogeochemical Implications of a Two-State Ecosystem. Seattle, WA. March, 1999.

University of British Columbia Geochemistry Seminar. Diatom control of new and export production in the equatorial Pacific. Vancouver, BC. October, 1998.

JGOFS Equatorial Pacific Synthesis Group meeting. Diatom control of new and export production in the equatorial Pacific. Seattle, WA. October, 1998.

Ocean Sciences Meeting, American Geophysical Union. Particle Export from the western and central equatorial Pacific. San Diego, CA. February, 1998.

Chemical Oceanography Departmental Seminar. Do diatoms control productivity in the central equatorial Pacific? UW Oceanography. January, 1998.

JGOFS Synthesis and Modeling Project Workshop. Sensitivity of ^{234}Th-based export to circulation in the equatorial Pacific. Snowbird, UT. July, 1997.

American Society for Limnology and Oceanography. Adsorption of ^{234}Th onto particles in the central equatorial Pacific. Santa Fe, NM. February, 1997.

Chemical Oceanography Departmental Seminar. Adsorption of ^{234}Th onto particles in the central equatorial Pacific. UW Oceanography. January, 1997.

Chemical Oceanography Departmental Seminar. ^{234}Th cycling and export production using JGOFS EqPac data. UW Oceanography. November, 1995.

NATO Advance Workshop on the Equatorial Pacific. Particle export during the FRANCE JGOFS FLUPAC cruise. (poster) June, 1995.

American Geophysical Union. ^{234}Th cycling and export production using JGOFS - EqPac data. San Francisco, CA. December, 1994.

The Oceanography Society. ^{234}Th and Particle cycling in the central equatorial Pacific. (poster) Honolulu, HI. July, 1994.

IMAGE EVALUATION
TEST TARGET (QA-3)

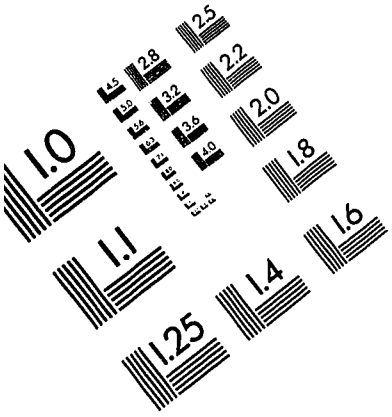

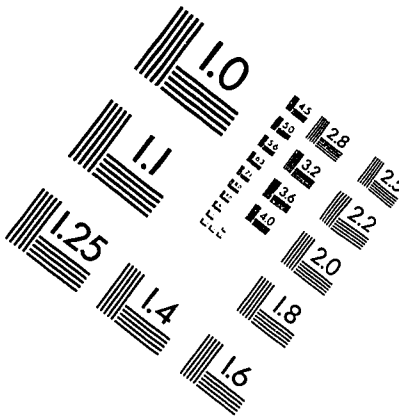

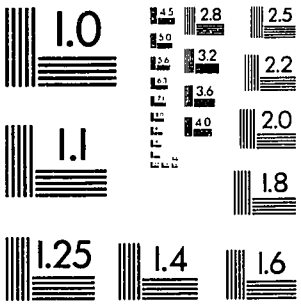

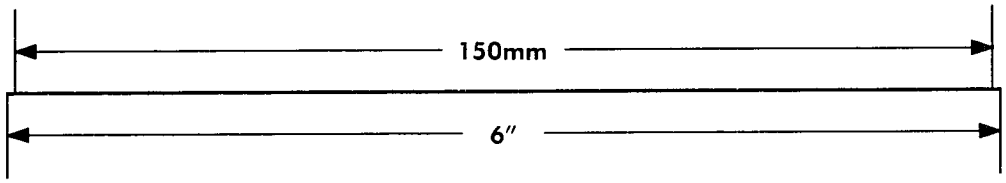

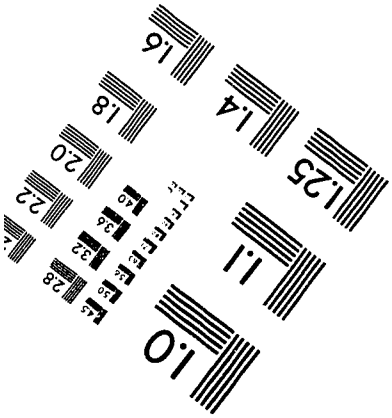

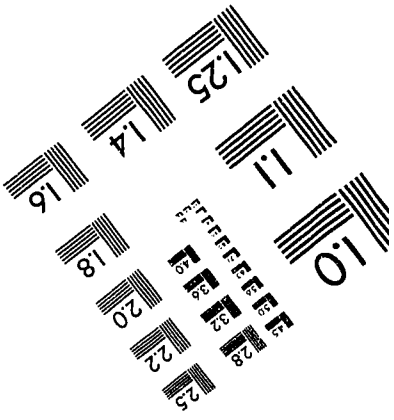

APPLIED IMAGE, Inc
1653 East Main Street
Rochester, NY 14609 USA
Phone: 716/482-0300
Fax: 716/288-5989